The role of mechanical forces in osteogenic differentiation, BMP signaling and early tissue formation processes in the context of bone healing

vorgelegt von
Dipl.-Ing. Sophie Görlitz
geborene Schreivogel
ORCID: 0000-0002-2302-8351

an der Fakultät III – Prozesswissenschaften der
Technischen Universität Berlin
zur Erlangung des akademischen Grades

Doktor der Ingenieurwissenschaften
-Dr.-Ing.-

genehmigte Dissertation

Promotionsausschuss:
Vorsitzender: Prof. Dr. Lorenz Adrian
Gutachter: Prof. Dr. Jens Kurreck
Gutachter: Prof. Dr. Roland Lauster
Gutachter: Prof. Dr. Georg N. Duda

Tag der wissenschaftlichen Aussprache: 02. Juni 2020

Berlin 2021

Für meine Familie

Danksagung

Mein ganz besonderer Dank geht an Dr. Ansgar Petersen, der mir nicht nur ermöglicht hat den Weg der Promotion einzuschlagen, sondern mir auch während dieser Zeit ein hervorragender Mentor war. Durch seine Vorschläge und konstruktive Kritik haben sich diese Arbeit, aber auch vorherige Präsentationen und Veröffentlichungen entscheidend verbessert. Weiterhin hat er durch die Zusammenstellung einer internationalen und interdisziplinären Arbeitsgruppe, deren Mitglieder sich sehr gut ergänzen, ein konstruktives und stimulierendes Arbeitsumfeld geschaffen. Ich bin mir sicher, dass mir das Wissen und die Fähigkeiten, die ich unter seiner Betreuung erworben habe, auf meinem weiteren Weg sehr helfen werden. Besten Dank für deine wertvolle Unterstützung.

Ein großer Dank geht auch an Prof. Georg Duda. Neben seinen wertvollen wissenschaftlichen Beiträgen, habe ich durch ihn einen guten Einblick in die Mechanismen der akademischen Welt erhalten. Weiterhin möchte ich mich bei Prof. Petra Knaus für ihre Unterstützung bedanken. Die Zusammenarbeit mit ihr und ihrer Arbeitsgruppe hat fruchtbare Ideen in mein Projekt gebracht. Auch Prof. Jens Kurreck danke ich, dass er die Betreuung dieser Arbeit aus universitärer Seite übernommen hat.

Natürlich möchte ich mich auch ganz herzlich beim gesamten jetzigem und ehemaligem CBM Team bedanken. Ihr habt meinen Arbeitsalltag enorm bereichert und ich habe die zahlreichen Frühstücke, Ausflüge und Abendveranstaltungen mit euch sehr genossen. Insbesondere möchte ich mich bei Aaron Herrera und Erik Brauer für die Zusammenarbeit bedanken. Ich konnte immer auf eure Unterstützung zählen und weiß eure Meinungen und Vorschläge sehr zu schätzen. Auch die verscheiden wissenschaftlichen Konferenzen, die wir gemeinsam besucht haben, werde ich in sehr guter Erinnerung behalten. Weiterhin bin ich sehr froh, dass Isabel Orellano, Ehsan Soodmand, Martina Tortorici, Janina Stadter und Parisa Khalaghi zum Team dazu gestoßen sind. Mit euch macht es einfach Spaß zusammen zu arbeiten. Auf keinen Fall darf ich Gabriela Korus und Iwona Cichocka vergessen. Sie haben mich nicht nur in die Welt der Histologie und Zellkultur eingeführt, sie hatten auch immer eine helfende Hand und ein offenes Ohr. Ich freue mich auch, dass unser Team nun durch Simone Cho unterstütz wird.

Die tägliche Labor- und Büroarbeit lebt von der gegenseitigen Unterstützung, daher möchte ich mich auch bei Maria Reichenbach, Aline Lückgen, Christian Bucher, Dag Wulsten, Thomas Sips, Julia Berkmann, Taimoor Hasan Qazi, Janosch Schoon und so vielen anderen bedanken.

Meinen allergrößten Dank verdient meine Familie, insbesondere mein Mann Richard, meine Eltern, meine Schwester und meine Großeltern. Ich kann mir keine bessere wünschen. Bei euch kann ich Ballast abwerfen und neue Energie tanken. Ihr seid immer für mich da und stärkt mir den Rücken. Auch meinen Schwiegereltern, meiner Schwägerin und meinem Schwager danke ich von Herzen für ihre Unterstützung. Ohne euch alle wäre ich nicht da wo ich jetzt bin.

Abstract

During bone fracture healing, cells are simultaneously subjected to extrinsic mechanical forces and to a variety of biochemical signals including the indispensable and clinically applied growth factor Bone Morphogenetic Protein 2 (BMP-2). *In vivo* experiments provide evidence that mechanical forces promote BMP-2-induced bone defect healing and *in vitro* studies report about a potentiation of BMP signaling by mechanical stimuli. Clinically, supra-physiological BMP-2 concentrations are used for fracture treatment, which can cause various side effects. Fine-tuned mechanical stimuli, either resulting from extrinsic loading or featured by advanced biomaterials, could in future improve the growth factor application by increasing its efficiency. However, to employ the power of the mechano-biochemical interaction, a deeper understanding how both stimuli control cell behavior independently and in combination is needed.

In this dissertation, the influence of extrinsic mechanical forces and BMP-2 on osteogenic cell differentiation and early tissue formation processes was investigated *in vitro* and the molecular mechanism underlying the mechano-regulated BMP signaling were explored. To realize *in vivo* loading scenarios in the well-controlled environment of an *in vitro* screening system, mechano-bioreactors in combination with 3D biomaterial matrices were utilized throughout this study.

In contrast to data from literature, osteogenic differentiation of primary human mesenchymal stromal cells was found to be down-regulated under cyclic compression. This could be explained by the specific experimental conditions that excluded autocrine stimulation. When the enrichment of secreted factors including BMP-2 in the cell culture medium was permitted, cyclic compression promoted osteogenic differentiation as it was observed under direct supplementation of BMP-2. Based on these observations, it was concluded that mechanical stimulation induces osteogenesis indirectly through a mechanically controlled secretion of BMP-2 and the resulting biochemical self-stimulation. This interpretation was underpinned by the absence of load-induced osteogenic differentiation when a specific BMP inhibitor was supplemented.

Besides a mechano-regulated increase in BMP-2 expression and secretion, mechanical stimuli trigger mechanotransduction pathways that directly crosstalk to BMP signaling enhancing Smad phosphorylation and target gene expression. However, the mechanical requirements and the molecular mechanism causing the crosstalk are poorly understood. By a systematic variation of the mechanical loading schemes, it was shown for the first time that cells feature a mechanical memory that leads to an increased signaling response to BMP-2 even when the mechanical signal has vanished. The mechanical memory is active upon long-term stimulation and is based inter alia on an enhanced and sustained expression of the BMP receptor type 1B. While transcriptional regulations are suggested to be an integral part of the mechanical memory, the immediate early induction of Smad phosphorylation upon concurrent mechanical and biochemical (BMP-2) stimulation is independent of any transcriptional regulation. Instead, specific integrin knockdown and F-actin stabilization experiments

revealed that integrin α_v as well as load-induced integrin and actin cytoskeleton remodeling are required for the immediate mechano-regulation of BMP signaling.

The relevance of the crosstalk for early tissue formation was investigated in the last part of the project. While, cyclic compression alone specifically altered mechanical, structural and compositional matrix cues, BMP-2 treatment had only minor effects. In a combination of both stimuli, the effects of cyclic compression were therefore dominating and no synergistic effects could be observed. Even though a role of the crosstalk for early tissue formation could not be verified, new insides into how mechanical stimulation influences ECM formation have been gained.

Taken together, this dissertation contributes to a profound understanding of how mechanical forces regulate osteogenic differentiation, BMP signaling and early tissue formation, processes, which are relevant in the context of bone regeneration. In a long-term perspective, these findings could help to optimize mechanical boundary conditions with respect to BMP signaling to increase the efficacy and safety of therapeutically used BMP-2. This study highlights the role of mechano-biochemical interactions in controlling cell behavior and motivate further research on growth factor signaling in a mechanical context.

Zusammenfassung

Während der Knochenheilung sind Zellen gleichzeitig mechanischen Kräften und einer Vielzahl von biochemischen Faktoren, einschließlich des klinisch angewandten Bone Morphogenetic Protein 2 (BMP-2), ausgesetzt. *In vivo* Experimente deuten darauf hin, dass mechanische Kräfte die BMP-2-induzierte Knochendefektheilung fördern und i*n vitro* Studien konnten eine Verstärkung des BMP Signalweges durch mechanische Stimulation zeigen. Zur klinischen Behandlung werden noch immer supra-physiologische BMP-2 Konzentrationen verwendet, die verschiedene Nebenwirkungen verursachen können. Optimierte mechanische Stimuli, ausgehend von extrinsischer Belastung oder von einem Biomaterial, könnten zukünftig dazu genutzt werden, die Effizienz des Wachstumsfaktors zu überhöhen. Um sich diese Interaktion zunutze zu machen, muss jedoch zunächst verstanden werden wie beide Stimuli unabhängig und abhängig voneinander das Zellverhalten beeinflussen.

In dieser Dissertation wurde sowohl der Einfluss von extrinsischen mechanischen Kräften und BMP-2 auf die osteogene Zelldifferenzierung und Gewebebildung untersucht, als auch der molekulare Mechanismus der der mechanischen Regulierung des BMP-Signalweges zugrunde liegt, erforscht. Um *in vivo* Belastungsbedingung in einer 3D Umgebung nachzubilden, wurde ein Bioreaktorsystem in Kombination mit makroporösen Biomaterialien in dieser Studie verwendet.

Im Gegensatz zu Literaturdaten, wurde die osteogene Differenzierung primärer humaner mesenchymaler Stromazellen durch zyklische Kompression herunterreguliert. Dies konnte durch die speziellen experimentellen Bedingungen erklärt werden, die eine autokrine Stimulation ausschlossen. Wenn eine Anreicherung von sezernierten Faktoren, einschließlich BMP-2, im Zellkulturmedium zugelassen wurde, förderte die zyklische Kompression jedoch die osteogene Differenzierung, was auch unter Supplementierung von BMP-2 beobachtet wurde. Basierend auf diesen Ergebnissen wurde der Schluss gezogen, dass die mechanische Stimulation die Osteogenese indirekt durch eine mechanisch kontrollierte Sekretion von BMP-2 und die daraus resultierende biochemische Selbststimulation induziert wird. Diese Interpretation wurde dadurch untermauert, dass eine Zugabe eines spezifischen BMP-Inhibitors zum Ausbleiben einer belastungsinduzierten osteogenen Differenzierung führte.
Neben einer mechano-regulierten Erhöhung der BMP-2-Expression lösen mechanische Stimuli Mechanotransduktionswege aus, die direkt mit dem BMP-Signalweg interagieren und die Smad-Phosphorylierung und die Expression von Zielgenen verstärken. Allerdings sind die mechanischen Anforderungen für eine Interaktion und der zugrundeliegende molekulare Mechanismus nur unzureichend verstanden.

Durch Variation der Belastungsparameter wurde erstmals festgestellt, dass Zellen bei langfristiger Vorstimulation ein mechanisches Gedächtnis entwickeln, welches sich auf den BMP-Signalweg auswirkt. Dieses Gedächtnis wird unter anderem durch eine belastungsinduzierte Erhöhung der BMP-Rezeptor-Typ-1B-Expression verursacht. Während transkriptionelle Regulationen für die Ausbildung eines mechanischen Gedächtnisses von großer Wichtigkeit sind, ist die sofortige und frühe Induktion der Smad-Phosphorylierung

durch gleichzeitiger mechanischer und BMP Stimulation unabhängig von einer Transkriptionsregulierung. Stattdessen konnte durch einen spezifischen Integrin-Knockdown und eine F-Aktin-Stabilisierung gezeigt werden, dass αv Integrine und der belastungsinduzierte Integrin- und Zytoskelettumbau für die sofortige Mechano-Regulation des BMP-Signalweges erforderlich sind.

Die Bedeutung der Interaktion für die frühe Gewebebildung wurde im letzten Teil des Projekts untersucht. Während die zyklische Kompression spezifisch mechanische, strukturelle und kompositorische Matrixeigenschaften veränderte, hatte die BMP-2-Behandlung nur geringe Auswirkungen. Bei einer Kombination beider Stimuli dominierten daher die Effekte der zyklischen Kompression und es konnten keine synergistischen Effekte beobachtet werden. Obwohl eine Rolle der Mechano-Regulation des BMP-Signalweges für die frühe Gewebebildung nicht verifiziert werden konnte, wurden neue Erkenntnisse darüber gewonnen, wie mechanische Stimulation die Bildung der extrazellulären Matrix beeinflusst.

Zusammengenommen tragen die Ergebnisse diese Dissertation zu einem tiefgreifenden Verständnis darüber bei, wie mechanische Kräfte die osteogenen Differenzierung, den BMP-Signalweges und frühe Gewebebildungsprozesse im Kontext der Knochenheilung regulieren. In Zukunft könnten diese Erkenntnisse dazu beitragen, die mechanischen Randbedingungen in Bezug auf den BMP-Signalweg zu optimieren, um die Wirksamkeit und Sicherheit von therapeutisch eingesetztem BMP-2 zu erhöhen. Die Ergebnisse heben die Rolle mechano-biochemischer Wechselwirkungen bei der Steuerung des Zellverhaltens hervor und motivieren zu weiteren Forschungen zur Wachstumsfaktorsignalwegen in einem mechanischen Kontext.

Table of Contents

Abstract ... **1**
Zusammenfassung ... **3**
Table of Contents ... **5**
List of figures ... **7**
List of tables ... **9**
1 Introduction ... **11**
1.1 Repair versus regeneration – bone as a model system for tissue regeneration ... 11
1.2 Bone fracture healing and regeneration ... 11
1.2.1 Bone Morphogenetic Proteins - growth factors essential for bone healing ... 13
1.2.2 Mechanical forces influence bone healing ... 13
1.2.3 Mechanical forces enhance BMP-2-induced bone healing ... 15
1.3 Sensing, transmitting and responding to mechanical cues ... 16
1.3.1 Integrin-mediated adhesions ... 16
1.3.2 Integrin-mediated mechanotransduction ... 18
1.3.3 Mechanical forces influence cell fate decisions ... 19
1.4 BMP signaling pathway ... 20
1.5 Mechanical signals integrate into the BMP pathway ... 23
1.5.1 Integrin-BMP receptor crosstalk ... 24
1.6 Mechanical forces and BMP-2 influence ECM formation ... 26
1.7 Motivation and Aims ... 28
2 Materials ... **30**
2.1 Optimaix collagen scaffold ... 30
2.2 Bioreactor used for mechanical stimulation ... 30
2.3 Bioreactor equipment and consumables ... 31
2.4 Flow chamber setup ... 32
2.5 Devices ... 33
2.6 Chemicals, reagents and kits ... 33
2.7 Buffer ingredients ... 34
2.8 Cell culture ... 35
2.8.1 Cells ... 35
2.8.2 Cell culture material ... 36
2.8.3 siRNAs, transfection reagents and transduction material ... 36
2.8.4 Growth factor and small molecular inhibitor ... 37
2.9 Materials for histology ... 37
2.9.1 Primary and secondary antibodies ... 38
2.9.2 Small molecular dyes for immunohistochemistry ... 39
2.10 RNA isolation, reverse transcription and qPCR ... 39
2.10.1 Primer ... 39
3 Methods ... **42**

3.1 Cell biological methods ... 42
3.1.1 Cell thawing and cultivation ... 42
3.1.2 Passaging and cryo-preservation ... 43
3.1.3 Seeding of collagen scaffolds ... 44
3.1.4 Lentiviral transduction of an actin marker ... 44
3.1.5 Transfection of small interfering RNA ... 45
3.1.6 Bioreactor cultivation, mechanical loading and BMP stimulation ... 46
3.2 Molecular biological methods ... 49
3.2.1 Ribonucleic acid isolation from collagen scaffolds ... 49
3.2.2 Reverse transcription, quantitative polymerase chain reaction and data evaluation ... 49
3.2.3 Cell lysis for protein analysis and extraction of ECM proteins ... 50
3.2.4 Sodium dodecylsulfate polyacrylamide gel electrophoresis ... 51
3.2.5 Western blotting and protein detection ... 51
3.3 Immunocytochemistry ... 52
3.3.1 Sample preparation including fixation and cryo-trimming ... 52
3.3.2 Immunofluorescence staining ... 52
3.4 Confocal multiphoton microscopy ... 53
3.4.1 Image acquisition and analysis ... 53
3.4.2 Live-cell-imaging and analysis ... 54
3.4.3 Mechano-imaging ... 55
3.5 Scaffold contraction analysis ... 56
3.6 Mechanical compression tests ... 56
3.7 Decellularization after *in vitro* tissue formation ... 57
3.8 Mass spectrometry ... 58
3.9 Statistical analysis and data presentation ... 58
4 Results ... 59
4.1 Load-induced osteogenic differentiation via BMP-2 ... 59
4.1.1 Cell morphology, proliferation and oxygen concentration inside scaffolds cultured in the bioreactor ... 59
4.1.2 Cyclic mechanical compression downregulates the expression of key osteogenic marker genes but upregulates BMP-2 expression ... 61
4.1.3 Limited biochemical conditioning of the culture medium during bioreactor culture ... 62
4.1.4 Cyclic mechanical compression enhances RUNX2 mRNA expression only in a BMP-enriched environment ... 63
4.2 Mechanistic investigations on the crosstalk between mechano-transduction and BMP signaling ... 68
4.2.1 The crosstalk is relevant in primary human cells of the mesenchymal lineage ... 68
4.2.2 Correlation between loading frequency and crosstalk duration ... 69

4.2.3 Focal adhesion number and size is increased by both, BMP-2 and mechanical loading in a frequency-dependent manner ... 72
4.2.4 Cells develop a mechano-memory impinging on BMP signaling ... 74
4.2.5 Mechanical signals regulate the BMP-pathway via integrins ... 76
4.2.6 Actin cytoskeleton remodeling is crucial for the crosstalk ... 78
4.3 The influence of the crosstalk on ECM formation ... 86
4.3.1 Load- induced tissue contraction and stiffening is reduced by BMP-2 ... 86
4.3.2 Mechanical loading increases collagen synthesis but reduces fibrillar collagen density and fiber alignment ... 88
4.3.3 BMP-2 and cyclic compression induce distinct gene expression changes ... 92
4.3.4 ECM protein composition is specifically altered by mechanical loading ... 94
5 Discussion ... 97
5.1 Mimicking mechanical loading conditions during the early phase of bone healing 97
5.2 Towards a deeper understanding how cyclic compression influences osteogenic differentiation ... 98
5.3 Cyclic compression possess an osteoinductive potential only in a BMP-enriched environment ... 99
5.4 Cyclic compression integrates into the BMP signaling pathway only in a ligand dependent manner ... 100
5.5 The mechano-sensitivity of BMP signaling is dependent on the loading frequency and timing ... 101
5.6 Integrin αv and load-induced integrin and F-actin reorganization processes are required for the crosstalk ... 105
5.7 Mechanical forces specifically alter mechanical, structural and compositional matrix cues ... 110
6 Summary and Conclusion ... 117
7 Outlook ... 120
8 Bibliography ... 121
Supplement ... 135
Abbreviations ... 139

List of figures

Figure 1-1: Important phases and factors in bone regeneration. ... 12
Figure 1-2: Mechanical conditions at the fracture site define the route of tissue differentiation and the mode of healing. ... 14
Figure 1-3: Mechanosensation by integrin adhesions ... 17
Figure 1-4: The complexity of integrin signaling ... 18
Figure 1-5: BMP signaling pathway and selected regulatory mechanisms. ... 22
Figure 1-6: Regulation of BMP signaling by mechanotransduction. ... 24
Figure 2-1: Bioreactor setup. ... 30

Figure 2-2: Schematic representation of the ibidi Pump System. 32
Figure 3-1: Analysis of protrusion remodeling. 54
Figure 3-2: Bioreactor-Microscope-Setup. 55
Figure 3-3: Schematic representation of scaffold contraction and calculation of total volume contraction ($V_{(V0-Vt)}$). 56
Figure 4-1: Bioreactor setup validation. 60
Figure 4-2: Cyclic compression downregulates the expression of key osteogenic marker genes but upregulates BMP2 expression. 62
Figure 4-3: Low BMP-2 concentrations in the conditioned medium. 63
Figure 4-4: Cyclic compression only increases RUNX2 expression, if rhBMP2 is added or an enrichment of cell-secreted BMP2 in the cell culture medium was permitted. 65
Figure 4-5: Cyclic compression does not increase RUNX2 expression, if BMP signaling is inhibited by rhNoggin. 67
Figure 4-6: Cyclic mechanical compression significantly increases the BMP-2-induced Smad1/5/8 phosphorylation in human primary MSCs and dermal fibroblasts (hdF) 69
Figure 4-7: Loading frequency influences strength and duration of Smad1/5/8 phosphorylation and ID gene expression. 70
Figure 4-8: Heat map summarizing the gene expression changes in response to 24h BMP-2 stimulation and/or mechanical loading of 1 Hz or 10 Hz. 71
Figure 4-9: Mechanical stimuli regulate gene expression in a frequency dependent manner. 72
Figure 4-10: Focal adhesion number and size is increased by BMP-2 treatment and by mechanical loading in a frequency-dependent manner. 73
Figure 4-11: Mechanical pre-stimulation induced a crosstalk on p-Smad and on gene expression level. 75
Figure 4-12: Only prolonged mechanical pre-stimulation induced a crosstalk on p-Smad level. 76
Figure 4-13 Validation of integrin αv knockdown in hFOBs. 77
Figure 4-14: Integrin αv knockdown reduced the crosstalk on Smad phosphorylation level. 78
Figure 4-15: Cyclic compression induced focal adhesion kinase and myosin light chain activation. 79
Figure 4-16: Effects of Jasplakinolide on actin cytoskeleton integrity and dynamics. 81
Figure 4-17: Dynamic actin remodeling induced by fluid shear stress is inhibited by Jasplakinolide. 83
Figure 4-18: F-actin stabilization by Jasplakinolide inhibits load-induced Smad phosphorylation and ID1 expression. 85
Figure 4-19: Load- induced scaffold contraction and stiffening is reduced by BMP-2 87
Figure 4-20: Cyclic mechanical compression increases collagen synthesis but reduces fibrillar collagen density 89
Figure 4-21: Cyclic compression changes the dependency of collagen density and tissue contraction. 90
Figure 4-22: Cyclic mechanical compression reduces fiber and cell alignment. 92
Figure 4-23: Gene expression analysis of selected ECM proteins and ECM modulators. 92

Figure 4-24: Cyclic compression induced distinct changes in the protein composition of the ECM. 95
Figure 5-1: Cyclic compression promotes osteogenic differentiation via BMP. 100
Figure 5-2: Schematic representation of how mechanical forces integrate into BMP signaling. 109
Figure 5-3: The regulation of collagen cross-linking by periostin. 114
Figure 5-4: Cyclic compression disturbs collagen cross-linking. 114
Figure 0-1 Pubmed search term statistics 135
Figure 0-2: Gene expression changes of TGFβ1, TGFβ3, FGF2, PDGF-A and VEGF-A, growth factors that influence osteogenic differentiation. 135
Figure 0-3: BMP2 stability during bioreactor culture. 136
Figure 0-4: Dynamic actin remodeling induced by cyclic compression and scaffold wall deformation under compression visualized using the Bioreactor-Microscope-Setup. 137
Figure 0-5: Fibrillar collagen density is reduced by cyclic compression after 2 weeks of cultivation. 137
Figure 0-6: Cyclic compression did not induce ERK1/2 or Src phosphorylation. 138

List of tables

Table 2-1: List of bioreactor equipment 31
Table 2-2: List of bioreactor consumables 32
Table 2-3: Consumables for the ibidi Pump System 32
Table 2-4: List of devices 33
Table 2-5: List of chemicals, reagents and kits 33
Table 2-6: Buffer compositions 34
Table 2-7 Material for siRNA transfection and lentiviral transduction 36
Table 2-8: List of growth factors and small molecular inhibitors 37
Table 2-9: Consumables for histology 37
Table 2-10: List of primary and secondary antibodies 38
Table 2-11: List of small molecular dyes used in immunohistochemistry 39
Table 2-12: Consumables and kits for RNA isolation, reverse transcription and pPCR 39
Table 2-13: List of primers for qPCR 39
Table 3-1 Summary of expansion media composition 43
Table 3-2: Volumes used for culture and trypsinization depending on the culture format 43
Table 3-3 Cell concentrations used for different cell types 44
Table 3-4 Plate layout for the transduction efficiency test. 45
Table 3-5 Calculations for seeding of one scaffold (volume = 80 µl) per condition 46
Table 3-6: Summary of experimental conditions 47
Table 3-7: FBS concentration and medium amount inside bioreactors depending on the type of experiment 48
Table 3-8 qPCR reaction steps 50
Table 3-9 General IF staining protocol 52
Table 3-10: Perfusion protocol 57

Table 0-1: Fold change (F.I.) gene expression in response to 24h BMP-2 stimulation and/or mechanical loading of 1 Hz or 10 Hz. 136
Table 0-2: Gene expression analysis of selected ECM proteins and ECM modulators. 138

1 Introduction

1.1 Repair versus regeneration – bone as a model system for tissue regeneration

Regeneration, a process by which the original structure and function of a tissue, organ or even whole body parts are fully restored, is fascinating and motivates the whole field of regenerative medicine. The question why some organisms regenerate while others not is still unanswered but there is a great endeavor to identify common themes of regeneration that if fully understood might revolutionize medical treatment [1]. In order to unravel regenerative processes, model organs and organisms are extensively studied, one of which is bone.

In the adult human body, bone is one of the few tissues that have the ability to fully regain their initial functionality after injury [2]. In other tissues, however, a repair process is initiated, which mainly involves the deposition of fibrous matrix and wound contraction by fibroblasts. The resulting scar tissue closes the wound but possesses, in comparison to the original tissue, different compositional, structural and mechanical properties, impairing the tissues functionality [3], [4]. Future regenerative therapies aim at scar-less healing by resembling endogenous regeneration cascades but therefore, a full understanding of regenerative processes like in bones is needed.

1.2 Bone fracture healing and regeneration

Depending on the size of the fracture gap and the mechanical stability at the fracture site, bone healing can follow two mechanisms, which are termed primary (also referred to direct healing) or secondary healing (also referred to endochondral ossification) [5]. Primary healing, a process in which bone is formed directly without the intermediate step of cartilage formation, requires absolute mechanical stability, a very small fracture gap (< 500 μm) and aerobic conditions [6]. In other instances, bone healing follows a complex multiphase process that is commonly divided into four overlapping phases: inflammatory, soft callus, hard callus and remolding phase [7] (see Figure 1-1). Directly after injury, a hematoma is formed and chemotactic signaling molecules are released attracting immune cells. They in turn secrete pro-inflammatory cytokines such as tumor necrosis factor-α (TNF-α), interleukin-1β (IL-1β) or IL-6 to further attract inflammatory cells [8]. The initial pro-inflammatory phase is gradually transferred into an anti-inflammatory phase characterized by the presence of Fibroblast Growth Factor -2 (FGF-2), Transforming Growth Factor-β (TGF-β), Platelet-Derived Growth Factor (PDGF) and Bone Morphogenetic Proteins (BMPs) [9]. These growth factors are essential for the recruitment, proliferation and differentiation of progenitor cells

[10]. Due to the secretion of chemoattractants and growth factors as well as their ability to remove necrotic tissue, immune cells play an important role in initiating the healing cascade [9]. During the inflammatory phase, the primary hematoma is remodeled into a fibrin-, fibronectin-, but also collagen-rich granulation tissue that serves as a scaffold for the establishment of the cartilaginous soft callus. Importantly, the structural organization of the fibrillar collagen network within the granulation tissue was recently shown to guide the following process of endochondral bone formation [11]. Recruited and proliferated mesenchymal stromal cells (MSCs) differentiate into chondroblasts and synthesize a cartilaginous matrix consisting of collagen II and glycoproteins. All fibrous tissue in the fracture gap will eventually be replaced by cartilage that bridges and stabilizes the fracture [12]. This process is followed by cartilage calcification. Hypertrophic chondrocytes and later osteoblast release membrane-derived-vesicles containing alkaline phosphatases (ALP), calcium phosphate complexes and proteoglycanases [13]. Glycoaminoglycans become degraded, calcium phosphate complexes are integrated into the collagenous matrix and the region will be revascularized. The established hard callus is still consisting of unorganized woven bone that is eventually remodeled into lamellar bone to fully restore the mechanical strength [14].

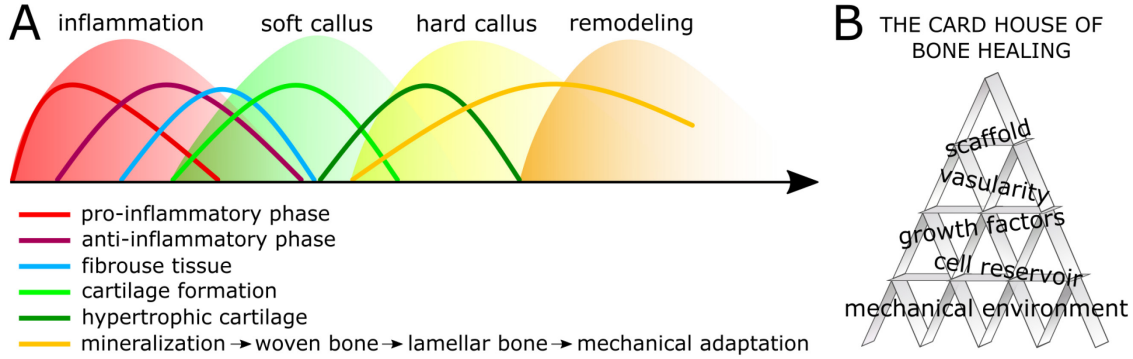

Figure 1-1: Important phases and factors in bone regeneration. (A) Consecutive and overlapping phases of bone regeneration after fracture. Figure adapted from [15] with permission from the publisher. (B) "The card house of bone healing". The authors' interpretation of the diamond concept for bone healing [16]–[18]. *Factors for successful healing are assembled in a card house, relating to the fragility of the process.*

All factors that influence and contribute to fracture repair, which are summarized in the "diamond concept" [16]–[18] (Figure 1-1B), must be tightly controlled in order to allow successful healing. The misbalance of one of the factors due to for example aging or obesity, can lead to delayed healing or non-union formation. Moreover, the natural self-healing capacity of bone is limited by the fracture size. Large bone defects resulting from e.g. tumor resection where large tissue quantities need to be restored, resemble an especially challenging situation [19]. The gold standard for the treatment of large bone defects is still the harvest of autologous material from the iliac crests of the pelvis, or the intramedullary

canal of long bones [20]. However, due to the known disadvantageous like donor site morbidity and limited amount of material [21], alternative treatment strategies are needed, which could include biomaterials, cells or growth factors. In fact, the clinical use of the growth factor BMP-2 has gained increasing importance.

1.2.1 Bone Morphogenetic Proteins - growth factors essential for bone healing

BMPs are one of the major signaling molecules orchestrating bone healing by regulating cellular processes like proliferation [22], migration [23] and differentiation [24]. The family of BMPs consists of 30 different members but not all of them are associated to bone [25]. During the different healing phases, the expression of individual BMP types is tightly regulated. BMP-2, -4 and -7 are highly upregulated in the periosteal region at the early phase of healing [26], whereas BMP-3, -4, -7 and -8 are expressed at later stages of endochondral ossification when the cartilaginous matrix is remodeled and calcified. BMP- 5 and -6 instead are expressed almost throughout the healing cascade [27]. Therefore, some BMP types are potent inducers of differentiation, while others regulate cell maturation. From *in vivo* knockout experiments it is known that specifically BMP-2 is indispensable for the initiation of fracture healing [28].

With the FDA (Food and Drug Administration) approval of recombinant human BMP-2 (rhBMP-2, InFUSE™, Medtronic, USA) for the treatment of tibial non-unions and spinal fusions, the growth factor has gained significant clinical relevance [25], [29]. Recombinant hBMP-2 is used either as an alternative or complementary treatment option for autologous bone grafting. Its administration has reduced the length of hospital stay [30], the rate of secondary interventions and the treatment failure rate [31]. However, still excessive and non-physiological amounts of rhBMP-2 are required (1.5 mg/ml are FDA-approved) to promote bone formation increasing the treatment costs and the risk of side effects like ectopic bone formation and osteoclast-mediated osteolysis [32]. In order to optimize the growth factor treatment, it is necessary to better understand signaling cascades and regulatory mechanisms.

1.2.2 Mechanical forces influence bone healing

Mechanical boundary conditions at the fracture site, mainly determined by the mechanical properties of the fixation device and musculoskeletal loadings, critically influence the course and outcome of bone healing [33]–[35]. Complete stability or excessive movements delay healing or can even cause non-union formation [36], [37]. In case of excessively rigid fixation, the healing bone is protected from normal stresses (stress shielding) resulting in bone-end resorption due to the lack of mechanical communication [38]. However, if the mechanical stability is too low, blood vessels become repeatedly disrupted and the healing cascade

cannot continue [37], [39]. These findings demonstrate, that mechanical conditions have to be adjusted carefully in order to promote healing.

Movements at the fracture site (interfragmentary movements (IFMs)) are differentiated in axial compression of the fracture fragments or relative movements causing shear stress. While the latter is considered to be detrimental, it is widely accepted that a moderate amount of axial compression promotes healing by stimulating callus formation [40]–[43]. *In vivo* animal studies and numerical simulation suggest that IFMs smaller than 15% of the fracture height allow undisturbed healing via endochondral ossification [37], [40], [44], [45]. Using FE modeling and histological data, mechanobiological models have been developed, describing how mechanical conditions define tissue differentiation and consequently the mode of fracture healing (Figure 1-2). According to the model by Claes and Heigele (1999), endochondral ossification occurs for strains less than ±15% and compressive pressure larger than −0.15MPa. However, larger mechanical stimuli result in the formation of connective and fibrous tissues [40].

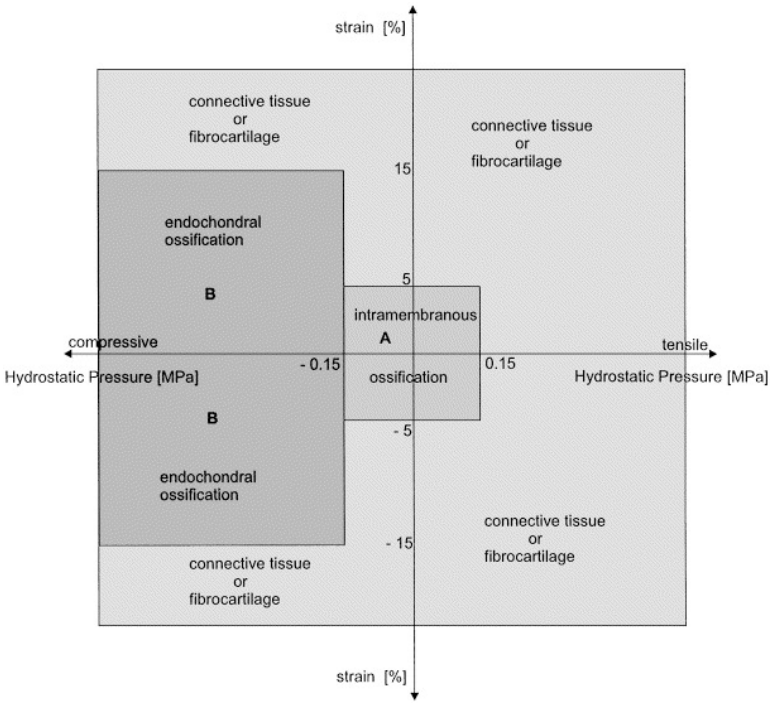

Figure 1-2: Mechanical conditions at the fracture site define the route of tissue differentiation and the mode of healing. Model is based on the correlation between mechanical condition and types of tissues in a fracture callus. Intermembranous ossification takes place in regions which are defined by a surface strain <±5% and a hydrostatic pressure <±0.15 MPa (region A). Endochondral ossification takes place in regions which are defined by surface strains <±15% and negative hydrostatic pressure values greater than −0.15 MPa. Figure taken from [40] *with permission of reuse from the publisher.*

Besides the magnitude of IFMs, the timing is critically important. Moderate movements during the early healing phase contributed to increased bone mineral density and stiffness [43], [46], while increased movements at later stages had contrary effects [46]. From this, the concept of reverse dynamization evolved, in which the fracture fixation stiffness changes from

low to high during the course of healing [47]. When this strategy, the change from flexible to rigid fixation, was applied at 1 week after surgery in a rat osteotomy model, healing was accelerated [48]. In humans, this beneficial effect could be reproduced in a pilot study [49] but further clinical studies are missing until now.

In summary, specifically the early healing phase is highly mechano-sensitive and optimization of biomechanical conditions during this stage has great potential to promote the subsequent healing cascade.

1.2.3 Mechanical forces enhance BMP-2-induced bone healing

Even though, rhBMP-2 is a very potent inducer of bone formation, it is increasingly recognized that the efficiency of rhBMP-2 is controlled by mechanical cues [47], [50]–[54]. The interplay between BMP-2 and mechanical forces was mainly investigated in critical-sized femoral defects in rats but clinical studies are missing so far. In animal experiments, the mechanical environment was tuned by using different fixator stiffnesses or by the active application of axial compression during healing.

Low- stiffness fixation (stiffness of 114 N/mm) accelerated rhBMP-2 induced bone healing in comparison to medium and high stiffness fixation (185 N/mm, 254 N/mm, respectively) [47]. Using the reverse dynamization approach it was found that the effect of BMP-2 can be even further promoted if mechanical loads are high during the early phase but rather low at later stages. Strikingly, given the strong osteoinductive capacity of rhBMP-2, fracture fixation using too low fixator stiffnesses (25.4 N/mm) can be detrimental to healing [50].

Additionally, external mechanical loading (10% axial compression, f = 0.01Hz, applied once a week) under rhBMP-2 treatment significantly enhanced mineralized tissue volume and mineral content at 2 weeks post-operation in comparison to the non-loaded control. In agreement with the study mentioned before, it was found that early mechanical stimulation seems to be beneficial but once a bony bridging is established loading loses its stimulatory capacity. Interestingly, in a critical-sized bone defect, mechanical stimulation alone does not induce bone formation but rather negatively affects callus formation [51].

These findings demonstrate that even if rhBMP-2 is a powerful therapeutic tool, its effectiveness is largely dependent on mechanical boundary conditions. It becomes clear, that certain amounts of mechanical stimulation have the ability to enhance the efficacy of rhBMP-2. This indicates a cooperative interaction of BMP-2 and mechanical forces that can be expected to be true also for endogenously expressed BMP-2. Still further investigations are needed to define optimal timing and magnitude of mechanical loading in combination with rhBMP-2 treatment. Although *in vitro* studies cannot resemble the physiological complexity,

they help to understand concepts of cellular behavior, which can be translated back into *in vivo* situations. Therefore, in this study, the sensitivity of the BMP signaling pathway for loading frequency, duration and timing were investigated on cellular level. These findings might in future help to improve mechanical boundary conditions during healing.

1.3 Sensing, transmitting and responding to mechanical cues

Due to intensive research in the field of cellular biomechanics during the past 20 years (see supplementary Figure 0-1), it is nowadays accepted that physical signals are as important as biochemical cues to control cellular behavior. Cells are not only influenced by external mechanical forces like tension, compression, shear and hydrostatic pressure [55] but also by the mechanical properties of the surrounding extracellular matrix (ECM) like rigidity [56], stress relaxation behavior [57] and topology [58]. Specialized organelles and structures including the primary cilium, ion-channels, G-protein-coupled receptors (GPCRs), cell adhesions sites, the cytoskeleton and also the nucleus perceive and transduce mechanical stimuli [59]. Given that a variety of different physical stimuli act simultaneously on the cell, it is likely that many of these sensors contribute to define cell behavior.

1.3.1 Integrin-mediated adhesions

Integrins are one of the most important mechanotransducers. They not only provide a molecular link between the ECM and the actin cytoskeleton but also mediate the conversion of physical into biochemical signals via cytoplasmic adaptor proteins [60]. Integrins form non-covalently linked heterodimeric complexes of α and β subunits, each of which is a single-spanning type I transmembrane protein with an extracellular ligand binding site, a transmembrane domain and a short cytoplasmic tail. From a combination of 18 α-subunits and 8 β-subunits, 24 different integrin subtypes are formed that specifically recognize ECM ligands such as fibronectin, collagen or laminin [61] (Figure 1-3A). Due to their ligand specificity, integrin expression patterns dependent on the composition of the ECM and are tissue-specific. Importantly, each integrin type triggers different combinations of downstream signaling pathways, which differentially affect cellular behavior [62]. Integrins are usually in their low affinity (bent-V shape) conformation. Unfolding into the high affinity (active) conformation is triggered either upon binding to the specific ECM ligand (outside-in activation) or upon binding of Talin to the cytoplasmic tail of the β-subunit (inside-out activation).

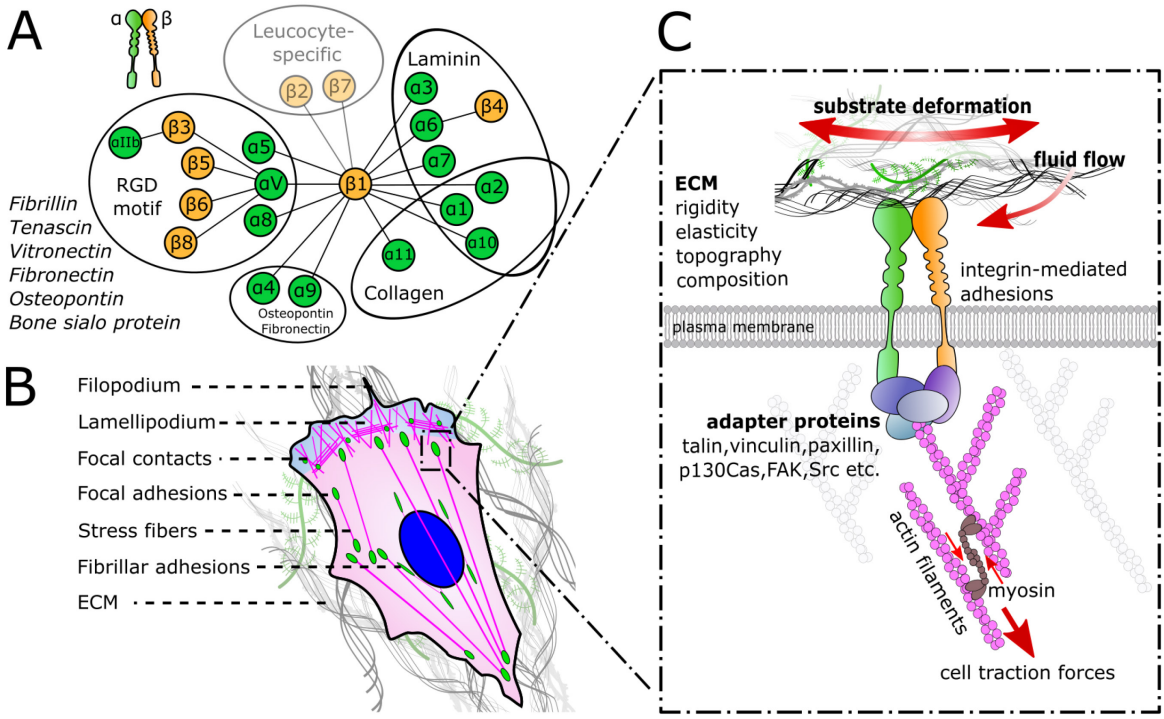

Figure 1-3: Mechanosensation by integrin adhesions. (A) Integrin subunits α and β form heterodimers, which specifically recognize ECM proteins or motifs (Arg-Gly-Asp (RGD)). (B) Illustration of an adherent, migrating cell containing diverse integrin-mediated adhesions. Focal complexes (FC) form within the lamellipodium and eventually mature to focal adhesions (FA), which are connected to thick actin stress fibers. Some FA transition into fibrillar adhesions, which are important for the remodeling of fibronectin. (C) Schematic drawing showing the principle structure of integrin-mediated adhesions. Integrin heterodimers bound to the ECM are connected via adapter proteins to the actin cytoskeleton allowing a bidirectional force transmission. Figure information taken from [63]–[65]

Integrin activation is followed by the recruitment of numerous adaptor proteins, by the assembly of actin filaments and the clustering to other integrins. Early adhesions formed within the lamellipodia or filopodia of motile cells are termed focal complexes (FC) or nascent adhesions (NA) (Figure 1-3B). As the leading edge is pushed forward by actin polymerization, the lamellipodium moves over the stationary NA. Within the lamella, most of the NA disassemble, whereas some eventually undergo a force dependent growth and maturation into focal adhesions (FA) [66]. FA are much larger, elongated and coupled to thick actin filaments cross-linked by α-actinin and myosin II (actin stress fibers). Myosin II, a motor protein, generates the tension that is necessary for FA assembly and stability [67], [68]. The contractile forces exerted by the actomyosin-network (cell traction force) are transmitted towards the ECM via FAs (Figure 1-3C). Mature FAs can transition into fibrillar adhesions, a specialized type of integrin-mediated adhesion, essential for the remodeling of fibronectin that contain tensin instead of talin [69].

1.3.2 Integrin-mediated mechanotransduction

Upon force-dependent FA maturation various adaptor proteins are recruited, which either reinforce the connection to actin filaments or mediate downstream signaling. The integrin adhesome within FAs can consist of 180 different proteins with approx. 700 interactions demonstrating the complexity of mechanotransduction [70], [71]. The conversion of mechanical into biochemical signals is mediated inter alia via the recruitment and activation of kinases such as focal adhesion kinase (FAK) and proto-oncogene tyrosine-protein kinase (Src) (see Figure 1-4). FAK is upstream of many pathways ultimately controlling cell motility, proliferation and survival. In the context of this work, it is important to note that FAK was shown to control adhesion stability and the activity of Rho-familiy GTPase, thereby taking part in the regulation of actin cytoskeletal dynamics. Autophosphorylation of FAK at Tyr397 leads to binding of Src, which in turn phosphorylates other tyrosine residues in FAK promoting its activity. The FAK-Src complex mediates the phosphorylation of p130Cas that in turn activates Rac1 leading to enhanced lamellipodia formation [72], [73]. Additionally, this complex phosphorylates paxillin resulting in increased focal adhesion turnover [74].

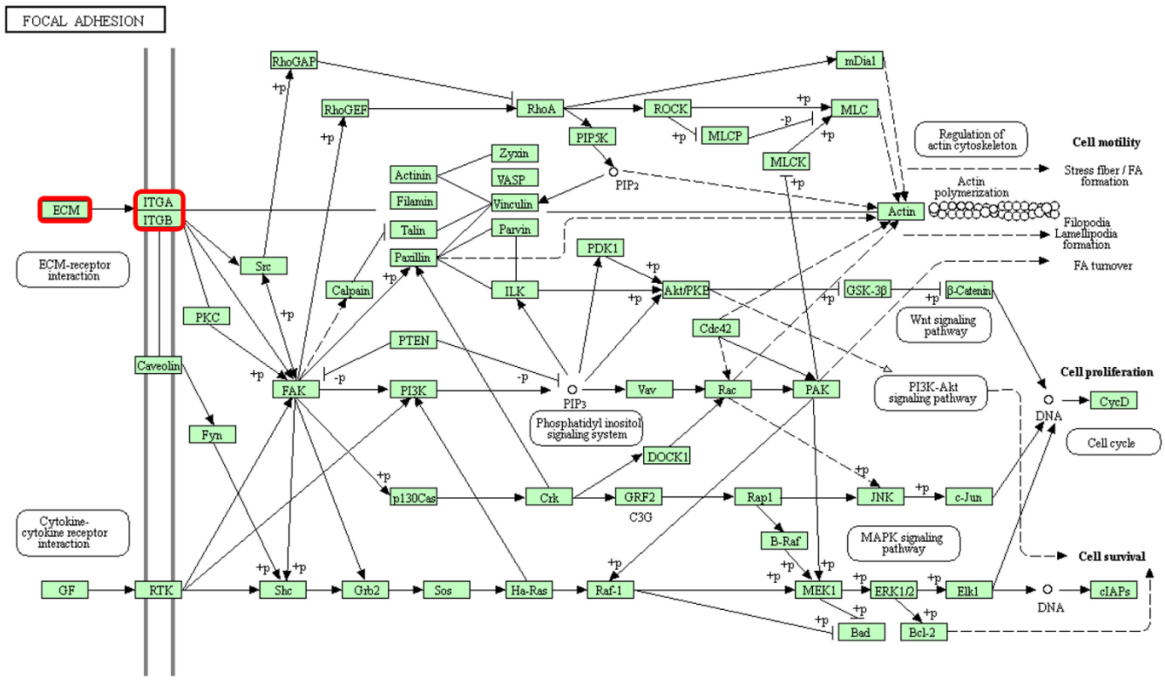

Figure 1-4: The complexity of integrin signaling. Pathway map showing integrin-mediated downstream signaling with consequences for cell motility, proliferation and survival. Map taken from KEGG (Kyoto Encyclopedia of Genes and Genomes) database with permission from Kanehisa Laboratories [75]–[77].

Integrin signaling-mediated remolding of FAs and the actin cytoskeleton is crucial for the adaptation to mechanical stimuli. Upon mechanical tension, cell traction forces increase through a cascade that involves RhoA/ROCK and the subsequent activation of myosin II [78]. Cyclic stretch and fluid flow trigger the reorientation of cells along with actin stress fiber realignment, which is further more regulated by FAK and Rho-kinases. Interestingly, stress

fibers oriented in the direction of stretch disassemble and reassemble in perpendicular direction, which is accompanied by FA reorientation [79], [80]. Additionally, FAK-mediated Rac1 activation induces the formation of lamellipodia upon tensile strain [81]. Mechanical forces not only induce cytoskeletal remodeling through kinase activation but also triggers the reorganization of protein interactions within the adhesom of FAs [82].

Whereas forces like fluid shear stress or compression are actively transmitted through FAs, rigidity is a passive mechanical parameter whose sensation requires active probing of the substrate. To deform the ECM, cells apply traction forces generated by the actomyosin cytoskeleton and transmitted through integrins. The generated traction force is thereby adapted to the ECM rigidity through a feedback mechanism. On stiff versus soft matrices, stress fiber assembly and cytoskeletal contractility is increased through the RhoA pathway [83].

In summary, integrin-based adhesions are important for the sensation, transduction and response to changes in the mechanical environment. As an immediate response, cells adapt by remodeling their cytoskeletal organization and adhesion sites to establish a new force equilibrium. On the long-term, this will have consequences for gene expression affecting proliferation, matrix production and differentiation.

1.3.3 Mechanical forces influence cell fate decisions

Since Engler *et al.* (2006) reported that MSCs can be directed into the neurogenic, myogenic and osteogenic lineage by plating them on matrices mimicking the tissue-specific stiffness of brain, muscle and collagenous bone, respectively, mechanical cues have gained increasing attention [56]. To date it is accepted that the physical environment, which is defined by the mechanical properties of the substrate as well as the type, frequency and magnitude of mechanical loading, affects stem cell differentiation. In the following, the response of stem cells, specifically MSCs, to external mechanical forces is summarized.

MSCs, adult progenitor cells residing in different mesodermal tissues such as bone marrow and fat, are often used to study the influence of physical cues in the context of regeneration, as they are actively recruited to the site of injury where they are subjected to increased tissue deformation [84], [85]. A wide range of experimental setups have been used to stimulate MSCs with mechanical forces *in vitro*. They can be generally categorized by the type of mechanical loading including tension, compression, fluid shear stress, ultrasound and vibration. These different modes of stimulations can be applied to cells cultured in tissue culture plates or in bioreactors in 2D or 3D. Despite this, many different experimental parameters influence the cell response, for example, scaffold properties (type of matrix, stiffness), biochemical medium supplements, donor age, cell density, and of course different

loading parameters (duration, magnitude, and frequency). As cell responses can be distinctly different depending on the culture dimension [86], a direct comparison of 2D and 3D results is often difficult. Therefore, here only studies investigating the influence of compressive force applied to MSCs seeded in a 3D biomaterial are summarized.

Depending on the scaffold material, loading parameters and -very importantly- medium supplements used, cyclic biomaterial deformation was reported to induce/enhance osteogenic or chondrogenic differentiation of MSCs. Interestingly, studies in which MSCs were cultured under chondrogenic or osteogenic medium found an enhanced chondrogenic [87]–[89] or osteogenic [90]–[92] differentiation under cyclic compression, respectively. However, if adipogenic medium was added, mechanical stimulation suppressed adipogenesis of MSCs [93]. Therefore, cyclic compression promoted the differentiation towards the osteo-chondral lineage predefined by the medium supplements. These investigations yet don't show whether mechanical stimulation directly induces osteo-chondral differentiation or just promotes the biochemical trigger.

Only a few studies used basal medium to investigate the direct impact of loading on MSC commitment. Michalopoulos *et al.* (2012) reported that cyclic compression of collagen-alginate sponges (f = 1 Hz, 4h/day, 21 days) induced osteogenic or chondrogenic differentiation of MSCs in a magnitude dependent manner. While 10% compression induces the expression of Runt-related transcription factor 2 (RUNX2), an early osteogenic transcription factor, 15% compression enhanced the expression of chondrogenic markers Sox 9 (SRY (sex determining region Y)-box 9) and aggrecan [94]. Furthermore, low magnitude compression of MSC seeded PCL/PLGA/TCP scaffolds increased Runx2 protein levels and the expression of other important osteogenic markers as osterix (OSX), ALP and osteopontin (OPN) [95]. Moreover and in addition to the classical osteogenic markers, mechanical loading was reported to induce the expression of the growth factor BMP-2 in MSCs [96], [97]. The fact that BMP signaling regulates the transcription of RUNX2 through the Smad pathway [98], points towards an involvement of BMP signaling in load-induced osteogenic differentiation.

However, if the observed pro-osteogenic effects of cyclic compression on MSCs are a direct consequence of mechano-regulated gene expression, or an indirect consequence of load-induced autocrine or paracrine signaling (e.g. via secretion and signaling of BMP2) remains an open question. This study aims to address this question by dissecting the direct mechanical influence from a mix influence of mechanics and BMP-2.

1.4 BMP signaling pathway

The BMP family belongs to the Transforming Growth Factor (TGFβ) superfamily of cytokines that fulfill functions in tissue development, homeostasis and healing but also disease [99].

Even though originally described as bone growth factors [100], BMPs regulate processes in many different tissues including cartilage [101], muscle [102], tendon [94], heart [104], vessles [105] and the neuronal system [106]. On the cellular level they control proliferation, migration, differentiation and apoptosis [107], [108].

After posttranslational processing, secretion and dimerization (homo- and heterodimers exist), BMPs can bind to hetero-tetrameric receptor complexes consisting of two type I and two type II transmembrane receptors. Both BMP receptor types feature an extracellular ligand-binding motif and an intracellular serine/threonine kinase domain. While type II receptors are constitutively active, type I receptors carry an additional glycine/serine-rich region (GS-box) that controls the kinase activity. Upon ligand binding, this region becomes phosphorylated by the type II receptor, leading to the activation of the type I kinase, which in turn activates Smad or non-Smad signaling pathways [109], [110]. The mode of ligand-receptor oligomerization defines the way of signal propagation. The canonical Smad pathway is activated when BMPs bind to preformed complexes (PFCs) of type I and II receptors. BMPs can furthermore bind to single type I receptors, forming a so-called BMP-induced signaling complex (BISC) to which type II receptors are recruited activating the non-Smad pathway [111].

The canonical Smad pathway is activated by C-terminal phosphorylation of recruited receptor-regulated Smads (R-Smads) by BMP receptor type I and subsequent complex formation with the common mediator Smad4. The trimeric transcription factor complex composed of two phosphorylated R-Smads and one Smad4 molecule, translocates into the nucleus and binds to elements in the promotor regions of BMP target genes to control their expression [112], [113]. Downstream target genes controlled by the Smad pathway are inter alia the family of Inhibitor of DNA binding (ID)-genes as one of the earliest [114], but also the osteogenic transcription factor RUNX2 [98].

Non-Smad pathways include a diversity of other downstream effectors like mitogen activated protein kinases (MAPK), such as p38 and ERK, which induce transcriptional responses by the activation of ATF2, c-Jun or c-Fos and further control the expression of osteopontin, ALP or collagen type 1 [115]. In addition, BMPs can induce immediate non-transcriptional responses like actin rearrangement and migration via phosphatidylinositol 3-kinase, small RhoGTPases and LIM kinases [107], [116].

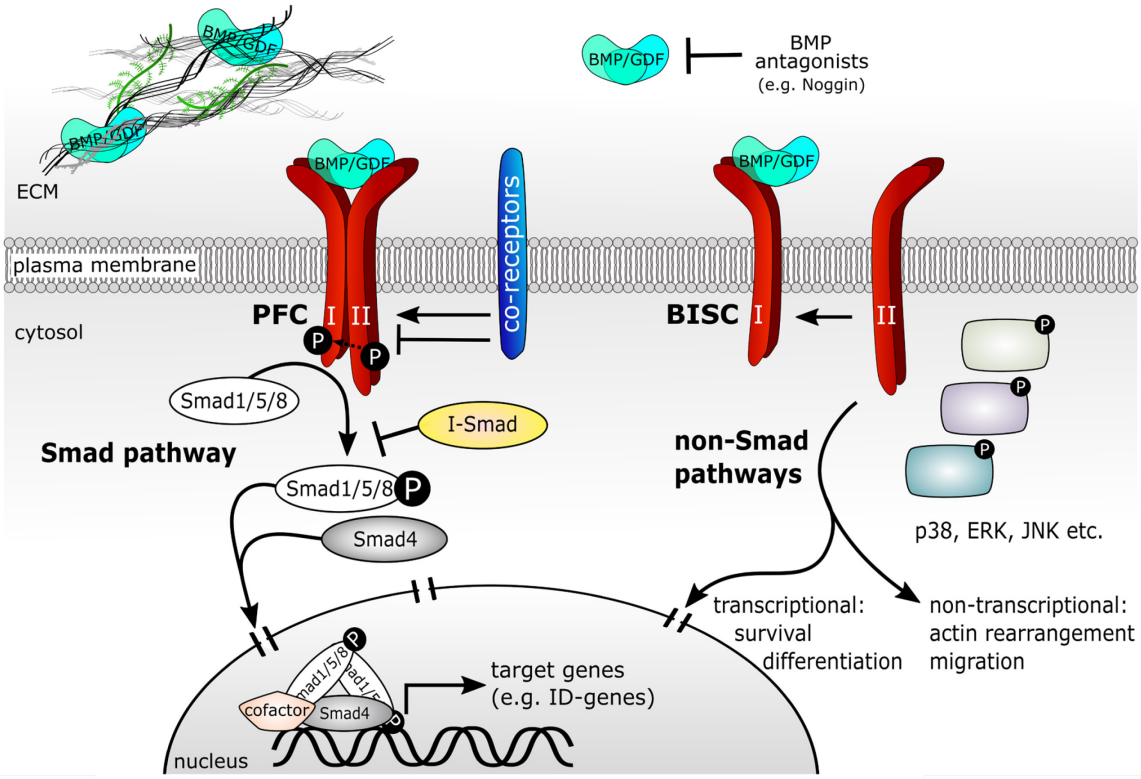

Figure 1-5: BMP signaling pathway and selected regulatory mechanisms. The dimeric ligand binds to its BMP receptor complex, which becomes activated. Subsequently, Smad1/5/8 transcription factors are phosphorylated, form a trimeric complex with Smad 4 and translocate into the nucleus. Together with transcriptional cofactors, they control the transcription of multiple target genes. Non-Smad pathways include a diversity of downstream effectors like MAPKs such as p38, ERK, JNK and others. Their activation leads to transcriptional and non-transcriptional responses. BMP signaling is controlled via multiple factors including the ECM, BMP antagonists, co-receptors and inhibitory Smads (I-Smads). Figure inspired by [111], [117].

The pleiotropic signaling responses upon pathway activation are based on the diversity of BMP ligands, of BMP receptors (4 type I and 4 type II receptors are known) [110] with different ligand-binding affinities, the tissue specific expression of receptors [118] and the modes of ligand-receptor oligomerization. To ensure context-specific and precise signal propagation, pathway activation and inactivation must be under tight control. This is realized by a large number of regulation systems on different levels. At the ligand level, secreted antagonists (e.g. Noggin, Chordin, Gremlin) inhibit signaling by binding BMPs and masking the receptor-binding epitope [119]. Furthermore, ECM proteins such as fibrillin bind and sequester BMPs in their inactive from [120]. At the receptor level, multiple co-receptors attenuate or enhance signaling activity. Intracellularly, inhibitory Smad 6 and 7 (I-Smads) compete for receptor binding [121] and MAPK and GSK3β-mediated R-Smad linker phosphorylation targeting R-Smads for proteasome-dependent degradation [122].

These regulatory mechanisms enhance or attenuate signaling and are crucial for physiological tissue function. However, in recent years it became more and more clear, that also the mechanical environment adds to these regulatory mechanisms.

1.5 Mechanical signals integrate into the BMP pathway

Several *in vitro* studies described a direct regulation of the BMP signaling pathway by mechanotransduction [96], [123]–[126]. Mechanical loading was described to activate Smad signaling in both a ligand dependent and independent manner. In osteoblasts this relation was discussed somewhat controversial. Some studies reported that loading alone was sufficient to activate R-Smads [123], [127], while others described a ligand dependent activation [96], [125]. These contradictory results might be explained by the experimental design that included a pre-cultivation on the biomaterial up to one week prior to loading versus a direct load application. In the case of pre-cultivation an autocrine ligand secretion could have led to the activation of the BMP pathway. Indeed, this assumption was supported by Wang *et al.* (2010) who reported that Noggin treatment abolished the load-induced BMP pathway activation [96].

A study performed by Kopf *et al.* (2012) sets the basis for the work presented here. They showed a ligand-dependent force-specific activation of R-Smads in human fetal osteoblast. Under BMP-2 stimulation and concurrent mechanical loading (f=1Hz, 10%), the phosphorylation of Smad1/5/8 was increased in intensity and duration in comparison to the BMP-2-only treated control. As the positive regulation was visible already after 15 min of stimulation, it was suggested that mechanotransduction events integrate into the BMP pathway already at the receptor level.

Moreover, the alterations on Smad-level were transmitted into transcriptional responses, as the expression of direct BMP target genes (ID1, ID2) as well as BMP ligands (BMP-2, -6) and the antagonist Noggin were regulated by mechanical stimulation. Mechanical loading alone was not sufficient to activate R-Smads, but components of the non-Smad pathway were induced ligand-independently. A strong induction of Akt, p38 and Erk1/2 phosphorylation after 15 min could be detected in response to loading, but no further enhancement under concurrent BMP-2 stimulation was observed [125].

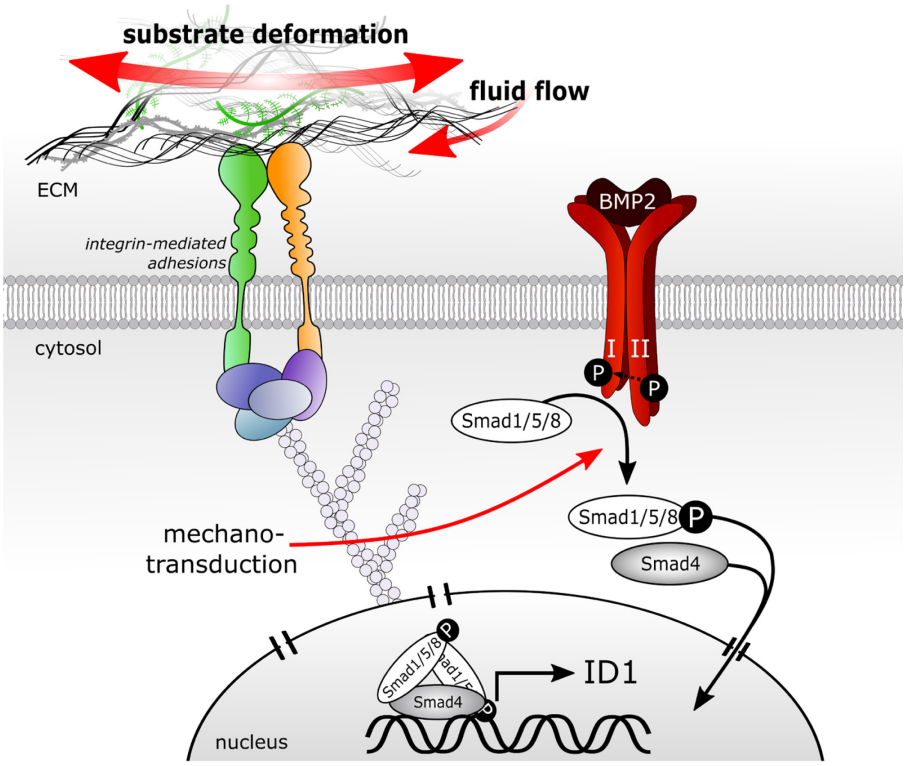

Figure 1-6: Regulation of BMP signaling by mechanotransduction. Mechanical forces like substrate deformation and fluid flow trigger mechanotransduction events, which enhance Smad1/5/8 phosphorylation and consequently BMP target gene expression. The exact mechanotransduction pathway feeding into the BMP pathway is unknown.

Even though the crosstalk between mechanotransduction and BMP signaling was described in several studies, the underlying mechanism is still not understood (Figure 1-6). Wang *et al.* (2010) attributed the regulation of BMP signaling by mechanical forces to the load-induces downregulation of Smurf1 expression, which mediates the protein degradation of Smads [96]. Others suggest an involvement of integrins and/or integrin mediated signaling, which is described in more detail in the following section [128], [129].

1.5.1 Integrin-BMP receptor crosstalk

Influence of integrins on basal BMP signaling

Different integrin subtypes have been found to co-localize with type I and II BMP receptors but contradicting statements were made concerning the influence of their association on BMP signaling.

Positive regulation of basal BMP signaling by integrins was described in human osteoblasts and osteosarcoma cells. In those cells, both BMP-receptor type I and II were found to co-localize with αv and β1 containing integrins [130]. Treatment with function-blocking αvβ, α1 and α2 antibodies reduced BMP-2-induced Smad transcriptional activity causing reduced ALP, osteocalcin, osteopontin and bone sialo protein mRNA levels, thereby leading to a reduction in osteogenic differentiation [130], [131]. Since blocking antibodies did not affect the BMP receptor- integrin co-localization, it is suggested that integrin signaling rather

than the physical interaction is responsible for the positive regulation [130]. In a recent study, genomic deletion of β1 integrins in osteoblasts also caused a reduction in BMP-2-induced expression of osteogenic marker genes like RUNX2, ALP, OCN and OSX [132].

However, other studies reported inhibiting effects of BMP receptor- integrin interaction on BMP signaling. In MC3T3, CHO cells, primary osteoblasts and bone marrow derived MSCs, BMP receptor type IA (BMPRIA) associated with integrin α1β1 shown by immunostainings and immunoprecipitation. The site of integrin binding was identified the same as for BMP-2-receptor binding [133] and knockdown of α1 integrin in CHO cells increased the level of Smad phosphorylation. Together this led to the suggestion that α1 integrin and BMP-2 competitively associate with the BMPRIA receptor [134]. In neuronal stem cells, β1 integrins interact with BMPRIA and IB and negatively influence the BMP- mediated astrocytic differentiation, while a loss of β1 integrins result in an enhanced differentiation [135].

The role of integrins for the mechanoregulation of BMP signaling

Integrin activation, clustering and signaling is influenced by extracellular substrate composition and stiffness as well as external mechanical stimuli like fluid flow or cell straining. The effect of substrate stiffness or fluid flow on BMP signaling events have been previously implicated with the interaction of BMP receptors and mechano-responsive integrins.

A study comparing the influence of soft versus stiff polyacrylamide gels (elastic moduli: $E_{\text{soft}} \sim$ 0.1–1k Pa and $E_{\text{stiff}} \sim$ 50–100 kPa) on bone marrow MSCs differentiation provided evidence for an integrin regulated trafficking of the BMP receptor. Cells on soft substrates did not spread and displayed reduced surface levels of β1 integrins due to increased caveolae-mediated internalization. Furthermore, on soft gels, BMP signaling was repressed indicted by a strong reduction in Smad phosphorylation in comparison to stiff gels. Due to the observed co-localization of BMPRIA and β1 integrins in intracellular vesicles, it was suggested that β1 integrins promote caveolae-mediated internalization of BMPRIA causing the decrease in Smad phosphorylation and promoted neuronal differentiation of MSCs on soft gels [136].

Interestingly, covalent incorporation of BMP-2 into soft substrates could override the influence of substrate elasticity on cell spreading. Via β3 integrins, C2C12 cells were able to spread and organizes their cytoskeleton as they would on stiff substrates. In addition, BMP-2-induced Smad signaling was found to be dependent on the inhibitory effect of β3 integrin signaling on glycogen synthase kinase 3 (GSK3) activity. This mechanism requires the activation of the downstream integrin signaling pathway Cdc42-Src-FAK-ILK [129], with ILK previously shown to negatively regulate GSK3 via phosphorylation [137].

One study also related the regulation of the BMP signaling cascade by fluid flow to the interaction of BMP receptors and integrins. In vascular endothelial cells, disturbed flow with

oscillatory shear stress (OSS) induces the ligand independent phosphorylation of Smad1/5 and activation of the BMP signaling cascade, which was proposed to be pro-atherogenic. The activation of Smad1/5 by OSS was attributed to the activation of the Shc/FAK/ERK pathway following the interaction of αvβ3 integrins and BMPRIB. This association was interestingly found to be mediated by the cytoplasmic kinase domain of BMPRII. Phosphorylated Smad1/5 in turn activated Runx2, mammalian target of rapamycin (mTOR) and p70S6 kinase signaling leading to increased proliferation of endothelial cells [128].

Even though the mechanism of fluid flow-induced Smad phosphorylation was proposed for vascular endothelial cells in an atherosclerosis model, it still remains to be elucidated in the context of bone healing, where different cell types and mechanical stimuli are relevant. This thesis aims to contribute to an enhanced understanding of how mechanical signals integrate into the BMP pathway in the context of bone by investigating the role of intergins and load-induced focal adhesion and actin cytoskeleton remodeling processes in human fetal osteoblasts.

1.6 Mechanical forces and BMP-2 influence ECM formation

Mechanical properties, structure and composition of the ECM influences how external mechanical forces are transmitted to the cell, how BMPs are recognized and in the end, how cells respond in terms of proliferation, migration and differentiation. Vice versa, it will be described in this section that external mechanical forces and BMP change the mechanical properties and composition of the ECM by regulating the expression of ECM proteins and remodeling enzymes. To understand these regulations, at first the composition and formation of the extracellular matrix will be explained.

A small excursion into the extracellular space: Although the ECM composition is highly tissue- specific, fundamentally it is composed of two main classes of molecules: fibrous proteins and proteoglycans, which are further divided into subgroups. The main fibrous proteins are collagens, elastins, fibronectins and laminins. Proteoglycan such as decorin, aggrecan or perlecan, are composite molecules consisting of a core protein, which is covalently linked to glycosaminoglycan (GAG) polysaccharide chains. Due to their hydrophilic character, proteoglycans hydrate the ECM and serve as ion storages [138].

The ECMs` mechanical properties are greatly defined by the amount and structural organization of collagens. Collagens are summarized in a family of 28 members that all feature triple helical motifs within their structure. Based on their supramolecular assembly, collagens can be further subdivided into fibril-forming, fibril-associated and network-forming collagens. Fibrillar collagens (type I, II, III, V and XI) assemble into higher ordered, long, cable-

like fibers, which mostly consists of not only one collagen type (heterotypic fibrils) [139]. The formation of fibrils is a complex processes starting with the assembly of the triple helix after numerous posttranslational modifications of the synthesized single proα-chain. The triple helix is secreted into the extracellular space where the propeptides at each end of the triple helix are cleaved enzymatically. The resulting tropocollagens self-assemble into staggered collagen fibrils, a process which is regulated by cell-adhesions like integrins and ECM proteins such as fibronectin and other collagens. Lysyl oxidases (LOX) covalently crosslink the tropocollagens, stabilizing the fibril and strengthening its mechanical properties [140]. Non-fibrillar collagens associate to and interconnect fibers and also serve as binding partners for proteoglycans [139].

Especially during regeneration processes, but also for tissue maintenance, ECM remodeling is essential. Dysregulation of ECM remodeling, however, can be the cause of many different diseases such as cancer, fibrosis or arthritis. Matrix degradation is mostly mediated by matrix metalloproteinase (MMPs), zinc-dependent endopeptidases that cleave both matrix and non-matrix proteins with different specificities and efficacies. Their proteolytic activity is controlled by tissue inhibitors of metalloproteinases (TIMPs) [141].

The interplay between matrix protein synthesis and degradation must be tightly orchestrated and mechanical forces and BMP take part in this regulation.

Tension applied to fibroblasts on 2D substrates or embedded in gels induced the expression of collagen type I and fibronectin [142]. Compression or relaxation, however, reduced the ECM production but increased the secretion of collagenases [143]–[145]. On the other hand, cyclic compression of open porous collagen scaffolds was shown to enhance procollagen-I and fibronectin secretion, but also collagen degrading MMP1, pointing towards and increased remodeling of the established ECM [146]. In tissue engineering approaches, mechanical stimulation have been employed to enhance the mechanical properties of the construct. Especially in the context of cartilage regeneration, cyclic mechanical compression was shown to induce collagen II and aggrecan deposition of chondrocytes [147], [148].

Interestingly, also BMP-2 has been shown to stimulate the secretion of cartilaginous matrix like collagen II, aggrecan and other proteoglycans but also matrix degrading enzymes in chondrocytes [149], [150]. As a potent osteoinducer it is not surprising that MSCs and osteoblasts increase their expression of bone ECM including osteocalcin, osteopontin, bone sialo protein and collagen I upon BMP-2 treatment in a dose-dependent manner [151]–[153]. The response of fibroblasts to BMP-2 was less studied, and if, rather in the context of scar formation. Scar tissue derived fibroblasts stimulated with BMP-2 showed an enhanced

deposition of collagen I, suggesting a role of BMP-2 in the formation of hypertrophic scars [154].

During bone healing, extracellular matrix formation is initiated directly with the end of the pro-inflammatory phase [15] and the early structural organization of collagen fibers within the fracture gap was shown to critically influence healing [11]. Given the importance of early ECM formation processes and the fact that both BMP-2 [149], [155] and mechanical forces [142]–[146] were independently described to influence such processes, it is even more important to study how ECM formation is influenced by their mutual interaction. As those mutual interactions might change individual effects, in this study the individual and mutual influences of cyclic mechanical loading and BMP-2 stimulation on ECM formation were compared. Since mechanical forces have already been shown to promote BMP signaling, it was hypothesized here that these effects are transduced to the ECM-level, meaning that cyclic loading is expected to increase the effect of BMP-2 stimulation on ECM formation.

1.7 Motivation and Aims

Even though bone is one of the few tissues in the human body that possess a great regeneration potential, its natural self-healing capacity faces limitations resulting in delayed healing or non-unions [2]. In such cases, BMP-2 is an established clinical treatment, which is applied instead of, or in combination with autologous bone grafting [32]. However, the high treatment costs and potential severe side effects due to supra-physiological concentrations used, motivate further research on how to optimize its application. Interestingly, *in vivo* experiments provide evidence that mechanical forces promote BMP-2-induced bone defect healing [51] and *in vitro* studies report about a potentiation of BMP signaling by mechanical stimuli [123], [125], [127], [128], [156]. Fine-tuned mechanical stimuli, either resulting from extrinsic loading or featured by advanced biomaterials, could in future improve the growth factor application by increasing its efficiency. However, to employ the power of the mechano-biochemical interaction, a deeper understanding how both stimuli control cell behavior independently and in combination is needed.

Therefore, this dissertation aims for an enhanced understanding of the molecular mechanisms mediating the described mechano-regulation of the BMP signaling and the role of the mutual interaction of mechanical signals and BMP-2 in controlling cell fate decision and ECM formation.

To accomplish this, the first objective was to dissect the direct effect of mechanical forces on osteo-differentiation of hMSCs from a mutual influence of mechanics and BMP. The underlying hypothesis was that mechanical stimulation would directly induce osteogenic

differentiation of hMSCs independent of BMP-2. To analyze the pure loading effect, experiments were conducted under diminished autocrine signaling, under BMP-2 supplementation as well as under the specific exclusion of BMP from the system.

After investigating the individual and mutual influences of BMP-2 and mechanical forces for osteogenic differentiation, the second step was to gain a deeper molecular understanding of how mechanical signals integrate into the BMP signaling pathway. The basis for further molecular investigations was set by a precise characterization of how mechanical parameters influence the signaling dynamics. Thereafter, the hypothesis was tested if mechanical forces integrate into the BMP pathway via integrin-mediated mechanosensation and the resulting actin cytoskeletal adaptation. For this, first focal adhesion and actin reorganization in response to mechanical loading and BMP stimulation were investigated and second, integrin expression and actin remodeling dynamics were manipulated.

Besides the known osteoinductive properties of BMP-2, evidences point towards an additional role in regulating tissue formation [149], [155], a process induced early during bone healing [15]. Since the early ECM is believed to influence subsequent healing processes, in a third step, the influence of mechanical loading and BMP-2 stimulation on early ECM formation processes was studied. It was hypothesized that mechanical stimulation would foster the growth factors` effects on ECM formation by enhancing BMP signaling. As collagens greatly define ECM structure and its mechanical properties [140], which vice versa influence cell behavior [56], [157], a particular focus was laid on collagen formation, as well as microtissue structuring and stiffening.

In summary, the findings reported in this dissertation aim to contribute to a deeper understanding how mechanical forces regulate osteogenic differentiation, BMP signaling and early tissue formation processes, thereby influencing bone regeneration. In a long-term perspective, the knowledge gained here about mechano-regulated cellular processes in the context of BMP-2 signaling might help to better employ the power of mechanical forces in critical bone healing scenarios.

2 Materials

2.1 Optimaix collagen scaffold

Marcoporous collagen scaffolds fabricated from purified porcine collagen suspensions using a directional freeze and freeze drying method [158] were provided by Matricel GmbH (Kaiserstraße 100, 52134 Herzogenrath, Germany). The collagen sponges are characterized by an aligned channel-like open-porous architecture providing optimal oxygen and nutrient supply. In its wetted state, the biomaterial exhibits a purely elastic behavior under repeated compression up to 20% of the scaffold height, therefore suitable for cyclic mechanical stimulations. In this study, scaffolds with collagen contents of 1.1 and 1.5 wt-% were used, which differ in their elastic moduli, while biomaterial architecture is not affected. Collagen scaffold were delivered dry, sterile and in a bulk material size of 30x40x3mm. Opened packages were stored in sterile containers at 4°C for further use.

2.2 Bioreactor used for mechanical stimulation

A custom-made mechano-bioreactor system, previously described by Petersen *et al.* (2012) was used to apply cyclic monoaxial compression to cell-seeded collagen scaffolds. The system was designed to mimic the mechanical environment in the hematoma during the early phase of fracture healing. The bioreactor can be separated in two compartments, the cell culture unit and the mechanical unit. The cell culture unit can be assembled under sterile conditions and consists of a reactor chamber, a medium reservoir allowing gas exchange and a micro pump (pump rate approx. 2.5 ml/min). The bioreactor chamber can be equipped with different scaffold-holders made from silicone, which offer space for up to 5 scaffolds with a diameter of 5 mm.

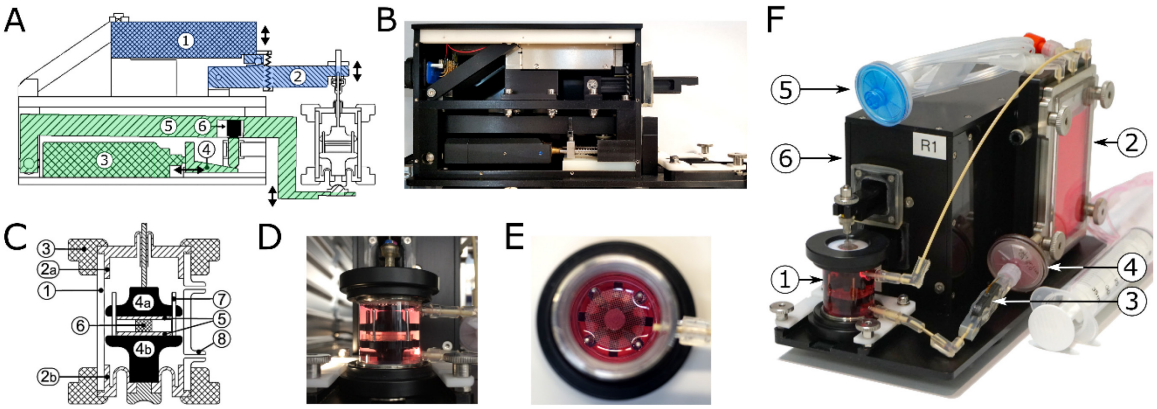

Figure 2-1: Bioreactor setup. Schematic view of the mechanical unit in cross-section (A), showing piezo actuator (1), cantilever for displacement amplification (2), linear actuator (3), wedge for translation to vertical movement (4), lower arm (5), and force sensor (6). Arrows indicate movement direction. Picture into the opened mechanical unit (B). Schematic view of the bioreactor chamber in cross-section (C), with glass housing (1), upper (2a) and lower (2b)

silicone sealings, threaded rings (3), upper (4a) and lower (4b) plunger, polyether ether ketone meshes (5), specimen (6), and centering pins (7). Picture of the bioreactor chamber with collagen scaffold inserted (D). View inside the chamber showing the position of the scaffold (E). Fully assembled bioreactor consisting of bioreactor chamber (1), medium reservoir (2), micropump (3), 5µm filter (4), pressure equalization tube (5) and mechanical unit (6). Schematic representations (A and C) were adapted from Petersen et al. 2012 [159].

The mechanical unit allows the application of defined loading patterns and the online-measurement of the force acting on the sample. It contains two electro-mechanical devices, a linear actuator and a piezo actuator for sample positioning and dynamic mechanical stimulation, respectively. The horizontal motion of the linear actuator is translated into vertical movement by a wedge, which slides underneath a bolt. The bolt deflects the lower bioreactor arm leading to a movement of the lower plunger in the bioreactor chamber. Inside the lower arm, a force sensor is mounted, which detects applied loads up to 15 N with a resolution of 1.5 mN. The piezo actuator is attached to a pivoted cantilever, which increases the displacement by three-fold. Both actuators are connected to their respective motor controllers. In addition to the eight individual bioreactor units, the system contains a micropump controller, a measurement data acquisition unit and a gassing system, listed in Table 2-1. The system can be controlled and automated via a LabView interface. Mechanical loading protocols, not only including the loading parameters (frequency, amplitude and duration) but also mechanical compression tests during culture time can be run up to weeks, while the data (force sensor, actuator positions) are recorded.

2.3 Bioreactor equipment and consumables

Table 2-1: List of bioreactor equipment

Equipment	Model	Manufacturer
Data Acquisition System	Spider 8	Hottinger Baldwin Messtechnik
Frequency Generator	180LF	Wavetek San Diego
Gassing system	MX 4/4	DASGIP Technologies
Incubator for bioreactors	-	Memmert
Interface for Pump Control	NI USB-6501	National Instruments
Linear Actuator Servocontroller	C-863 Mercury™	Physik Instrumente
Micropump	mp6	Bartels Mikrotechnik
Mircopump Controller	8CH	MTL Charite- Med. Tech. Labore
Micropump Desktop Controller	EDP0604	thinXXS
Piezo Actuator	E-621.SR in E-500.621	Physik Instrumente

Table 2-2: List of bioreactor consumables

Item	Ordering #	Manufacturer
30 ml syringes	629502	CODAN Medical
Blue Filters Minisart 0.2 µm	16534K	Sartorius Stedim
Brown Filters Minisart 5 µm	17594Q	Sartorius Stedim
Perfusor	8722935	B.Braun

2.4 Flow chamber setup

The Ibidi Pump system (10902, Ibidi GmbH) used in this dissertation was kindly provided by the Lab of Petra Knaus at the Freie Univerität Berlin. The setup, shown in Figure 2-2, consists of a fluidic unit, a pump which is controlled via a PumpControl software and disposable parts, such as perfusion sets and flow chamber slides (Table 2-3). The fluidic unit is equipped with a sterile perfusion set (fluidic reservoirs and tubing) connected to the flow chamber slide and performs the switching operation to create the unidirectional flow. The fluidic unit is further coupled to the ibidi pump via two connectors, one electrical connection to control the valve and a tubing for the pressurized air. To protect the pump from the moisture inside the cell culture incubator, in which the fluidic unit is placed, the warm air passes through a drying bottle.

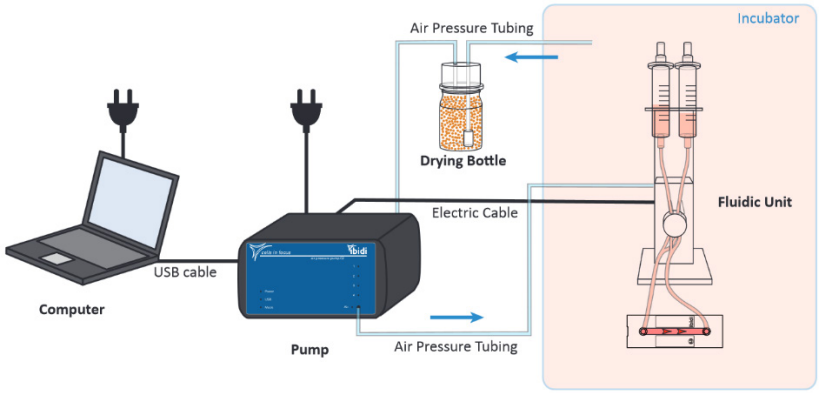

Figure 2-2: Schematic representation of the ibidi Pump System. The fluidic unit is placed into the cell culture incubator, while the pump and drying bottle are outside. Image taken from the instruction manual of the ibidi Pump System.

Table 2-3: Consumables for the ibidi Pump System

Item	Ordering #	Manufacturer
µ-Slide I $^{0.8}$ Luer	80176	Ibidi
Perfusion set	10962	Ibidi

2.5 Devices

Table 2-4: List of devices

Device	Model	Manufacturer
Autoklave	5L steam pot	Fissler
Cell counter	Casy Modell TT	Casy
Centrifuge (1.5-2 ml Eppendorf tubes)	Heraeus Fresco 17	Thermo Fischer
Centrifuge (15, 50 ml Falcon tubes)	Rotofix 32	Hettich
Clean bench	Safe2020	Thermo Fischer
	Herasafe	Heraeus
Cryotome	CM1950	Leica
CO_2 incubator cell culture	APT.line™	Binder
Confocal multiphoton microscope	TCS SP5	Leica Microsystems
Gel electrophoreses chamber	SureLock™ Mini-Cell	Thermo Fischer
Heating plate/stirrer	-	VWR
Ibidi Pump System	10902	Ibidi
Microplate reader	Infinite pro 2000	Tecan
Microscope	DM IL LED	Leica
Multipipette	Picus 5-120L	BIOHIT/Satorius
Spectrophotometer (NanoDrop)	ND-1000	Thermo Fischer
PCR cycler	Mastercycler gradient	Eppendorf
pH Electrode	SenTix®	WTW Weilheim
Power supply	Power Pac HC	Bio-Rad
Scale	Scout pro 400g	Ohaus
Thermomixer	Thermomixer comfort	Eppendorf
Ultrasound bath	SONOREX SUPER RK 100H	Schalltec
Vacuum pump	AC1 PH-MTR Serie 71	Pfeiffer Vacuum
Water bath	WNB 7-45	Memmert
Western blot	XCell II™	Thermo Fischer
Western blot imaging system	Odyssey	Li-Cor

2.6 Chemicals, reagents and kits

Table 2-5: List of chemicals, reagents and kits

Item	Ordering #	Manufacturer
10% SDS solution	15553027	Thermo Fischer
10% Triton X-100 solution	93443	Sigma Aldrich

Item	Ordering #	Manufacturer
4x protein loading buffer	928-40004	Li-COR
Acetonitril, Ultra LC-MS (ROTISOLV > 99,98%)	HN40.2	ROTH
Acetonitrile with 0.1% trifluoracetic acid (LC-MS)	34976	FLUKA
Alamar Blue®	DAL1025	Thermo Fischer
Ammonium bicarbonate (for LC-MS)	A6141-500G	Sigma Aldrich
Bovine Serum Albumin	8076.2	Carl Roth
Cell tracker green (CMFDA)	ab145459	abcam
cOmplete™, Mini Protease Inhibitor	4693124001	Roche
DMSO (anhydrous) ≥99%	276855	Sigma Aldrich
DNase I (700U)	10104159001	Roche
Luciferase assay system	E4030	Promega
HEPES (hydroxyethyl-piperazineethane-sulfonic acid buffer)	L1613	Merck
Nitrocellulose membrane	10600002	GE healthcare
NuPAGE™ 4-12% Bis-Tris Protein Gels	NP0336BOX	Thermo Fischer
NuPAGE™ MES SDS Running Buffer	NP0002	Thermo Fischer
NuPAGE™ MOPS SDS Running Buffer	NP0001	Thermo Fischer
Odyssey® Blocking Buffer (TBS)	P/N 927-50000	Li-Cor
PageRuler™ Plus Prestained Protein Ladder	26619	Thermo Fischer
Paraformaldehyde 4 wt.%	1.04005.1000	Merck Millipore
Phosphate-Buffered Saline with Ca^{2+}/Mg^{2+}	14040 - 091	Thermo Fischer
PhosSTOP™ phosphatase inhibitor	4906845001	Roche
Pierce™ BCA Protein Assay Kit	23225	Thermo Fischer
RIPA lysis buffer	806	Cell Signaling
Trifluoroacetic acid (Uvasol for spectroscopy)	1.08262.0025	Merck-Millipore
Trypsin (Sequencing Grade Modified, LC-MS)	V5111	Promega
Water with 0.1% (v/v) formic acid (for LC-MS)	84867.320	VWR Chemicals
Water with 0.1% Trifuoroacetic acid (for LC-MS)	84871.320	VWR Chemicals

2.7 Buffer ingredients

Table 2-6: Buffer compositions

Chemicals	concentration	Ordering #	Manufacturer
Ammonium chloride solution			
NH_4Cl	25 mM	1.01145.0500	Merck Millipore
PBS	1x	14190-094	Thermo Fischer

Chemicals	concentration	Ordering #	Manufacturer
Western blot transfer buffer			
Glycin	192 mM	0079.2	Carl Roth
Tris base	25 mM	T6066	Sigma Aldrich
Methanol	20 vol.%	0082.3	Carl Roth
TBS-T (1x) Western blotting, pH 7.6			
NaCl	136 mM	567440-1KG	Merck Millipore
Tris	20 mM	108.382	Merck Millipore
Tween-20	0.1%	P1379-100ml	Sigma Aldrich
TBS-T (1x) Immunofluorescent staining, pH 8.2			
NaCl	150 mM	567440-1KG	Merck Millipore
Tris	50 mM	108.382	Merck Millipore
Tris-HCl	50 mM	T3253	Sigma Aldrich

2.8 Cell culture

2.8.1 Cells

Human fetal osteoblasts (hFOBs 1.19)

hFOBs, immortalized by SV40 pUCSVtsA58 vector transfection, were purchased from ATCC (Manassas, Virginia, USA) and used for mechanistic investigation on the crosstalk between BMP signaling and mechanotransduction.

Primary human mesenchymal stromal cells (hMSCs)

Human MSCs were isolated from bone marrow aspirates of patients who underwent total hip endoprosthesis. The isolation was performed by the Core Unit "cell harvesting" at the Berlin-Brandenburg Center for Regenerative Therapies (BCRT). Cells were validated for their osteogenic differentiation potential by stimulation with osteogenic medium and the subsequent analysis of ALP activity and calcium amount in the ECM.

Primary human dermal fibroblasts (hdF)

Human dermal fibroblasts were isolated form skin samples. Experiments were conducted using cells obtained from one male donor at the age of 26.

The isolation of primary human mesenchymal stromal cells and fibroblasts from patient-derived material was approved by the Institutional Review Board of the Charité Berlin. All patients gave their written consent.

2.8.2 Cell culture material

Item	Ordering #	Manufacturer
Biopsy Punch 5 mm	48501	Pfm medical AG
Chamber slides (8 well)	80826	Ibidi
Culture Flasks (75 cm^2, 175 cm^2, 300 cm^2)	734.2315	TPP
DMEM Dulbecco's Modified Eagle Medium (low glucose (LG))	D5546	Biochrom GmbH
DMEM Dulbecco's Modified Eagle Medium (high glucose (HG))	41965-039	Gibco® Life Technologies
DMEM Dulbecco's Modified Eagle Medium and Ham's F-12	11320-082	Thermo Fischer
FBS Superior (fetal bovine serum)	S0615	Biochrom GmbH
Geneticin disulphate (G418)-solution	CP11.3	Carl Roth
GlutaMAX™	35050-038	Thermo Fischer
MEM Non-Essential Amino Acids Solution (NEA)	K0293	Biochrom GmbH
Mr. Frosty™ freezing container	5100-0001	Thermo Fisher
Multiwell-Plates (6, 12, 24, 96 wells)	353046	BD Biosciences
Nutridoma-SP	11011375001	Roche
Penicillin/Streptomycin (P/S)	A2213	Biochrom AG
PBS- Phosphate-Buffered Saline (w/o $Ca^{2}+/Mg^{2}+$)	14190-094	Thermo Fischer
Trypsin/EDTA (10x)	59418C-10ml	Biochrom GmbH

2.8.3 siRNAs, transfection reagents and transduction material

Table 2-7 Material for siRNA transfection and lentiviral transduction

Item	Ordering #	Manufacturer	Storage
siRNA transfection			
Lipofectamine™ RNAiMAX	13778500	Thermo Fisher	4°C
Opti-MEM™ serum-free	51985034	Thermo Fischer	4°C

siRNA (Silencer® select) ITGαv	s7568	Thermo Fisher	-20°C
siRNA Lincode Non-targeting #1	D-001320-01-05	Dharmacon	-20°C
Lentiviral transduction			
Hexadimethrine bromide (Polybrene)	TR-1003-G	Sigma-Aldrich	-20°C
Puromycin	A1113802	Thermo Fisher	-20°C
rLV-Ubi-LifeAct-TagGFP2 Lentiviral Vector	60141	Ibidi	-80°C

2.8.4 Growth factor and small molecular inhibitor

Table 2-8: List of growth factors and small molecular inhibitors

Item	Dissolved in	Stock concentration	Ordering #	Manufacturer	Storage
rhBMP-2	1 mM HCl	1mg/ml	-	AG Prof. Dr. Thomas Müller*	-80/4°C
Jasplakinolide	DMSO	1 mM	420107	Calbiochem	-20°C

2.9 Materials for histology

Table 2-9: Consumables for histology

Item	Ordering #	Manufacturer
Antibody diluent	S3022	Dako
Bovine Serum Albumin	A7906-100g	Sigma Aldrich
Cover slips	01-2446	Langenbrinck
Fluoromount-G®	0100-01	Southern Biotech
Microscope slides	08.100 00	Marienfeld
Normal donkey serum	017-000-1212	Jackson Immunoresearch
Normal goat serum	S-1000	Vector Laboratories
Normal horse serum	S-2000	Vector Laboratories
Scalpels	5518067	Aesculap AG
Tissue-Tek® Cryomold	4566	Sakura Finetek
Tissue-Tek® O.C.T.™ Compound	4583	Sakura Finetek

*Molekulare Pflanzengenetik, Lehrstuhl für Molekulare Pflanzenphysiologie und Biophysik, Julius-Maximilians-Universität Würzburg

2.9.1 Primary and secondary antibodies

Table 2-10: List of primary and secondary antibodies

Target	source	clonality	Ordering #	Manufacturer
Primary antibodies				
Collagen 1	Rabbit	Monoclonal	ab138492	Abcam
FAK	Rabbit	Monoclonal	13009	Cell Signaling Technology
GAPDH	Rabbit	14C10 monoclonal	2118	Cell Signaling Technology
pERK1/2 (Thr202/Tyr204)	Rabbit	Monoclonal	4370	Cell Signaling Technology
pFAK(Y397)	Rabbit	Monoclonal	8556	Cell Signaling Technology
pMLC (S19)	Mouse	Monoclonal	3675	Cell Signaling Technology
pPaxilin (Y118)	Rabbit	Polyclonal	2541	Cell Signaling Technology
pSmad 1/5 (S463/465)	Rabbit	Monoclonal	9516	Cell Signaling Technology
p-Src(Y416)	Rabbit	Monoclonal	6943	Cell Signaling Technology
Secondary antibodies				
Target	**source**	**conjugation**	**Ordering #**	**Manufacturer**
Anti-mouse IgG	Goat	Cy3-conjugated	405309	Biolegend
Anti-mouse IgG	Goat	Alexa Fluor 488-conjugated	A11001	Thermo Fischer
Anti-rabbit IgG	Donkey	Cy3-conjugated	711-165-152	Jackson Immunoresearch
Anti-rabbit IgG	Donkey	Alexa Fluor 488-conjugated	A21206	Thermo Fischer
Anti-rabbit IgG	Goat	IRDye® 800CW	925-32211	Li-Cor
Anti-mouse IgG	Goat	IRDye® 680RD	925-68070	Li-Cor

2.9.2 Small molecular dyes for immunohistochemistry

Table 2-11: List of small molecular dyes used in immunohistochemistry

Item	Concentration/ storage	Ordering #	Manufacturer
Alexa Fluor™ 488 Phalloidin	6.6 µM in MeOH at -20°C	A12379	Thermo Fischer
Alexa Fluor™ 633 Phalloidin	6.6 µM in MeOH at -20°C	A22284	Thermo Fischer
DAPI (4',6-Diamidino-2-Phenylindole, Dihydrochloride)	5 mg/ml in dH_2O at -20°C	D1306	Thermo Fischer
DRAQ5	5 mM at 4°C	424101	Biolegend

2.10 RNA isolation, reverse transcription and qPCR

Table 2-12: Consumables and kits for RNA isolation, reverse transcription and pPCR

Item	Ordering #	Manufacturer
Ethanol EMPROVE®	1009861000	Merck Milipore
iQ™ SYBR® Green Supermix	170-8882	Bio-Rad
iScript™ cDNA Synthesis Kit	170-8891	Bio-Rad
Nuclease-free water	AM9937	Thermo Fischer
Optically clear flat 8 cap strips	TCS1080	Thermo Fisher
PureLink® DNase	12185010	Thermo Fischer
PureLink® RNA Mini Kit	12183018A	Thermo Fischer
RNaseZAP®	AM9780	Thermo Fischer
Semi- skirted 96 well PCR plate	AB0900	Thermo Fisher

2.10.1 Primer

Table 2-13: List of primers for qPCR

Gene	Protein	Function	Primer sequence 5'→ 3' forward (fwd) and reverse (rev)	
BMP-1	Bone morphogenetic protein 1	Matrix metallo-proteinase	fwd	CTCCATCAAAGCTGCAGTTCC
			rev	CGGGATCTACCTCTCCATCTC
BMP-2	Bone morphogenetic protein 2	BMP ligand	fwd	CATGCCATTGTTCAGACGTT
			rev	CAACTGGGGTGGGGTTTT
BMP-4	Bone morphogenetic protein 4	BMP ligand	fwd	CCACGAAGAACATCTGGAGAAC
			rev	ATACGGTGGAAGCCCCTTT

BMP-6	Bone morphogenetic protein 6	BMP ligand	fwd	GCAGACCTTGGTTCACCTTATG
			rev	AGAATGTGTGTCCCCAGCA
BR1A	BMP type I receptor 1a	BMP signaling	fwd	TTCGATGGCTGGTTTTGCTC
			rev	ACGACGTCTGCTTGAGATGC
BR1B	BMP type I receptor 1b	BMP signaling	fwd	CCTGGAGAATCCCTGAGAGAC
			rev	AGTCCTTTGGACCAGCAGAG
BR2	BMP type I receptor 2	BMP signaling	fwd	GTTGGAGCTGATTGGCCGAG
			rev	TTTACAGCAACTGGACGCTC
c-fos	FBJ murine osteosarcoma viral oncogene homolog	Mechano-sensitive TF	fwd	CAAGCGGAGACAGACCAACT
			rev	AGATCAAGGGAAGCCACAGA
COL1A2	Collagen alpha-2(I) chain	ECM proteins	fwd	AGCCGGAGATAGAGGACCAC
			rev	GGCCAAGTCCAACTCCTTTT
COL6A1	Collagen alpha-1(VI) chain	ECM proteins	fwd	ACTGCGTATCAAGAAGGGG
			rev	TCGTTCACAGCATCCTCCAG
DLX2	Distal-less homeobox 2	BMP target	fwd	GGCGTTTCCAAAAGACTCAA
			rev	CGAAGCACAAGGTGGAGAAG
EEF1A1	eukaryotic translation elongation factor 1 alpha 1	House-keeping gene	fwd	AACACAGGTGTCGTGAAAAC
			rev	AAGACCCAGGCATACTTGAA
ELN	Elastin	ECM proteins	fwd	TTTTATCCAGGGGCTGGTCTC
			rev	AGAGCCCCCGGAAAGGTAAC
FGF2	Fibroblast growth factor 2	growth factors	fwd	AGCGGCTGTACTGCAAAAAC
			rev	AGCCAGGTAACGGTTAGCAC
FN1	Fibronectin	ECM proteins	fwd	CAGCCAGTAGCTTTGTGGTC
			rev	GCATCAGGCGCTGTTGTTT
FBLN1	Fibulin 1	ECM proteins	fwd	CGGATGGCCACTCATCAGAAG
			rev	GCACCATCCTGCATTCTTTGG
HPRT1	hypoxanthine phosphoribosyl-transferase 1	House-keeping gene	fwd	TATGGACAGGACTGAACGTC
			rev	TGATGTAATCCAGCAGGTCA
ID1	Inhibitor of DNA binding 1	BMP target	fwd	GCTGCTCTACGACATGAACG
			rev	CCAACTGAAGGTCCCTGATG
ID2	Inhibitor of DNA binding 2	BMP target	fwd	GTGGCTGAATAAGCGGTGTT
			rev	TGTCCTCCTTGTGAAATGGTT
ITGα1	Integrin subunit alpha 1	Cell adhesion	fwd	ACGCTGCTGCGTATCATTCA
			rev	CACCTCTCCCAACTGGACAC
ITGα5	Integrin subunit alpha 5	Cell adhesion	fwd	TGGCCTTCGGTTTACAGTCC
			rev	GGTGCAGTTGAGTCCCGTAA
ITGαv	Integrin subunit alpha v	Cell adhesion	fwd	TCAGCAAGGCAATGCTCCAT
			rev	GAGGGCAAGATCCCGCTTAG
ITGβ1	Integrin subunit beta 1	Cell adhesion	fwd	CTGCGAGTGTGGTGTCTGTA
			rev	CACAGGATCAGGTTGGACCG
ITGβ3		Cell adhesion	fwd	ACCAGTAACCTGCGGATTGG

	Integrin subunit beta 3		rev	TCCGTGACACACTCTGCTTC
ITGβ5	Integrin subunit beta 5	Cell adhesion	fwd	ATACCTGGAACAACGGTGGAG
			rev	AGATCCTCAGGCTGATCCCA
LOX	Lysyl oxidase	ECM regulation	fwd	TGGCCGACCCCTACTACATC
			rev	TGGGGAAATCTGAGCAGCAC
LOXL1	Lysyl oxidase homolog 1	ECM regulation	fwd	TGTACCGGCCCAACCAGAAC
			rev	GATGCTTGCACATAGTTGGGG
MMP1	Interstitial collagenase	ECM regulation	fwd	ACATGAGTCTTTGCCGGAGG
			rev	ATCCCTTGCCTATCCAGGGT
MMP13	Collagenase 3	ECM regulation	fwd	TTGAGCTGGACTCATTGTCG
			rev	TCTCGGAGCCTCTCAGTCAT
Noggin	Noggin	BMP antagonist	fwd	GCCAGCACTATCTCCACATCC
			rev	GGGTGTTCGATGAGGTCCAC
TGFB1	Transforming growth factor 1	growth factors	fwd	GGCCTTTCCTGCTTCTCAT
			rev	GTCCTTGCGGAAGTCAATGT
TGFB2	Transforming growth factor 2	growth factors	fwd	ACTGTCCCTGCTGCACTTTT
			rev	GGGGTCTTCCCACTGTTTTT
TGFB3	Transforming growth factor 3	growth factors	fwd	ATGAGCACATTGCCAAACAG
			rev	ATTGGGCTGAAAGGTGTGAC
TGFBI	TGF-beta induced protein	ECM proteins	fwd	TACGAGTGCTGTCCTGGATATG
			rev	GTTTGAGAGTGGTAGGGCTGC
TNC	Tenascin	ECM proteins	fwd	GTGAAAAACAATACCCGGGGC
			rev	CCGTAGGTCAGCTCAATGCC
THBS1	Thrombospondin	ECM proteins	fwd	TCTGCAAAAAGGTGTCCTGC
			rev	AGAACAGGAGGTCCACTCGG
POSTN	Periostin	ECM proteins	fwd	CAGCAGTTTTGCCCATTGACC
			rev	CAGCAGTTTTGCCCATTGACC
RUNX2	Runt-related transcription factor 2	Osteogenic marker	fwd	CTCCTACCTGAGCCAGATGA
			rev	CGGGGTGTAAGTAAAGGTGG
Smad7	Smad familiy member 7	BMP signaling	fwd	TGCAACCCCTACCACTTCAGC
			rev	GAGACATGCTGGCGTCTGAG
Smurf1	SMAD specific E3 ubiquitin protein ligase 1	BMP signaling	fwd	AATGAAGATGCGACCGAAAG
			rev	AGCCCGTAATAAGGATTCAGC
Smurf1	SMAD specific E3 ubiquitin protein ligase 2	BMP signaling	fwd	TCCTCGGCTGTCTGCTAACT
			rev	GGGACTGTCAGGCATTCTGT
SPP1	Osteopontin	Osteogenic marker	fwd	TCACCTGTGCCATACCAGTTA
			rev	TCATGGCTTTCGTTGGACTT
VEGFA	Vascular endothelial growth factor A	growth factors	fwd	CAGAAGGAGGAGGGCAGAAT
			rev	CTGCATGGTGATGTTGGACT

3 Methods

3.1 Cell biological methods

3.1.1 Cell thawing and cultivation

Cryopreserved cells ($1x10^6$ per cryo-vial) were thawed at 37°C in the water bath under constant movement of the cryo-vial until only a small piece of ice remained. The vial was transferred into the clean bench and as soon as the ice disappeared completely, cells were transferred into a cell culture flask containing the respective pre-warmed expansion medium (Table 3-1). The day after, the medium was exchanged in order to remove the DMSO containing freezing medium.

Human fetal osteoblasts (hFOBs) were cultured in a 1:1 mixture of Dulbecco's Modified Eagle Medium (DMEM) and Ham's F-12 (11320-033; Thermo Fischer Scientific) supplemented with 1 vol.-% penicillin/streptomycin (P/S: A 2212; Biochrom), 0.3 mg/ml Geneticin (CP11.3; Carl Roth) and 10 vol.-% fetal bovine serum (FBS: S0615; Biochrom). hFOB were grown at 34°C and 5% CO_2 in a humid incubator until ~80% confluence was reached (after 3-4 days). For further expansion, cells were split in a ratio of 1:4, which corresponds to approx. 2800 cells/cm^2. Cells were used from passage six to 15.

Primary human mesenchymal stromal cells (hMSCs) isolated from bone marrow were expanded in DMEM low glucose (D5546; Sigma Aldrich) supplemented with 1 vol.-% P/S, 1 vol.-% GlutaMAX™ (35050-038, Life Technologies) and 10 vol.-% FBS. hMSCs were expanded at 37°C and 5% CO_2 in a humid incubator until ~80 to 90% confluence was reached and split for further cultivation at a density of approx. 3300 cell/cm^2 ($1x10^6$/T300 flask). Cells were used between passages three to five.

Primary human dermal fibroblasts (hdF) isolated from skin biopsies were cultured in DMEM high glucose (# 41965; Gibco, Invitrogen) supplemented with 10% FBS, 1% P/S and 1% Nonessential Amino Acids (NEA: K0293; Biochrom). hdF were expanded at 37°C and 5% CO_2 in a humid incubator until 100% confluence was reached. For further culture cells were split at a density of approx. 3300 cell/cm^2 ($1x10^6$/T300 flask). Cells were used between passages four to nine.

C2C12-BREluc were expanded in DMEM low glucose supplemented with 10 vol.% FBS, 1 vol.% GlutaMAX™ and 0.5 mg/ml Geneticin at 37°C with 5% CO_2 in a humidified incubator until ~70% confluence was reached (every 2-3 days). For further expansion cells were split at a concentration of 1100 cells/cm^2 ($2x10^5$/T175 flask) into a new culture flask. Cells were used from passage eight to 15.

Table 3-1 Summary of expansion media composition

Component	hFOB	hdF	hMSC	C2C12-BREluc
DMEM (high glucose)		x		
DMEM (low glucose)			x	x
DMEM F-12	x			
FBS	10 vol.-%	10 vol.-%	10 vol.-%	10 vol.-%
P/S	1 vol.-%	1 vol.-%	1 vol.-%	1 vol.-%
G418	0.6 vol.-%			1 vol.-%
GlutaMAX™			1 vol.-%	
NEA		1 vol.-%		

3.1.2 Passaging and cryo-preservation

Cell passaging was performed by trypsinization using 1x Trypsin/EDTA solution (59418C, Biochrom) at 37°C after two washing steps with 1x phosphate buffered saline (PBS: 14190-094, Thermo Fisher). Cells were incubated for approx. 2-3 min with trypsin until they detached and the reaction was stopped with the according expansion medium. Cells were resuspended and given through a cell strainer to separate and remove aggregates. Cell concentration was determined using the CASY™ Cell Counter (Model TT, Roche) by diluting 70 µl of the cell suspension in 7 ml CASY® ton. At the same time, cell suspension was centrifuged at 375 x g for 6 min‡ or 325 x g for 8 min†. Thereafter, supernatant was sucked off and cell pellet was resuspended in expansion medium to a concentration required for the type of experiment.

Table 3-2: Volumes used for culture and trypsinization depending on the culture format

Flask	Medium vol.	PBS wash	Trypsin/EDTA	Medium to stop
T75	15 ml	5 ml	1 ml	4 ml
T175	35 ml	10 ml	2† / 2.5‡ ml	8†/7.5‡ ml
T300	60 ml	25 ml	4† /5‡ ml	16†/15‡ ml

For cell freezing, a concentration of $2x10^6$ cells/ml was adjusted and suspension was incubated on ice for 5 min. The freezing medium containing the respective expansion medium, 20% FBS and 20% DMSO (anhydrous, Sigma Aldrich) was prepared and chilled on ice to 4°C. Cryo-vials were filled with 500 µl of the cell suspension and 2x250 µl of the freezing

† hMSC, hFOB, C2C12-BREluc
‡ hdF

medium in two consecutive steps (final ratio 1:1). Vials were transferred into the -80°C freezer overnight and finally stored in the gas phase of the liquid nitrogen container.

3.1.3 Seeding of collagen scaffolds

Cylindrical samples of 5 mm diameter were cut from the collagen scaffold sheet using a sterile biopsy punch. Scaffold cylinders were dipped into the prepared cell suspension (see Table 3-3) that was immediately soaked up until the scaffold was completely filled. Seeded scaffolds were placed into a 12-well-plate without additional medium. During a 60 min incubation, the cells were allowed to adhere to the scaffold walls. Subsequently, the scaffolds were washed in fresh expansion medium to remove unattached cells and placed in a 12 well plate on PEEK (polyether ether ketone) meshes. The meshes enable improved supply from the bottom. Depending on the type of experiment performed, scaffolds were either pre-incubated for one[§] or two[**] days in the cell culture incubator prior to bioreactor experiments.

Table 3-3 Cell concentrations used for different cell types

Cell type	Cell concentration	Cell number / scaffold	Experiment
hFOBs, hdF, hMSC	5000 cells/µl	~$3.25x10^5$	mechanistic investigations
hdF	7500 cells/µl	~$4.875x10^5$	ECM formation
hMSC	2500 cells/µl	~$1.625x10^5$	load-induced osteogenesis

3.1.4 Lentiviral transduction of an actin marker

To visualize and follow the remodeling of filamentous actin (F-actin) in living cells, the GFP tagged F-actin binding peptide LifeAct (17-amino acid long) was introduced into hFOBs by viral transduction. In contrast to GFP-actin or other actin labeling methods, LifeAct was not found to interfere with the actin dynamics[160]. A lentiviral vector was selected since it mediates efficient transduction and stable integration into the genome of many different cell types. The rLV-Ubi-LifeAct-TagGFP2 Lentiviral Vector (60141) containing 100µl of $1x10^7$ TU/ml was purchased from Ibidi and the transduction was performed according to the manufacture´s instruction under Safety Level 2 conditions.

The transduction efficiency was evaluated before by testing MOIs (multiplicity of infection) of 0.5, 1 and 2. hFOBs were seeded in a 48 well plate at different concentrations (30, 50 and 70% confluence). The next day, medium was removed and 200 µL transduction medium, containing no antibiotics, 10% heat inactivated FCS and 8 µg/ml hexadimethrine

[§] ECM formation, load-induced osteogenic differentiation
[**] Mechanistic investigations

bromide (Polybrene), was added. A 1:10 dilution of the lentiviral vector was prepared in PBS and added to the cells according to Table 3-4. After a 20 hours incubation the medium containing the lentiviral particles was removed and 200 µl fresh expansion medium was added.

Table 3-4 Plate layout for the transduction efficiency test. Volumes taken from the 1:10 dilution of the vector

	Lentiviral Titer 10^6 TU/mL		
	3200 cells/well	**4800 cells/well**	**6500 cells/well**
MOI	µl	µl	µl
0.5	1.6	2.4	3.25
1	3.2	4.8	6.5
2	6.4	9.6	13
total	50.75		

At the fifth day after transduction, the transduction efficiency was evaluated under the fluorescence microscope according to that a MOI 2 and a confluence of 50% was selected for the final transduction.

Finally, hFOBs in P4 were seeded at 50% confluence ($4.8x10^4$ cells/well) in a 6 well plate and transduced as described. At the fifth day, cells were transferred into a $25cm^2$ cell culture flask for expansion. The positive selection started on the next day by adding 1µg/ml puromycin to the culture medium. The day after, dead cells were removed by medium exchange that was repeated every 3 days until only transduced cell remained. The efficiency of the selection process was thereafter evaluated by FACS analysis. Stable expressing hFOBs are called in the following hFOB-LA.

3.1.5 Transfection of small interfering RNA

Knockdown of integrin (ITG) αv was performed by lipid-based transfection of small interfering RNAs (siRNAs) into hFOBs using Lipofectamine™ RNAiMAX (13778500, Thermo Fisher) according to the manufacture´s instruction. siRNA (A) and RNAiMax (B) dilutions were prepared separately in serum-free Opti-MEM™ (51985034, Thermo Fischer) as shown in Table 3-5. To from siRNA-lipid complexes, solution A and B were mixed in a 1:1 ratio and incubated for 5 min. Cell suspension at a concentration of $1x10^5$ cells/µl in antibiotic-free expansion medium was added to the siRNA-lipid complexes in a 1:1 ratio and incubated for further 5 min. Thereafter, cell suspension was transferred into a 48 well plate and scaffolds (Ø = 5 mm) were seeded as described in section 3.1.3 and incubated for two days prior to bioreactor experiments. The reverse transfection method, meaning simultaneous cell seeding and transfection, was selected since it reached higher efficiencies then transfection of already seeded scaffolds. A nonspecific siRNA (scrambled, scr) was used as a negative control to determine the effect of lipid-based transfection in all RNAi-experiments. In general, nuclease-

free consumables (filter tips, tubes and water) and antibiotic-free cell culture medium for transfection and the subsequent experiment was used.

Table 3-5 Calculations for seeding of one scaffold (volume = 80 µl) per condition

	A1	A2	B
	siITG αv	scr	RNAiMAX dilution
siRNA stock concentration	20 µM	100 µM	-
siRNA working concentration	25 nM	25 nM	-
siRNA (µl)	1 µl of a 1:10 dilution in water	2 µl of a 1:100 dilution in water	-
Opti-MEM	20 µl	20 µl	2 x 20 µl
RNAiMAX	-	-	2 x 0.25 µl

3.1.6 Bioreactor cultivation, mechanical loading and BMP stimulation

The assembly of the bioreactor cell culture units was performed under sterile conditions. Pre-warmed medium was filled into syringes and transferred via perfusor tubes inside the reservoirs. Depending on the type of experiment and its duration, the medium amount and the FBS concentration varied (see Table 3-7). Additional medium supplements were added according to the used cell type as summarized in Table 3-1. The medium was pumped into the bioreactor chamber until the lower sample holder was covered, thereby preventing sample dehydration during scaffold positioning. Carefully the cell-seeded scaffolds were placed into the custom-made silicon holders and covered with another PEEK mesh. The upper plunger was inserted, the chamber was sealed and the complete unit was mounted onto the mechanical subunit in the incubator. Thereafter, gas mixing and pump control units were connected and activated. Rough positioning of the plungers was carried out manually using the LabView interface, while fine tuning was performed using a force-controlled automated sample positioning protocol. Further experimental settings were dependent on the respective research aim and are described in the following:

3.1.6.1 Load-induced osteogenic differentiation

To study the influence of load-induced autocrine signaling, in particular the enrichment of BMP-2, on hMSC differentiation, three experimental conditions were selected, which are listed in Enrichment of autocrine factors in the cell culture medium during bioreactor cultivation was promoted by placing five scaffolds (Ø = 5 mm) into each chamber and by reducing the volume of cell culture medium to 12 ml. On the other hand, autocrine factors

were strongly diluted in reactors containing only one scaffold and 27 ml medium. Additionally, to compare the impact of medium conditioning to direct BMP-2 stimulation, 135 ng/ml recombinant human BMP-2 was added at day 4 of cultivation into bioreactors containing one scaffold and 27 ml medium.

Table 3-6.

Enrichment of autocrine factors in the cell culture medium during bioreactor cultivation was promoted by placing five scaffolds (Ø = 5 mm) into each chamber and by reducing the volume of cell culture medium to 12 ml. On the other hand, autocrine factors were strongly diluted in reactors containing only one scaffold and 27 ml medium. Additionally, to compare the impact of medium conditioning to direct BMP-2 stimulation, 135 ng/ml recombinant human BMP-2 was added at day 4 of cultivation into bioreactors containing one scaffold and 27 ml medium.

Table 3-6: Summary of experimental conditions

	Experimental condition	**Scaffolds per reactor**	**Medium volume**	**Cell to medium ratio (cells/ml)**
1	Enabling autocrine stimulation	5	12 ml	$6.25x10^4$
2	Disabling autocrine stimulation	1	27 ml	$0.56x10^4$
3	BMP-2 addition	1	27 ml	$0.56x10^4$

hMSC were subjected to cyclic compression with a frequency of 1 Hz and an amplitude of 10%. Mechanical loading was applied periodically with 3h stimulation and 5h break. Loading resulted in a compression of the scaffold in the direction of the scaffold pores. At the end of the experiment, cells were either fixed in 4% PFA (IF) or lysed in the RNA isolation lysis buffer (qPCR).

3.1.6.2 Mechanistic investigations

Two days after scaffold seeding and culture in growth medium containing 10 % FBS, scaffolds were transferred into the bioreactor. For short- term bioreactor experiments up to 120 min, FBS-free cell culture medium was used. After positioning, samples were left untreated for three hours in order to decrease unspecific background signaling due to the presence of growth factors in FBS and as a consequence of mechanical deformations that the sample experiences when mounted in to the reactor chamber. Next, BMP-2 was diluted to 4185 ng/ml in starvation medium and 0.5 ml was injected into the bioreactor reservoir to reach a final concentration of 135 ng/ml. The respective loading protocol was started immediately afterwards. To study the crosstalk dynamics, cells were stimulated with cyclic uniaxial mechanical loading with different frequencies (0.03, 1 and 10 Hz), amplitudes (5% and 10%

of the scaffold height) and durations (15, 30, 90, 120 min, 24h). At the end of the experiment, cells were either fixed in 4% PFA (IF) or lysed in the respective assay buffer for further analysis (WB, qPCR).

To investigate whether load-induced actin cytoskeleton rearrangement processes are necessary for the crosstalk, different small molecular inhibitors (Table 2-8) were used during bioreactor experiments. Jasplakinolide (Jas) was used to stabilize actin filaments. Jas at a concentration of 0.1 µM was supplemented to the medium at the beginning of the experiment so that cells were treated for three hours prior to BMP-2 stimulation and mechanical loading. As a control to Jas treated samples, DMSO was supplemented to the medium. After the starvation phase, scaffolds were subjected to cyclic mechanical compression of 10% with a frequency of 1 Hz for 90 min in this particular experiment. Thereafter, cells were either fixed in 4% PFA (IF) or lysed in the respective assay buffer for further analysis (WB, qPCR).

3.1.6.3 Consequences of the crosstalk for ECM formation

As described in section 3.1.6.2, samples were left untreated for three hours in order to decrease unspecific background signaling. Next, BMP-2 was diluted and injected into the bioreactor reservoir (final concentration of 135 ng/ml in 15 ml) and loading protocol was started. hdF in collagen scaffolds were allowed to form ECM during one and two weeks bioreactor culture under BMP-2 stimulation and cyclic mechanical loading. To enable fibrillar collagen formation, cell culture medium contained ascorbic acid at a concentration of 1.36 mM. Bioreactor culture of two weeks required half a medium exchange on day seven. Scaffolds were subjected to cyclic compression with a frequency of 1 Hz and an amplitude of 10%. Cyclic compression was applied periodically with 3h stimulation and 5h break in the direction of the scaffold pores. BMP-2 (135 ng/ml) was added at day one, five and 10, while medium without BMP-2 was added to unstimulated controls. BMP-2 was injected at the start of each mechanical stimulation phase. At the end of the experiment, cells were either fixed in 4% PFA (IF) or lysed in the respective assay buffer for further analysis (WB, qPCR).

Table 3-7: FBS concentration and medium amount inside bioreactors depending on the type of experiment

Type of experiment	**Cell type**	**Experiment duration**	**Medium volume**	**FBS concentration**
Mechanistic studies	hFOBs, hdFs, hMSCs	≤ 2h	15 ml	0%
	hFOBs	24h	15 ml	1%
ECM formation	hdFs	one and two weeks	15 ml	2%
Osteogenic differentiation	hMSCs	one week	27 ml or 12 ml	10%

3.2 Molecular biological methods

3.2.1 Ribonucleic acid isolation from collagen scaffolds

For RNA isolation, exclusively nuclease-free materials (filter tips, tubes, water) were used and all surfaces and the equipment were wiped with RNaseZap™ (AM9780, Thermo Fisher).

Total RNA was isolated using the PureLink® RNA Mini Kit (12183018A, Thermo Fischer) and DNA digestion was performed using ON-column PureLink® DNase (12185-010, Thermo Fischer). Isolation from cells grown in 2D were performed according to the manufacture's instruction. For 3D collagen scaffold cultures, however modifications were implemented, which are described in the following.

At the desired endpoint of the experiment, scaffolds were placed onto a sterile filter paper to removethe culture medium and subsequently transferred into a tube containing 500 µl lysis buffer supplemented with 1 vol.-% β-mercaptoethanol. Tubes were vortexed and frozen at -80°C at least overnight. For the isolation, samples were thawed and centrifuged at 3000 x g through a 10 µl pipette tip, which was loaded with a glass bead hindering the scaffold from passing, while collecting the total lysate at the tube bottom. The empty scaffold was discarded and the lysate was processed according to the manufacture's instruction.

Finally, the elution of the RNA was performed twice with nuclease-free water pre-warmed to 60°C to increase the yield. RNA concentrations were measured using a NanoDrop Spectrophotometer.

3.2.2 Reverse transcription, quantitative polymerase chain reaction and data evaluation

For each sample, 500 ng RNA was transcribed to complementary DNA using the iScript™ cDNA Synthesis Kit (#170-8891, BIO-RAD) according to the manufacture's instruction. The transcription was performed inside the Mastercycler® gradient (Eppendorf). The resulting cDNA was stored for further qPCR analysis at -20°C.

Quantitative determination of messenger RNA transcription was performed using the SYBR green- based PCR. The reaction mixture contained 5 ng cDNA, 500 nM Primer (100 µM stock concentration) and 50% of the iQ™ SYBR® Green Supermix (170-8882, Bio-Rad). The reaction was performed in an iQ™5 Real-Time PCR Detection System (Bio-Rad) following the steps listed in Table 3-8. The assessed C_T values were processed according to the efficiency corrected $\Delta\Delta C_T$–method [161]. The primer efficiencies listed in Table 2-13 were determined by measuring a cDNA standard curve as described elsewhere [162]. Melting curves were recorded to check for non- specific amplifications, like primer dimers. Three different housekeeping genes (Hypoxanthine Phosphoribosyltransferase 1 (HPRT), Beta-2-

Microglobulin (B2MG) and Eukaryotic Translation Elongation Factor 1 Alpha 1 (EEF1A)) were tested for their stable expression under mechanical loading and BMP stimulation and HPRT was selected for normalization.

Table 3-8 qPCR reaction steps

	Cycle 1	**Cycle 2 (40x)**			**Cycle 3**	**Cycle 4 (80x)**
step	initiation	denaturation	annealing	elongation	denaturation	melting
°C	95	95	60	72	95	55-95(0.5 incr.)
min	3	0:30	0:30††	0:30††	1	0:10††

3.2.3 Cell lysis for protein analysis and extraction of ECM proteins

For the analysis of intracellular proteins, cells were lysed using 1x RIPA lysis buffer (9806, Cell Signaling Technology) supplemented with protease (cOmplete™, 4693124001, Roche) and phosphatase inhibitors (PhosSTOP™, 4906845001, Roche), while extracellular proteins were extracted by an adapted protocol described previously[163].

Intracellular protein extraction: Cells harvested from 2D surfaces were washed once in 500 µl ice-cold PBS and subsequently lysed in 100 µl RIPA buffer. After 5 min incubation on ice, cells were scraped off using a pipette tip and lysate was collected and frozen at -20°C. Cells from scaffold cultures were washed in 200 µl ice-cold PBS by placing it on a filter paper, which first removed the culture medium and subsequently the PBS. The sample was transferred into 100 µl RIPA buffer vortexed thoroughly and incubated on ice for 4 min. Thereafter, lysates were sonicated for 30 seconds to increase the extraction efficiency and again vortexed thoroughly. A 10 µl pipette tip with a glass bead was placed into the tube and loaded with the scaffold. By centrifugation for 2 min at 3000 x g at 4°C, the scaffold was dried and the lysate was collected and subsequently stored at -20°C.

Extracellular matrix extraction: Scaffolds were transferred to -80°C and frozen samples were pulverized under liquid nitrogen conditions using custom-made silicone vessels and steel pestles. Scaffold powder was dissolved in 200 µl of ECM extraction buffer I, vortexed thoroughly and sonicated at 4°C for 2 min inside an ultrasound bath. Thereafter, 100 µl of ECM extraction buffer II was added, vortexed and samples were centrifuged at 5000 x g for 2 min to remove insoluble fragments. The supernatant was collected and stored at -20°C.

†† Measurement of fluorescent intensity

3.2.4 Sodium dodecylsulfate polyacrylamide gel electrophoresis

The gel electrophoresis was conducted using the NuPAGE® electrophoresis system (Thermo Fischer) and NuPAGE™ 4-12% Bis-Tris protein gels. Lysates were mixed with 4x LDS loading buffer (Li-Cor) and heated for 4 min at 95°C to denature the proteins. Samples were cooled down to 4°C on ice, centrifuged briefly and lysates were loaded onto gradient gels clamped into XCell SureLock™ Mini-Cell container (Thermo Fisher). In addition, a pre-stained protein marker (26619, Thermo Fisher) was loaded to monitor the gel electrophoresis and to indicate the location of the proteins of interest. SDS-PAGE was run with 1x MES buffer at 150V for 80-90 min until the desired protein separation was achieved. Finally, polyacrylamide gels were removed from the plastic case and processed as described in the following section.

3.2.5 Western blotting and protein detection

Gel and nitrocellulose membrane were equilibrated for 5 min in transfer buffer, which was prepared according to Table 2-6. Thereafter, the blotting sandwich was assembled in the following order from bottom to top: filter paper, gel, membrane, filter paper. The sandwich was placed between blotting sponges soaked with transfer buffer and fitted inside the XCell Blot module (Thermo Fisher). The module was mounted inside the XCell SureLock™ Mini-Cell container, filled with transfer buffer and the transfer was run at 30V for one hour.

Next, the membrane was rinsed in TBS, incubated for another hour in Odyssey® Blocking Buffer (TBS) (P/N 927-50000, Li-Cor) under constant shaking, before it was cut as desired. Membrane sheets were further incubated overnight at 4°C in the respective primary antibody dilution, which was prepared according to the manufacture´s instruction. The next day, membranes were washed three times with TBS-T and incubated with the secondary antibody (Li-Cor) diluted 1:15000-1:20000 in 3% BSA/TBS-T for two hours at room temperature. The secondary antibody is coupled to an InfraRed-Dye, therefore the subsequent steps were performed protected from light.

Finally, membranes were washed three times for 10 min with TBS-T and one time with TBS to remove excess secondary antibody, before proteins of interest could be detected using the Li-Cor Odyssey® infrared imaging system (Li-Cor Biosciences). The signal intensity of the detected protein bands were quantified in the Li-Cor software by contouring the respective band with a rectangular ROI. The signal intensity of the protein of interest was normalized to GAPDH or β-Actin.

3.3 Immunocytochemistry

3.3.1 Sample preparation including fixation and cryo-trimming

Cells cultured on 2D surfaces or in collagen scaffolds were fixed in 4% paraformaldehyde (PFA) at room temperature for 15 min or for at least 5 hours, respectively. To quench the reaction, samples were incubated in 25 mM ammonium chloride solution (in PBS) for one hour at room temperature. After two times consecutive washing in PBS, scaffold samples were infiltrated at 37°C by a 5% gelatin/sucrose solution overnight. Gelatin was solidified at 4°C for 30-60 min and scaffolds were cut along the symmetry axis using a scalpel. Scaffold halves were transferred into PBS and gelatin was washed out at 37°C during repetitive exchange (3-4x) of PBS every one hour. To generate a plane imaging surface, the cut sides of the scaffold halves were trimmed in a cryotome. Therefore, the samples were embedded into Tissue-Tek® (Sakura Finetek) and snap-frozen on a metal bar placed into liquid nitrogen. In the cryotome, approx. 200 µm was trimmed off the surface in 10 µm steps and the Tissue-Tek® was subsequently washed out with PBS at 37°C.

3.3.2 Immunofluorescence staining

Proteins of interest were stained indirectly by coupling a fluorophore-conjugated antibody to a primary antibody that specifically recognized and bound to an epitope of the protein. The immunofluorescence (IF) staining protocol was adapted to each antibody combination and combined with nuclei or actin labeling using small molecule probes. An overview of the procedure including pre-treatments, blocking and antibody incubation is listed in Table 3-9. Wash buffer composition and materials used for IF stainings can be found in Table 2-6 and in section 2.9, respectively.

Table 3-9 General IF staining protocol

Step	Condition	Time
Wash (optional)	0.025% TBS-T	10 min
Permeabilization (optional)	0.1-0.5% TBS-T pH 8.2	10 min
Wash	0.025% TBS-T	3 x 10 min
Blocking I	1% BSA/TBS	10 min
Blocking II	5% normal serum (NS)/1%BSA/TBS	30 min
Primary antibody	different concentrations in diluent (Dako)	overnight, 4°C
Wash	0.025% TBS-T	3 x 10 min

Secondary antibody	different concentrations diluted in 5%NS/1%BSA/TBS	2h
Wash	0.025% TBS-T	3 x 10 min
DNA staining	DAPI (in Ampuwa) or Draq5 (in TBS)	15 or 60 min
Wash	Ampuwa or TBS	3 x 10 min
Storage	PBS	4°C

Actin labeling via Alexa Fluor-coupled phallotoxins (Phalloidin) was combined with the secondary antibody incubation step. All steps including the fluorophore were conducted in the dark to avoid photobleaching.

3.4 Confocal multiphoton microscopy

3.4.1 Image acquisition and analysis

Images were acquired using a Leica TCS SP5 confocal microscope equipped with an Argon-, two Helium-Neon- and a Mai Tai HP multiphoton laser. Overview scans and images of small structures such as focal adhesions were obtained by using the 25x (image size 620 x 620 µm) or 63x (98.5 x 98.5 µm) water immersion objective, respectively. Second harmonic generation (SHG), a phenomenon in which two photons of the same wavelength within specific molecular structures generate one photon with halve the wavelength but twice the frequency, was utilized to visualize fibrillar collagen in a label-free manner [164]. Both, porcine collagen of the scaffold as well as newly *in vitro*-deposited collagen mediates the photon conversion by its ordered fibrillar architecture. In this case, the wavelength was set to 910 nm and signal was detected in the range of 450-460 nm. In general, photons were detected either using an internal photomultiplier or an external non-descanned detector (NDD). To compare different samples, all settings like laser power, z-spacing, detection range etc., were kept constant. Recorded images were analyzed in Fiji, a packaged distribution of ImageJ, using different custom-made macros.

Analysis of focal adhesion number and size per cell was performed from Phospho-Paxillin (Tyr118) (#2541, cell signaling) stainings. Recorded z-stacks were transferred into a maximum projection, cell outlines were contoured in the actin-channel and the p-Pax-channel was binarized. Number and size of adhesions per cell were determined by particle tracking. Particle size was categorized and normalized to the total number of particles per cell.

Analysis of signal density and orientation was performed for fibrillar collagen recorded by second harmonic imaging (SHI). For the quantification of collagen density, z-stacks were

summed up and scaffold pores were contoured manually so that only the *in vitro*-deposited collagen was captured. The density was calculated by summing up a background subtracted histogram and dividing it by the ROI (region of interest) area. Orientation distribution was analyzed from maximum projections, which were previously aligned to the pore orientation, using the ImageJ plugin OrientationJ [165].

3.4.2 Live-cell-imaging and analysis

Time-lapse live-cell imaging was performed to investigate migration or actin reorganization processes. Therefore, the Leica TCS SP5 confocal microscope described above, was used in combination with a custom-made incubation chamber and a gassing unit to maintain cell culture conditions.

For migration experiments, cells seeded in collagen scaffolds were stained by cell tracker green (ab145459, abcam) at a dilution of 1:1000 in 0% FBS containing medium for 1h at 37°C. Cells were washed once in cultivation medium and scaffolds were transferred into a custom-made silicone holder mounted in a stainless steel chamber with an optical view field. At minimum four different scaffolds positions were marked and images were acquired every 30 minutes using the 25x objective at a resolution of 512 x 512 pixel with 4 µm z-spacing. Cell migration velocity was analyzed from 3D stacks using the TrackMate [166] ImageJ pugin.

For imaging of actin remodeling processes, hFOB-LA were seeded in 8-well chamber slides (80826, Ibidi) and 5 µm image stacks with a z-spacing of 1 µm were recorded every 6 seconds over 3 min using the 63x objective at 1024 x 1024 pixel resolution. Protrusion dynamics of whole cell protrusions were analyzed using a custom-made Image marco. In brief, z-stacks were projected, cell outlines were contoured for each time point and the area in between two consecutive ROIs was determined. Mean area change over time was calculated for the image sequence. Representative images showing the cell outline change over time were prepared using the QuimP [167] ImageJ plugin.

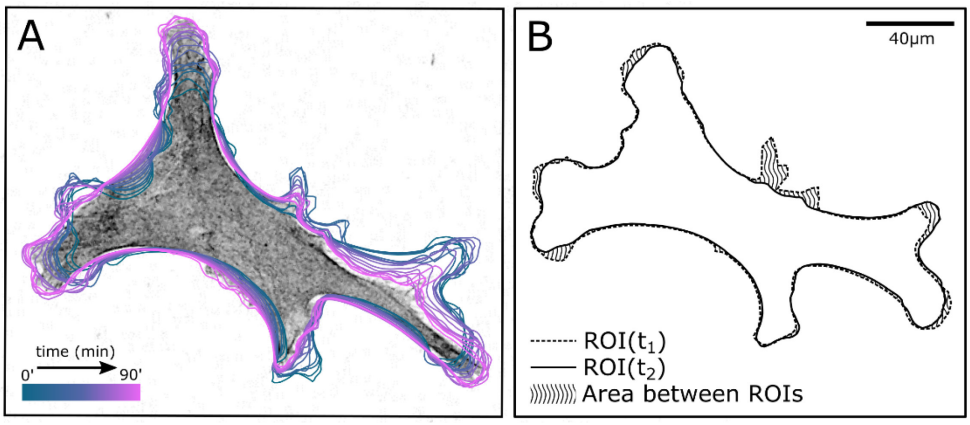

Figure 3-1: Analysis of protrusion remodeling. Exemplary image sequence showing a LifeAct®-transduced hFOB during the course of 90 min (images acquired every 5 min) (A). The recording was processed using the QuimP [167] *ImageJ plugin to illustrate cell morphology changes over time by the color-coded outline. Assessment of the cell area*

change as a measure for actin remodeling dynamics (B). The shaded area between cell outlines indicates the area change from time point 1 to 2 which was measured between all consecutive images using ImageJ.

3.4.3 Mechano-imaging

Bioreactor-Microscope-Setup: To image cell seeded scaffolds in the bioreactor, both the mechanical and the cell culture unit needed to be modified. The lower silicone sealing of the bioreactor chamber, containing the lower plunger and the silicone sample holder, was replaced by a silicone sealing with circular glass window (8 mm diameter, 0.2 mm thickness). The scaffold sample is now positioned directly on the glass window bottom. Due to the changed sample position, the upper star-shaped plunger needed to be replaced by a small round stamp (6 mm diameter), glued to a PEEK mesh of the same size. In the original setup, the bioreactor chamber is resting on the lower arm of the mechanical unit that would block the newly introduced optical window. Therefore, the lower arm was modified by introducing an opening of the size of the glass window. The window can be inserted and clamped tightly into the opening, enabling both sample positioning and imaging.

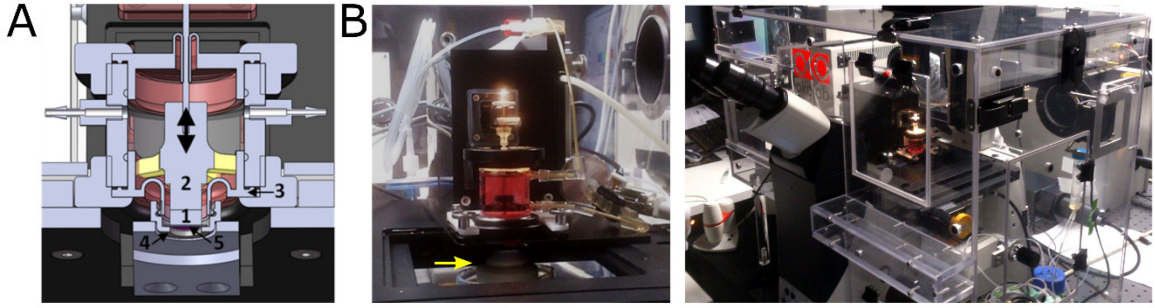

Figure 3-2: Bioreactor-Microscope-Setup. Schematic representation of the modified bioreactor chamber (A) with scaffold (1), modified upper piston (2), modified silicon sealing (3) sample cup (4) and glass window for optical access with inverted microscope (5). Pictures showing the modified bioreactor setup on the Leica TCS SP5 confocal microscope (B). The yellow arrow indicates the microscope objective below the optical window of the chamber.

The modified bioreactor setup was combined with the Leica TCS SP5 confocal microscope by placing the whole mechanical unit on top of the microscope table after removing the condenser head. The gas mixing unit, pump and motor controller were connected and the sample was brought into contact with the upper stamp by using a force-controlled automated sample positioning protocol. After precise positioning, the optical window of the bioreactor chamber was aligned with the 25x or 63x objective for imaging. For straining experiments, hFOB-LA or hFOBs stained with cell tracker green were used. Images were acquired either directly after mechanical loading or during stepwise scaffolds compression.

Flow chamber setup: The Ibidi Pump System, which is owned by the Lab of Petra Knaus at the Freie Univerität Berlin, was used for the application of fluid shear stress to hFOB-LA. The experiments were conducted according to the manufacture´s instruction in collaboration with Dr. Maria Reichenbach. In brief, hFOB-LA were seeded inside µ-slides (80176, Ibidi) at a concentration of $1.2x10^5$ cells/ml one day prior to the flow experiment. Growth medium was

exchanged to FBS-free starvation medium buffered with 20 mM HEPES (L 1613, Merck) and incubated for two hours. µ-Slides were transferred to the Leica TCS SP5 confocal microscope and connected to the pump system also containing HEPES-buffered FBS-free starvation medium. Thereafter, cells were allowed to rest for an additional hour before actin remodeling under static conditions was recorded according to section 3.4.2. Laminar shear stress of 5 dyn/cm^2 was applied and time-lapse images under flow were recorded at time point 10, 30 and 90 min. Subsequently, the inhibitor Jasplakinolide (0.05 µM) was added into the medium reservoir and time-lapse videos were recorded after 10 and 20 min. Actin remodeling dynamics was quantified as described in section 3.4.2.

3.5 Scaffold contraction analysis

Cell-mediated scaffold contraction was assessed by scanning the sample at day one after seeding (t_0) and at the end of the experiment (t_1) using a commercially available digital scanner (Epson Perfection V200). Therefore, samples were placed inside a 48-well-plate filled with expansion medium specific for the cell type used (Table 3-1) and scanned both in top and side view. The cross-sectional area was determined from top views by manual contouring of the scaffold outline. The side view was used for the measurement of the scaffold height by calculation the mean distance between bottom and top. From these values, the total volume contraction (in %) was calculated as described in Figure 2-2.

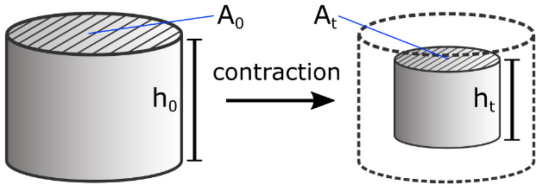

$$V_{(V_0\text{-}V_t)}\,[\%] = \frac{(A_0 * h_0 - A_t * h_t) * 100}{A_0 * h_0}$$

Figure 3-3: Schematic representation of scaffold contraction and calculation of total volume contraction ($V_{(V0\text{-}Vt)}$).

3.6 Mechanical compression tests

The scaffolds mechanical properties were assessed by performing mono-axial compression tests using the BOSE ElectroForce Mechanical TestBench equipped with a 50 g load cell (Model 31 Low load cell, Honeywell Corp.). To calculate the elastic modulus from the data obtained by compression testing, the scaffold-dimensions were assessed prior to the measurement. Empty scaffolds or native cell seeded scaffolds were placed into a custom-made chamber filled with PBS. The chamber consists of the same upper and lower star-shaped plunger that were also used in the bioreactor, to which PEEK meshes are glued distributing the applied force. Three consecutive compression cycles at a speed of 0.05 mm/s and a displacement of 10 or 20% of the scaffold height (adjusted for each sample individually) were performed with a resting time of 30 seconds at 0, 10 and 20% displacement.

Recorded load/displacement curves were converted into stress (σ)/strain (ε) curves according to:

$$\sigma[Pa] = \frac{m * g}{A} \qquad 3.1$$

m = mass [g]
g = 9.81 m/s² (gravitational acceleration)
A = cross sectional area [m²]

$$\varepsilon = \frac{l}{\Delta l} \qquad 3.2$$

l = length [m]
Δl= change in length [m]

The Young's modulus, as a measure for the material stiffness, corresponds to the slope of the stress/strain curve in the linear region (equation 3.3).

$$E\ [Pa] = \frac{\sigma}{\varepsilon} \qquad 3.3$$

3.7 Decellularization after *in vitro* tissue formation

Scaffolds seeded with hdF were cultured for two weeks in the bioreactor as described in section 3.1.6.3. In preparation for mass spectrometry analysis of the ECM, cellular components were removed from *in vitro*-grown micro-tissues by detergent-based decellularization and DNA digestion using DNase I. Decellularization was performed in an in-house developed perfusion system consisting of individual sample chambers connected via silicone tubes to a peristaltic pump and detergent reservoirs. Samples were actively perfused with a fluid velocity of 2.5 ml/min. The decellularization protocol used here (Table 3-10) was previously established and optimized to preserve many soft ECM components while removing most of the cellular components.

Table 3-10: Perfusion protocol

Step	**Condition**	**Time**
ddH_2O	sterile deionized water with 1x cOmplete™ protease inhibitor and 5 mM Tris (pH 8)	60 min
detergent treatment	0.05% SDS in deionized water	20 min
PBS wash	PBS with Ca^{2+}/Mg^{2+}	2 x 20 min
DNA digestion	DNasesI (350U/ml) dissolved in PBS (with Ca^{2+}/Mg^{2+})	5h
detergent treatment	0.025% SDS in deionized water	20 min
wash	sterile deionized water	20 min

Thereafter, samples were frozen at -80°C and subsequently freeze dried.

3.8 Mass spectrometry

Mass spectrometry of decelluarized samples was performed by the Core Unit "Tissue Typing" and conduced as described previously [168]. In brief, decelluarized and freeze dried samples were subjected to tryptic digestion at 37 °C for 3h and overnight. Peptides were extracted with trifluoridic acid (0.1% (w/v)), desalted with ZipTip and analyzed by LC/ESI–MS. Peptides were separated using an analytical UHPLC System (Dionex Ultimate 3000 RSLC, Thermo-Fisher) and analyzed by a ESI-QTOF-mass spectrometer (Impact II, Bruker). Mass spectra were evaluated using PEAKSX+ software (PEAKS Studio 10.5 (Bioinformatics Solutions Inc., Waterloo, Canada) [169] automatically searching the SwissProt database. MS/MS ion search was performed with the following set of parameters: a) taxonomy: homo sapiens (human) (20366 sequences); b) proteolytic enzyme: trypsin; c) maximum of accepted missed cleavages: 2; d) mass value: monoisotopic; e) peptide mass tolerance 10 ppm; f) fragment mass tolerance: 0.05 Da; and g) variable modifications: oxidation (M), deamidation (N,Q) and acetylation (N-therm). Only proteins with scores corresponding to $p < 0.01$ and with at least two identified peptides were considered.

3.9 Statistical analysis and data presentation

Data analysis was performed using Microsoft Excel 2016. The OriginPro 2015G (OriginLab Corporation) software was used for the graphical presentation and statistical analysis of the obtained data. Box and line plots show mean values with standard deviation. Box and whisker plots display the maximum and the minimum, the upper and lower quartile and the median marked as a horizontal line of all data points. For statistical analysis, the non-parametric, two-sided Mann- Whitney-U test was performed. For the comparison of multiple groups the *p*-value was corrected according to the Bonferroni method using the following equation:
$p^* = p \cdot n$, with n=number of statistical tests. P values < 0.05 were considered as statistical significant. Different significance levels are indicated as: # $p<0.1$; * $p<0.05$; ** $p<0.01$; and *** $p<0.001$.

4 Results

4.1 Load-induced osteogenic differentiation via BMP-2

In the first part of this thesis, the direct influence of cyclic mechanical loading on the osteogenic differentiation of primary human bone marrow MSCs (hBMSCs) is being investigated and dissected from the effect of load-induced autocrine signaling, in particular of BMP-2. Multiple studies examined the influence of mechanical loading on stem cell differentiation, including osteogenic commitment (see section 1.3.3 and reviews [55], [170]). Motivated by a tissue engineering approach, the majority of these studies used osteoinductive medium supplements, bone derived scaffolds or hydrogels with limited supply masking effects of loading on cell fate decision. Even in studies working without additional osteogenic triggers, the influence of load-induced autocrine signaling was not investigated. Therefore, it still remains unclear whether the observed mechano-sensitivity is a direct consequence of cyclic compression, an indirect effect of altered supply or a specific modulation of autocrine BMP signaling.

To elucidate this, special emphasis was put on the selection of the experimental setup and its physiological relevance. Therefore, the *in vitro* setup used here was specifically chosen to resemble the mechanical environment during the early phase of bone healing as it was observed *in vivo*. The bioreactor was used to simulate interfragmentary compression that occur as a consequence of weight bearing in the rage of reported data for external fixation in bone healing in sheep [37], [43], [159]. The utilized scaffolds are characterized by low elastic moduli mimicking the soft tissue matrix in the fracture gap and have been shown to successfully induced endochondral ossification in a rat bone defect model [11]. Due to its elastic deformation behavior, the material withstands repetitive compression, as it was shown previously [171]. As the stiffness of the substrate that cells adhere to is known to be an important regulator influencing cellular behavior [56], scaffolds with bulk stiffnesses of 3.4 kPa (scaffold A) and 12.3 kPa (scaffold B) were used in this study (Figure 4-1A). To additionally strengthen the *in vivo* relevance, primary hBMSCs obtained from at least five donors were used.

4.1.1 Cell morphology, proliferation and oxygen concentration inside scaffolds cultured in the bioreactor

Bioreactor cultivation and cyclic compression might have altered the cell morphology and proliferation that could cause differences in the later on investigated migration and differentiation behavior. Therefore, it was verified in the beginning that neither bioreactor culture, nor cyclic compression have major influences on cell morphology and number by

comparing hBMSC-seeded scaffolds cultured for seven days in the bioreactor (with and without cyclic compression) to hBMSC-seeded scaffolds cultured for one and seven days in the cell culture incubator (static). Images acquired using confocal multiphoton imaging (Figure 4-1B), showed no differences in cell distribution and morphology between different culture time points (one or seven days) and conditions (static, bioreactor without cyclic compression, bioreactor with cyclic compression). Cells were homogeneously distributed throughout the scaffold and showed an elongated morphology in the direction of the scaffold pores. Analysis of the cell density seven days after seeding neither showed significant differences between static and bioreactor culture nor an alteration in response to cyclic compression (Figure 4-1C). The comparison with the cell density one day after seeding revealed that the cells remained viable but did not proliferate significantly in the microenvironment provided by the scaffold. The oxygen concentration, measured by opto-chemical microsensors introduced into the sample, showed only a slight decrease from the surface (20.7/20.5%) to the center of the sample (18.9/18.5%) at day 3/7 of culture (Figure 4-1E).

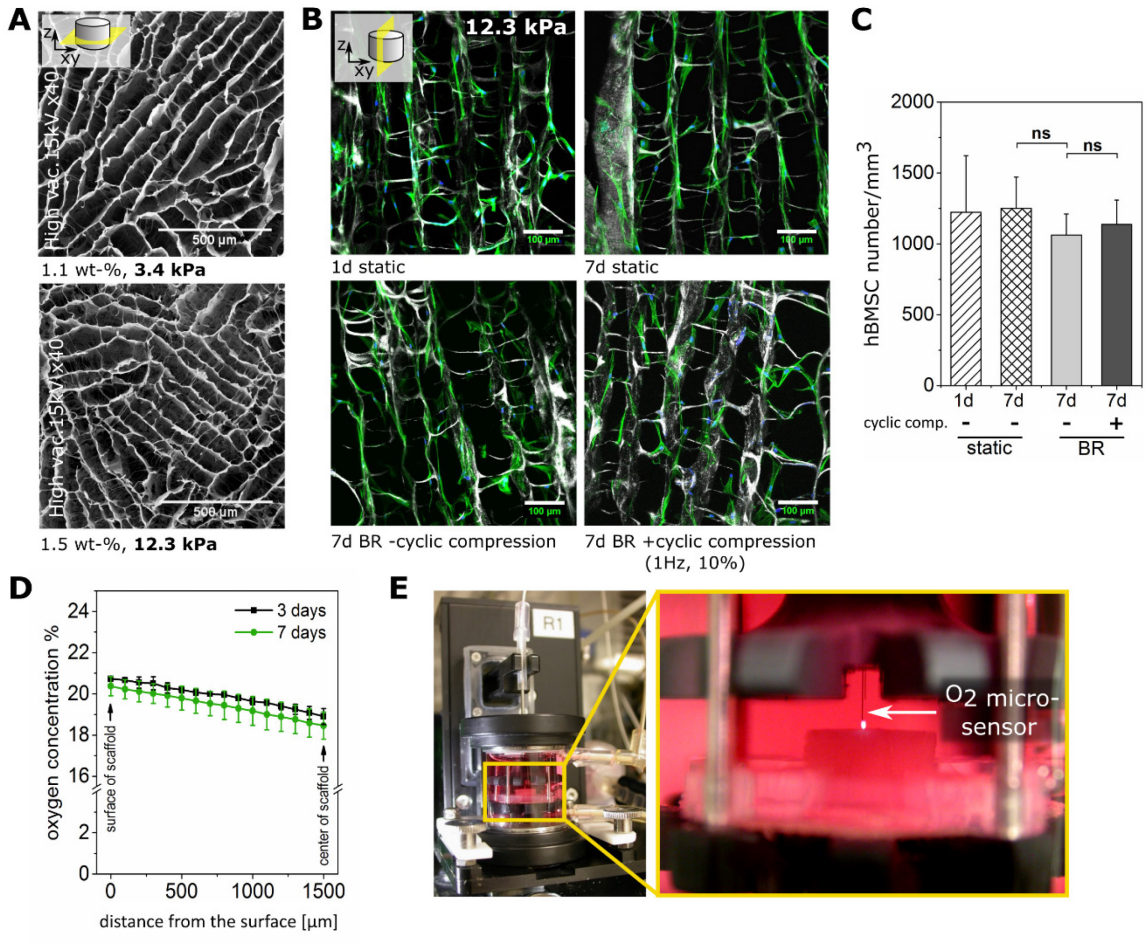

Figure 4-1: Bioreactor setup validation. (A) Electron microscopy image of the two scaffold prototypes with collagen solid contents of 1.1 and 1.5 wt-%. (B) Bioreactor consisting of reactor chamber (1), medium reservoir (2), micro pump (3), filter (4), pressure equalization tube (5) and the mechanical unit (6). (C Close-up of the bioreactor chamber with collagen scaffold inserted. (D) Human BMSCs obtained from three donors were seeded in collagen scaffolds and

cultured for one or seven days in well plates under static conditions or in the bioreactor with and without cyclic compression (f=1Hz, 10% axial compression). Representative confocal images showing hBMSCs in the collagen scaffold (white), stained with phalloidin (green) and DAPI (blue) to visualize the F-actin fibers and the cell nuclei, respectively. (E) Cell density (cells/mm^3) inside the scaffold as analyzed from confocal image stacks (mean ± SD, 3 donors, ns = not significant). (F) Concentration of oxygen measured inside the scaffold depending on the distance from the scaffold surface (mean ± SD, n=2 scaffolds per time point). Figure modified from [172] *with permission form the publisher.*

This verified that the cells were well-supplied even in the center of the scaffold throughout the duration of the experiment. Consequently, a potentially improved supply resulting from enhanced fluid flow under cyclic compression could be excluded. Thus, the effects of cyclic compression on gene expression and protein secretion reported in this study could be linked to direct mechanical consequences of cyclic compression. In contrast, supply in other, less open-porous biomaterials might be significantly enhanced by cyclic compression (reduced hypoxia, increased viability) as reported before for cell-seeded fibrin hydrogels [173].

4.1.2 Cyclic mechanical compression downregulates the expression of key osteogenic marker genes but upregulates BMP-2 expression

Next, the impact of cyclic mechanical compression on the mRNA expression of osteogenic marker genes was quantified by qPCR (Figure 4-2). Therefore, hBMSCs were seeded in collagen scaffolds and subjected to cyclic compression of 5% and 10% magnitude. Surprisingly, the median fold-change mRNA expression levels of RUNX2 (early transcription factor for osteogenesis) were reduced in both scaffold types in response to 10% compression, with statistical significance for scaffold A [$\widetilde{FC}(RUNX2)_{scaffA,10\%}$= 0.8, p = 0.0002; $\widetilde{FC}(RUNX2)_{scaffB,10\%}$= 0.81]. Cyclic compression of 5% significantly decreased the RUNX2 expression in scaffold A [$\widetilde{FC}(RUNX2)_{scaffA,5\%}$= 0.7, p = 0.01] while no change was visible in scaffold B [$\widetilde{FC}(RUNX2)_{scaffB,5\%}$= 0.98]. The median mRNA expression of osteocalcin (BGLAP) and collagen type 1 α 2 (COL1A2) were also decreased for both scaffold stiffnesses and loading magnitudes in comparison to the uncompressed controls. Statistical significant downregulation was reached for BGLAP in response to 10% compression in scaffold B [$\widetilde{FC}(OC)_{scaffB,10\%}$= 0.56, p= 0.0007].

The median expression of osteopontin (SPP1) under 5% cyclic compression remained unchanged, whereas 10% compression significantly increased the SPP1 expression for the softer scaffolds [$\widetilde{FC}(OP)_{scaffA,10\%}$= 2.24, p = 0.01] but not for the stiffer. Interestingly, mechanical stimulation induced an upregulation of BMP-2 mRNA expression in scaffold B at 5 and 10% and in scaffold A at 10% compression. Statistical significance was reached at 10% compression in scaffold B [$\widetilde{FC}(BMP2)_{scaffB,10\%}$= 1.5, p = 0.02].

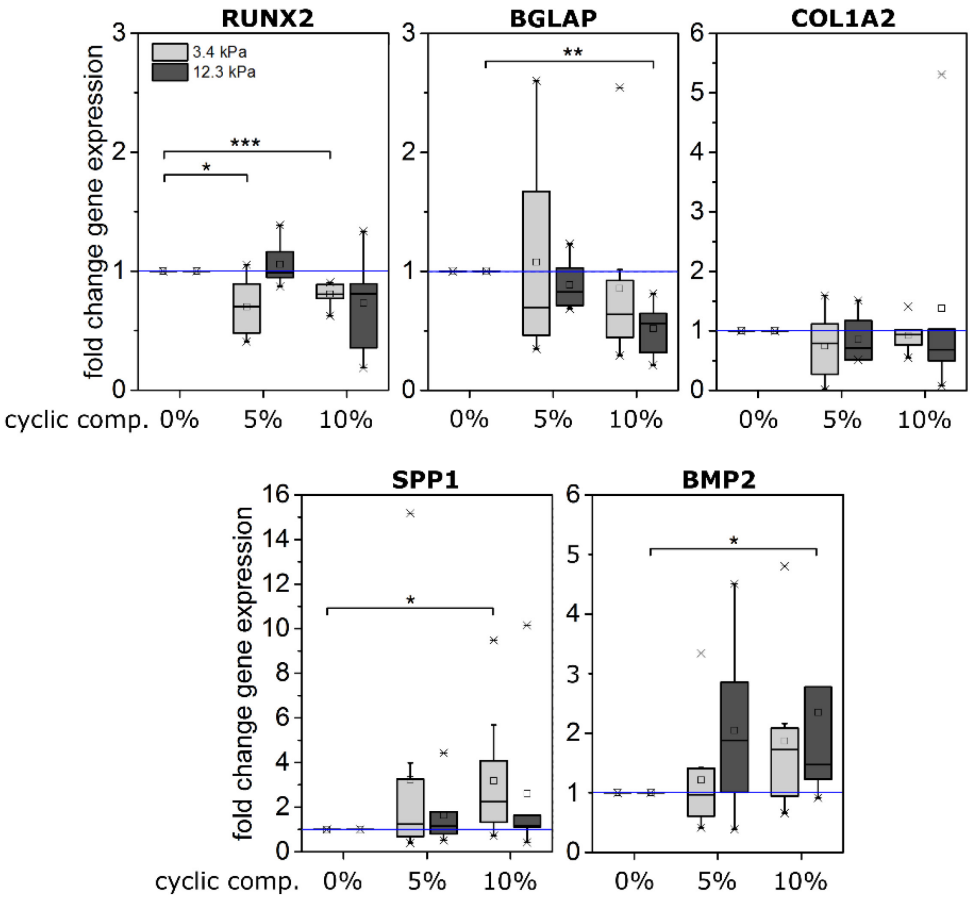

Figure 4-2: Cyclic compression downregulates the expression of key osteogenic marker genes but upregulates BMP2 expression. Human BMSCs obtained from various donors were seeded in collagen scaffolds of 3.4 kPa (n=8 donors)/ 12.3 kPa (n=6 donors) stiffness, respectively. Scaffolds were cultured in the bioreactor and stimulated with 5% or 10% intermittent cyclic compression or left unstimulated (0%). mRNA expression was analyzed by qPCR. Fold change expressions to the 0% control group of the respective scaffold type are depicted in box and whisker plots. Figure reproduced from [172].

In summary, we found a clear downregulation of important osteogenic marker genes, especially of RUNX2, in response to cyclic mechanical compression. However, BMP-2, a potent inducer of osteogenic differentation, was clearly upregulated under 10% cyclic compression.

4.1.3 Limited biochemical conditioning of the culture medium during bioreactor culture

To study whether the observed increase in BMP-2 gene expression resulted in an increased protein secretion, BMP-2 protein concentrations were analyzed using an enzyme-linked immunosorbent assay (ELISA) specific for human BMP-2 (Figure 4-3). Since BMP-2 gene expression was significant upregulation in hBMSCs seeded in scaffold B (12.3 kPa) and stimulated with 10% cyclic compression, this condition was analyzed in comparison to the unstimulated control (0%).

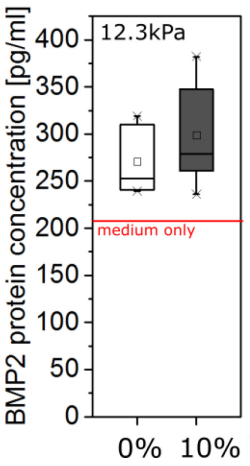

Figure 4-3: Low BMP-2 concentrations in the conditioned medium. BMP-2 concentration in the conditioned bioreactor media was analyzed using a human BMP2 ELISA. Only the medium of hBMSCs seeded in scaffold B (12.3 kPa) and stimulated with 10% intermittent cyclic compression was analyzed in comparison to the unstimulated control (0%), as this condition induced a significant upregulation of BMP-2 gene expression. Figure modified from [172].

In agreement with the expression data, a slight increase of BMP-2 secretion was detected in culture media of samples stimulated with 10% compression [$\tilde{\beta}(BMP2)_{0\%}$= 252 pg/ml, $\tilde{\beta}(BMP2)_{10\%}$= 280 pg/ml]. However, the detected BMP-2 concentrations were in general very low and only slightly above the BMP-2 concentration detected in the culture medium without cells. According to Katagiri [174], these concentration are not capable to stimulate an osteogenic response. This result can be explained by the comparably low cell number in respect to the large medium volume ($1.5x10^5$ cells/ 27 ml medium = $5.6x10^3$ cells/ml) in the bioreactors. The cell-to-medium ratio in the bioreactor was approximately nine times lower compared to typical 2D culture conditions ($5x10^4$ cells/ml). Therefore, the gene expression data shown in Figure 4-2 was obtained from bioreactor experiments under a strong dilution of secreted proteins. The observed gene regulations thus represented consequences of cyclic compression without relevant contributions of autocrine biochemical stimulation.

4.1.4 Cyclic mechanical compression enhances RUNX2 mRNA expression only in a BMP-enriched environment

With the goal to promote medium conditioning and autocrine BMP-2 signaling, the ratio between cell number and medium volume was increased in subsequent experiments. The number of scaffolds per bioreactor was increased from one to five and the medium volume was reduced from 27 ml to 12 ml (minimal filling volume of the bioreactor) resulting in an increase in cell-to-medium ratio from R_{low}=$0.56x10^4$ to R_{high}=$6.25x10^4$ cells/ml. Additionally, we conducted separate control experiments where 5 nM (135 ng/ml) recombinant human BMP-2 (rhBMP-2) was added at day 4 of bioreactor cultivation, to compare the impact of medium conditioning to direct BMP-2 stimulation. These experiments were conducted using the 12.3 kPa scaffold and the five donors of the six that showed a consistent downregulation in RUNX2 expression upon cyclic compression.

As expected, the increase in cell-to-medium ratio enabled a significant 5.5-fold increase of BMP-2 concentration (p = 0.004) in the cell culture medium from $\tilde{\beta}(\mathrm{BMP2})_{\mathrm{Rlow,-cyclic\ comp.}}$ = 252 pg/ml to $\tilde{\beta}(\mathrm{BMP2})_{\mathrm{Rhigh,-cyclic\ comp.}}$=1395 pg/ml (Figure 4-4B, light grey vs. light blue box). In response to cyclic compression the BMP-2 concentration increased slightly but significantly (Fig. 4B, dark blue vs. light blue box, [$\tilde{\beta}(\mathrm{BMP2})_{\mathrm{Rhigh,+cyclic\ comp.}}$ = 1623 pg/ml]). This is in agreement with the observed increase in BMP-2 gene expression under load strengthening the assumption that cyclic compression triggers a positive feed-forward loop for BMP-2.

Next, we analyzed the concentration of BMP-2 in the conditioned media collected from bioreactors that were supplemented with rhBMP-2. Also here mechanical loading increased BMP-2 concentration slightly but non-significantly (Figure 4-4B, dark vs. light orange box). It has to be mentioned that the detected BMP-2 concentrations were overall very low compared to the initially added amount of rhBMP-2 (135 ng/ml). To understand this discrepancy, we analyzed the BMP-2 stability in the bioreactor. Therefore, 135 ng/ml rhBMP-2 was added to the bioreactor experiment (conducted without cells) and medium samples were collected after 30min and at day 1, 3, 5 and 7 (supplementary Figure 0-3). Already after one day, the BMP2 concentration decreased to about one third and declined further during culture. Together this indicated that BMP-2 stability is transient under cell culture conditions.

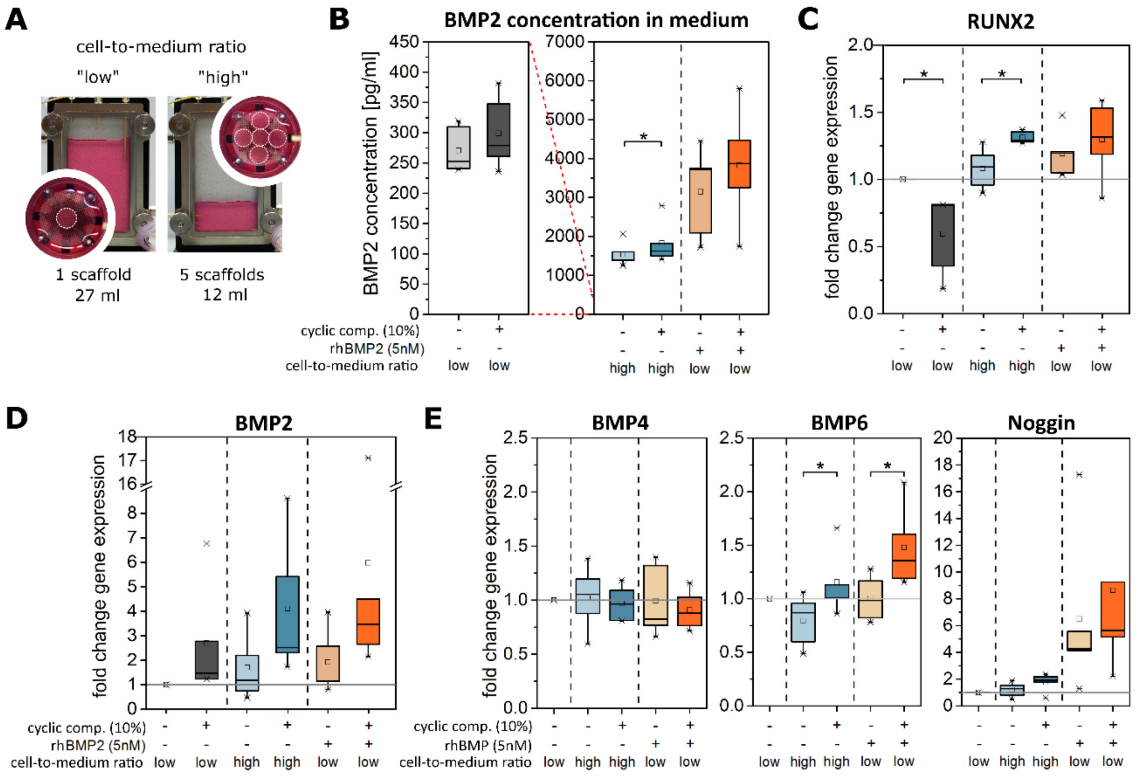

Figure 4-4: Cyclic compression only increases RUNX2 expression, if rhBMP2 is added or an enrichment of cell-secreted BMP2 in the cell culture medium was permitted. Data was obtained from three different experimental conditions: 1. Human BMSCs were seeded in collagen scaffolds (12.3 kPa) and cultured with or without cyclic compression (f=1Hz, ε=10%) for six days. 2. BMSCs were additionally stimulated with recombinant human BMP2 (rhBMP2, 5nM) added at the fourth day of cultivation (+ rhBMP2). 3. The cell number was increased five times and the medium volume was reduced from 27ml to 12ml ("high cell-to-medium ratio"). (A) Illustration of low vs high cell-to-medium ratio. (B) Human BMP2 ELISA of collected bioreactor media from all loading experiments was conducted. The relative gene expressions of (C) RUNX2, (D) BMP2, (E) BMP4, -6 and Noggin normalized to the untreated control (low cell-to-medium-ratio, without cyclic compression) (n=5 hBMSC donors B-E). Figure reproduced from [172].

Signaling initiated by BMP-2 directly stimulates the expression of RUNX2 and balances its transcriptional activity [175], [176]. Therefore, BMP-2 is an important trigger for early osteogenic responses. Consequently, the observed upregulation of BMP-2 expression in response to mechanical loading led us to the assumption that hBMSCs would trigger themselves towards osteogenic differentiation (enhance RUNX2 expression) in response to cyclic loading under increased cell-to-medium ratio R_{high}.

Strikingly, under R_{high} conditions, RUNX2 expression was significantly upregulated in response to cyclic compression in comparison to the uncompressed control (Figure 4-4C, dark blue box, $[\widetilde{FC}(RUNX2)_{Rhigh,+cyclic\ comp.} = 1.3, p = 0.036]$). This finding stands in strong contrast to the regulation of RUNX2 in response to cyclic loading under R_{low} conditions in the original setup (Figure 4-4C, gray box, $[\widetilde{FC}(RUNX2)_{Rlow,+cyclic\ comp.} = 0.8, p = 0.021]$). Additionally, RUNX2 expression under rhBMP-2 supplementation was also further enhanced by cyclic compression (Figure 4-4C, dark orange box $[\widetilde{FC}(RUNX2)_{+rhBMP2,+cyclic\ comp.} = 1.3]$). This indicated that BMP-2 is capable to alter the cell's gene expression response to mechanical loading. Moreover, in response to (i) the increase of the cell-to-medium ratio from R_{low} to R_{high}

and (ii) the supplementation of rhBMP-2, concurrent cyclic compression further enhanced the expression of BMP-2, suggesting a positive feed-forward regulation by biochemical self-stimulation (Figure 4-4D, dark blue and dark orange box, [$\widetilde{FC}(BMP2)_{Rhigh,+cyclic\ comp.}$= 2.5, $\widetilde{FC}(BMP2)_{+BMP2,+cyclic\ comp.}$= 3.5]).

To investigate the involvement of possible further feed-forward components we also analyzed the expression of BMP-4, -6 and -7, as well as the expression of the BMP antagonist Noggin (Figure 4-4E). Expression of BMP-4 was not affected by neither condition and BMP-7 transcription was not detected. BMP-6 expression, instead, was found to be sensitive to cyclic compression. Under rhBMP-2 supplementation, loading induced a 1.4-fold increase in BMP-6 transcription, while in the R_{high} condition, only a slight 1.1-fold increase was detected. Taking into account the observed mechano-sensitivity of BMP-6 expression, a potential contribution to the RUNX2 regulation cannot be excluded. However, in comparison to the according changes in BMP-2 expression, the contribution of regulations in BMP-6-expression are regarded to be low. Noggin expression strongly increased by 4.3-fold in response to rhBMP-2 treatment and increased further to 5.6-fold by cyclic compression. Under high cell-to-medium ratio, cyclic compression increased Noggin transcription by 1.9-fold. The regulation of Noggin expression under both conditions is line with the increased BMP2 expression and medium concentration. Noggin inhibits BMP2, -4, -7 and -14 from binding to the BMP receptor. BMP6 however is more resistant to noggin inhibition [177]. Additionally, the expressions of Transforming growth factor beta-1 and 3 (TGFβ1 and β3), Fibroblast Growth Factor-2 (FGF2), Platelet-derived Growth Factor-A (PDGF) and Vascular Endothelial Growth Factor-A (VEGF-A) that are of relevance in osteogenic differentiation were analyzed (supplementary Figure 0-2). FGF-2 and PDGF-A expressions were not regulated by any of the treatments. TGFβ1, TGFβ3 and VEGF-A expressions were increased in response to cyclic compression under rhBMP-2 stimulation. However, in the high cell-to-medium ratio group, only the expression of TGFβ3 was increased by 1.35-fold upon cyclic compression, while the others were not consistently regulated. No statistical significant differences could be found. Therefore, in comparison to the 2.5-fold change in BMP-2 expression change under cyclic compression ($\widetilde{FC}(BMP2)_{Rhigh,+cyclic\ comp.}$= 2.5) only modest changes were detected.

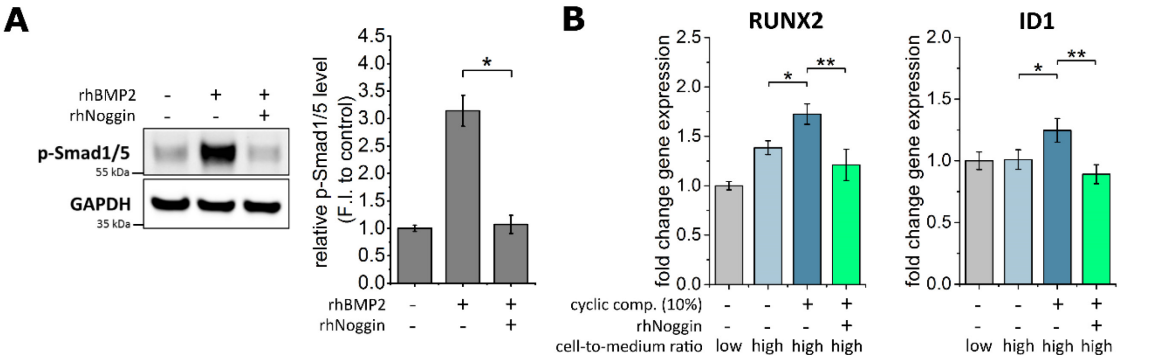

Figure 4-5: Cyclic compression does not increase RUNX2 expression, if BMP signaling is inhibited by rhNoggin. (A) Validation of rhNoggin efficiency by western blot analysis of p-Smad1/5 level after rhBMP2 stimulation. Phosphorylation was normalized to GAPDH (n=3, one donor). (B) Scaffolds were cultured under high cell-to-medium ratio with or without 10% cyclic compression and with or without rhNoggin stimulation (100ng/ml, added at day 1, 3, 5) and RUNX2 and ID1 expression were analyzed. Gene expressions were analyzed by qPCR. HPRT1 was used as the reference gene and expressions were normalized to the untreated control (low cell-to-medium-ratio, without cyclic compression) (n≥4 for one donor). Figure reproduced from [172].

To finally verify that the load-induced increase in RUNX2 expression is mediated by BMP-2, in the next experiment BMP-2 was depleted from the system by recombinant human Noggin. At first, the effect of the rhNoggin on BMP signaling was validated in a separate experiment by western blot analysis investigating the phosphorylation of the transcription factor Smad1/5 (Figure 4-5A). While Smad1/5 phosphorylation was increased by 3-fold in response to 5 nM rhBMP-2, no increase was detected if cells were treated with rhBMP-2 and rhNoggin (12 nM). Next, for the proof of concept experiment, one hBMSC donor representing the group was selected. Cells were cultured under R_{high} conditions with or without cyclic compression and rhNoggin (100 ng/ml equals 2.2 nM) which was added at day 1, 3 and 5. Again RUNX2 expression was significantly upregulated in response to cyclic compression, however treatment with rhNoggin abolished the effect of compression completely. The RUNX2 expression was significantly reduced when rhNoggin was supplemented. Furthermore, the expression of ID1 (inhibitor of DNA binding 1), a common only used BMP target gene, was investigated. Under R_{high} conditions, ID1 expression was significantly induced by cyclic compression and significantly reduced by rhNoggin treatment (Figure 4-5B).

Taken together, the results show that cyclic compression strongly downregulated the expression of RUNX2 when the cell-to-medium ratio was low and BMP self-conditioning was impeded by dilution. However, after increasing the ratio, cyclic compression significantly upregulated RUNX2 expression. Both observation, (i) that rhBMP-2 stimulation led to a very similar result as the increase in cell-to-medium ratio and (ii) that the load-induced effect on RUNX2 and ID1 expressions were abolished by rhNoggin treatment, verify the role of BMP-2 as the relevant mechano-regulated signaling factor controlling RUNX2 and consequently osteogenesis.

4.2 Mechanistic investigations on the crosstalk between mechano-transduction and BMP signaling

So far it was found, that the increased BMP expression in response to cyclic compression contributes to a positive feed-back loop enhancing RUNX2 expression. In addition, cyclic compression not only increases the expression of but also the sensitivity for BMP-2. In a ligand dependent manner, mechanical stimulation was shown to enhanced BMP-2-signaling. Even though the mechano-regulation of BMP signaling was described previously, still many questions are unanswered: Is the observed mechano-regulation a general phenomenon, or exclusive for some cell types? What mechanical requirements need to be met to regulate BMP signaling? How is the dynamics of BMP signaling altered? Which mechanotransduction pathway is involved? The following part aims to address those questions.

4.2.1 The crosstalk is relevant in primary human cells of the mesenchymal lineage

The regulation of the BMP signaling pathway by external mechanical stimuli has been described in several cell types, including cell lines like C2C12 myoblasts [178], MC3T3-E1 [179] and human fetal osteoblasts (hFOB) [125] as well as primary cells like murine and rat osteoblasts [123], [127] or human vascular endothelial cells [128]. However, primary human cells from the mesenchymal lineage have not been tested so far.

For the relevance of the study and to investigate the influence of BMP-2 and mechanical stimulation on extracellular matrix formation (section 4.3) and osteogenic differentiation (section 4.1), it was required to verify the existence of the crosstalk in primary human fibroblasts and MSCs. Therefore, Smad1/5/8 phosphorylation, an immediate early event downstream of the BMP receptor, was investigated in hMSCs and hdFs upon treatment with BMP-2 and mechanical loading. The cell line hFOBs, which was used in a previous study investigating the mechano-regulation of BMP signaling [125], was selected as a reference. The conditions selected for the experiments (duration and loading parameters) have been validated in hFOBs (see section 4.2.2) before and were found to result in maximum crosstalk strength.

Cell-seeded collagen scaffolds were subjected for 90 min to BMP-2 stimulation, cyclic uniaxial compression (e=10% of the scaffold height, f= 1Hz) or a combination of both and Smad1/5/8 phosphorylation was analyzed by western blotting. BMP-2 treatment resulted in an increase in Smad phosphorylation, which was notably the highest for hdF. Importantly, concurrent mechanical loading led to the significant increase of the BMP-2-induced Smad phosphorylation consistently in all cells tested. Even though the fold change increase of B/L

to the control is the same for hFOBs and hdF, the effect of loading reflected by the difference between B/L and B is the highest for hFOBs. In none of the cells, mechanical stimulation alone was not able to induce a phosphorylation of Smads. Taken together the results obtained here with the studies mentioned above, it can be suggested, that the effect of external mechanical stimuli on BMP signaling represents a fundamental regulatory mechanism to control the effectiveness of BMPs.

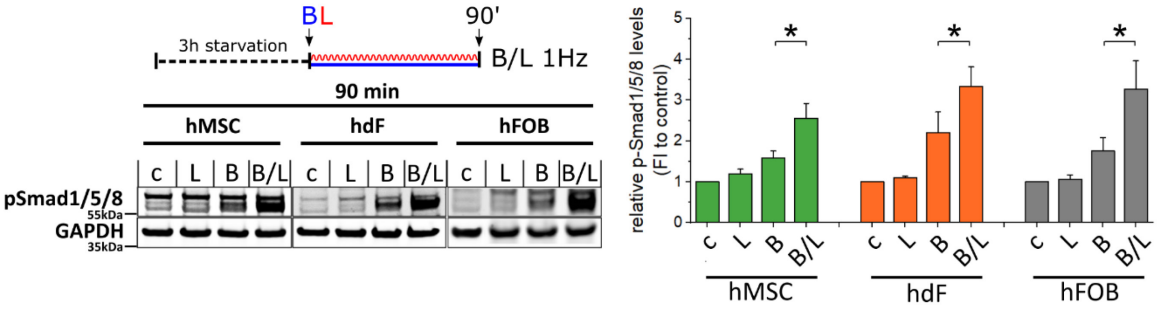

Figure 4-6: Cyclic mechanical compression significantly increases the BMP-2-induced Smad1/5/8 phosphorylation in human primary MSCs and dermal fibroblasts (hdF). hFOBs, hMSCs and hdFs seeded in collagen scaffolds were subjected for 90 min to BMP-2 stimulation, cyclic uniaxial compression (e=10% of the scaffold height, f= 1Hz) or a combination of both. Thereafter, cells were lysed and Smad1/5/8 phosphorylation levels were determined via western blotting. Signal intensities were related to GAPDH and the fold changes to the untreated controls were calculated, n=3 from one donor.

4.2.2 Correlation between loading frequency and crosstalk duration

The crosstalk between mechanotransduction and BMP signaling was shown to be induced by different mechanical forces, including laminar and oscillatory shear stress [124], [127], [128], mechanical stretch [180] and compression [123], [125]. However, a systematic investigation of how different loading parameters of the same force magnitude influence the duration and strength of BMP signaling is missing. Such investigations would, however, be important to defined parameters optimally supporting BMP signaling and furthermore, to gain insides into the dynamics of this regulation. Therefore here, the impact of the loading frequency on early BMP signaling events was investigated in a time-dependent manner.

Collagen scaffolds seeded with hFOBs were subjected for 30, 90, or 120 min to BMP stimulation and cyclic mechanical compression of selected frequencies (0.03 Hz, 1 Hz and 10 Hz) and Smad1/5/8 phosphorylation was examined via western blotting (Figure 4-7 A-D). The expression of ID1 and ID2, early BMP target genes, was analyzed after 90 min by qPCR (Figure 4-7 E).

Already after 30 min, mechanical stimulation induced a significant increase in Smad phosphorylation in comparison to the BMP-only treated control for all frequencies applied. However, the crosstalk induced by 0.03 Hz loading was significantly reduced in comparison to 1 Hz, while no significant difference was detected between 1 Hz and 10 Hz. After 90 min of

stimulation, the maximum increase in Smad phosphorylation was reached for 1 Hz and 10 Hz loading, while 0.03 Hz could not maintain the crosstalk. Whereas the Smad phosphorylation induced by 1 Hz loading decreased after 120 min to the level of the BMP-only treated control, high frequency loading with 10 Hz maintained the maximum phosphorylation level, therefore inducing a prolonged crosstalk. The frequency dependent phosphorylation of Smads is furthermore reflected in the expression level of ID1 and ID2. Especially the ID1 transcription increases with increasing frequency. Interestingly, even 0.03 Hz loading, which only mildly and transiently increased the Smad phosphorylation, increased the ID1 expression by two-fold.

Taken together, a positive correlation between the frequency of mechanical loading and the duration of the crosstalk was observed, which is indicated by a prolonged increase of Smad phosphorylation.

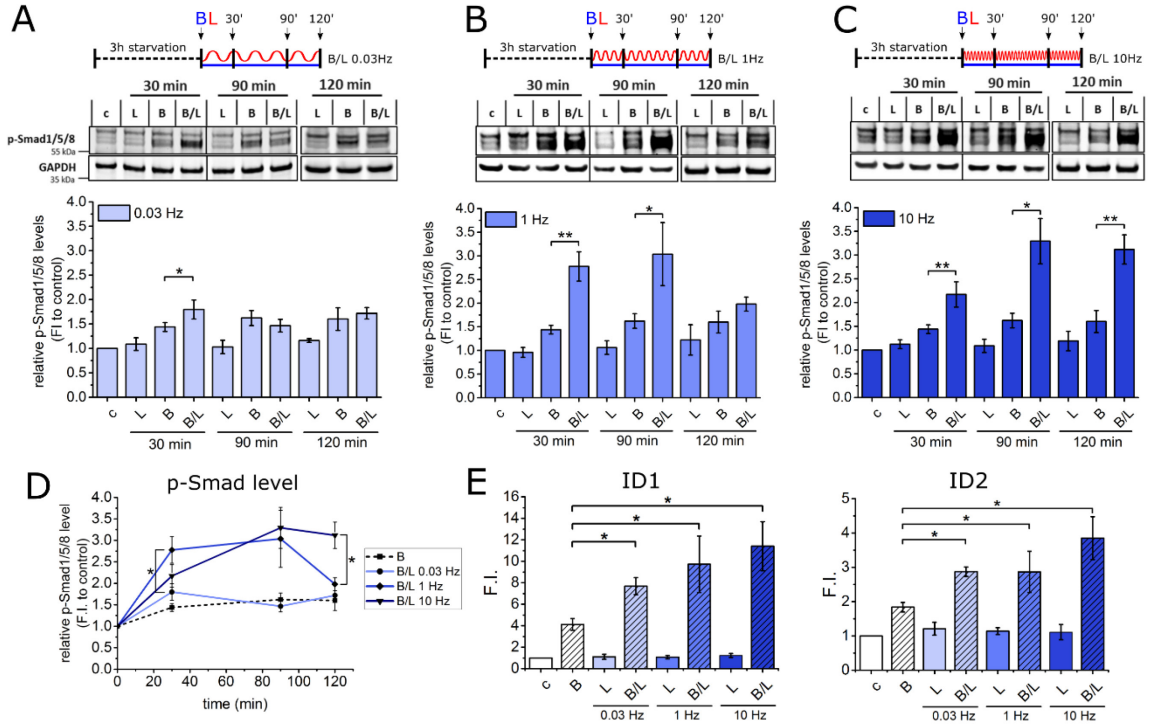

*Figure 4-7: Loading frequency influences strength and duration of Smad1/5/8 phosphorylation and ID gene expression. Human FOBs seeded on collagen scaffolds were subjected for 30, 90 or 120 min to BMP-2 stimulation, mechanical loading (10% compression) or a combination of both. Loading frequencies of 0.03 Hz, 1 Hz and 10 Hz were applied to analyze the impact on (A-D) SMAD1/5/8 phosphorylation, determined using western blot analysis and on (E) ID1 and ID2 expression, determined via qPCR (relative to HPRT expression) (n = 3, *p < 0.05, **p<0.01).*

To further examine whether the initial frequency-dependent effects on Smad phosphorylation and early gene expression persist or equilibrate at a later time point, hFOBs were continuously stimulated for 24h with BMP-2 and mechanical loading. Since 0.03 Hz was not expected to cause any changes in comparison to the BMP-treated control, this condition was excluded from further examinations. Direct BMP-targets, osteogenic markers and genes

related to the perception of mechanical forces were included in the evaluation. The heatmap summarizes the regulation of the tested genes with induction or reduction of expression labeled in red or blue, respectively (Figure 4-8). The predominantly red-colored heatmap clearly illustrates the overall anabolic effect of the treatments. The expression analysis indeed revealed a frequency-dependent increase of transcription even after 24h. For all genes regulated, the response to 10 Hz loading was stronger in comparison to 1 Hz.

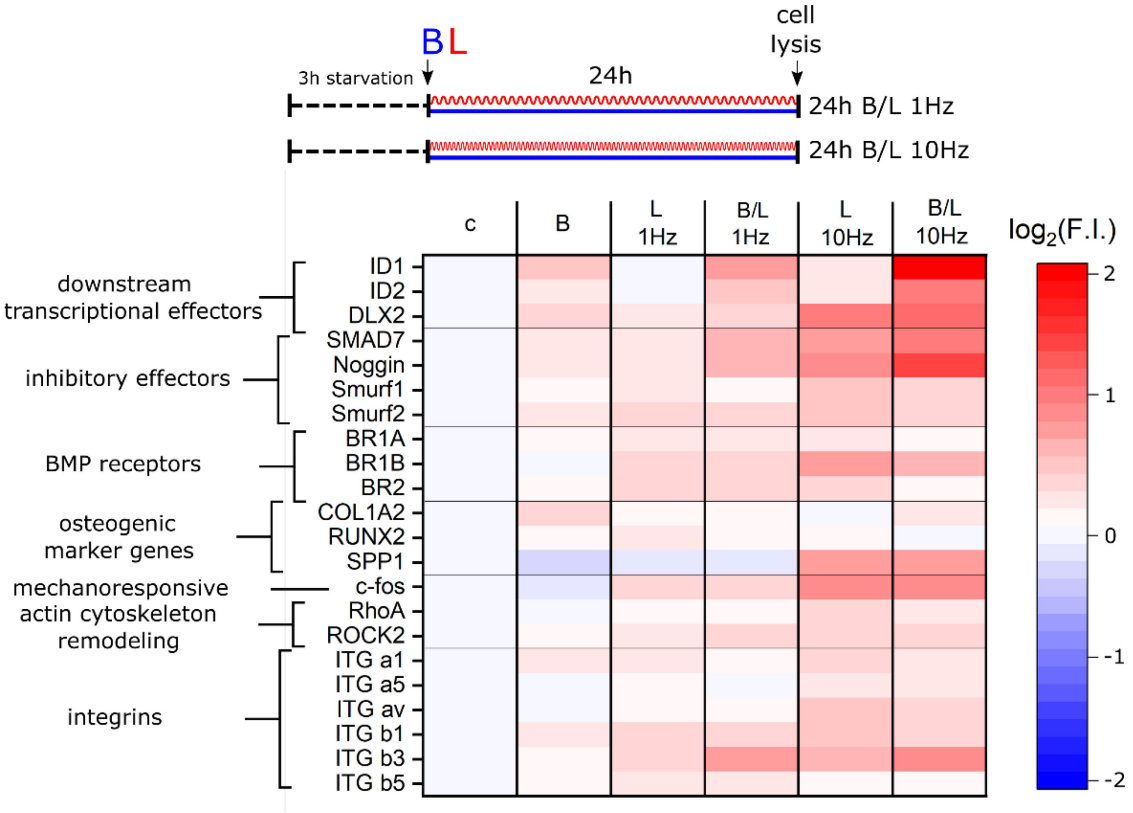

Figure 4-8: Heat map summarizing the gene expression changes in response to 24h BMP-2 stimulation and/or mechanical loading of 1 Hz or 10 Hz. Induction and reduction of expression is labeled in red and blue respectively, while white indicates no change in comparison to the untreated control (c), n=4. The values of the fold changes and log2(F.I.), on which the heat map is based, are depicted in Table 0-1 in the supplement.

Mechanical stimulation with 10 Hz further enhanced significantly the BMP-induced expression of both, positive (ID1, ID2) and negative regulators (Noggin, Smad7) of the BMP pathway, while 1 Hz had only minor effects (Figure 4-9). Interestingly, the expressions of BMP receptor type 1B but not type 1A or type 2 were found to be significantly increased by mechanical loading in a frequency-dependent manner, whereas BMP-treatment alone had no effect. The expressions of the osteogenic marker genes RUNX2 and COL1A2 were unaffected by the treatment, but osteopontin (SPP1) was significantly up-regulated in response to 10 Hz loading. C-fos, a transcription factor known to be a target of mechanotransduction [181], was used as a positive control for mechanical loading. As expected, the expression of c-fos increased with increasing frequency.

Moreover, the expression of specific integrin subtypes was analyzed, which were selected according to the previously determined integrin expression profile of hFOBs (obtained in personal communication with Dr. Maria Reichenbach, Knaus lab, FU Berlin). Integrin αv, β1 and β3 expressions were increased by mechanical loading, while α1, α5 and β5 were not affected. Mechanical loading especially induced the integrin β3 expression, which was further promoted under concurrent BMP-2 treatment, even though BMP-treatment alone had no impact. Interestingly, the heterodimer of integrin αvβ3 binds to RGD-containing ECM proteins, like osteopontin, which were all mechano-sensitive

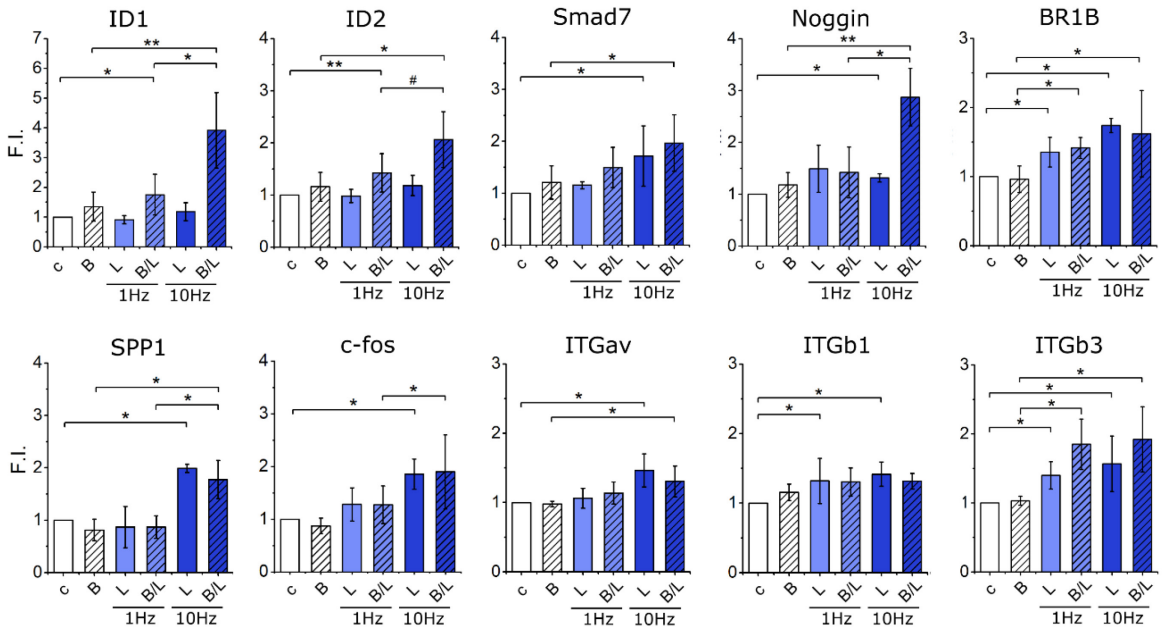

Figure 4-9: Mechanical stimuli regulate gene expression in a frequency dependent manner. hFOBs were seeded in collagen scaffolds, transferred into the bioreactor and stimulated for 24h with BMP-2 and/or mechanical loading (1 Hz or 10 Hz). Thereafter, cells were lysed and gene expression was analyzed via qPCR (n≥3).

In summary, frequency-dependent effects on early Smad phosphorylation persisted and transduced to the level of BMP target gene expression. The results revealed that mechanical loading with 10 Hz significantly increases the crosstalk duration in comparison to 1 Hz.

4.2.3 Focal adhesion number and size is increased by both, BMP-2 and mechanical loading in a frequency-dependent manner

To investigate whether the increased integrin expression was transduced into an increased assembly of focal adhesions (FAs), hFOBs were stained for the focal adhesion marker phospho-Paxillin (pPax) after a 24 hours treatment with BMP-2 and/or mechanical loading (1 Hz or 10 Hz). The confocal microscopy images and the corresponding quantifications show a strong influence of the treatments on cellular attachment to collagen walls (Figure 4-10 A-C). While untreated cells assembled little and small FA complexes, treatment with BMP-2, mechanical loading and a combination of both increased the amount of FAs significantly. The total number of FAs in cells treated with BMP-2 and 1 Hz loading was comparable and not

increased by a combination of both treatments. However, mechanical stimulation with 10 Hz under concurrent BMP-2 treatment, further increased the BMP-2- and load-only effect significantly (Figure 4-10 B). Furthermore, the percentage of cells with FAs larger than 0.7 μm^2 increased about 1.5 fold under a combined treatment of BMP-2 and 1 Hz loading and about 2 fold under BMP-2 and 10 Hz loading.

Interestingly, BMP-2 and 1 Hz mechanical stimulation induced equal FA number and size distributions, even though BMP-2 in contrast to 1 Hz loading did not enhance integrin expressions. Therefore, it is suggested that BMP-2 treatment mainly promoted integrin clustering. Both, the strong increase in integrin expression under 10 Hz loading and the increased integrin clustering under BMP-2 consequently led to the synergistic increase of FA size and amount under concurrent stimulation.

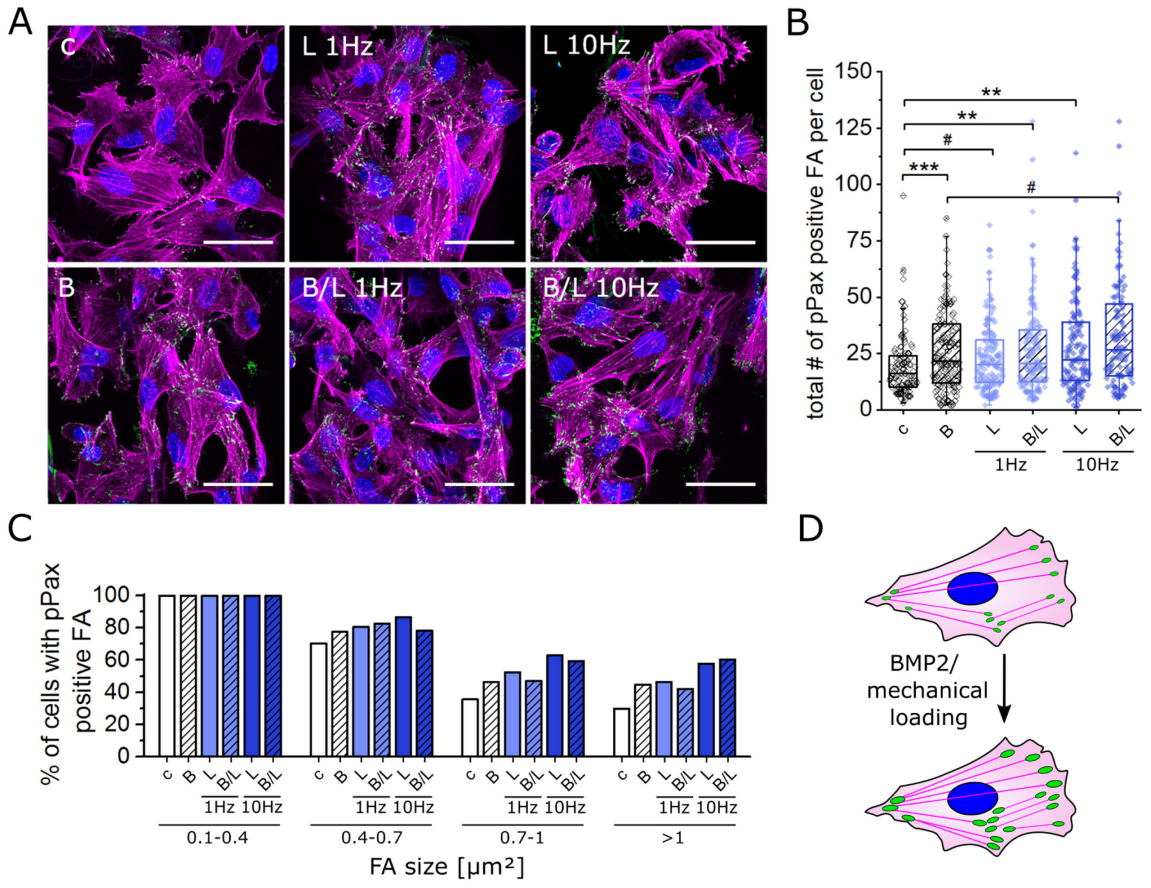

Figure 4-10: Focal adhesion number and size is increased by BMP-2 treatment and by mechanical loading in a frequency-dependent manner. hFOBs were seeded in collagen scaffolds, transferred into the bioreactor and stimulated for 24h with BMP-2 and/or mechanical loading (1 Hz or 10 Hz). Cells were fixated and stained for phospho-Paxillin (green), F-actin using phalloidin (pink) and nuclei using DAPI (blue). (A) Representative confocal images of stained hFOBs. Scale bar represents 50 µm. (B) Amount of phospho-Paxillin positive FA per cell and (C) percentage of cells with FAs of different size classes was assessed in ImageJ (see paragraph 3.4.1) (in total >110 cells pre condition, n=3). (D) Schematic drawing illustrates the increase in FA size and amount due to BMP-2 and mechanical stimulation.

The observed increase in integrin expression and FA assembly together with the increased expression of BMP receptor type IB under mechanical stimulation without the

application of BMP-2, was especially interesting since both, an increased amount of BMP receptors and the described BMP receptor-integrin interaction (see paragraph 1.5.1) would promote BMP signaling. A 24 hours stimulation with cyclic compression, could therefore induced gene expression changes, which could enhance BMP signaling once cells are exposed to BMP-2.

Consequently, two further hypothesis arose:

(1) Long-term mechanical loading sensitize the cells for BMP-2 so that the crosstalk between BMP signaling and mechanotransduction induced by subsequent concurrent mechanical and BMP-2 stimulation would be even further increased.

(2) Long-term mechanical loading leads to the establishment of a "mechano-memory", which would be sufficient to mediate the crosstalk, even though mechanical and BMP-2 stimulation are not concurrently applied.

4.2.4 Cells develop a mechano-memory impinging on BMP signaling

To examine whether mechanical pre-stimulation even further promotes the crosstalk between BMP signaling and mechanotransduction in comparison to no pre-stimulation (hypothesis (1)), cells were continuously stimulated for 24h before *and during* BMP-2 treatment. To examine whether cells establish a "mechano-memory", which would mediate the crosstalk (hypothesis (2)), cells were mechanically stimulated prior to but *not during* BMP-2 treatment. The pre-load conditions were compared to 90 min concurrent BMP-2 and mechanical stimulation with a frequency of 1 Hz (= crosstalk control), as this induced the maximum crosstalk strength (see Figure 4-7).

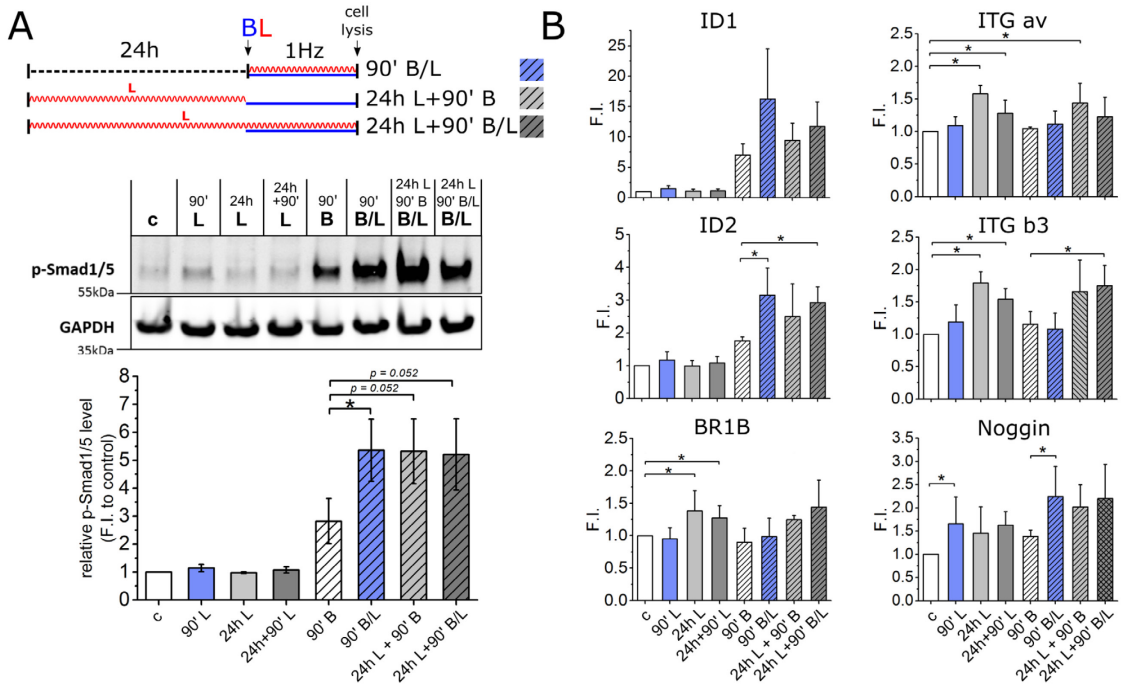

Figure 4-11: Mechanical pre-stimulation induced a crosstalk on p-Smad and on gene expression level. hFOBs were seeded in collagen scaffolds, transferred into the bioreactor and stimulated with mechanical loading for 24h. Thereafter, cells were stimulated with BMP-2 (5nM) for 90 min with or without concurrent mechanical loading. Cells were lysed and (A) p-Smad1/5 levels were determined by western blot and (B) gene expression was analyzed via qPCR (n≥3).

Gene expression analysis confirmed the previously observed significant increase in BMP receptor type 1B, integrin αv and β3 expression by 24h mechanical loading (Figure 4-11 B). However, in contrast to hypothesis (1), this adaptation to mechanical stimulation did not further promote Smad phosphorylation under BMP-2 treatment in comparison to the crosstalk control (Figure 4-11 A). It could be assumed, that differences could not be observed because Smad phosphorylation was already in saturation. Therefore, it would be interesting to investigate earlier time points in potential follow-up studies.

Most strikingly, when cells were mechanically stimulated prior to but *not during* BMP-2 treatment, Smad phosphorylation was equally increased as in the crosstalk-control. This demonstrated that mechanical pre-stimulation was able to induce a mechano- memory, which was sufficient to promote Smad phosphorylation even if the direct mechanical trigger was missing. Consequently, this experiment suggests that the mechano-regulation of BMP signaling at the Smad-level does not exclusively depend on *concurrent* BMP and mechanical stimulation.

Even though Smad phosphorylation levels were equal for all three crosstalk-conditions, the expression of BMP target genes ID1 and ID2 were reduced by mechanical pre-stimulation in comparison to the crosstalk-control (Figure 4-11B). This implies, that intracellular negative regulators of the BMP pathway, which might interfere with the translocation of Smads into the nucleus or suppress the binding of Smads at the promoter region, have been activated by mechanical stimulation decreasing BMP target gene expression.

In summary, cellular adaptation processes in response to 24 hours mechanical pre-stimulation persisted and were able to promote BMP signaling with different efficiencies on different signaling levels.

It is assumed that during 24 hours cyclic compression, cells have fully adapted to the changed mechanical environment, meaning non- transcriptional such as adhesion and cytoskeletal adaptations but also transcriptional responses including some negative control mechanisms have been initiated until a new mechanical equilibrium was established (assumption based on [182]). However, what happens if the time of pre-stimulation is reduced so that cells not jet fully adapted on all levels to the change in mechanics? By investigating this, the contribution of load-induced gene expression regulation (slow processes) in comparison to adhesion and cytoskeletal remodeling (fast processes) for the establishment of the mechano-memory can be estimated.

Therefore, the pre-stimulation time was reduced to 90 and 30 min prior to 90 min BMP stimulation and phosphorylation levels of Smad1/5 were again analyzed (Figure 4-12A).

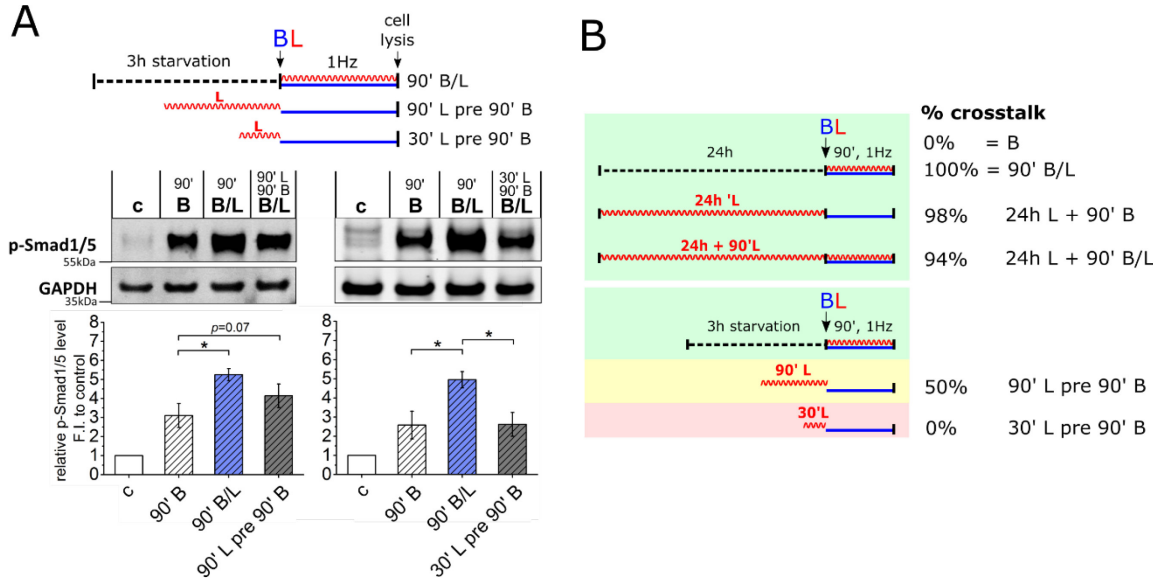

Figure 4-12: Only prolonged mechanical pre-stimulation induced a crosstalk on p-Smad level. (A) hFOBs were seeded in collagen scaffolds, transferred into the bioreactor and stimulated with mechanical loading for 90 min or 30 min. Thereafter, cells were stimulated with BMP-2 (5nM) for 90 min with or without concurrent mechanical loading. Cells were lysed and p-Smad1/5 levels were determined by western blot (n=3). (B) Summary of pre-loading conditions and their efficiencies (in %) to potentiate Smad1/5 phosphorylation (=crosstalk). The maximum crosstalk strength (90 min concurrent mechanical loading (1Hz) and BMP-2 stimulation) was set to 100%, while BMP-2-only treatment was set to 0%.

Interestingly, 90 min pre-loading could already induce an increased Smad1/5 phosphorylation in comparison to BMP-only control. Compared to the crosstalk control, however, phosphorylation levels were reduced. In fact, this condition reached around 50% of the crosstalk strength induced by the crosstalk-control (f = 1Hz, t = 90 min), if the BMP-only control is set to 0% (Figure 4-12B). Short pre-loading of 30 min had no effect on the BMP-induced Smad phosphorylation and was therefore insufficient to trigger a crosstalk.

Figure 4-12B summarizes the pre-loading conditions and their efficiency to induce an enhanced Smad phosphorylation. The calculated percentages of crosstalk strength show that the shorter the time of pre-loading, the weaker the crosstalk.

4.2.5 Mechanical signals regulate the BMP-pathway via integrins

Stimulation with BMP-2 and mechanical loading increased the expression of BMP receptor type B1, integrin αv and β3 (Figure 4-11) as well as the size and amount focal adhesions (Figure 4-10). Taking into account the described interaction of different integrin and BMP receptor subtypes (see paragraph 1.5.1), it was hypothesized that mechanical stimulation would increase BMP-2-induced Smad phosphorylation through interactions between BMPRs and integrins. Due to the specific regulation of integrin αv and β3 expression, the role of αvβ3

integrins for the crosstalk was investigated via siRNA mediated integrin αv knockdown. Since αv integrin is the only relevant interaction partner for integrin β3 in hFOBs (the fibrinogen receptor αIIbβ3 is mainly relevant in platelets [183]) a knockdown of integrin αv in turn reduces the amount of active integrin β3. Therefore, both integrin αv and β3 are no longer available as interaction partners for the BMP receptors.

Scaffold seeding and lipofectamine-mediated siRNA transfection was performed at the same time, since transfection of already seeded scaffolds was less efficient. A nonspecific siRNA (scrambled, scr) was used as a negative control in all RNAi-experiments. Knockdown efficiencies were validated via qPCR and western blot analysis two days after seeding and transfection. Integrin αv mRNA expression and protein amount were reduced respectively by about 90% and 60% in comparison to the scr control (Figure 4-13 A and B). Immunofluorescence staining of integrin αv after transfection (cells seeded on 2D chamber slides) show the absence of integrin αv-positive focal adhesion complexes in most of the cells. Interestingly, cells were less spread and established a more spindle-like morphology in comparison to the scr control (Figure 4-13 C).

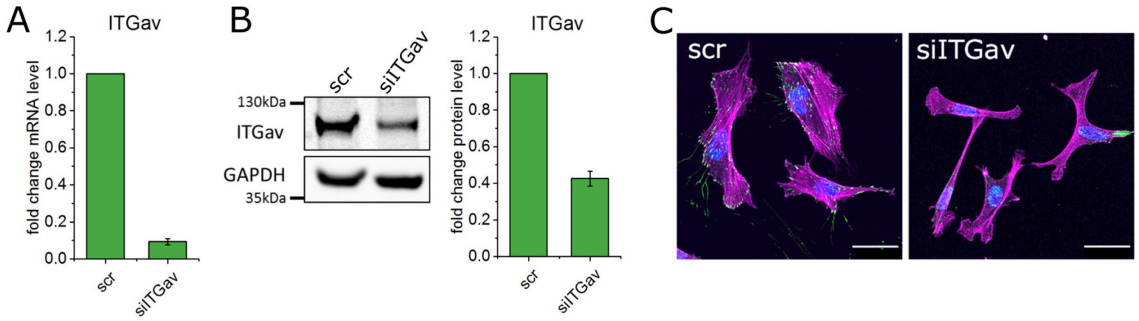

Figure 4-13 Validation of integrin αv knockdown in hFOBs. Human FOBs were transfected with siRNAs targeting integrin αv or a non-targeting control (scr) (30nM) using lipofectamin and simultaneously seeded either into collagen scaffolds or on 2D chamber slides. Two days after seeding, knockdown efficiencies were validated via qPCR (A) and western blot analysis (B) from cells grown in the scaffold. Representative images show hFOBs on chamber slides stained for integrin αv (green), F-actin (pink) and nuclei (blue). Scale bar represents 50 µm.

After the successful validation of the integrin αv knockdown, its impact on the crosstalk between BMP signaling and mechanotransduction was investigated. Therefore, bioreactor experiments were performed with transfected cells under crosstalk-control conditions (1 Hz, 10%, 90 min, 5nM rhBMP-2) and Smad phosphorylation was analyzed.

In the scr control, mechanical loading further increased the BMP-2-induced Smad phosphorylation significantly by 2-fold. Since the induction strength is comparable to results of previous experiments using non-transfected hFOBs (see Figure 4-7), the transfection procedure itself was not affecting the crosstalk. Knockdown of integrin αv, however, reduced the total integrin αv protein levels consistently and significantly by about 50-60% in comparison to the scr control. Strikingly, this influenced the sensitivity of BMP signaling to mechanical stimulation, while basal signaling was unaffected. The Smad phosphorylation

upon concurrent BMP-2 and mechanical stimulation was still significantly increased, however only by 1.36-fold. Therefore, the sensitivity to mechanical stimulation was reduced by about 65% in comparison to the scr control with a p- value of 0.06. It is assumed that an increase in knockdown efficiency would also increase the effect on the crosstalk. In summary, αvβ integrins play an important role for the crosstalk between BMP signaling and mechanotransduction.

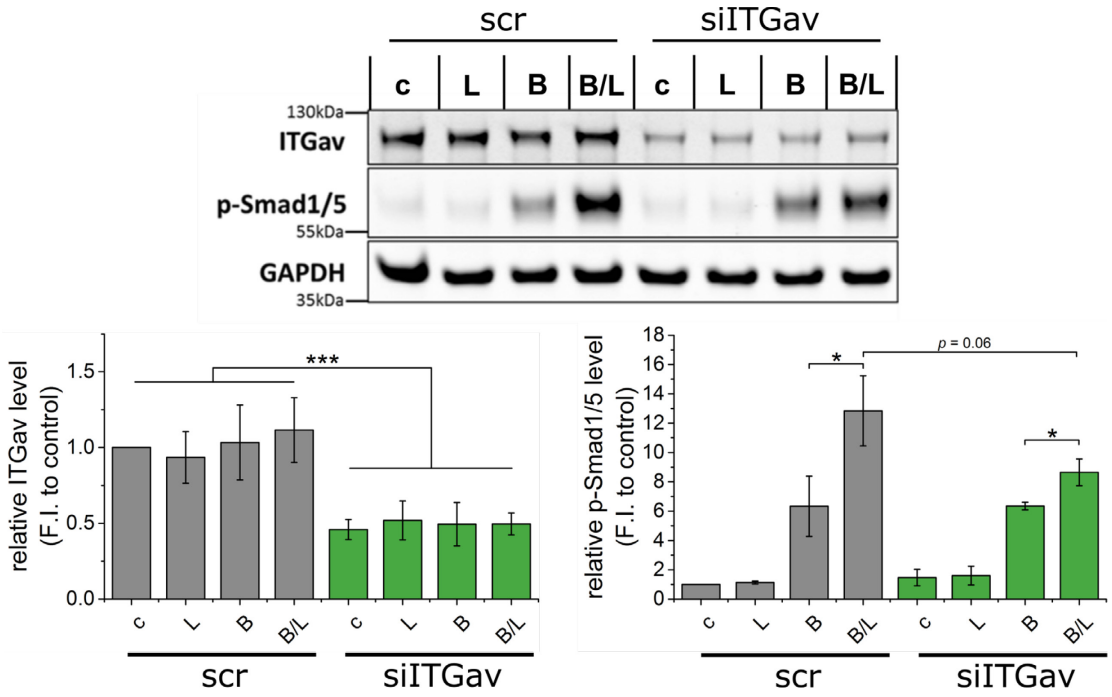

Figure 4-14: Integrin αv knockdown reduced the crosstalk on Smad phosphorylation level. Human FOBs were transfected with siRNAs targeting integrin αv or a non-targeting control (scr) (30nM) using lipofectamin and simultaneously seeded into collagen scaffolds. Two days after, scaffolds were transferred into the bioreactor, starved for 3h and subsequently stimulated with 5nM BMP-2 and/or cyclic mechanical compression (1 Hz, 10%) for 90 min. Protein levels of integrin αv and phosphorylated Smad1/5 were quantified via western blotting. Bar charts depict relative fold changes in comparison to the unstimulated scr control (n=4).

If a direct interaction of intergins and BMP receptors is assumed to mediate the integration of mechanical signals into the BMP pathway, is this interaction already existing under static conditions, or is it only established in response to mechanical stimulation? The latter scenario would imply that load-induced remodeling/reorganization of intergins and BMP receptors must have preceded an interaction. In the following, it was analyzed whether a remodeling process is a prerequisite for the crosstalk.

4.2.6 Actin cytoskeleton remodeling is crucial for the crosstalk

It was found that mechanical stimulation induces the expression of specific integrin subtypes and the clustering into FAs (Figure 4-10), already indicating a load-induced remodeling process at the plasma membrane. The rearrangement of FAs upon mechanical stimulation is mediated through integrin signaling that also induces the remodeling of structurally and

mechanically connected actin fibers. A primary integrin effector controlling FA turnover and lamellipodia formation is focal adhesion kinase (FAK). Upon integrin engagement, FAK is recruited and activated via autophosphorylation at tyrosine 397. Its phosphorylation level in relation to the total protein amount was examined in response to cyclic compression in a time dependent manner (Figure 4-15A). In comparison to the static control, a significantly increased Y397 phosphorylation was detected after 30 min of mechanical loading that remained high until the 90 min time point. Interestingly, this time dependent behavior correlated with the load-induced increase in p-Smad level at 30 and 90 min. The total FAK levels remained constant during the loading period and were equal to the static control. The increased FAK activation points towards an enhanced integrin clustering and signaling in response to cyclic compression. A prominent downstream pathway of FAK activation is the RhoA/ROCK pathway, which controls the activity of myosin II by phosphorylation of the myosin light chain (MLC) subunit. Cyclic compression increased the MLC phosphorylation in a time dependent manner reaching significance after 90 min of stimulation (Figure 4-15B).

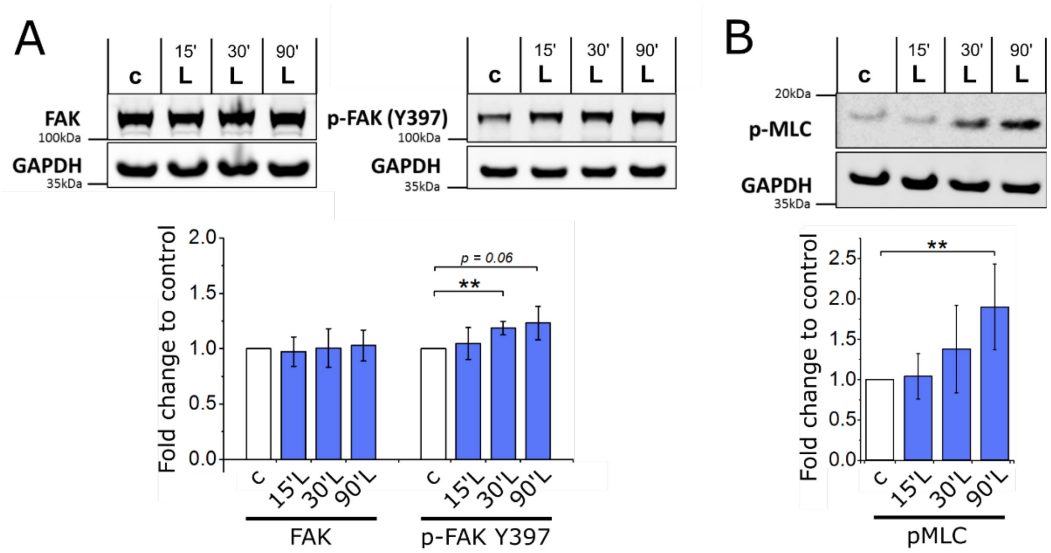

Figure 4-15: Cyclic compression induced focal adhesion kinase and myosin light chain activation. Human FOBs seeded in collagen scaffolds were subjected for 15, 30 or 90 min to cyclic compression (1Hz, 10%). The total protein level of FAK, its phosphorylation at tyrosine 397 and the phosphorylation of MLC was analyzed by western blot (n=4).

This indicated a load-induced reinforcement of the actin cytoskeleton that goes along with an actin remodeling and adaptation process. The myosin-mediated increased tensile force of the cytoskeleton acts on integrin adhesion sites and fosters the clustering of FA. Since integrin signaling induces actin cytoskeleton remodeling that in turn cause the remodeling of integrin-mediated adhesions, there is a mutual interaction of integrins/ FAs and the actin cytoskeleton. Due to this connection, it was hypothesized that load-induced actin cytoskeletal remodeling is an important mechanotransduction process to mechanically enhance BMP signaling, as it in turn regulates integrin remodeling. To investigate the relevance of load-

induced actin cytoskeletal remodeling for the crosstalk, cells were treated with the actin cytoskeleton stabilizer Jasplakinolide (Jas). Given the great diversity of actin modulatory agents, Jas was chosen specifically for its described inhibitory function on actin filament depolymerization, stabilizing the network and interfering with its remodeling. Jas, an actin binding macrocyclic peptide, was originally isolated from marine sponge and its concentration dependent effect on the actin cytoskeleton were described before [184]. Therefore, hFOBs were treated over three hours (the duration of starvation in bioreactor experiments) with different Jas concentrations and cell morphology and actin cytoskeleton organization was analyzed. Representative fluorescent images of phalloidin-stained hFOBs (in 2D) treated with 0.05 µM or 0.1 µM Jas or equal amounts of DMSO (serving as negative control) are shown in Figure 4-16A. DMSO treatment did not affect the organization of the F-actin stress fibers into a dense network. Jas at concentration of 0.05 µM increased the thickness but reduced the amount of actin stress fibers in most of the cells. Furthermore, actin aggregates formed in the perinuclear region. Due to the competitive binding of Jas and phalloidin, phalloidin signal intensity was reduced. The cell morphology was barely affected by the treatment with 0.05 µM in comparison to the DMSO treated control. However, at a concentration of 0.1 µM, the actin cytoskeleton completely collapsed into an unorganized actin mass around the nucleus. In contrast, cells seeded into collagen scaffold were less sensitive to the inhibitor. Cell morphology was maintained but some actin aggregates were present at the concentration of 0.1 µM Jas. Therefore, for following 2D experiments 0.05 µM Jas and for 3D experiments 0.1 µM Jas were selected. These concentrations already show effects on actin organization without inducing major changes to the cell morphology.

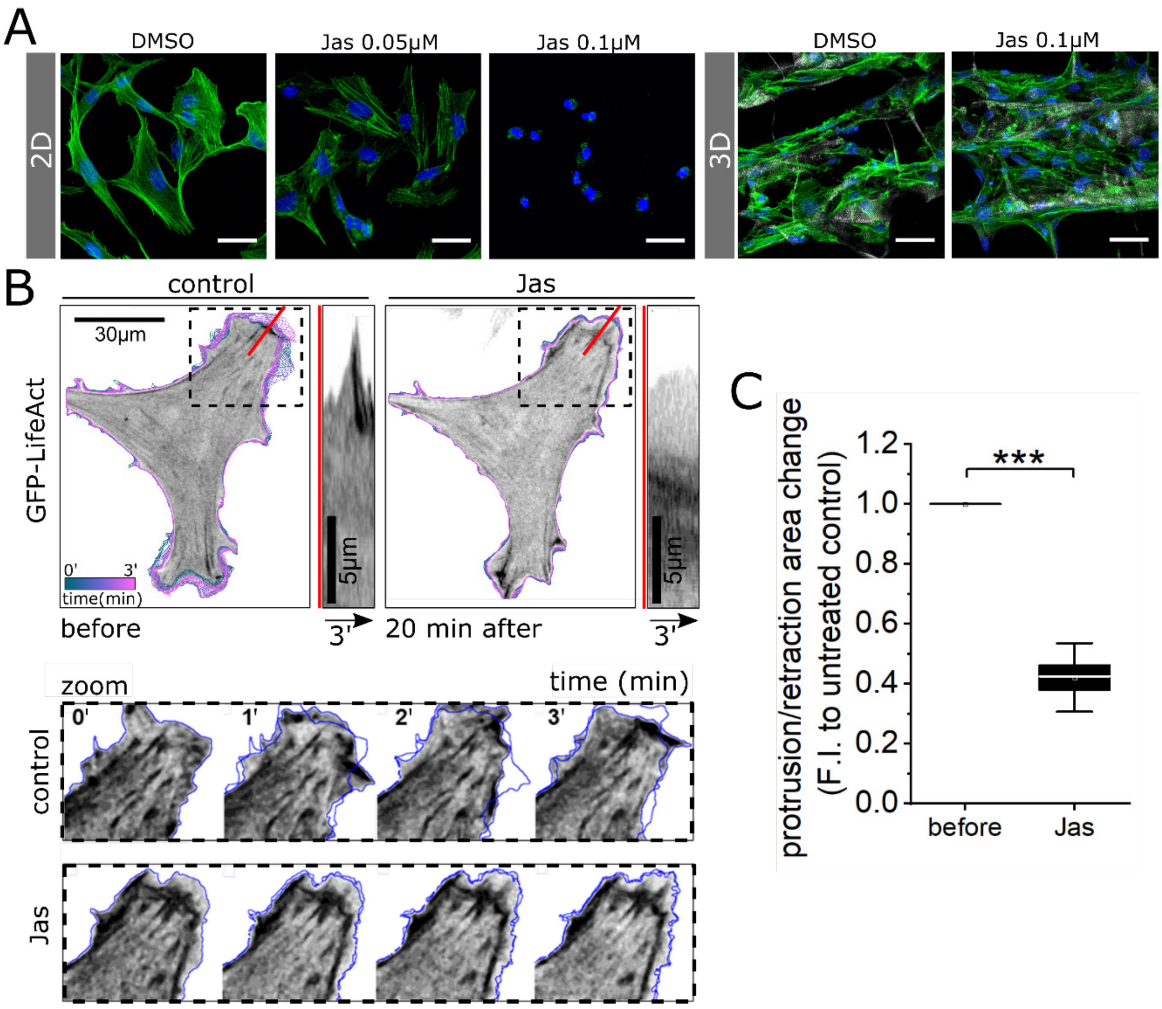

Figure 4-16: Effects of Jasplakinolide on actin cytoskeleton integrity and dynamics. (A) Concentration and culture system dependent effects of Jas. Human FOBs seeded onto collagen coated glass slides or into the collagen scaffold were treated for 4.5h with 0.05µM Jas, 0.1µM Jas or with the solvent DMSO in starvation medium. Thereafter, cells were fixed and stained. Representative confocal images show F-actin (green) and nuclei (blue) and collagen scaffold (white) (scale bar = 50µm). (B) Representative images showing the dynamic protrusion remodeling of GFP-LifeAct expressing hFOBs during a time frame of three minutes before and after inhibitor treatment. The remodeling dynamics is visualized by an overlay of all cell outlines colored according to frame number from blue to pink. The kymographs, taken along the red lines, illustrate the different protrusion dynamics. A zoom into the lamellipodia region illustrates the fast remodeling. Blue lines indicate the cell border changes between (C) Quantification of the protrusion/retraction area change before and after Jas treatment (20-45 min after). The protrusion/retraction area change was normalized to the untreated control (=before treatment), n = 12.

To validate its effects on actin cytoskeleton remodeling processes, time-lapse microscopy was performed using GFP-LifeAct expressing hFOBs. LifeAct is an F-Actin binding peptide coupled to GFP, which was reported to be less interfering than a direct coupling of GFP to actin monomers[160]. Cells seeded on collagen-coated glass slides were recorded every 10 seconds during a time frame of 3 min. Since protrusion dynamics differ from cell to cell, depending on the current phase of cell cycle and whether a cell is migrating or static, protrusion dynamics of the same cell before and after Jas treatment were compared. The cell outlines were marked and the area in between two consecutive outlines was measured to assess the area change (extension and retraction) per time frame. Area changes during one minute were summed up and averaged over the three recorded minutes. To better illustrate

the protrusion dynamics, all cell outlines colored according to frame number from blue to pink were overlaid and depicted in Figure 4-16B for a representative cell. Additionally, kymographs show the time dependent movement of a selected position within the lamellipodia. The resulting image sequences showed a highly dynamic remodeling of protrusion sites before Jas supplementation (Figure 4-16B). The kymograph illustrates the fast extension and retraction of the lamellipodium covering approx. ±5 µm and also visualizes the time dependent accumulation of actin in this region. Jas treatment drastically decreased the fast protrusion remodeling observed in control cells. The protrusions almost remained "frozen", only slowly sliding forward. Additionally, the change in fluorescence signal intensity over time visible in the kymograph shows, that in contrast to the control, actin was retracted from the outer cortex. Quantification of the protrusion dynamics, underlines the impression of the image sequences: Jas significantly reduced the area change per min. Taken together, Jas inhibited fast actin remolding processes especially visible in protruding lamellipodia.

The here collected data concerning FA growth and increased FAK and MLC phosphorylation in response to mechanical loading suggest, that cytoskeletal remodeling processes are triggered. However, a direct proof of the assumption that the dynamics of actin remodeling is increased in hFOBs upon exposure to mechanical stimulation was missing. Furthermore, it was necessary to validate the efficiency of Jas to stabilize the cytoskeleton even under loading conditions. In a first attempt to visualize and quantify actin remodeling dynamics in response to mechanics, the bioreactor was modified to allow *in situ* time-lapse confocal microscopy. Therefore, a glass window was implemented at the bottom of the bioreactor chamber and the upper plunger was elongated. The collagen scaffold seeded with GFP-LifeAct expressing hFOBs was positioned onto the glass, the plunger was adjusted on top and the bioreactor was placed onto the microscope table. Time-lapse imaging was performed before and after cyclic compression, as imaging during compression was impossible since the rate of image acquisition was lower than the stimulation frequency. Due to the increased imaging volume in 3D the frequency of image acquisition decreased drastically so that, to investigate the very fast protrusion dynamics, not the whole cell body could be recorded. Furthermore, position selected before cyclic compression could not be re-imaged afterwards because of a slight, uncontrollable drift of the scaffold within the bioreactor system. Moreover, it became obvious that scaffold walls deform inhomogenously under compression, aggravating the comparison of actin remodeling at different positions within the scaffolds. Due to these limitations, recorded image sequences could only exemplary show the change in protrusion dynamics, but no quantifications were possible (see supplementary Figure 0-4).

Although substrate deformation caused by cyclic compression of the scaffold, is regarded to be the most prominent mechanical trigger, cells also experience fluid flow induced by the

cyclic compression of the scaffold in the bioreactor. By using a 2D flow chamber setup (Ibidi) it was interestingly found that fluid shear stress alone enhances early and late BMP signaling events (data obtained by Dr. Maria Reichenbach, FU Berlin, Knaus Lab). To simplify imaging of actin remolding in response to mechanical stimuli, this flow chamber setup was combined with the confocal microscope (in cooperation with Dr. Maria Reichenbach, FU Berlin, Knaus Lab). GFP-LifeAct expressing hFOBs were seeded into the flow chambers and image stacks were recorded every 10 seconds over 3 min before and during fluid flow stimulation at 90 min (=flow) as well as after 30 min Jas treatment.

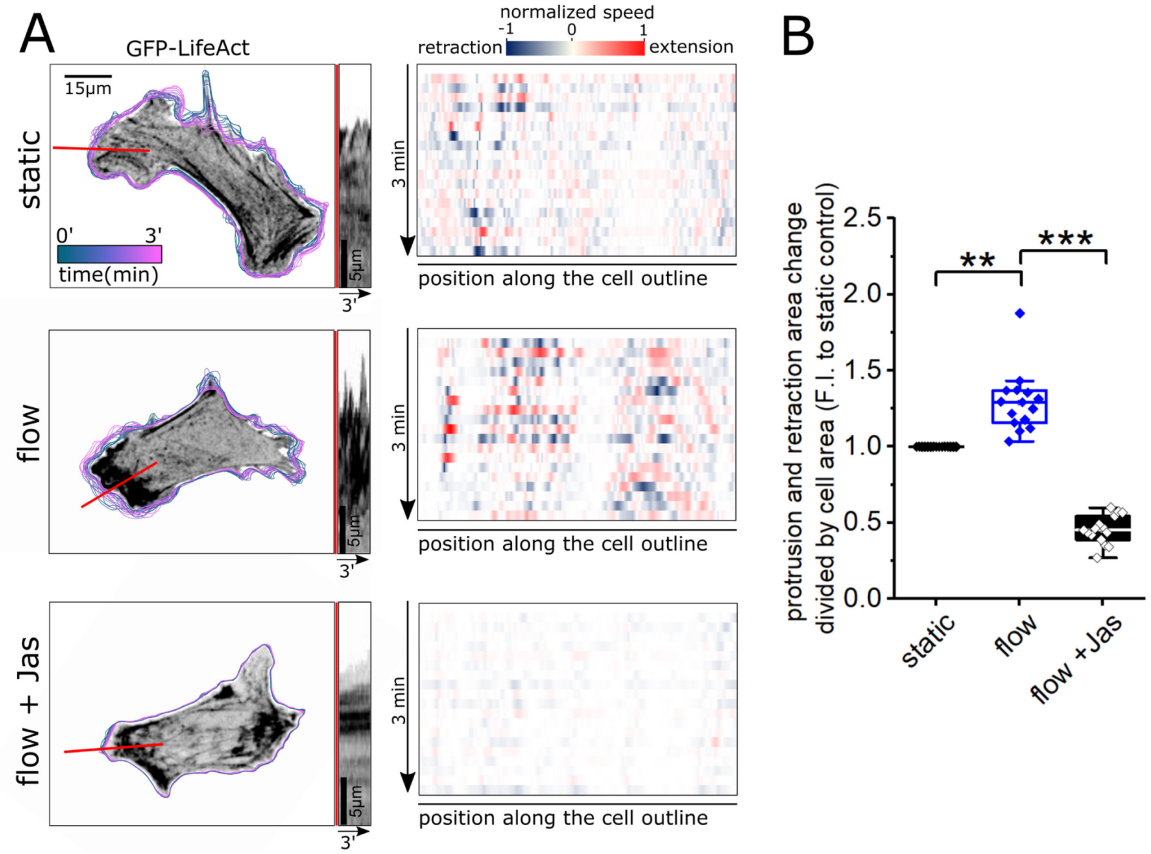

Figure 4-17: Dynamic actin remodeling induced by fluid shear stress is inhibited by Jasplakinolide. GFP-LifeAct expressing hFOBs seeded in Ibidi flow chambers were stimulated with fluid flow (5dyn/cm²) and Jas (0.05µM) was supplemented after 90 min. Fast actin remolding processes were recorded during 3 min before (=static) and during fluid flow stimulation 90 min (=flow) as well as after 30 min Jas treatment (=flow + Jas). (A) Representative images show the cell outline change over 3 min. The cell outlines are colored according to frame number from blue to pink. The kymographs, taken along the red lines, illustrate the different protrusion dynamics. The motility map below shows the speed of nodes along the cell outline normalized to the maximum speed. Red shades represent expanding regions, blue shades contracting regions. (B) Quantification of the cell area change per time frame divided by the total cell area and normalized to the static control (n=15 cells in 3 experiments).

As described before, changes of protrusion dynamics were compared within the same cell. Under static conditions, cells dynamically extended and retracted the protrusion sites representatively illustrated in Figure 4-17A by the overlaid cell outlines and the kymograph. Additionally, the speed of nodes positioned in regular distances along the cell outline was tracked using Quimp an ImageJ plugin and displayed in motility maps, with red shades represent expanding regions and blue shades contracting regions (middle vertical panel). The

node speed was normalized to the maximum node speed measured in all images sequences acquired for the cell. The dynamic changes of the cell outline, the increased extension and retraction visible in the kymograph and the enhanced speed of extension and retraction depicted in the motility map, clearly showed the increased protrusion dynamic of cells stimulated with fluid flow. Especially obvious is the increased accumulation of actin in the lamellipodia region in a fluctuating manner. Furthermore, fluid flow induced the polarization of the cell in this example. This was however not observed for all the recorded cells. For the analysis of this particular experiment, the area change per minute was normalized to the cell area as the cell morphology was changing significantly during the time course of the experiment. Without normalization, area changes of a large cell in comparison to a small cell would always be greater. A statistically significant increase in cell area change was quantified for cells stimulated with fluid flow at both time points. Strikingly, also under continuous fluid flow, Jas strongly reduced the protrusion dynamics of the cells. In some cases, the lamellipodia were even completely retracted. As in the previous 2D experiments under static condition (Figure 4-16), cells appeared “frozen” and a fluctuation of actin accumulation was completely inhibited. The area change was significantly reduced by the treatment with Jas. Even though a direct experimental proof is missing, it can be speculated that this is also happening in 3D during the loading experiments in the bioreactor using 0.1µM Jas.

In summary, it was found that Jas inhibited the load-induced dynamic remodeling of the actin cytoskeleton, especially visible in the reorganization of protrusion sites. Since the actin network is linked to integrin–mediated adhesions, a disturbed actin reorganization will in turn impair remodeling of adhesion sites. However, the load-induced remodeling of adhesion sites and the actin cytoskeleton, are fundamental first events leading to the establishment of a new force equilibrium. Therefore, it was proposed that an interference with the load-induced actin remodeling would disturb mechanotransduction and would moreover hinder a load-induced interaction between integrins and BMP receptors.

Since Jas was proven to efficiently inhibit actin remodeling dynamics induced by mechanical stimulation, the agent was regarded a good candidate to test the hypothesis whether load-induced dynamic remodeling of the actin cytoskeleton mediates the mechano-regulation of BMP signaling. Therefore, bioreactor experiments with and without Jas were performed under crosstalk-control condition (t=90 min, *f*=1Hz, A=10%, 5nM BMP-2), which is known to increase Smad phosphorylation significantly. Jas or equal amounts of DMSO were supplemented to the starvation medium, bioreactors were assembled, hFOB-seeded scaffolds were positioned and starved for 3h. Thereafter, cells were subjected for 90 min to BMP-2 stimulation, mechanical loading (1 Hz, 10%) or a combination of both. Subsequently, cells

were harvested for western blotting or qPCR to analyze p-Smad levels or ID1 expression, respectively (Figure 4-18A B).

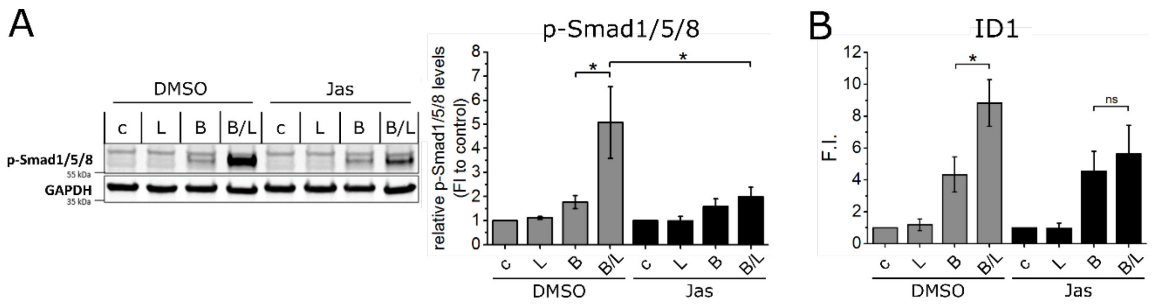

Figure 4-18: F-actin stabilization by Jasplakinolide inhibits load-induced Smad phosphorylation and ID1 expression. Human FOBs seeded in collagen scaffolds were incubated for 3 h in starvation medium supplemented with 0.1 µM Jasplakinolide (Jaspl). Subsequently, scaffolds were subjected for 90 min to BMP-2 stimulation, mechanical loading (1 Hz, 10%) or a combination of both. (A) The phosphorylation of Smad1/5/8 was analyzed by western blot and (B) ID1 expression was determined via RT-qPCR (n = 3).

In the DMSO treated control samples, cyclic compression significantly increased Smad1/5/8 phosphorylation under concurrent BMP-2 stimulation in comparison to BMP-2-only stimulation. Under Jas treatment, however, cyclic compression did not increase p-Smad levels and in comparison to the crosstalk-control, phosphorylation was significantly downregulated. This is mirrored in the expression of ID1. Whereas cyclic compression under concurrent BMP-2 stimulation significantly increased ID1 expression under DMSO treatment, there was no difference under Jas treatment (Figure 4-18B). Consequently, Jas treatment abolished the positive effect of cyclic compression almost completely, while basal BMP signaling remained unaffected. Together with the observed inhibition of actin remodeling, this led to the conclusion, that actin cytoskeletal adaptation in response to cyclic compression is a prerequisite for the mechano-regulation of BMP signaling.

4.3 The influence of the crosstalk on ECM formation

BMP-2 is known for its strong osteoinductive potential and its influence on cell differentiation in the context of bone healing is well studied. However, the growth factor should not be reduced to this feature alone, as it was described to influence cell migration [23], proliferation [22], angiogenesis [219] and evidences point towards an additional role in steering early extracellular matrix formation processes [149], [155]. Therefore, the question arose whether mechanical stimulation would not only increase the growth factors` potential to induce osteogenic differentiation but also foster its effects on tissue formation.

The influence of cyclic compression and BMP-2 stimulation on extracellular matrix formation was investigated using human primary fibroblasts known as tissue forming cells. For these experiments BMP-2 concentration (5nM) and mechanical loading protocol (f=1Hz and ε=10%, 3h cyclic compression, 5h break) used were identical to previously performed differentiation experiments described in section 4.1. The selected experimental parameters were proven to induce a crosstalk on Smad phosphorylation level at 90 min in fibroblasts as shown in section 4.2.1. Therefore, it was hypothesized that cyclic compression increases the BMP-2 effect on early tissue formation.

4.3.1 Load- induced tissue contraction and stiffening is reduced by BMP-2

Tissue contraction is regarded as an essential process during tissue healing to re-establish the lost tissue pretension [185]. Therefore, macroscopic deformation of the scaffold was investigated after bioreactor culture. Scaffold dimensions were assed in radial and axial direction, before (0d) and after bioreactor culture (7d), (example images in Figure 4-19 A) to calculate the scaffold volume contraction (%). A significant increase in volume contraction of mechanically loaded compared to control samples was observed. The separation into axial and radial contraction demonstrates, that this is not only due to increased tissue compaction resulting from the axially applied load (Figure 4-19 C), but also due to active cell-mediated contraction perpendicular to the loading direction (Figure 4-19 D). BMP-2 stimulation slightly increased the volume contraction in comparison to the control. However interestingly, in combination with cyclic compression, BMP-2 slightly reduced the load-induced tissue contraction.

Mechanical properties of the cell substrate are known to influence cell behavior [56]. To characterize the effect of cyclic compression and BMP-2 on the mechanical properties of the early tissue, mono-axial compression tests of native samples were performed to assess the compressive stiffness. Since the compression tests were conducted in the direction of the scaffold pores that provide resistance to the newly deposited tensed collagen fibers, it is expected, that collagen contributes manly by occupying the space in the pores and not by its

tensile load-bearing capacity. The measured stiffness, therefore, mostly depends on the cross-sectional area of the bulk material (a reduction in cross-sectional area due to contraction results in densification) but also on the amount of deposited ECM.

Indeed, an increased radial contraction correlated with an increased Young's modulus (*E*) here expressed as compressive stiffness (Figure 4-19 E). Both cyclic loading and BMP-2 enhanced tissue stiffness in comparison to the control, reaching statistically significant difference for the loaded group. Unexpectedly however, under concurrent BMP-2 and mechanical stimulation, BMP-2 reduced the load-induced scaffold stiffening.

In summary, both tissue contraction and stiffening due to cyclic compression were reduced by BMP-2 stimulation.

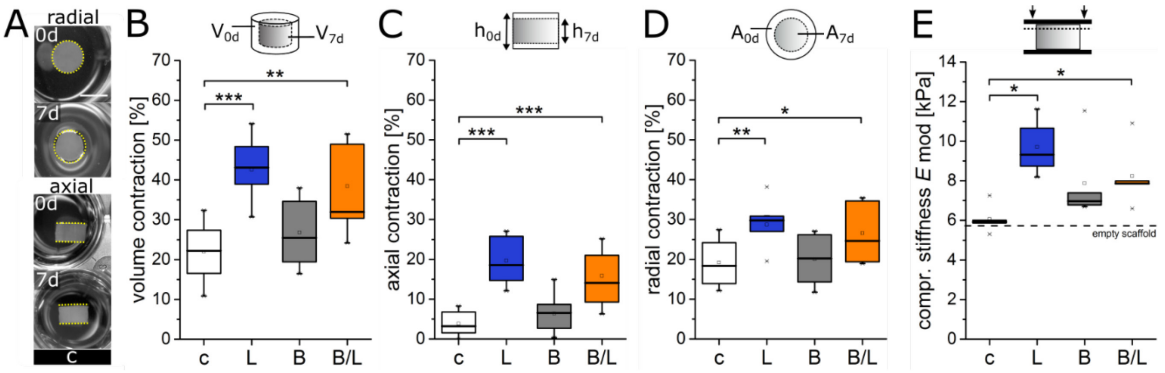

Figure 4-19: Load- induced scaffold contraction and stiffening is reduced by BMP-2. Human fibroblasts seeded in 1.5-wt% collagen scaffolds were cultured for seven days in the bioreactor under intermitted cyclic compression (f=1Hz, ε=10%, 3h load, 5h break), rhBMP2 (5nM) or a combination of both. (A) Representative images of fibroblast-seeded collagen scaffold cultured under control conditions showing radial and axial contraction at day 0 and 7. (B-D) Quantification of volume, axial and radial contraction [%] of scaffolds after seven days dependent on the culture condition (n=8). (E) Compressive stiffness E [kPa] of native samples after seven days dependent on the culture condition (n=5).

Tissue contraction is not only dependent on cell traction forces but also on the amount of fibrillar collagen. Indeed, a linear dependency between biomaterial contraction and fibrillar collagen density was shown previously, indicating a mechanical contribution of tensioned collagen fibrils in the contraction process [171]. In the following, it was investigated whether the observed differences in scaffold contraction can be correlated to differences in collagen content. Based on previous findings that BMP-2 and cyclic compression individually increased collagen I expression [154] and the secretion of procollagen I C-peptide [159] in fibroblasts, respectively, it was hypothesized that both stimuli independently but specifically in combination increase contraction and tissue stiffening due to increased fibrillar collagen formation.

4.3.2 Mechanical loading increases collagen synthesis but reduces fibrillar collagen density and fiber alignment

To verify that fibroblasts increase collagen secretion upon cyclic loading, the concentration of procollagen I C-peptide (PIP) was measured in the harvested conditioned culture medium using ELISA (Figure 4-20 C). Collagen is synthesized and secreted in its pro-form that is cleaved by collagen peptidases to remove the end-termini before it is eventually assembled into collagen fibrills. The concentration of the soluble C-terminal peptide directly correlates with the amount of collagen synthesized. Cyclic compression significantly increased the PIP concentration in the medium. BMP-2 stimulation, however, had no effect on collagen I synthesis. In agreement with this the PIP concentrations under the BMP-2+load condition were similar to the load-only group. Consequently, the question arose whether the increased collagen secretion under cyclic compression would also result in an increased deposition of collagen fibrils that are known to serve as a structural network for tissue repair processes.

Collagen type I was visualized in the ECM using an antibody staining and confocal microscopy (Figure 4-20 A). The monoclonal collagen I antibody is directed to the amino acid sequence at position 1200-1300 of human collagen I, binding to fibrillar and non-fibrillarized collagen, therefore visualizing the whole proportion of deposited collagen. Interestingly and in contrast to the PIP measurement, the signal intensity per mm^3 quantified from confocal images was similar in control, loaded and BMP-2 stimulated samples, with a slight reduction under combined treatment (Figure 4-20 D). The increased secretion was therefore not leading to an increased deposition of collagen I into the ECM. However, since scaffold contraction was increased under cyclic compression (Figure 4-19 B-D) and contraction was previously described to correlate linearly with the amount of fibrillar collagen [171], it was hypothesized that the proportion of fibrillar vs non-fibrillar collagen would increase under load.

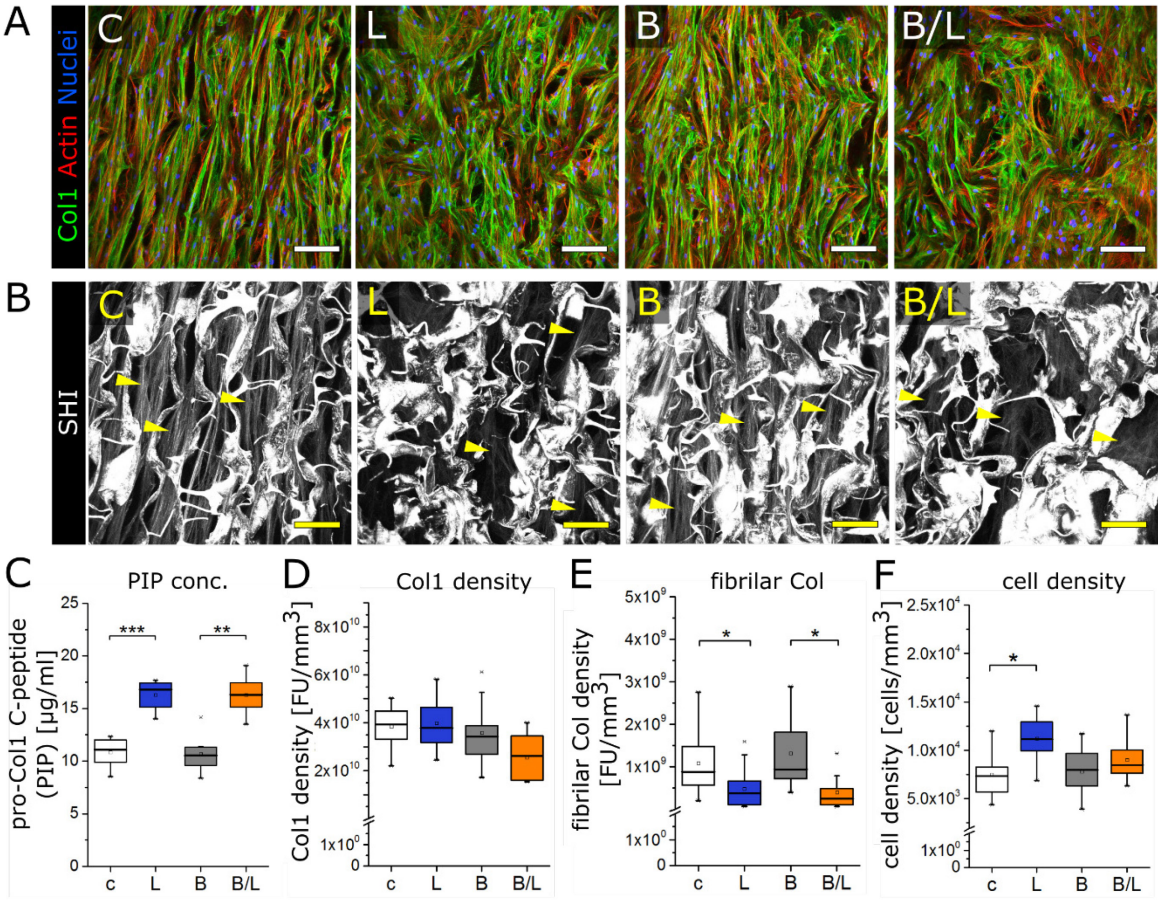

Figure 4-20: Cyclic mechanical compression increases collagen synthesis but reduces fibrillar collagen density. Human fibroblasts seeded in 1.5-wt% collagen scaffolds were cultured for seven days in the bioreactor under intermitted cyclic compression (f=1Hz, ε=10%, 3h load, 5h break), rhBMP2 (5nM) or a combination of both. (A) Representative confocal multiphoton images showing stainings for collagen 1 (green), F-actin (red), nuclei (blue) and (B) fibrillar collagen visualized by SHG (white) after seven days. Yellow arrows indicate newly deposited collagen fibers within the collagen walls of the scaffold. Scale bar = 100µm. (C) Quantification of Procollagen type I C-peptide (PIP) concentration inside culture medium using ELISA. Quantification of (D) collagen 1 density (antibody staining), (E) fibrillary collagen density and (F) cell density from confocal images.

To investigate this, second harmonic imaging (SHI), a label-free method to visualize fibrillar collagen was used. Under control conditions and BMP-2 treatment, thick bundles of newly deposited fibrillar collagen were visible in scaffold pores (Figure 4-20 B). Cyclic compression, however, reduced the second harmonic signal intensity drastically. Even in combination with BMP-2, the inhibitory effect of cyclic compression was dominating. Quantification of the fibrillar collagen density inside collagen pores confirmed the visual impression; cyclic compression significantly reduced the density of SHI-visualizable collagen bundles even in combination with BMP-2 (Figure 4-20 E). This is not related to the cell number, as the cell density in loaded samples even increased due to scaffold contraction (Figure 4-20 F). Frist investigations on further tissue maturation at the 2 week time point indicate, that fibrillar collagen density remains decreased under cyclic compression, even though BMP-2 stimulation seems have a small rescuing effect (supplementary Figure 0-5).

The observation that tissue contraction increased while at the same time fibrillar collagen density was reduced stands in contrast to the previously observed linear correlation between macroscopic contraction and fibrillar collagen depositions by fibroblasts from different donors, which strongly differed in their ability to deposit fibrillar collagen [171]. To better compare the current finding with previous results obtained by Brauer *et al*. [171], the tissue contraction was plotted in relation to the fibrillar collagen density combining the data obtained here with the data obtained by Brauer *et al.* (2019) (Figure 4-21A). In comparison to the linear dependency between tissue contraction and fibrillar collagen density observed by Brauer *et al.* (2019), it becomes obvious, that cyclic compression drastically changed the described interdependency as these conditions strongly deviate from the linear fit. Control and BMP-2 treated samples, however, nicely fit into this linear correlation, with the BMP-2 treated samples slightly shifted upwards along the line.

Against the assumption, that cyclic compression would increase the proportion of fibrillar vs non-fibrillar collagen, the opposite was the case. This becomes even clearer when calculating the ratio between Col1 density (determined by antibody staining, showing both fibrillar and non-fibrillar collagen) and fibrillar collagen density (Figure 4-21B). This ratio shows the proportion of non-fibrillar collagen in the samples and demonstrates that the proportion of non-fibrillar collagen strongly increased under cyclic compression in comparison to control and BMP-2 treated samples.

The ratio between PIP concentration and fibrillar collagen density is 3-fold higher in samples treated with cyclic compression in comparison to the control or BMP-2 treated samples. This demonstrates that under cyclic compression much more collagen I has been secreted than assembled into collagen bundles (Figure 4-21C).

Together this indicates that under cyclic compression the amount of collagen is reduced with progression of collagen maturation; secretion (PIP), embedding (Col1 immunofluorescent staining), fiber assembly (SHI of collagen fibrils).

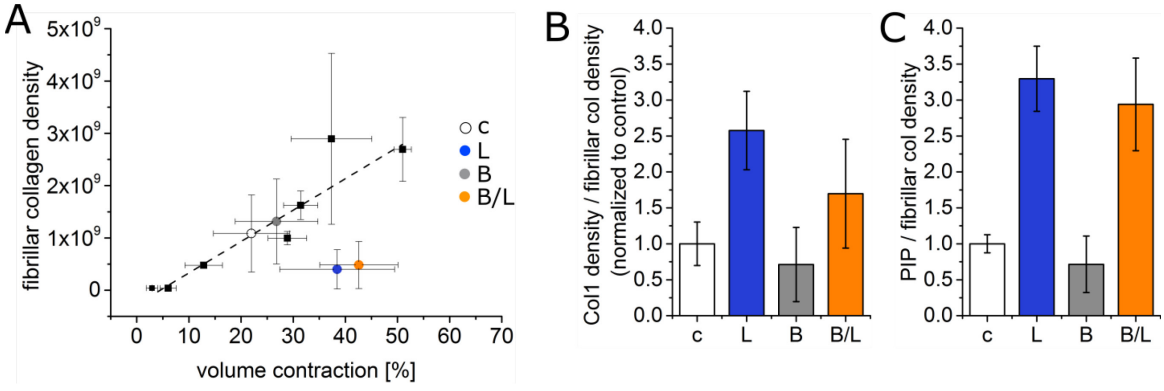

Figure 4-21: Cyclic compression changes the dependency of collagen density and tissue contraction. (A) Correlation of fibrillar collagen density and scaffold contraction. Data for linear correlation (black dots and dotted line) based on

7 fibroblast donors was obtained and kindly provide by Erik Brauer [171]*. (B) Ratio of collagen 1 (staining) and fibrillar collagen density. (C) Ratio of PIP and fibrillar collagen density.*

Even though almost equal amounts of Col1 were deposited into the ECM under all conditions (Fig. 4-20D), the assembly into collagen fibers, which can be detected using SHI, was different. A closer look onto the structure of collagen fibers within the pore reveals an altered organization under cyclic compression (Figure 4-22A). In control and BMP-2 treated samples, fibers show a uniform alignment along the scaffold pores, while under cyclic compression a more unorganized meshwork of fibers was established. When quantifying the collagen fiber orientation distribution from both SHI and Col1 staining under the different culture conditions (Figure 4-22B), it becomes clear that the anisotropic alignment adopted under control and BMP-2 conditions is strongly reduced towards a more isotropic orientation upon cyclic compression. As the ECM alignment follows the orientation of the cell, it was not surprising that F-actin and collagen fibers orientation are similar. Also on the level of ECM organization, the effect of cyclic compression dominated over the BMP-2 effect.

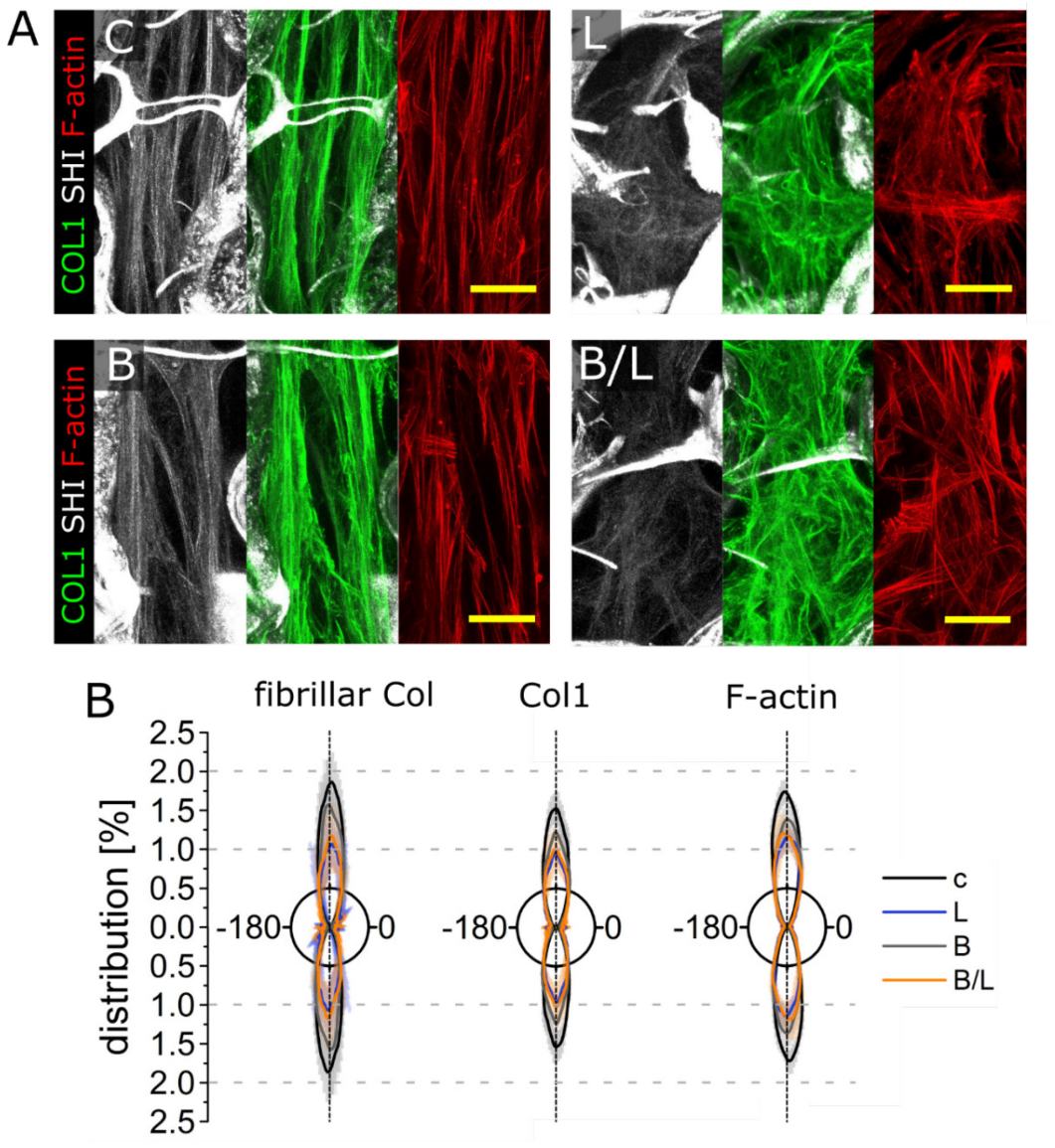

Figure 4-22: Cyclic mechanical compression reduces fiber and cell alignment. (A) Representative confocal multiphoton images showing collagen 1 (green) visualized by an antibody staining, fibrillar collagen (white) visualized by SHG and F-actin (red) visualized by phalloidin staining. Scale bar = 50µm (B) Comparison of fiber orientation distribution (percent of total) of fibrillary collagen, collagen 1 and F-actin signal relative to local pore orientation. Polar diagrams show mean value as solid line and standard deviation as color/gray band.

4.3.3 BMP-2 and cyclic compression induce distinct gene expression changes

To further investigate the regulation of collagens and collagen modulating proteins by BMP-2 and cyclic compression, gene expression analysis were performed. Gene expression changes in fibroblasts cultured for seven days in the bioreactor under intermitted cyclic compression were assessed using qPCR. Specifically, the expression of important fibrillar collagens, soft ECM proteins and enzymes involves in collagen fibrillogenesis and remodeling were investigated and are summarized in the heat map (Figure 4-23). These candidates have been selected due to their abundance in MS analysis (described in the paragraph below) and because of their regulatory capacity on collagen metabolism. At the first glance it can be seen, that cyclic compression increased the expression of most of the genes investigated, while a more diverse regulation was observed under BMP-2 stimulation. In a combination, the impact of mechanical stimulation on gene regulation seemed dominant, although BMP-2 treatment dampened the strong load-effect. This could lead to the suggestion, that the ECM established under cyclic compression is subjected to a higher turnover than under control conditions.

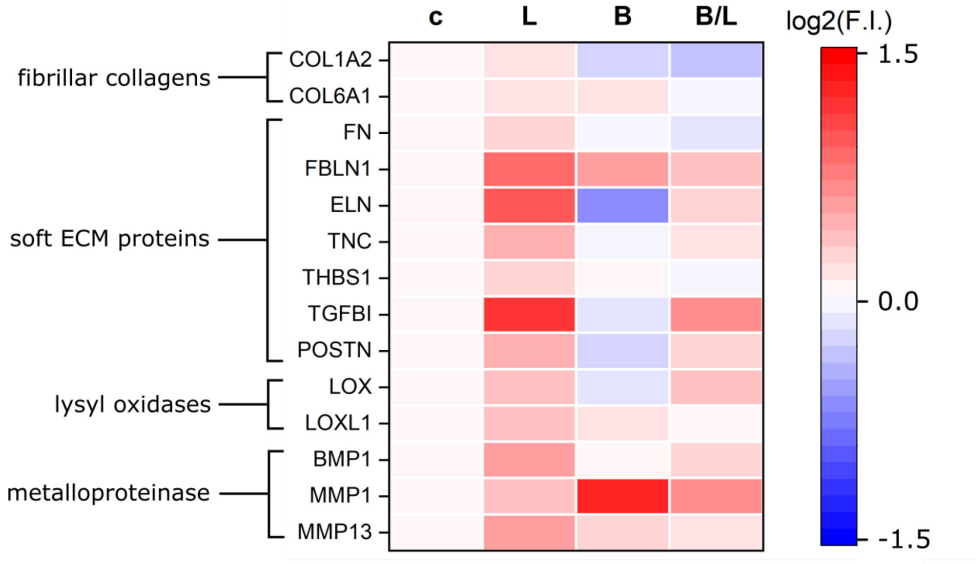

Figure 4-23: Gene expression analysis of selected ECM proteins and ECM modulators. Human fibroblasts seeded in 1.5-wt% collagen scaffolds were cultured for seven days in the bioreactor under intermitted cyclic compression (f=1Hz, ε=10%, 3h load, 5h break), rhBMP2 (5nM) or a combination of both. mRNA expression was determined via qPCR (expressions relative to HPRT). Heat map shows the log2 of the fold change towards the untreated control (n=3). The values of the fold changes and log2(F.I.), on which the heat map is based, are depicted in Table 0-2 in the supplement.

In detail, cyclic compression induced a strong 2-fold up-regulation of fibulin (±0.3), elastin (±0.4), TGFβ-induced protein (±0.3, TGFBI) and 1.5-fold on bone morphogenetic protein type-1 (±0.4, BMP-1) and matrix metalloproteinase-13 (±0.2, MMP13) expression. In contrary to what the name suggests, BMP-1 is a matrix metalloproteinase that cleaves the C-terminal

propeptide of secreted tropocollagen. The cleaved C-peptide was quantified in the medium (Figure 4-20C) and found to be elevated under cyclic compression, which would be in agreement to the increased BMP-1 expression. However, even though the increased PIP concentration in the medium would also suggest an enhanced collagen I synthesis, the expression of COL1A2 after one week is only slightly increased by cyclic compression. It might be suggested that an increased collagen I expression at an early time point caused an increased secretion and an enrichment of soluble tropocollagen I. In contrast to the reduction in fibrillar collagen density in response to cyclic compression, lysyl oxidase (LOX) and lysyl oxidase like protein (LOXL1) were slightly increased. Since these enzymes mediate the covalent cross-linking of staggered collagen fibrils, an increase in their expression should in turn increase fibrillar collagen density, which stands in contrast to the histological observation (Figure 4-20). This discrepancy might be explained by an increased expression of the collagenase MMP13, suggesting increased collagen degradation. The increase in expression of TGFβ-induced protein, could point towards elevated levels of TGFβ secreted by fibroblasts under compression, since its expression is, as the name suggests, induced by the growth factor. The proteins specific function, however is still a matter of debate [186].

BMP-2 stimulation alone induced a strong 2.25-fold up-regulation of MMP1 (±0.4), a 1.5-fold increase in fibulin-1 expression and a down regulation of elastin and COL1A2 expression with a fold change of 0.6(±0.2) and 0.8(±0.3), respectively. Especially the regulation of elastin is distinctly different under cyclic compression or BMP-2 stimulation. Elastin is a fibrillar protein, which provides elasticity to tissues [187]. In this regard, it would be especially interesting to investigate if the changed elastin levels would change the tissues´ stress relaxation behavior, a material property which was previously shown to influence cell function [188]. Although, MMP1 expressions was elevated and COL1A2 expression was decreased under BMP-2 treatment in comparison to the control, previous histological quantifications of collagen 1 and fibrillar collagen density (Figure 4-20) do not indicate an increased collagen degradation. In the follow-up investigations, the activity of MMPs should be assessed, as MMP gene expression and enzyme activity might differ.

Under concurrent BMP-2 and mechanical stimulation, gene regulations are not as pronounced as under their individual influence but similarities can be observed. As in response to mechanical loading alone, a combination of both treatments increased the expression of TGFβ-induced protein in comparison to the control, however with reduced strength as in comparison to mechanical treatment alone (L=2-fold(±0.3) vs B/L=1.5-fold(±0.2)). As under BMP-2 treatment alone, a combination of both treatments increased the MMP1 expression by 1.5-fold (±0.2) and decreased the COL1A2 expression by 0.8-fold (±0.03) in comparison to the control. The regulation of MMP1 might contribute to the decreased

fibrillar collagen density observed in the ECM. The decreased COL1A2 expression is, however, in disagreement with the increased PIP concentration detected in the culture medium. In general, as qPCR analysis only represent the transcriptional activity of the cell at the time of lysis, it might be necessary to investigate the gene expression in a time dependent manner.

In summary, the gene expression analysis of selected ECM proteins and ECM modulators show that each condition; cyclic compression, BMP-2 or a combination of both, trigger distinctly different gene expression patterns, which suggest the formation of distinct, biochemically different ECMs. The strength of gene regulation under concurrent BMP-2 and mechanical stimulation was overall reduced in comparison to the individual treatments. This is pointing towards a mutual balancing of effects that might be of importance for regenerative processes.

To investigate whether gene expression regulations reflect the ECM protein composition, in the following mass spectrometry (MS) analysis were conducted. Since here the effect of cyclic loading on ECM formation particularly collagen formation was most intriguing, first MS analysis were focused on a comparison between static and dynamic culture.

4.3.4 ECM protein composition is specifically altered by mechanical loading

To investigate the composition of the ECM established under static conditions and under cyclic compression (both cultured in the bioreactor) via mass spectrometry, samples had to be decellularization, as the amount of cellular proteins would greatly overlay ECM proteins. The detergent-based decellularization approach using a perfusion system was previously established [171] and the protocol was adapted with the aim to preserve many ECM proteins, while removing most of the cellular components.

Figure 4-24A, represents a summary of all proteins detected in the matrices of both control and mechanically stimulated samples after decellularization. For a better overview, proteins were grouped into extracellular (blue) and cellular (gray) compartments. To increase the accuracy and reliability of the analysis, here only those proteins are depicted, which were identified by two peptides.

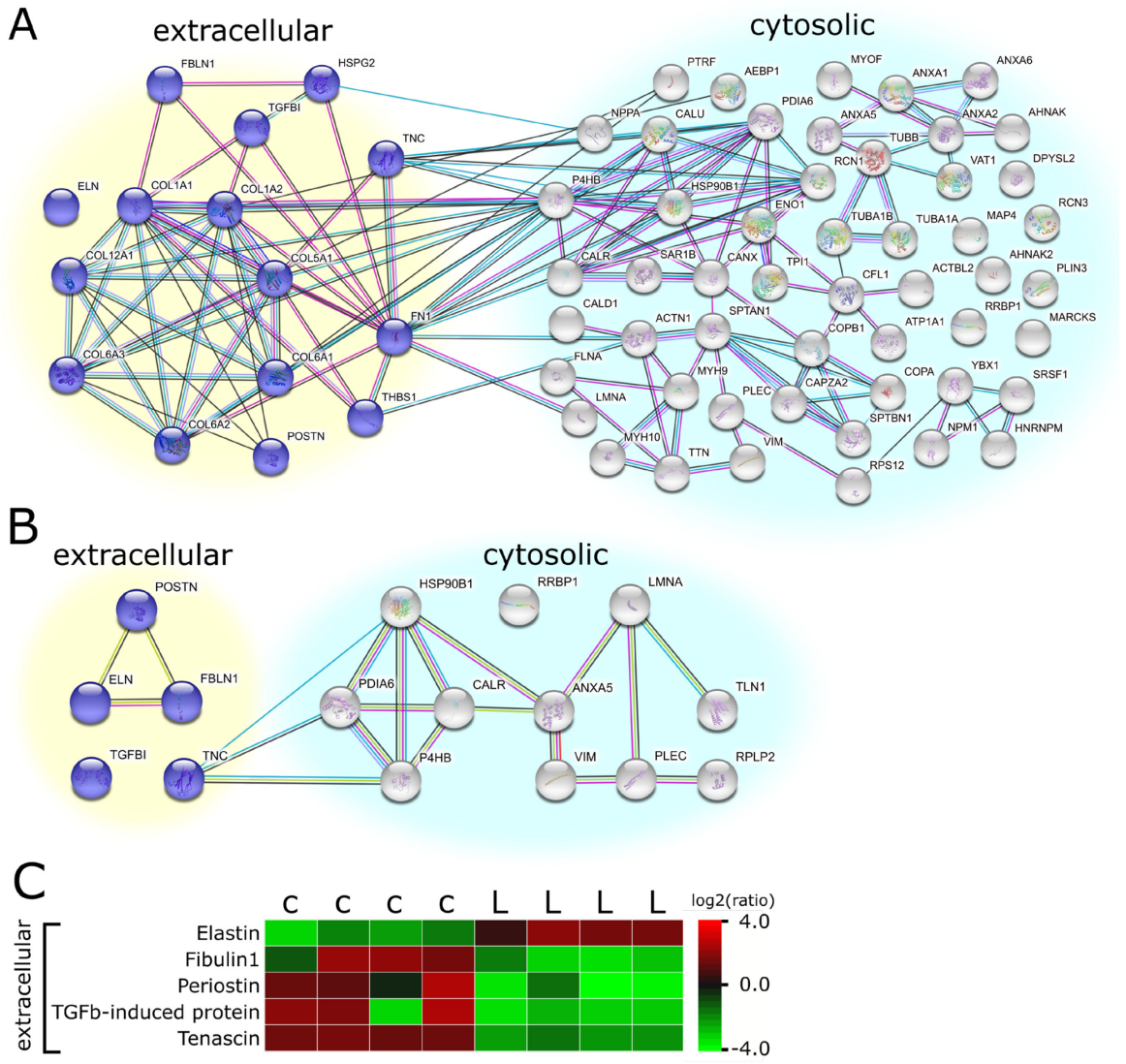

Figure 4-24: Cyclic compression induced distinct changes in the protein composition of the ECM. Human dF seeded in collagen scaffolds were cultured for 2 weeks in the bioreactor with (L) or without (c) 10% cyclic compression (f=1Hz, cycles of 3h stimulation and 5h break). Samples were decellularized, freeze dried and mass spectrometry analysis was performed. (A) Protein networks of all proteins detected in the two conditions grouped into extracellular (blue) and cytosolic (grey) proteins. (B) Network of proteins with significantly changed abundance between the conditions grouped into extracellular (blue) and cytosolic (grey) proteins. (C) Heat map of the log2 ratios of the abundance of each sample relative to the average abundance (only ECM proteins) (n=4).

The MS analysis securely identified 15 ECM proteins and 53 cellular proteins in all samples. Among those ECM proteins detected, five were significantly regulated with a fold change of ≥2 (Figure 4-24B). The abundance of elastin was increased, while fibulin-1, periostin, TGFβ-induced protein and tenascin were very consistently reduced under cyclic compression (Figure 4-24C). Interestingly, the regulation of elastin by cyclic compression is in agreement with the gene expression analysis (Figure 4-23). However, protein regulations of fibulin-1, periostin, TGFβ-induced protein and tenascin are in disagreement with the gene expression data. Although the expressions of fibulin-1, periostin, TGFβ-induced protein and tenascin were increased, their amount in the ECM was significantly reduced. This again highlights the importance to investigate all levels of the protein synthesis to gain a

comprehensive understanding. In agreement with the quantification of collagen 1 density (antibody staining against COL1A1), also MS analysis did not detect a change in the abundance of COL1A1. This observation again points towards a decelerated collagen fibrillogenesis under cyclic compression. In this context, it is interesting to mention that periostin is known to be involved in collagen-crosslinking (for details see section 5.7 of the discussion). Therefore, the MS analysis helps to understand why collagen fibrillogenesis might be disturbed under mechanical loading

In summary, the results obtained by MS analysis revealed distinct differences in the biochemical composition of extracellular matrices grown under static conditions or under cyclic compression. Since integrins specifically recognize ECM proteins, it is assumed that alterations in the biochemical ECM signature alter integrin adhesion and expression patterns and thereby potentially also BMP signaling.

5 Discussion

5.1 Mimicking mechanical loading conditions during the early phase of bone healing

To increase the physiological relevance of this work, special emphasis was laid onto the experimental design. The early healing phase is especially sensitive to mechanical signals and is believed to lay the ground for the entire repair process. Indeed, allowing limited interfragmentary movement in the early phase was shown to enhance fracture healing in a sheep model [43]. Axial interfragmentary movement was reported to be the main loading regime in animal osteotomy models with an external fixator [189]. Interfragmentary compression that occurs as a consequence of weight bearing in experimental bone healing studies was reported to range between 10 - 33% [37], [43] and 2 - 20% [40], [190] of the fracture gap for sheep and rat osteotomies, respectively. According to the reported *in vivo* data and in agreement with previous studies investigating the impact of mechanical loading on cell differentiation [91], [92], [94], [191], strain regimes of 5% and 10% were selected. To mimic the load pattern during human locomotion [192], a sinusoidal compression with a frequency of f= 1 Hz was applied in this study using the mechano-bioreactor. In summary, the loading parameters used in this study were chosen to represent regimes occurring *in vivo*, more specifically, to mimic the mechanical environment in the early fracture gap.

The biomaterial used in this study was made from fibrillar collagen, a component of the extracellular matrix that is a relevant cell substrate throughout the bone healing process [11]. The macroporous architecture assures a three-dimensional cell morphology and provides enhanced nutrient and oxygen supply for the cells even in the center for the scaffold. Collagen crosslinking during production protects the scaffolds from fast enzymatic degradation. Both, collagen crosslinking and its elastic deformation behavior, allowed repetitive compression without major shape-changes even over long periods of time [11], [171]. By changing the solid content, the wall stiffness was tuned without affecting the pore architecture (Figure 4-1). As the stiffness of the substrate that cells adhere to is known to be an important regulator influencing cellular behavior [56], scaffolds with bulk stiffnesses of 3.4 kPa and 12.3 kPa were to investigate load-induced osteogenic differentiation. The utilized scaffolds are characterized by low elastic moduli mimicking the physical environment in the fracture gap early after bone injury where a soft tissue matrix is present within the fracture gap.

5.2 Towards a deeper understanding how cyclic compression influences osteogenic differentiation

Multiple studies examined the influence of mechanical loading on stem cell differentiation, including osteogenic commitment (see section 1.3.3 and reviews [55], [170]). Motivated by a tissue engineering approach, the majority of these studies used osteoinductive medium supplements, bone derived scaffolds or hydrogels with limited supply masking effects of loading on cell fate decision. Even in studies working without additional osteogenic triggers, the influence of load-induced autocrine signaling was not investigated. Therefore, it remained unclear whether the observed mechano-sensitivity is a direct consequence of cyclic compression, an indirect effect of altered supply or a specific modulation of autocrine BMP signaling. In this dissertation, the direct influence of cyclic mechanical loading on the osteogenic differentiation of primary human bone marrow MSCs (hBMSCs) was investigated and dissected from the effect of load-induced supply changes and autocrine signaling, in particular of BMP-2. To investigate osteogenic differentiation, the expressions of common osteogenic markers were analysed.

Runx2 (Cbfa 1), a member of the RUNT domain gene family, is an indispensable transcription factor for osteoblast differentiation [193]. In this study the expression of RUNX2 in hBMSCs was found to be downregulated upon cyclic compressive loading (Figure 4-2). This observation stands in contrast to previous reports in which comparable experimental setups were used [91], [92], [94], [95]. It is known that Runx2 regulates the expression of osteoblast specific genes such as collagen type 1, bone sialoprotein, osteocalcin and RUNX2 itself [194]. Thus, the downregulation of COL1A2, which encodes the pro-alpha2 chain of type I collagen and osteocalcin observed in this study is most likely a consequence of the downregulation of RUNX2. Only one study was identified that reported an inhibitory effect of mechanical stimulation on the RUNX2 expression and, consequently, on other osteogenic markers. In this study, continuous application of mechanical loading over up to 10 days, might be responsible for the negative impact [195]. However, this can be excluded as an explanation in our study, since here only intermittent loading (repeated cycles of 3h cyclic compression and 5h break) was applied.

In contrast to RUNX2, COL1A2 and osteocalcin, a significant upregulation was found for osteopontin mRNA expression in response to 10% compression in the softer scaffold A (E=3.4 kPa). A possible explanation for this discrepancy is that osteopontin expression is regulated by an alternative mechanism independent of RUNX2. The expression of osteopontin was previously found to be sensitive to mechanical stimulations [91], [196]. Osteopontin is an abundant non- collagenous protein in the extracellular matrix of bones and serves as a cell

attachment point mediated through integrin binding [197]. It is conceivable that hBMSCs establish stronger attachments to their substrate in response to cyclic deformation of the walls by increased osteopontin secretion.

In summary, aside from osteopontin, all investigated osteogenic marker genes were found to be downregulated in response to cyclic compression. This surprising finding contradicts the majority of literature on this topic. A reason for the discrepancy may be found in the specific experimental conditions. In comparison to others, we can exclude previously reported indirect effects of mechanical loading on oxygen concentration and nutrient supply inside the biomaterial due to the chosen macroporous architecture [173]. A further major difference is the low total cell number in relation to the volume of cell culture medium in the bioreactor ($1.5x10^5$ cells/ 27ml medium) compared to the cultivation of 3D cell seeded constructs in well plates with low medium volume [91], [94], [95]. This in combination with the small but decisive fluid flow in the bioreactor, lead to a strong dilution of signaling proteins secreted by the cells (here demonstrated for BMP-2, Figure 4-4) and hinder autocrine biochemical self-stimulation.

5.3 Cyclic compression possess an osteoinductive potential only in a BMP-enriched environment

As an indicator for an osteogenic response to cyclic compressive loading, and in contrast to the osteogenic genes mentioned above, BMP-2 expression and secretion were found to be enhanced. This is in line with previous studies, reporting about a mechanosensitive BMP-2 expression [97], [198]. The growth factor BMP-2 is known to be an indispensable player during bone repair [28] and it's in vivo administration leads to bone defect healing [199]. In fact, BMP signaling regulates the transcription of RUNX2 through the activation of the Smad transcription factors [176]. Based on this connection, we hypothesized that cyclic compression does not induce osteogenic differentiation per se but only in presence of BMPs. The addition of rhBMP-2 in combination with cyclic compression caused a strong enhancement of RUNX2 and BMP-2 gene expression. This observation is remarkable, since in the absence of rhBMP-2, cyclic compression suppressed the transcription of RUNX2 mRNA. Hence, it indicates that BMP-2 is capable to alter the cell's gene expression response to cyclic compression. Strikingly, after increasing the cell-to-medium ratio in bioreactor experiments the fold change expression of RUNX2 was significantly increased in response to 10% cyclic compression even in the absence of an additional rhBMP-2 stimulus. The changed culture conditions enabled a significant enrichment of BMP-2 in the culture medium, confirmed by ELISA quantification (Figure 4-4B). Cyclic compression further increased BMP-2 expression and secretion pointing to an autocrine BMP-mediated increase of RUNX2 expression.

Treatment with rhNoggin verified the importance of cell-secreted BMP-2 in inducing RUNX2 expression under cyclic compression (Figure 4-5). That rhNoggin treatment did not fully recapitulate R_{low} conditions under which RUNX2 expression was downregulated, could have two reasons, either the concentration of rhNoggin was not sufficient to fully inhibit BMP-2 signaling, or a BMP-independent mechanism is additionally acting under R_{high} conditions. A BMP-2-mediated induction of osteogenic differentiation under cyclic compressive load was previously postulated [96], [97]. Rui *et al.* (2011) correlated an upregulation of BMP2 expression under loading conditions to an increased expression of either RUNX2 or ALP in rat tendon derived stem cells. However, the hypothesis was not proven by the exclusion of BMP-2 from their systems as it was done here by the dilution effect (in R_{low} condition) and the addition of rhNoggin (in R_{high} condition). Wang *et al.* (2010) instead showed in a 2D setting using the MC3T3-E1 cell line, that Noggin treatment abolished ALP expression induced by mechanical loading (four-point bending device), thereby demonstrating the role of BMP in this context. Our findings highlight the physiological relevance of load-induced effects for cell differentiation processes in a 3D bone healing context, since primary human bone marrow-derived MSCs from multiple donors were utilized.

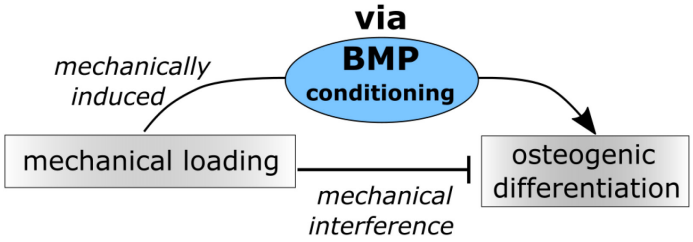

Figure 5-1: Cyclic compression promotes osteogenic differentiation via BMP. In this study, mechanical stimulation alone did not promote osteogenic differentiation but enhanced the expression of BMP-2. It is proposed that mechanical loading is able to promote osteogenic differentiation via autocrine signaling through BMP-2.

It was found that the increase of BMP expression in response to cyclic compression contributes to a positive feed-back loop enhancing osteogenesis (see Figure 5-1). In addition, cyclic compression not only increases the expression of but also the sensitivity for BMP-2. It was shown in human fetal osteoblasts [125] and in hBMSCs (Figure 4-6) that cyclic compression enhances BMP-2-signaling events under concurrent BMP-2 stimulation. These two mechano-regulated processes – an increased expression of BMP-2 and an increased sensitivity for BMP-2 – seem to contribute jointly to the osteogenic commitment of hBMSCs under cyclic mechanical compression.

5.4 Cyclic compression integrates into the BMP signaling pathway only in a ligand dependent manner

The transcriptional regulation of RUNX2 is controlled by several transcription factors and mechanisms and is not jet fully understood. The described transcriptional regulators,

Smad1/5 [176] and DLX5 [200] (Distal-Less Homeobox 5) are important enhancers binding to the promoter region of RUNX2. Smad proteins need to be activated by phosphorylation and form a trimeric complex to function as transcription factors. Phosphorylation is mediated by the BMP receptor complex upon BMP-ligand binding [113]. DLX5 is a direct target gene of BMP-Smad signaling specifically induced by BMP-2 or BMP-4 [200]. The Smad pathway is therefore crucially important to enhance RUNX2 expression. To induce RUNX2 expression via mechanical stimulation, mechanotransduction events would need to directly (ligand independently) activate the BMP-Smad pathway. This was tested in short-term bioreactor experiments analyzing the BMP pathway under cyclic compression. However, in all cell types tested here (hFOB, hMSC, hdF, Figure 4-6), cyclic compression alone did not induce Smad1/5/8 phosphorylation or ID1 expression. In the literature it is still discussed controversial whether mechanical forces activate Smad signaling in a ligand dependent or independent manner. Some studies reported that loading alone was sufficient to activate R-Smads [123], [127] while others described a ligand dependent activation in osteoblastic cells [96], [125]. This discrepancy may be explained by the use of different experimental setups including the type of force (fluid shear stress vs cyclic compression) and pre-incubation of cells up to 7 days prior to loading without medium exchange. Although, fluid shear stress and cyclic compression might trigger distinct mechanotransduction pathways differently affecting Smad signaling, shear stress alone did not stimulate R-Smad phosphorylation in hFOBs (data obtained by Dr. Maria Reichenbach, FU Berlin, Knaus Lab), which is in contrast to Kido *et al.* [127]. In case of a pre-incubation of cells up to 7 days prior to loading without medium exchange, it is likely that mechanical forces induced Smad phosphorylation due to autocrine BMP secretion. This assumption is supported by a study showing, that Smad phosphorylation in response to mechanical stimulation was abolished after the addition of noggin during the loading experiments [96]. For these experiments, stimulation by autocrine BMP secretion was avoided by exchanging the culture medium to starvation medium only 3h prior to cyclic compression as well as by using large medium volumes. Therefore, it is concluded here that mechanotransduction pathways only activate BMP-Smad signaling in a ligand dependent manner. This also serves as an explanation for the observation that cyclic compression enhances RUNX2 expression only in a BMP-enriched environment as it was described in section 5.3.

5.5 The mechano-sensitivity of BMP signaling is dependent on the loading frequency and timing

As discussed in the previous section, mechanical forces have no influence on BMP signaling in the absence of the BMP ligand. However, in the presences of BMP, mechanical forces are

strikingly able to enhance the growth factor´s signaling. This mechano-regulation of BMP signaling, here also referred to as the crosstalk between mechanotransduction and BMP signaling, was described before using different cell types and experimental conditions. While different types of forces like oscillatory fluid shear stress [124], [127], [128], cyclic tension [180] and compression [123], [125] were found to promote BMP signaling, systematic investigations of how different loading parameters of the same force influence the duration and strength of BMP signaling were missing. Such investigations would, however, be important to defined parameters optimally supporting BMP signaling and furthermore, to gain insides into the dynamics of this regulation.

Therefore here, the impact of the loading frequency on early BMP signaling events was investigated in a time dependent manner. Cyclic biomaterial compression with a frequency of 1 Hz was chosen as it represents the frequency of human locomotion and was previously shown to enhance Smad1/5/8 phosphorylation [125]. Additional frequencies of 10 Hz, representing muscle contraction [201] and a comparably low frequency of 0.03 Hz were selected for comparison. As expected, the loading frequency strongly influenced the strength and the duration of early and late BMP signaling events. Whereas the crosstalk strength was saturated at 1Hz, the crosstalk duration at Smad and gene expression levels increased with increasing frequency. The increase in the crosstalk duration was especially obvious when analyzing the gene expression after 24 hours showing an increase in BMP target genes (ID genes, noggin, Smad7) only for 10 Hz. Therefore, frequency-dependent effects on early Smad phosphorylation persisted and transduced to the level of BMP target gene expression, confirming the importance of the loading frequency for a long-term cell response.

It is proposed that the magnitude and duration of Smad-phosphorylation following cyclic loading are a measure of how strong mechanotransduction pathways are activated and how fast cells adapt to the changed mechanical environment. Evidence for this is provided by the frequency dependent regulation of c-fos expression (see fig. 4-8). C-Fos is a highly mechano-responsive gene [181] that was shown to be induced via integrin-FAK signaling [202]. Furthermore, this conclusion is based on literature reports analyzing frequency dependent mechanotransduction responses. An increasing alignment of endothelial cells perpendicular to the stretch direction, going along with stress fiber reorientation, was observed with increasing stretch frequency (0.01 Hz , 0.1 Hz, 1 Hz) [203]. This was attributed to a frequency-dependent increased in p38 phosphorylation, as the reorientation was hindered by the inhibition of the p38 pathway [204]. Furthermore, cyclic pull on a fibronectin coated ferromagnetic beads attached to vascular cells increased ERK1/2 phosphorylation in a frequency dependent manner (from 0.5 to 2 Hz) by two-fold. Since fibronectin binding is mediated via integrin receptors, activation of the ERK1/2 pathway was attributed to

frequency-dependent integrin signaling [205]. The frequency-dependent regulation of mechanotransduction pathways is also relevant on the tissue level, as the bone formation rate in the rat tibiae [206] or ulna [207] increased with increasing frequency of cyclic bending (0.05, 0.1, 0.2, 0.5, 1 and 2 Hz) or compression (1, 5, 10 Hz), respectively. Interestingly, it was found that lower compression load (N) was needed at 10 Hz in comparison to 1 Hz compression to yield the same bone formation rates [207].

Based on the similar frequency dependency observed in *in vivo* studies, it is therefore suggested, that the crosstalk between mechanotransduction and BMP signaling is involved in the adaptation of bones to mechanical loading.

Strikingly, cyclic compression alone was found to increase the expression of BMP receptor 1B but not BR1A or BR2, whereas BMP-2 treatment had no effect on either of the receptors. A thorough literature research did not reveal other studies reporting about a mechano-regulation of BMP receptor expression. The present work thus adds another important information to understand how mechanical signals regulate BMP signaling.

Cyclic compression was also found to increase the expression of integrin αv and β3 in a frequency-dependent manner, whereas the expression of integrin α1, α5 and β5 were not regulated. Even though BMP-only treatment had no effects on integrin expression, BMP-2 stimulation under concurrent cyclic compression further enhanced integrin β3 expression highlighting the mutual interaction between mechanotransduction and BMP signaling. Despite the unchanged integrin expression levels upon BMP-2 stimulation, both BMP-2 treatment and cyclic compression increased the size and amount of integrin-mediated adhesions visualized by p-paxillin staining. This led to the suggestion that BMP-2 treatment mainly promoted integrin clustering, but comparable literature data is missing to confirm this assumption. It can be concluded that the strong increase in integrin expression under 10 Hz loading and the increased integrin clustering under BMP-2 led to the synergistic increase of FA size and amount under concurrent stimulation. Consistent with the results presented here, mechanical forces were previously shown to induce the expression of specific integrin subtypes [208] and growth of adhesion sites [209].

The observed increase in integrin expression and FA assembly, together with the increased expression of BMP receptor type 1B under mechanical stimulation was especially interesting since both, an increased amount of BMP receptors and the described BMP receptor-integrin interaction [128], [130] could promote BMP signaling.

Consequently, two hypotheses arose:

(1) Long-term mechanical loading sensitize the cells for BMP-2 so that subsequent concurrent mechanical and BMP-2 stimulation would even further increase the crosstalk.

(2) Long-term mechanical loading leads to the establishment of a “mechano-memory”, which would be sufficient to mediate the crosstalk, even though mechanical and BMP-2 stimulation are not concurrently applied.

Against the hypothesis (1), mechanical pre-stimulation did not further increase BMP signaling, neither on p-Smad level nor on gene expression level, under subsequent concurrent mechanical and BMP-2 stimulation. On p-Smad-level, this might be explained by a potential saturation of phosphorylation already under crosstalk-control conditions (90 min, 1Hz, 10%, 5nM BMP-2). As a consequence a further increase of Smad phosphorylation due to pre-stimulation could not be detected. Evidence for this is provided by the analysis of frequency-dependent Smad phosphorylation, where the p-Smad level reached saturation at 90 min for 1Hz and 10 Hz. Therefore, the result could be further supported by the investigation of an earlier time point (30 min), where a saturation is not jet reached.

Hypothesis (2) was tested by an experiment where mechanical stimulation was applied for 30 min, 90 min and 24 hours prior to but *not during* BMP-2 treatment. Intriguingly, it was observed that long-term mechanical pre-stimulation over 24h induces a persistent mechanical activation sufficient to increase Smad phosphorylation under BMP stimulation even in the absence of a direct mechanical trigger. This observation is the first prove for the existence of a so-called *mechano-memory* concerning the crosstalk between BMP-2 and cyclic mechanical compression. Interestingly, the shorter the time of mechanical pre-stimulation was chosen, the weaker was the effect. While 24 hours were as efficient as the crosstalk-control, 90 min only reached 50% of the controls’ crosstalk strength and 30 min was too short to induce a mechano-memory (Figure 4-12). This observation provides valuable information about the kinetics of the mechano-memory which is relevant to identify the underlying mechanisms. Cellular adaptation processes involving cytoskeletal reorganization or conformational changes of proteins are taking place within minutes after the onset of mechanical stimulation [210], [211]. Adaptation processes due to transcriptional regulations, however, take several hours [182]. Therefore, during 30 min cyclic compression cells potentially have remodeled their cytoskeleton and might already have reinforced their adhesion sites, but transcriptional regulations haven’t had any effects yet. After 90 min of mechanical stimulation, cytoskeleton and adhesion site have adapted and the first effects of transcriptional regulations might contribute to meet the new mechanical requirements. After 24h non-transcriptional and transcriptional responses have potentially established a new mechanical equilibrium. Since only 24 hours pre-loading was as efficient as the crosstalk-control, it is assumed that mechanical information need to be translated and stored in transcriptional regulations in order to persist beyond the phase of mechanical stimulation. It is suggested, that the observed mechano-memory is inter alia mediated by the load-induced

increase in BMP receptor type 1B expression that would lead to an increase in the amount of receptors available for ligand binding and Smad phosphorylation. Additionally, taking into account the here described role of integrin αvβx, a load-induced increase in expression of integrin αv and β3 as well as FA clustering could lead to increase in BMP receptor-integrin interactions, thereby promoting BMP signaling.

Physiologically, the existence of a mechanical memory is of high importance for tissue homeostasis, growth and adaptation like exercise-driven muscle or bone strengthening. In this context, the here described mechano-memory concerning the crosstalk between BMP-2 signaling and mechanical loading might play an important role in bone metabolism. It is suggested that cyclic loading during exercise increases the expression of endogenous BMP-2 (paragraph 4.1). The growth factor accumulates over time in the extracellular environment and triggers BMP signaling, which is enhances by mechanical stimulation even if the person is already resting. However, it still needs to be elucidated how long-lasting this effect is, in other words on what time-sale the information in the memory is vanishing. Therefore, in potential follow-up experiments, BMP-2 should be added at different time points (e.g. 15, 30 and 90 min) after pre-loading. Concerning the existing literature, the phenomenon of mechanical memory has been exclusively investigated with respect to passive biophysical cues like substrate rigidity [182] but not with respect to active and alternating mechanical forces. For example, prolonged culture of hMSCs on stiff matrices that led to nuclear translocation of YAP (yes-associated protein 1), a mechano-sensitive transcription factor, prevented YAP re-localization into the cytosol even when cells were subsequently cultured on soft matrices. These extended pre-cultures on stiff substrates biased hMSCs towards osteogenic differentiation on soft substrates [212]. The application of prolonged external forces might have a similar effect on YAP and osteogenic differentiation but a YAP mediated mechano-memory on BMP signaling is unlikely, since the effects on Smad phosphorylation are at the level of the receptor and not at nuclear level.

5.6 Integrin αv and load-induced integrin and F-actin reorganization processes are required for the crosstalk

While transcriptional regulations are suggested to be an integral part of the mechano-memory, the early induction of Smad phosphorylation upon *concurrent* mechanical and BMP-2 stimulation must be, due to its immediateness, independent of any transcriptional regulation. However, the question remains which mechano-responsive structure facilitates the fast integration of mechanical signals into the BMP pathway? The Smad phosphorylation investigated in detail in this thesis is an immediate early BMP signaling event. Since mechanical forces enhance BMP receptor-mediated Smad phosphorylation already after 15

min, mechanoresponsive structures at the level of the plasma membrane are potential candidates that facilitate the crosstalk.

Two prominent mechanosensitive structures located at the plasma membrane are ion channels and integrins. But also the BMP receptors themselves could possibly function as mechano-receptors. Reports from literature motivate to investigate a possible *integrin*- BMP signaling crosstalk. Integrins were reported to interact with BMP receptors leading to positive or negative regulations of basal BMP signaling depending on the context (cell type and experimental conditions) [130], [213]. But intergins could also be involved in the mechano-regulation of BMP signaling. Interestingly, a study by Zhou *et al. (2013)* investigating the fluid flow- mediated phosphorylation of Smad1/5 in endothelial cells (EC), proposed that: "*oscillatory shear stress induces synergistic interactions between specific BMPRs and integrin to activate Smad1/5 through the Shc/FAK/ERK pathway, which leads to the activation of the Runx2/mTOR/p70S6K pathway to promote EC proliferation*" [128]. However, this study distinguishes itself strongly from the present work. Firstly, ECs in contrast to hFOBs respond in a BMP-ligand independent manner to mechanics and secondly, the application of fluid flow in 2D instead of cyclic compression in 3D. Therefore, it still remains to be elucidated in the context of bone healing, where different cell types and mechanical stimuli are relevant. Here it was hypothesized, that integrin αv and β3, which were specifically increased in expression upon mechanical stimulation, are important for the integration of mechanical signals into the BMP pathway. Since the knockdown of integrin αv reduced Smad1/5 phosphorylation under mechanical stimulation in comparison to the crosstalk-control (Figure 4-14), it is suggested that αv- βx integrins are involved in the mechano-regulation of BMP signaling. However, since αv not only interacts with β3 but also β1, β5, β6 and β8 [64] it is still open which integrin αv-heterodimer is responsible. In a next step a β3 integrin knockdown is suggested to be performed to verify or falsify the hypothesis. It is however important to mention that all αv-heterodimers are RGD-binding receptors (fibronectin, osteopontin, tenascin and other soft ECM components). Changing the ECM composition or the substrate stiffness, both influencing the expression/activation of integrins, will therefore indirectly control the integration of active mechanical signals into the BMP pathway. It is hypothesized that cells on soft vs. stiff substrates will differently respond to mechanical stimulation in regards to BMP signaling amplification. However until today, only stiffness dependent basal BMP signaling was investigated [136], [214].

Here it was shown that αv integrins are involved in the mechano-regulation of BMP signaling, but further investigations need to clarify whether this is due to a direct physical integrin-BMPR association, or indirectly via integrin signaling events. Zhou *et al.* (2013) proposed an activation of Smad1/5 through the Shc/FAK/ERK pathway in endothelial cells.

However, while FAK phosphorylation increased under cyclic compression (Figure 4-15), ERK and Shc phosphorylation were not found to be regulated in the present study (supplementary Figure 0-6). Therefore, different mechanisms of integration might be existing in osteoblasts versus endothelial cells.

If a direct interaction of intergins and BMP receptors is assumed to mediate the integration of mechanical signals into the BMP pathway, the question remains whether this interaction already existed under static conditions, or whether it needs to be established in response to mechanical stimulation? The latter scenario would imply that load-induced remodeling/reorganization of intergins and BMP receptors must have preceded an interaction. A load-induced reorganization of focal adhesions was observed here (Figure 4-10) and is described in the literature [215]. To prevent reorganization and thereby an integrin-BMPR interaction in response to mechanical loading, the actin cytoskeleton stabilizer Jasplakinolide was used. Since activated integrins are connected to the actin cytoskeleton and a structural reorganization of the actin cytoskeleton under fluid flow orchestrates the reorganization of adhesions [80], an inhibition of actin remolding would consequently inhibit integrin-adhesion remodeling.

At first it was verified by time-lapse imaging under fluid flow that mechanical stimulation indeed triggers a dynamic actin remolding process, as it was previously described [79], [80], [216]. In cells stimulated with fluid flow, area and speed of protrusion extension and protrusion retraction was increased, which is a measure for the actin remodeling dynamics. Additionally, the phosphorylation of myosin light chain, the regulatory subunit of the myosin motor protein, was increased significantly under cyclic compression, indicating a load-induced reinforcement of the actin cytoskeleton that goes along with a remodeling and adaptation process.

Secondly, the previously described stabilizing-effect of Jasplakinolide on actin remodeling processes [217] was proven under static and flow conditions (Figure 4-17). In agreement with Cramer *et al.* (1999) Jasplakinolide inhibited the dynamic remodeling of protrusion. It should be noted that the effect of Jasplakinolide was extremely concentration dependent. High concentrations (≥0.1µM in 2D (Figure 4-16) and >0.5 µM in 3D (data not shown)) led to a gross disruption of actin organization and the formation of actin aggregates, which is in accordance with previous investigations [184], [218]. Since a disintegration of the actin cytoskeleton structure would not only alter immensely the cell morphology but also cellular mechanosensation, the concentration and timing of Jasplakinolide stimulation was adjusted carefully. By doing so, actin remodeling could be blocked without major alterations of the actin organization and cell morphology. In this case, the actin filaments are still taking part in mechanotransduction processes by transmitting mechanical tension to other proteins.

However, certainly by changing the actin dynamics, also other load-induced processes were altered. Even though in turn the remodeling of adhesions sites is reduced, it is assumed that integrin signaling is not altered.

After proving the ability of Jasplakinolide to efficiently inhibit actin remodeling dynamics in response to mechanical stimulation, the agent was used to test the hypothesis whether load-induced dynamic remodeling of the actin cytoskeleton and associated integrin adhesion remodeling is essential for the mechano-regulation of BMP signaling. Jas treatment during the bioreactor experiment abolished the positive effect of cyclic compression almost completely, while basal BMP signaling remained unaffected (Figure 4-18). It is thus proposed here that actin cytoskeletal adaptations in response to cyclic compression is a prerequisite for the mechano-regulation of BMP signaling. It is suggested that the stabilization of the actin cytoskeleton hinders the remodeling of integrins in the plasma membrane and in turn their interaction with BMP receptors. Certainly, this needs to be elucidated further, for example by using proximity ligations assays to assess a reduction of integrin-BMPR interaction upon Jasplakinolide treatment.

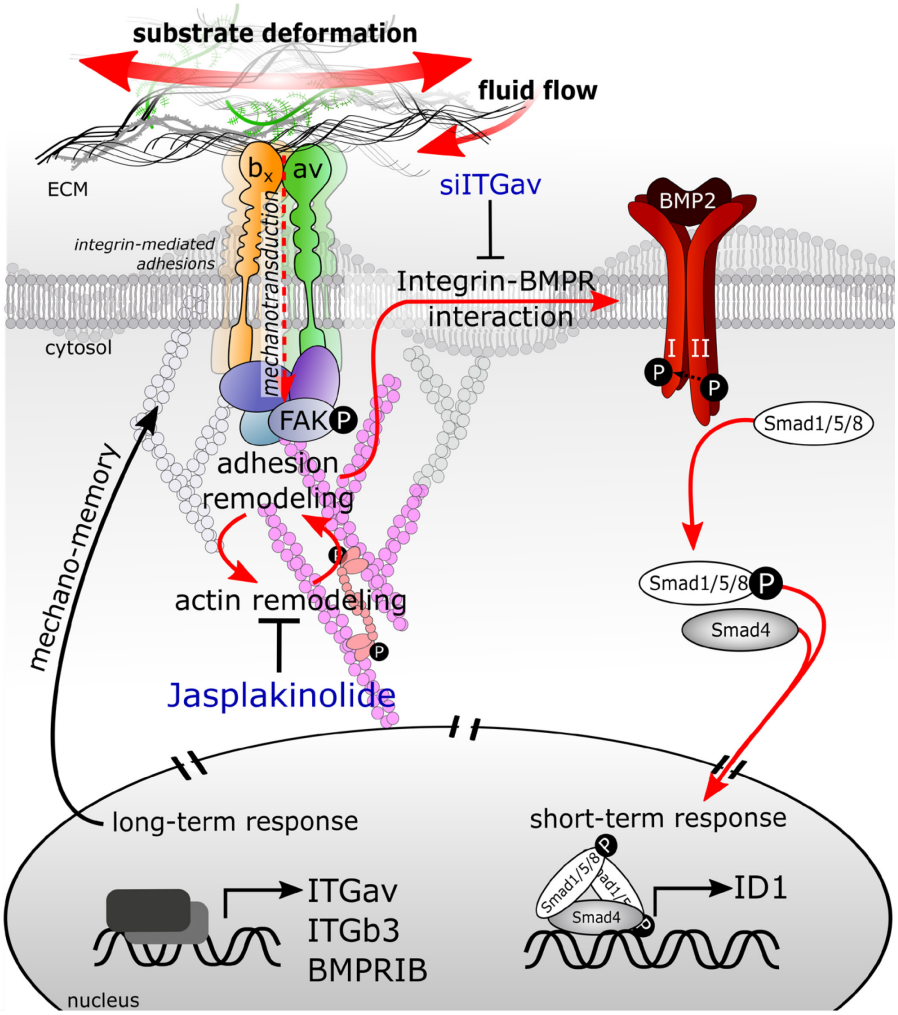

Figure 5-2: Schematic representation of how mechanical forces integrate into BMP signaling. Mechanical stimulation induces mechanotransduction via integrin signaling (via FAK) which leads to the remodeling of the actin cytoskeleton associated with increased protrusion dynamics, which in turn stimulates integrin-adhesion remodeling. The dynamic reorganization and maturation of adhesion sites causes increased interactions of αv-βx integrins and BMP receptors, which leads to the amplification of Smad1/5 phosphorylation and early target gene expression (ID1). Knockdown of integrin αv reduces the amount of interaction partners for the BMP receptor, thereby reducing the mechanosensitivity of BMP signaling. Inhibition of load-induced actin remodeling hinders the remodeling of adhesions and in turn the interaction of αv-βx intergins and BMP receptors. Long-term mechanical stimulation will trigger the expression of BMP receptor Ib (BMPRIB) and integrin αv (ITGav) and β3 (ITGb3) possibly responsible for the mechano-memory of BMP signaling.

In summary, (i) the load-induced growth of FA adhesions going along with a reorganization of integrins, (ii) the decrease in crosstalk efficiency after integrin αv knockdown (iii) the decreased crosstalk after F-actin stabilization and (iv) the known BMP receptor-integrin interaction [128], [130] led to the interpretation that the induction of intergin reorganization in response to mechanical loading and BMP-2 stimulation causes increased interactions of αv-βx integrins and BMP receptors, which leads to the amplification of Smad1/5 phosphorylation. A knockdown of integrin αv reduces the amount of interaction partners for the BMP receptor, thereby reducing the mechano-sensitivity of BMP signaling. Inhibition of load-induced actin remodeling hinders the reorganization of intergins and in turn the interaction of αv-βx integrins and BMP receptors. Long-term mechanical stimulation

triggers the expression of BMP receptor Ib and integrin αv and β3 proposed to be responsible for the mechano-memory of BMP signaling.

5.7 Mechanical forces specifically alter mechanical, structural and compositional matrix cues

BMP-2 is known for its strong osteoinductive potential and its influence on cell differentiation in the context of bone healing is well studied. However, the growth factor should not be reduced to this feature alone, as it was described to influence process which happen much earlier during the bone healing cascade. These processes include, cell migration [23], proliferation [22], angiogenesis [219] and evidences point towards an additional role in steering early extracellular matrix formation processes [149], [155]. During bone healing, extracellular matrix formation is initiated directly with the end of the pro-inflammatory phase [15] and the early structural organization of collagen fibers within the fracture gap was shown to critically influence healing [11]. Given the importance of early ECM formation processes and the fact that both BMP-2 [149], [155] and mechanical forces [142]–[146] were independently described to influence such processes, it is even more important to study how ECM formation is influenced by their mutual interaction. To better understand a potential crosstalk, in this study the individual and mutual influences of cyclic mechanical loading and BMP-2 stimulation on ECM formation were compared. Since mechanical forces have already been shown to promote BMP signaling, it was hypothesized here that this positive effect is transduced to the ECM-level. This means that cyclic loading was expected to further enhance BMP-2-specific ECM alterations under concurrent treatment.

For the investigation of ECM formation processes in 3D, the macroporous collagen scaffold, which was previously used as an *in vitro* tissue formation model system [146], [171], [220], was selected. Due to its high porosity, it provides space for the fibroblasts to de-novo deposit ECM and furthermore allows ECM imaging and reliable quantification of the cell-derived fibrillar collagen, as it is spatially and structurally distinguishable from the scaffold walls. In addition, the macroscopic stiffness of the scaffold selected here (5.9 ± 0.6kPa) allows for a slow cell-mediated biomaterial contraction during culture (Figure 4-19). This feature is very interesting, since tissue contraction represents an important process during tissue repair to re-establish the tissue pretension, which was destroyed upon injury [185], [221]. However, cells alone are not capable to contract the scaffold. Instead, contraction requires the gradual conversion and storage of cell forces into cell-deposited, pre-tensioned collagen fibers [171]. Additionally, fibrillar collagens are an integral structural component of the ECM, greatly defining its mechanical properties [140]. Material properties like structure and stiffness in

turn greatly influence cell behavior such as cell signaling, specifically BMP signaling [136], [222] and differentiation [56], [58]. Therefore in this thesis, ECM formation processes were analyzed with a special focus on how mechanical and BMP-2 stimulation impact tissue contraction, stiffening and structuring, processes which are influences by collagen formation and which vice versa affect cell behavior.

Effects of BMP-2 treatment: Here is was found that, BMP-2 treatment led to a slightly enhanced tissue contraction and stiffening in comparison to the control (see Figure 4-19). Due to the increased contraction and the accompanied bending of the collagen walls, the alignment of collagen fibers and cells were in turn slightly reduced (see Figure 4-22). No changes could be observed on the level of collagens. Neither the expression of collagen I or VI, nor the concentration of secreted pro-collagen type I, nor the amount of collagen type I deposited into the matrix, nor the fibrillar collagen density was changed in comparison to the control (see Figure 4-20 and Figure 4-23). However, since the amount of fibrillar collagen correlated with the amount of tissue contraction [171], it might be assumed that BMP treatment potentially stimulates cellular contractility, which is supported by other studies [54], [223]. Gene expression analysis revealed a strong upregulation of MMP1 transcription by BMP stimulation (see Figure 4-23), which is in agreement with a previous study [224]. MMP1 is a collagenases cleaving collagen type I, II and III [225], while only type I and III are secreted by fibroblasts. This would point towards an increased degradation of the collagenous ECM, which was however not reflected in the quantification of collagen. To further validate the regulation of MMP1 and other MMPs, it would be necessary to investigate the MMP protein levels and their activity using for example zymographic analyses. Additionally, the expression and protein levels of tissue inhibitor of metalloproteinases (TIMPs) should be examined since they control the activity of MMPs [141]. Even if no changes on the level of collagens were observed, gene expression analysis showed an upregulation of fibulin-1 and a strong downregulation of elastin expression in response to BMP stimulation. Fibulin-1 is a family member of eight glycoproteins and its function has been associated with cell adhesion and matrix remodeling due to integrin and metalloproteinase interactions, respectively [226]. Furthermore, fibulin-1 deficient mice show a clear bone phenotype with reduced bone volume and mineralization. It can be found in the ECM surrounding osteoblasts and was suggested to function as a positive regulator of BMP signaling in mice [227]. Elastin is secreted as tropoelastin that is cross-linked via lysyl oxidases to form elastin fibers onto preformed bundles of fibrillin microfibrils. As the name suggests, elastin fibers provide elasticity to tissues. While a regulation of elastin expression by BMPs has not been described so far, TGFβ1 was found to have pro-elastogenic activities [187].

Taken together, even though some minor changes on tissue contraction, stiffening and gene expression have been observed, a clear and dominant BMP-effect on ECM formation was not detected for the analyzed parameters. Prolonged culture times and a profound mass spectrometry analysis might be necessary to identify the expected BMP-matrix phenotype. Even though the responsiveness of fibroblasts to 5nM BMP-2 stimulation was verified before the experiment (Figure 4-6), it could be possible that higher BMP-2 concentrations are required to observe an effect.

Effects of cyclic compression: Most striking was the effect of cyclic compression on matrix formation. At first, a significantly increased tissue contraction was observed in axial and radial direction (see Figure 4-19). Although the collagen scaffold is fully elastic, upon deposition of ECM a composite material is formed consisting of collagens, elastic fibers and water-binding glycosaminoglycans that is characterized by viscoelastic mechanical properties and a certain stickiness. Repeated axial compression consequently led to a tissue compaction in the loading direction. However, since most of the materials respond with radial expansion upon axial compression, the radial contraction perpendicular to the loading direction observed here, must have been driven by active cell forces triggered by mechanical stimulation. Going along with the increase in contraction and the accompanied deformation of the collagen walls, the cells and the ECM adopted a more isotropic orientation (see Figure 4-22). Furthermore, a tissue stiffening was observed likely as a result of tissue densification. Interestingly, mass spectrometry revealed an increased abundance of elastin in the matrices of loaded samples. As described above, elastin fibers provide elasticity to tissues, therefore, it is found in great amounts in tissues, which are subjected to dynamic loads, like blood vessels, ligaments and skin. Static stretching has been shown before to induce elastin expression in smooth muscle cells [228]. However, cyclic stretching (5 and 10% for 24h) of periodontal ligament fibroblasts decreased elastin expression [229]. It might be speculated that fibroblasts try to counteract the increasing compaction of their environment by introducing an elastic ECM component.

Intriguingly, the increase in tissue contraction and stiffening was not accompanied by an increase, but a significant reduction in the amount of fibrillar collagen (see Figure 4-21). This again might suggests that cellular contraction forces might be accelerated in response to loading. Indeed, increased matrix stiffness [230] and mechanical tension [231] triggered the transdifferentiating of fibroblasts into myofibroblast, which feature a strong contraction ability. An immunohistological staining for α-smooth muscle actin, a myofibroblast marker, might be a way to clarify whether mechanical loading indeed increases cell contractility leading to the here-observed contraction of scaffold-based *in vitro* tissues.

The significantly reduced fibrillar collagen density observed under mechanical stimulation stands in striking contrast to (i) the strong and significantly upregulated secretion of pro-collagen type I C-peptide, (ii) the unchanged collagen I density assessed via specific antibody staining and (iii) unchanged collagen type I and VI abundance assessed via MS analysis. Also after 2 weeks of culture, fibrillar collagen density remained decreased in comparison to the control indicated by preliminary experiments (see supplementary Figure 0-5). Therefore in conclusion, cyclic compression disturbed the assembly of thick fibrillar collagen bundles, raising the question how and at which stage fibrillogenesis is disturbed?

Collagen fibril formation is a complex multistage process starting with the intracellular assembly of triple helices from synthesized and modified single proα-chains. After secretion of the soluble procollagen molecules, the propeptides at each end of the triple helix are cleaved enzymatically. The C-propeptide, which was measured in the culture medium (see Figure 4-20), is cleaved by the metalloproteinase BMP-1 and by other members of tolloid-like metalloproteases [140]. In agreement with the increased C-propeptide concentration, the expression of BMP-1 was increased under mechanical stimulation (Figure 4-23). The resulting tropocollagens self-assemble into staggered collagen fibrils, a process which is regulated by cell-adhesions like integrins and other ECM proteins like fibronectin. To stabilize the fibril and strengthen its mechanical properties, lysyl oxidases (LOX) need to covalently crosslink the tropocollagens [140]. Even though the expression of lysyl oxidases was slightly increased in mechanically stimulated samples, the density of fibrillar collagen was significantly reduced (see Figure 4-20). This discrepancy might be explained by an insufficient activation of lysyl oxidases in the extracellular space. This assumption is based on the finding that periostin, a protein participating in lysyl oxidase activation, was significantly reduced the matrices of mechanically stimulated samples (see Figure 4-24). Due to its multi-domain structure, periostin is an important scaffolding protein binding to ECM proteins (collagen I and V, fibronectin, tenascin C, and laminin), enzymes (BMP-1, LOX) and integrins [232]. Importantly, BMP-1 not only cleaves the propeptide of collagens but also the propeptide of LOX to activate its enzymatic activity [233]. The activated LOX in turn catalyzes the covalent cross-linking of staggered collagen fibrils. Periostin supports BMP-1-mediated proteolytic activation of LOX, by bringing the interacting proteins in close proximity, thereby facilitating and accelerating collagen cross-linking (Figure 5-3) [232], [234].

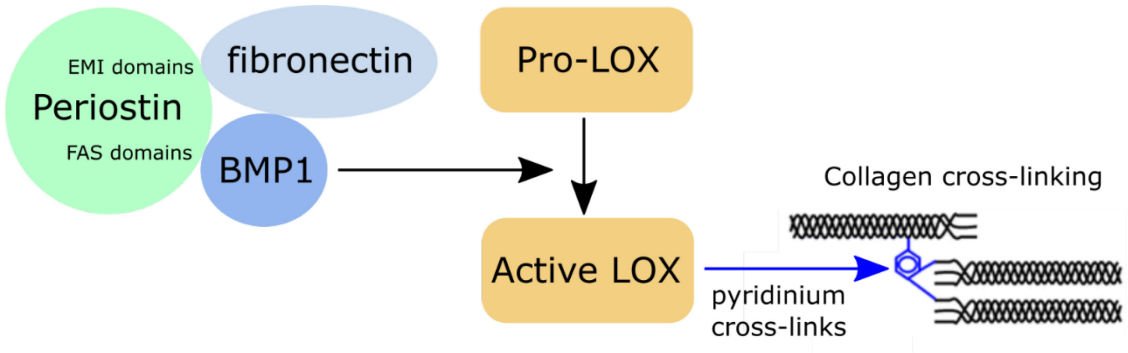

Figure 5-3: The regulation of collagen cross-linking by periostin. Periostin binds to fibronectin via its EMI domain and to BMP-1 through its FAS-1 domain, thereby promoting the deposition of BMP-1 into the ECM. BMP-1 activates LOX by proteolytic cleavage of the precursor LOX (Pro-LOX). Active LOX synthesizes pyridinium cross-links to interconnect collagen fibers. Figure modified from [235] *with permission from the publisher.*

Its physiological relevance is highlighted even more as periostin deficient mice exhibit reduced collagen cross-linking [236]. Here, the reduced periostin abundance in the ECM of samples subjected to cyclic compression could be one reason for the load-induced reduction of fibrillar collagen density. Collagen fibrils might self-assembly into staggered fibrils but their insufficient cross-linking leads to fibril disruption under cyclic compression. The increased secretion of collagen I and expression of BMP1, periostin and lysyl oxidases might be a compensation mechanism, which was for some reason insufficient.

The finding that cyclic compression reduced the density of fibrillar collagen is contradicting the expectation that cells in a highly mechanically unstable environment aim to stabilize the tissue by an increased deposition of load-bearing fibrillar collagen. This together with the finding that cyclic compression strongly increase the secretion of pro-collagen type I, leads to the suggestion, that cell indeed aim at stabilizing their environment with the help of collagen, but mechanical loading disturbs collagen fibrillogenesis (see Figure 5-4).

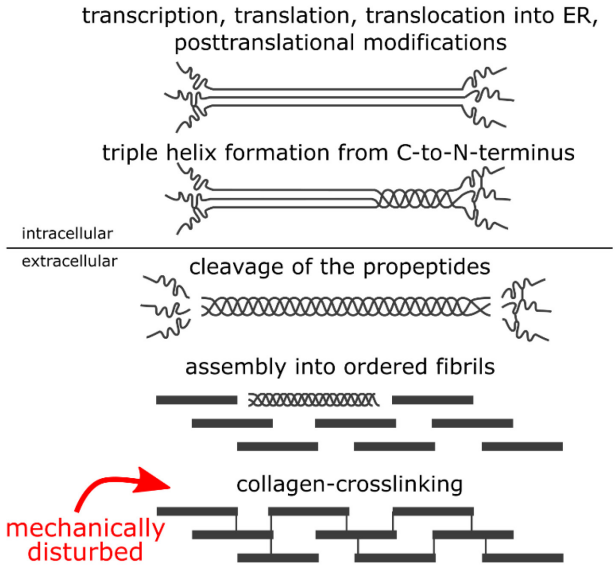

Figure 5-4: Cyclic compression disturbs collagen cross-linking. After transcription, translation and translocation into the rough endoplasmic reticulum and posttranslational modifications single proα-chains associate via the C-terminus. The triple helix is formed from C-to-N terminus and thereafter secreted into the extracellular space. After enzymatic cleavage of the propeptides the helices assemble into ordered fibrils. These fibrils are finally stabilized by inter and intramolecular cross-links. Mechanical stimulation is proposed to disturb the step of collagen cross-linking. Figure information taken from [140].

Next to the reasonable explanation, that collagen cross-linking is insufficient due to the significantly reduced deposition of periostin into the ECM, it might also be a pure mechanical interference with the process of fibril formation. It might be that 5 hours rest during the loading intervals are too short to sufficiently stabilize collagen fibrils leading to mechanically disruption during the subsequent loading phase.

Although mechanical stress has been previously reported to alter collagens on different levels of its biosynthesis, comprehensive studies investigating the influence of mechanics in a 3D environment on all levels of collagen synthesis, as it was performed here, are missing. Therefore, it is difficult to integrate the current findings into the existing literature and only individual aspects will be compared here. The expression of collagen type I was described to be differently regulated depending on the loading regime. While cyclic tension applied to fibroblasts seeded onto collagen coated silicon membranes induced an increase in collagen expression [142], relaxation of fibroblast- seeded pre-stretched membranes induced a reduction of collagen type I expression [144]. In line with the here presented data, the secretion of the procollagen C-peptide was found to be upregulated in response to cyclic biomaterial compression [159]. In contrast to the present finding, collagen fibril formation, visualized by SHG imaging, was reported to increase upon the application of cyclic stretch to osteoblasts seeded onto flexible PDMS membranes coated with fibronectin [237]. The contradiction might be due to the differences in culture dimensions. However, studies visualizing collagen fibril formation under cyclic compression in a 3D environment by SHG imaging are missing. The present work is the first to performed comprehensive investigations from collagen gene expression to final collagen fibers and therefore delivers new insights on how collagen biosynthesis is regulated by cyclic compression.

An interpretation of the current findings in the context of wound healing, suggests that different loading regimes might be favorable for different processes. While BMP signaling and osteogenic differentiation are promoted by cyclic compression with a frequency of 1Hz and an amplitude of 10%, fibrillar collagen formation and consequent mechanical stabilization is disturbed. In bone regeneration, mechanical instability (in the range of 5-15% strain [40]) would lead to healing via endochondral ossification, a process in which a cartilaginous phase is proceeding mineralization [6]. If mechanical forces hinder the early formation of a fibrillar collagen-rich ECM, which characterizes bone tissue and serves as a template for mineral crystal deposition [238], an intermediate step aiming at tissue stabilization is required to proceed. Cartilage most probably fulfills this function: its proteoglycan-rich ECM could act as a “shock absorber” and establishes the mechanical stability that is needed for successful collagen fibrillogenesis. This assumption is supported by the fact that bones heal via direct ossification (intermembranous healing) in case of mechanical stability (and small fracture

gaps) [6]. Following the interpretation line, these conditions would allow for a formation of a collagen fiber network, in which mineral crystal can be immediately deposited – an intermediate step of cartilage is not required.

Effects of concurrent BMP-2 treatment and cyclic compression: Due to the previously described mechanosensitivity of the BMP pathway, it was hypothesized, that mechanical stimulation would also enhance the BMP-effects on early tissue formation. However, due to the weak influence of BMP-2 stimulation and the strong effects of cyclic compression on ECM formation, the load-effect was dominating in samples concurrently stimulated. Also, no synergistic effects have been observed, however conversely, BMP-2 dampened the impact of mechanical stimulation for some parameters investigated. This was the case for tissue contraction and stiffening (see Figure 4-19). Samples concurrently stimulated with BMP-2 and mechanical loading were, even though not significant, less contracted and softer than samples only treated mechanically. This might be due to increased tissue remodeling but further investigations are needed to prove this assumption. Also, the strong increase in gene expression induced by mechanical stimulation of for example fibulin-1, elastin or TGFβ-induced protein, was reduced by a stimulation with BMP-2 (see Figure 4-23). Additionally, although after one week of culture BMP-2 did not influence the load-induced downregulation of fibrillar collagen density, preliminary experiments over two weeks indicate a rescuing ability of BMP-2 (see supplementary Figure 0-5).

An *in vivo* study investigating the interaction of BMP-2 stimulation and mechanical boundary conditions in a rat critical-sized femoral defect model (5 mm) using three distinctly different external fixator stiffness, indeed showed that their mutual interaction does have implications beyond the induction of osteogenic differentiation [54]. Using gene expression profiling performed at day 3 and 7, distinct differences in the expression patterns of genes involved in extracellular matrix formation and cellular contractility were observed. While a rigid fixation led to an increased expression of genes related to ECM remodeling, flexible fixation triggered the expression of genes related to inflammatory response and cellular contractility. Since the semi-rigid fixation showed the best healing outcome, it becomes clear that mechanical stimuli need to be tightly balanced in order to positively cooperate with BMP-2. Overall, literature concerning the influence of BMP-2 and mechanical stimulation on ECM formation is very limited and we are just starting to understand their mutual interactions. Further research will be needed to interpret the present findings in the context of bone regeneration and wound healing.

6 Summary and Conclusion

Mechanical forces are, as one factor of the diamond concept [16], critically influencing bone healing with detrimental effects if interfragmentary forces are too low or too high, but beneficial effects if optimized. However, in order to employ the great potential of mechanical forces, its effects on molecular, cellular and tissue level need to be understood and combined to a universal model. To contribute to a profound understanding, in the first part of this thesis, the direct influence of cyclic mechanical loading on osteogenic differentiation of primary hBMSCs was investigated excluding effects of altered supply, autocrine stimulation and further osteogenic triggers (e.g. medium supplements). The outcomes revealed that cyclic compressive loading per se does not trigger osteogenic differentiation but instead causes a downregulation of RUNX2 and osteocalcin expression. Osteogenic differentiation, indicated by increased RUNX2 expression, was only promoted by cyclic compression, if an enrichment of secreted factors including BMP-2 in the cell culture medium and resulting autocrine signaling was permitted. This is striking, as it implies that the presence of BMP-2 changes the cells response to mechanical stimulation. The proposed BMP-mediated osteogenesis under cyclic compression was underpinned by the absence of load-induced osteogenic differentiation when a specific BMP inhibitor was supplemented. This observation provides evidence that mechanical stimulation induces osteogenic differentiation via a mechano-regulated autocrine feedback mechanism involving BMP-2 [172].

Mechanical forces promote BMP signaling not only indirectly via the regulation of ligand expression, but also directly by enhancing BMP signaling events at the receptor level that further translates into the level of target gene expression. The aims of the second part of this project, were to investigate the influence of mechanical loading parameters on the mechano-sensitivity of BMP signaling to define optimal mechanical parameters and to gain a deeper molecular understanding of how mechanical signals regulate the BMP signaling pathway. It was found that the intensity and duration of Smad phosphorylation and target gene expression was strongly affected by the loading frequency. While the intensity of Smad phosphorylation reached saturation at 1Hz, the duration of the crosstalk increased with increasing frequency, which was indicated by a prolonged increase of Smad phosphorylation. Moreover, these frequency-dependent effects on early Smad phosphorylation persisted and transduced to the level of BMP target gene expression. The results revealed that high frequency loading is most effectively supporting BMP signaling. Strikingly, these investigations also revealed a so far unknown mechano-regulation of BMP receptor type 1B expression. Together with the observed mechanically-induced increase in integrin expression

and clustering this lead to the hypothesis that cells would establish a “mechano-memory” upon long-term mechanical pre-loading. Indeed, here it could be shown for the first time that long-term mechanical pre-stimulation induces a persistent mechano-memory sufficient to increase Smad phosphorylation under BMP stimulation even in the absence of a direct mechanical trigger. Since this effect decreased with decreasing pre-loading durations, it is concluded that the crosstalk induced by a mechano-memory requires additional transcriptional adaptations like BMP receptor 1B expression. While transcriptional regulations are suggested to be an integral part of the mechanical memory, the immediate early induction of Smad phosphorylation upon concurrent mechanical and biochemical (BMP-2) stimulation is independent of any transcriptional regulation. However, the way how mechanical signals integrate into the BMP pathway in such an immediate manner is still unknown. To gain a deeper understanding of the molecular mechanism responsible for the mechano-regulation of BMP signaling, the hypothesis was tested that mechanical forces integrate into the BMP pathway via mechanotransduction through the integrin-F-actin-axis. In this thesis, it was found that mechanical stimulation induces an increased integrin clustering, integrin activation (indicated by increased p-FAK(Y397) levels) and F-actin cytoskeleton remodeling. Furthermore, integrin αv knockdown and F-actin stabilization decreased the efficiency of mechanical forces to amplify BMP signaling. Together with the known BMP receptor-integrin interaction, it is concluded that the increased adhesion remodeling in response to mechanical loading and BMP-2 stimulation causes increased interactions of αv-βx integrins and BMP receptors, which leads to the amplification of Smad1/5 phosphorylation. The knockdown of integrin αv reduced the amount of interaction partners for the BMP receptor, thereby reducing the mechano-sensitivity of BMP signaling. Inhibition of load-induced actin remodeling blocks the remodeling of adhesions and in turn the interaction of αv-βx integrins and BMP receptors.

In the third part for the thesis, the influence of mechanical stimulation and BMP treatment on extracellular matrix formation was investigated. The hypothesis was tested that mechanical stimulation would not only increase the growth factors` potential to induce osteogenic differentiation but also foster its effects on tissue formation. Therefore, human fibroblasts were subjected to cyclic compression and BMP-2 stimulation and resulting ECM properties were investigated with the focus on collagen. However, only minor changes on tissue contraction, stiffening and gene expression have been observed under BMP-only treatment and a clear and dominant BMP-effect on ECM formation could not be detected for the analyzed parameters. Mechanical stimulation on the other hand, significantly increased tissue contraction, stiffness and collagen type 1 secretion but surprisingly reduced the density

and structural alignment of fibrillar collagen fibers. This led to the conclusion that cyclic compression disturbed the process of collagen fibrillogenesis. Analysis of the ECM composition by MS revealed a consistent and significant increase in elastin, but a reduction of fibulin1, periostin, tenascin and TGFβ-induced protein. Therefore, mechanical forces specifically altered mechanical, structural and compositional matrix cues, which might in turn alter cellular behavior. Under concurrent cyclic compression and BMP-2 stimulation, the effect of cyclic compression was dominating. Synergistic effects were not observed, however conversely, BMP-2 slightly dampened the impact of mechanical stimulation on some parameters investigated such as tissue contraction, stiffening and gene expression. This might point towards an increased tissue remodeling that could be beneficial in the context of regeneration but further investigations are needed. Even though the hypothesis that mechanical stimulation would increase the BMP-effects on early tissue formation could not be proven here, important new insides into how mechanical stimulation influences ECM formation have been gained.

It became clear, that different processes in the healing cascade favor different mechanical boundary conditions loading regimes. While, BMP signaling and osteogenic differentiation were promoted by mechanical signals, fibrillar collagen formation requires mechanical stability.

Taken together, the main conclusions of this dissertation are:

(1) Mechanical stimulation induces osteogenic differentiation indirectly through a mechanically controlled secretion of BMP-2 and the resulting biochemical self-stimulation.
(2) Cells feature a mechanical memory, established via transcriptional regulation that leads to an increased signaling response to BMP-2 even when the mechanical signal has vanished.
(3) The immediate mechano-regulation of BMP signaling requires the presence of integrin α_v as well as load-induced integrin and actin cytoskeleton remodeling.
(4) Mechanical stimulation specifically modulates mechanical, structural and compositional extracellular matrix cues, which are suggested to in turn influence cell behavior

This thesis therefore contributes to a profound understanding of how mechanical forces regulate osteogenic differentiation, BMP signaling and early tissue formation - important processes during bone regeneration.

7 Outlook

The mechanical boundary conditions at the fracture site critically influence bone healing and a mechano-biological optimization of interfragmentary movements, especially during the early phase of healing, has great potential to promote the subsequent healing cascade. The power of mechanical forces is in part based on the amplification of the BMP signaling pathway enhancing the effectiveness of endogenous and therapeutic BMP-2. With future personalized medicine, the fracture fixation system should account for the individual mechano-biological requirements that depend on the location and type of fracture. Personalized computational models of the patients' fracture could help to simulate *in vivo* loads resulting from different fixation systems. Intelligent fixation systems, which are equipping with strain gauges and load sensors could realize postoperative validations and further control. However, even though optimal mechanical parameters could be derived from this work and studies in animal models, there needs to be further research in humans using for example the mentioned intelligent fixations systems (which would need to be developed). Knowing from this study that high frequency loading most effectively amplifies BMP signaling, it could be possible to implement postoperative physiotherapy using whole body vibration training with optimized parameters that indeed has been shown to be beneficial for bone healing in rodents [239], [240]. However, knowing that collagen fibrillogenesis favors mechanical stability, also the timing of load application post-operation would need to be optimized. Furthermore, local external mechanical stimulation could be conceivable. Currently, in-house developed air pressure controlled compression cuffs are under establishment in the Julius Wolff Institute that apply 1Hz cyclic compression externally to a femoral fracture in mice. The external massage shows promising first results on bone healing, although the underlying mechanism needs further elucidation.

A profound understanding of the molecular mechanism underlying the regulation of BMP signaling by mechanical forces might in the future lead to the identification of therapeutic candidates, which if targeted could amplify BMP signaling even without the application of external forces. This could be for example relevant for elderly immobile patients.

With regard to the specific alteration of ECM properties by mechanical stimulation, future work should investigate progenitor cell responses like proliferation, migration, differentiation and signaling on those matrices. Since material properties like stiffness influence cellular fate decision [56] and BMP signaling (unpublished data), it is likely that the ECM established under mechanical stimulation specifically modulates cell behavior. The resulting findings could inspire specific biomaterial designs for bone regeneration.

Together, this work contribute to a better understanding of the signaling cascades and matrix formation processes involved in bone regeneration process. A mechanistic understanding of those processes is very valuable as is allows the knowledge-transfer to other tissues.

8 Bibliography

[1] M. Maden, "The evolution of regeneration - where does that leave mammals?," *Int. J. Dev. Biol.*, vol. 62, no. 6-7–8, pp. 369–372.

[2] K. Schmidt-Bleek, A. Petersen, A. Dienelt, C. Schwarz, and G. N. Duda, "Initiation and early control of tissue regeneration – bone healing as a model system for tissue regeneration," *Expert Opin. Biol. Ther.*, vol. 14, no. 2, pp. 247–259, Feb. 2014.

[3] D. T. Corr and D. A. Hart, "Biomechanics of Scar Tissue and Uninjured Skin.," *Adv. wound care*, vol. 2, no. 2, pp. 37–43, Mar. 2013.

[4] A. M. Segura, O. H. Frazier, and L. M. Buja, "Fibrosis and heart failure," *Heart Fail. Rev.*, vol. 19, no. 2, pp. 173–185, Mar. 2014.

[5] C. Sfeir and L. Ho, "Fracture repair," *Bone Regen. repair*, no. 11, pp. 21–44, 2005.

[6] T. Tosounidis, G. Kontakis, V. Nikolaou, a. Papathanassopoulos, and P. V Giannoudis, "Fracture healing and bone repair: an update," *Trauma*, vol. 11, no. 3, pp. 145–156, 2009.

[7] M. Greenbaum and I. Kanat, "Current concepts in bone healing. Review of the literature," *J. Am. Podiatr. Med. Assoc.*, vol. 83, no. 3, pp. 123–129, Mar. 1993.

[8] P. Kolar *et al.*, "The Early Fracture Hematoma and Its Potential Role in Fracture Healing," *Tissue Eng. Part B Rev.*, vol. 16, no. 4, pp. 427–434, Aug. 2010.

[9] K. Schmidt-Bleek *et al.*, "Inflammatory phase of bone healing initiates the regenerative healing cascade," *Cell Tissue Res.*, vol. 347, no. 3, pp. 567–573, Mar. 2012.

[10] R. Dimitriou, E. Tsiridis, and P. V. Giannoudis, "Current concepts of molecular aspects of bone healing," *Injury*, vol. 36, no. 12, pp. 1392–1404, 2005.

[11] A. Petersen *et al.*, "A biomaterial with a channel-like pore architecture induces endochondral healing of bone defects," *Nat. Commun.*, vol. 9, no. 1, p. 4430, Dec. 2018.

[12] M. E. Bolander, "Regulation of Fracture Repair by Growth Factors," *Exp. Biol. Med.*, vol. 200, no. 2, pp. 165–170, Jun. 1992.

[13] T. A. Einhorn, A. Hirschman, C. Kaplan, R. Nashed, V. J. Devlin, and J. Warman, "Neutral protein-degrading enzymes in experimental fracture callus: A preliminary report," *J. Orthop. Res.*, vol. 7, no. 6, pp. 792–805, Nov. 1989.

[14] H. M. Frost, "A determinant of bone architecture. The minimum effective strain.," *Clin. Orthop. Relat. Res.*, no. 175, pp. 286–92, May 1983.

[15] K. Schmidt-Bleek, B. J. Kwee, D. J. Mooney, and G. N. Duda, "Boon and Bane of Inflammation in Bone Tissue Regeneration and Its Link with Angiogenesis," *Tissue Engineering - Part B: Reviews*, vol. 21, no. 4. Mary Ann Liebert Inc., pp. 354–364, 01-Aug-2015.

[16] P. V Giannoudis, T. a Einhorn, and D. Marsh, "Fracture healing: The diamond concept," *4th Eur. Clin. Symp. Bone Tissue Regen.*, vol. 38, Supple, no. 0, pp. S3–S6, 2007.

[17] A. Moghaddam, B. Thaler, T. Bruckner, M. Tanner, and G. Schmidmaier, "Treatment of atrophic femoral non-unions according to the diamond concept: Results of one- and two-step surgical procedure," *J. Orthop.*, vol. 14, no. 1, p. 123, 2017.

[18] B. M. Willie *et al.*, "Designing biomimetic scaffolds for bone regeneration: why aim for a copy of mature tissue properties if nature uses a different approach?," *Soft Matter*, vol. 6, no. 20, p. 4976, 2010.

[19] P. H. Locker, J. Arthur, T. Edmiston, R. Puri, and B. R. Levine, "Management of Bone Defects in Orthopedic Trauma.," *Bull. Hosp. Jt. Dis.*, vol. 76, no. 1, pp. 278–284, Mar. 2018.

[20] R. Dimitriou, E. Jones, D. McGonagle, and P. V Giannoudis, “Bone regeneration: current concepts and future directions,” *BMC Med.*, vol. 9, no. 1, p. 66, 2011.

[21] T. A. St John *et al.*, “Physical and monetary costs associated with autogenous bone graft harvesting.,” *Am. J. Orthop. (Belle Mead. NJ).*, vol. 32, no. 1, pp. 18–23, Jan. 2003.

[22] O. Fromigué, P. J. Marie, and A. Lomri, “Bone morphogenetic protein-2 and transforming growth factor-beta2 interact to modulate human bone marrow stromal cell proliferation and differentiation.,” *J. Cell. Biochem.*, vol. 68, no. 4, pp. 411–26, Mar. 1998.

[23] S. Liu *et al.*, “Recombinant human BMP-2 accelerates the migration of bone marrow mesenchymal stem cells: Via the CDC42/PAK1/LIMK1 pathway in vitro and in vivo,” *Biomater. Sci.*, vol. 7, no. 1, pp. 362–372, Jan. 2019.

[24] G. Sánchez-Duffhues, C. Hiepen, P. Knaus, and P. ten Dijke, “Bone morphogenetic protein signaling in bone homeostasis,” *Bone*, vol. 80, pp. 43–59, Nov. 2015.

[25] I. Dumic-Cule, M. Peric, L. Kucko, L. Grgurevic, M. Pecina, and S. Vukicevic, “Bone morphogenetic proteins in fracture repair,” *Int. Orthop.*, vol. 42, no. 11, pp. 2619–2626, Nov. 2018.

[26] A. H. Reddi and N. S. Cunningham, “Initiation and promotion of bone differentiation by bone morphogenetic proteins,” *J. Bone Miner. Res.*, vol. 8, no. S2, pp. S499–S502, Dec. 2009.

[27] H. CHENG *et al.*, “OSTEOGENIC ACTIVITY OF THE FOURTEEN TYPES OF HUMAN BONE MORPHOGENETIC PROTEINS (BMPS),” *J. Bone Jt. Surgery-American Vol.*, vol. 85, no. 8, pp. 1544–1552, Aug. 2003.

[28] K. Tsuji *et al.*, “BMP2 activity, although dispensable for bone formation, is required for the initiation of fracture healing.,” *Nat. Genet.*, vol. 38, no. 12, pp. 1424–9, Dec. 2006.

[29] O. P. Gautschi, S. P. Frey, and R. Zellweger, “Bone morphogenetic proteins in clinical applications.,” *ANZ J. Surg.*, vol. 77, no. 8, pp. 626–31, Aug. 2007.

[30] K. R. Garrison *et al.*, “Clinical effectiveness and cost-effectiveness of bone morphogenetic proteins in the non-healing of fractures and spinal fusion: a systematic review.,” *Health Technol. Assess.*, vol. 11, no. 30, pp. 1–150, iii–iv, Aug. 2007.

[31] S. Wei, X. Cai, J. Huang, F. Xu, X. Liu, and Q. Wang, “Recombinant human BMP-2 for the treatment of open tibial fractures.,” *Orthopedics*, vol. 35, no. 6. pp. e847–e854, 01-Jun-2012.

[32] A. W. James *et al.*, “A Review of the Clinical Side Effects of Bone Morphogenetic Protein-2.,” *Tissue Eng. Part B. Rev.*, vol. 22, no. 4, pp. 284–97, 2016.

[33] D. C. Betts and R. Müller, “Mechanical regulation of bone regeneration: theories, models, and experiments.,” *Front. Endocrinol. (Lausanne).*, vol. 5, p. 211, Jan. 2014.

[34] G. N. Duda *et al.*, “Mechanical boundary conditions of fracture healing: borderline indications in the treatment of unreamed tibial nailing.,” *J. Biomech.*, vol. 34, no. 5, pp. 639–50, May 2001.

[35] V. Glatt, C. H. Evans, and K. Tetsworth, “A Concert between Biology and Biomechanics: The Influence of the Mechanical Environment on Bone Healing.,” *Front. Physiol.*, vol. 7, p. 678, 2016.

[36] M. Steiner, L. Claes, A. Ignatius, U. Simon, and T. Wehner, “Numerical Simulation of Callus Healing for Optimization of Fracture Fixation Stiffness,” *PLoS One*, vol. 9, no. 7, p. e101370, Jul. 2014.

[37] H. Schell *et al.*, “Mechanical induction of critically delayed bone healing in sheep: Radiological and biomechanical results,” *J. Biomech.*, vol. 41, no. 14, pp. 3066–3072, Oct. 2008.

[38] K. Aalto, T. Holmström, E. Karaharju, J. Joukainen, P. Paavolainen, and P. Slätis, “Fracture repair during external fixation: Torsion tests of rabbit osteotomies,” *Acta Orthop. Scand.*, vol. 58, no. 1, pp. 66–70, Jan. 1987.

[39] D. R. Carter, P. R. Blenman, and G. S. Beaupré, “Correlations between mechanical stress history and tissue differentiation in initial fracture healing,” *J. Orthop. Res.*, vol. 6, no. 5, pp. 736–748, Sep. 1988.

[40] L. . Claes and C. . Heigele, “Magnitudes of local stress and strain along bony surfaces predict the course and type of fracture healing,” *J. Biomech.*, vol. 32, no. 3, pp. 255–266, Mar. 1999.

[41] D. R. Epari, W. R. Taylor, M. O. Heller, and G. N. Duda, “Mechanical conditions in the initial phase of bone healing.,” *Clin. Biomech. (Bristol, Avon)*, vol. 21, no. 6, pp. 646–55, Jul. 2006.

[42] M. Mehta, G. N. Duda, C. Perka, and P. Strube, “Influence of gender and fixation stability on bone defect healing in middle-aged rats: a pilot study.,” *Clin. Orthop. Relat. Res.*, vol. 469, no. 11, pp. 3102–10, Nov. 2011.

[43] P. Klein *et al.*, “The initial phase of fracture healing is specifically sensitive to mechanical conditions.,” *J. Orthop. Res.*, vol. 21, no. 4, pp. 662–9, 2003.

[44] P. J. Prendergast, R. Huiskes, and K. Søballe, “ESB Research Award 1996. Biophysical stimuli on cells during tissue differentiation at implant interfaces.,” *J. Biomech.*, vol. 30, no. 6, pp. 539–48, Jun. 1997.

[45] M. S. Ghiasi, J. Chen, A. Vaziri, E. K. Rodriguez, and A. Nazarian, “Bone fracture healing in mechanobiological modeling: A review of principles and methods.,” *Bone reports*, vol. 6, pp. 87–100, Jun. 2017.

[46] A. E. Goodship, J. L. Cunningham, and J. Kenwright, “Strain rate and timing of stimulation in mechanical modulation of fracture healing.,” *Clin. Orthop. Relat. Res.*, no. 355 Suppl, pp. S105-15, Oct. 1998.

[47] V. Glatt *et al.*, “Improved Healing of Large Segmental Defects in the Rat Femur by Reverse Dynamization in the Presence of Bone Morphogenetic Protein-2,” *J. Bone Jt. Surgery-American Vol.*, vol. 94, no. 22, pp. 2063–2073, Nov. 2012.

[48] N. Bartnikowski *et al.*, “Modulation of fixation stiffness from flexible to stiff in a rat model of bone healing,” *Acta Orthop.*, vol. 88, no. 2, pp. 217–222, Mar. 2017.

[49] C. B. Howard, O. Elishoov, Y. Matan, R. Mosheiff, and M. Liebergall, “Can changing the mechanical environment increase the speed of fracture healing? A pilot study in tibial fractures,” *Inj. Extra*, vol. 40, no. 10, p. 230, Oct. 2009.

[50] V. Glatt, N. Bartnikowski, N. Quirk, M. Schuetz, and C. Evans, “Reverse Dynamization: Influence of Fixator Stiffness on the Mode and Efficiency of Large-Bone-Defect Healing at Different Doses of rhBMP-2.,” *J. Bone Joint Surg. Am.*, vol. 98, no. 8, pp. 677–87, Apr. 2016.

[51] C. Schwarz, D. Wulsten, A. Ellinghaus, J. Lienau, B. M. Willie, and G. N. Duda, “Mechanical Load Modulates the Stimulatory Effect of BMP2 in a Rat Nonunion Model,” *Tissue Eng. Part A*, vol. 19, no. 1–2, pp. 247–254, 2013.

[52] J. D. Boerckel, Y. M. Kolambkar, H. Y. Stevens, A. S. P. Lin, K. M. Dupont, and R. E. Guldberg, “Effects of in vivo mechanical loading on large bone defect regeneration,” *J. Orthop. Res.*, vol. 30, no. 7, p. 1067, Jul. 2012.

[53] S. Herberg *et al.*, “Combinatorial morphogenetic and mechanical cues to mimic bone development for defect repair.,” *Sci. Adv.*, vol. 5, no. 8, p. eaax2476, Aug. 2019.

[54] C. Schwarz *et al.*, “The Interaction of BMP2-Induced Defect Healing in Rat and Fixator Stiffness Modulates Matrix Alignment and Contraction.,” *JBMR plus*, vol. 2, no. 3, pp. 174–186, May 2018.

[55] R. M. Delaine-Smith and G. C. Reilly, *The Effects of Mechanical Loading on Mesenchymal Stem Cell Differentiation and Matrix Production*, 1st ed., vol. 87. Elsevier Inc., 2011.

[56] A. J. Engler, S. Sen, H. L. Sweeney, and D. E. Discher, "Matrix Elasticity Directs Stem Cell Lineage Specification," *Cell*, vol. 126, no. 4, pp. 677–689, 2006.

[57] O. Chaudhuri *et al.*, "Hydrogels with tunable stress relaxation regulate stem cell fate and activity," *Nat. Mater.*, vol. 15, no. 3, pp. 326–334, Mar. 2016.

[58] M. Werner *et al.*, "Surface Curvature Differentially Regulates Stem Cell Migration and Differentiation via Altered Attachment Morphology and Nuclear Deformation.," *Adv. Sci. (Weinheim, Baden-Wurttemberg, Ger.*, vol. 4, no. 2, p. 1600347, 2017.

[59] D. E. Ingber, "Cellular mechanotransduction: putting all the pieces together again.," *FASEB J.*, vol. 20, no. 7, p. 27, 2006.

[60] M. Barczyk, S. Carracedo, and D. Gullberg, "Integrins.," *Cell Tissue Res.*, vol. 339, no. 1, pp. 269–80, Jan. 2010.

[61] R. O. Hynes, "Integrins: bidirectional, allosteric signaling machines.," *Cell*, vol. 110, no. 6, pp. 673–87, Sep. 2002.

[62] S. Seetharaman and S. Etienne-Manneville, "Integrin diversity brings specificity in mechanotransduction," *Biol. Cell*, vol. 110, no. 3, pp. 49–64, Mar. 2018.

[63] G. Marsico, L. Russo, F. Quondamatteo, and A. Pandit, "Glycosylation and Integrin Regulation in Cancer," *Trends in Cancer*, vol. 4, no. 8. Cell Press, pp. 537–552, 01-Aug-2018.

[64] S. Seetharaman and S. Etienne-Manneville, "Integrin diversity brings specificity in mechanotransduction," *Biol. ot Cell*, vol. 110, pp. 49–64, Jun. 2018.

[65] Z. Sun, S. S. Guo, and R. Fässler, "Integrin-mediated mechanotransduction.," *J. Cell Biol.*, vol. 215, no. 4, pp. 445–456, Nov. 2016.

[66] C. K. Choi, M. Vicente-Manzanares, J. Zareno, L. A. Whitmore, A. Mogilner, and A. R. Horwitz, "Actin and α-actinin orchestrate the assembly and maturation of nascent adhesions in a myosin II motor-independent manner," *Nat. Cell Biol.*, vol. 10, no. 9, pp. 1039–1050, 2008.

[67] M. Chrzanowska-Wodnicka and K. Burridge, "Rho-stimulated contractility drives the formation of stress fibers and focal adhesions.," *J. Cell Biol.*, vol. 133, no. 6, pp. 1403–15, Jun. 1996.

[68] A. M. Pasapera, I. C. Schneider, E. Rericha, D. D. Schlaepfer, and C. M. Waterman, "Myosin II activity regulates vinculin recruitment to focal adhesions through FAK-mediated paxillin phosphorylation," *J. Cell Biol.*, vol. 188, no. 6, pp. 877–890, Mar. 2010.

[69] C. J. McCleverty, D. C. Lin, and R. C. Liddington, "Structure of the PTB domain of tensin1 and a model for its recruitment to fibrillar adhesions," *Protein Sci.*, vol. 16, no. 6, pp. 1223–1229, Jun. 2007.

[70] R. Zaidel-Bar, S. Itzkovitz, A. Ma'ayan, R. Iyengar, and B. Geiger, "Functional atlas of the integrin adhesome," *Nat. Cell Biol.*, vol. 9, no. 8, pp. 858–867, Aug. 2007.

[71] E. R. Horton, P. Astudillo, M. J. Humphries, and J. D. Humphries, "Mechanosensitivity of integrin adhesion complexes: role of the consensus adhesome.," *Exp. Cell Res.*, vol. 343, no. 1, pp. 7–13, 2016.

[72] S. K. Mitra, D. A. Hanson, and D. D. Schlaepfer, "Focal adhesion kinase: In command and control of cell motility," *Nature Reviews Molecular Cell Biology*, vol. 6, no. 1. pp. 56–68, Jan-2005.

[73] D. Chodniewicz and R. L. Klemke, "Regulation of integrin-mediated cellular responses through assembly of a CAS/Crk scaffold.," *Biochim. Biophys. Acta*, vol. 1692, no. 2–3, pp. 63–76, Jul. 2004.

[74] R. Zaidel-Bar, R. Milo, Z. Kam, and B. Geiger, "A paxillin tyrosine phosphorylation switch regulates the assembly and form of cell-matrix adhesions," *J. Cell Sci.*, vol. 120, no. 1, pp. 137–148, Dec. 2006.

[75] M. Kanehisa and S. Goto, "KEGG: kyoto encyclopedia of genes and genomes - Release 72.1, December 1, 2014 ," *Nucleic Acids Res*, vol. 28, no. 1, pp. 27–30, 2000.

[76] M. Kanehisa, "Toward understanding the origin and evolution of cellular organisms.," *Protein Sci.*, Aug. 2019.

[77] M. Kanehisa, Y. Sato, M. Furumichi, K. Morishima, and M. Tanabe, "New approach for understanding genome variations in KEGG," *Nucleic Acids Res.*, vol. 47, no. D1, pp. D590–D595, Jan. 2019.

[78] E. C. Lessey, C. Guilluy, and K. Burridge, "From mechanical force to RhoA activation.," *Biochemistry*, vol. 51, no. 38, pp. 7420–32, Sep. 2012.

[79] C. F. Lee, C. Haase, S. Deguchi, and R. Kaunas, "Cyclic stretch-induced stress fiber dynamics - Dependence on strain rate, Rho-kinase and MLCK," *Biochem. Biophys. Res. Commun.*, vol. 401, no. 3, pp. 344–349, Oct. 2010.

[80] D. Verma, F. Meng, F. Sachs, and S. Z. Hua, "Flow-induced focal adhesion remodeling mediated by local cytoskeletal stresses and reorganization.," *Cell Adh. Migr.*, vol. 9, no. 6, pp. 432–40, 2015.

[81] J. T. Parsons, "Focal adhesion kinase: the first ten years.," *J. Cell Sci.*, vol. 116, no. Pt 8, pp. 1409–16, Apr. 2003.

[82] H. B. Schiller and R. Fässler, "Mechanosensitivity and compositional dynamics of cell-matrix adhesions," *EMBO Reports*, vol. 14, no. 6. pp. 509–519, Jun-2013.

[83] A. Elosegui-Artola, X. Trepat, and P. Roca-Cusachs, "Control of Mechanotransduction by Molecular Clutch Dynamics," *Trends in Cell Biology*, vol. 28, no. 5. Elsevier Ltd, pp. 356–367, 01-May-2018.

[84] Z.-J. Liu, Y. Zhuge, and O. C. Velazquez, "Trafficking and differentiation of mesenchymal stem cells," *J. Cell. Biochem.*, vol. 106, no. 6, pp. 984–991, 2009.

[85] R. Bielby, E. Jones, and D. McGonagle, "The role of mesenchymal stem cells in maintenance and repair of bone," *Injury*, vol. 38, no. 1, pp. S26–S32, 2007.

[86] A. Riedl *et al.*, "Comparison of cancer cells in 2D vs 3D culture reveals differences in AKT-mTOR-S6K signaling and drug responses," *J. Cell Sci.*, vol. 130, no. 1, pp. 203–218, Jan. 2017.

[87] P. Angele *et al.*, "Cyclic, mechanical compression enhances chondrogenesis of mesenchymal progenitor cells in tissue engineering scaffolds," *Biorheology*, vol. 41, no. 3, pp. 335–346, Jan. 2004.

[88] Z. Li, S. J. Yao, M. Alini, and M. J. Stoddart, "Chondrogenesis of human bone marrow mesenchymal stem cells in fibrin-polyurethane composites is modulated by frequency and amplitude of dynamic compression and shear stress," in *Tissue Engineering - Part A*, 2010, vol. 16, no. 2, pp. 575–584.

[89] A. H. Huang, M. J. Farrell, M. Kim, and R. L. Mauck, "Long-term dynamic loading improves the mechanical properties of chondrogenic mesenchymal stem cell-laden hydrogel.," *Eur. Cell. Mater.*, vol. 19, pp. 72–85, Feb. 2010.

[90] A. Sittichockechaiwut, A. M. Scutt, A. J. Ryan, L. F. Bonewald, and G. C. Reilly, "Use of rapidly mineralising osteoblasts and short periods of mechanical loading to accelerate matrix maturation in 3D scaffolds," *Bone*, vol. 44, no. 5, pp. 822–829, 2009.

[91] A. Sittichokechaiwut, J. H. Edwards, a M. Scutt, and G. C. Reilly, "Short bouts of mechanical loading are as effective as dexamethasone at inducing matrix production by human bone marrow mesenchymal stem cell.," *Eur. Cell. Mater.*, vol. 20, pp. 45–57, 2010.

[92] M. Jagodzinski *et al.*, "Influence of perfusion and cyclic compression on proliferation and differentiation of bone marrow stromal cells in 3-dimensional culture," *J. Biomech.*, vol. 41, no. 9, pp. 1885–1891, 2008.

[93] B. Sen, Z. Xie, N. Case, M. Ma, C. Rubin, and J. Rubin, "Mechanical strain inhibits adipogenesis in mesenchymal stem cells by stimulating a durable β-catenin signal," *Endocrinology*, vol. 149, no. 12, pp. 6065–6075, Dec. 2008.

[94] E. Michalopoulos, R. L. Knight, S. Korossis, J. N. Kearney, J. Fisher, and E. Ingham, "Development of Methods for Studying the Differentiation of Human Mesenchymal Stem Cells Under Cyclic Compressive Strain," *Tissue Eng. Part C Methods*, vol. 18, no. 4, pp. 252–262, 2012.

[95] K. Shin Kang, Y. Hun Jeong, J. Min Hong, W.-J. Yong, J.-W. Rhie, and D.-W. Cho, "Flexure-based device for cyclic strain-mediated osteogenic differentiation.," *J. Biomech. Eng.*, vol. 135, no. 11, p. 114501, 2013.

[96] L. Wang *et al.*, "Involvement of BMPs/smad signaling pathway in mechanical response in osteoblasts," *Cell. Physiol. Biochem.*, vol. 26, no. 6, pp. 1093–1102, 2010.

[97] Y. F. Rui, P. P. Y. Lui, M. Ni, L. S. Chan, Y. W. Lee, and K. M. Chan, "Mechanical loading increased BMP-2 expression which promoted osteogenic differentiation of tendon-derived stem cells.," *J. Orthop. Res.*, vol. 29, no. 3, pp. 390–6, Mar. 2011.

[98] K. S. Lee *et al.*, "Runx2 is a common target of transforming growth factor beta1 and bone morphogenetic protein 2, and cooperation between Runx2 and Smad5 induces osteoblast-specific gene expression in the pluripotent mesenchymal precursor cell line C2C12.," *Mol. Cell. Biol.*, vol. 20, no. 23, pp. 8783–92, Dec. 2000.

[99] C. Sieber, J. Kopf, C. Hiepen, and P. Knaus, "Recent advances in BMP receptor signaling.," *Cytokine Growth Factor Rev.*, vol. 20, no. 5–6, pp. 343–55, Jan. 2009.

[100] M. R. Urist and B. S. Strates, "Bone morphogenetic protein.," *J. Dent. Res.*, vol. 50, no. 6, pp. 1392–406.

[101] N. Tsumaki *et al.*, "Bone Morphogenetic Protein Signals Are Required for Cartilage Formation and Differently Regulate Joint Development During Skeletogenesis," *J. Bone Miner. Res.*, vol. 17, no. 5, pp. 898–906, May 2002.

[102] A. Stantzou *et al.*, "BMP signaling regulates satellite cell-dependent postnatal muscle growth," *Development*, vol. 144, no. 15, pp. 2737–2747, Aug. 2017.

[103] F. Klatte-Schulz *et al.*, "An investigation of BMP-7 mediated alterations to BMP signalling components in human tenocyte-like cells.," *Sci. Rep.*, vol. 6, no. 1, p. 29703, Sep. 2016.

[104] H. Chen *et al.*, "BMP10 is essential for maintaining cardiac growth during murine cardiogenesis.," *Development*, vol. 131, no. 9, pp. 2219–31, May 2004.

[105] A. García de Vinuesa, S. Abdelilah-Seyfried, P. Knaus, A. Zwijsen, and S. Bailly, "BMP signaling in vascular biology and dysfunction," *Cytokine Growth Factor Rev.*, vol. 27, pp. 65–79, Feb. 2016.

[106] S. V. Hegarty, G. W. O'Keeffe, and A. M. Sullivan, "BMP-Smad 1/5/8 signalling in the development of the nervous system," *Prog. Neurobiol.*, vol. 109, pp. 28–41, Oct. 2013.

[107] C. Hiepen *et al.*, "BMP2-induced chemotaxis requires PI3K p55γ/p110α-dependent phosphatidylinositol (3,4,5)-triphosphate production and LL5β recruitment at the cytocortex," *BMC Biol.*, vol. 12, no. 1, p. 43, May 2014.

[108] D. O. Wagner, C. Sieber, R. Bhushan, J. H. Börgermann, D. Graf, and P. Knaus, "BMPs: from bone to body morphogenetic proteins.," *Sci. Signal.*, vol. 3, no. 107, p. mr1, Feb. 2010.

[109] K. Miyazono, S. Maeda, and T. Imamura, "BMP receptor signaling: Transcriptional targets, regulation of signals, and signaling cross-talk," *Cytokine Growth Factor Rev.*,

vol. 16, no. 3, pp. 251–263, Jun. 2005.

[110] V. S. Salazar, L. W. Gamer, and V. Rosen, "BMP signalling in skeletal development, disease and repair," *Nat. Rev. Endocrinol.*, vol. 12, no. 4, pp. 203–221, Apr. 2016.

[111] A. Nohe *et al.*, "The Mode of Bone Morphogenetic Protein (BMP) Receptor Oligomerization Determines Different BMP-2 Signaling Pathways," *J. Biol. Chem.*, vol. 277, no. 7, pp. 5330–5338, Feb. 2002.

[112] B. M. Chacko *et al.*, "Structural Basis of Heteromeric Smad Protein Assembly in TGF-β Signaling," *Mol. Cell*, vol. 15, no. 5, pp. 813–823, Sep. 2004.

[113] J. Massague, J. Seoane, and D. Wotton, "Smad transcription factors," *Genes Dev.*, vol. 19, no. 23, pp. 2783–2810, Dec. 2005.

[114] A. Hollnagel, V. Oehlmann, J. Heymer, U. Rüther, and A. Nordheim, "Id genes are direct targets of bone morphogenetic protein induction in embryonic stem cells.," *J. Biol. Chem.*, vol. 274, no. 28, pp. 19838–45, Jul. 1999.

[115] C.-F. Lai and S.-L. Cheng, "Signal Transductions Induced by Bone Morphogenetic Protein-2 and Transforming Growth Factor-β in Normal Human Osteoblastic Cells," *J. Biol. Chem.*, vol. 277, no. 18, pp. 15514–15522, May 2002.

[116] C. Gamell *et al.*, "BMP2 induction of actin cytoskeleton reorganization and cell migration requires PI3-kinase and Cdc42 activity," *J. Cell Sci.*, vol. 121, no. 23, pp. 3960–3970, Dec. 2008.

[117] J. Kopf, P. Paarmann, C. Hiepen, D. Horbelt, and P. Knaus, "BMP growth factor signaling in a biomechanical context," *BioFactors*, vol. 40, no. 2, pp. 171–187, 2014.

[118] T. D. Mueller and J. Nickel, "Promiscuity and specificity in BMP receptor activation," *FEBS Letters*, vol. 586, no. 14. No longer published by Elsevier, pp. 1846–1859, 04-Jul-2012.

[119] O. Avsian-Kretchmer and A. J. W. Hsueh, "Comparative Genomic Analysis of the Eight-Membered Ring Cystine Knot-Containing Bone Morphogenetic Protein Antagonists," *Mol. Endocrinol.*, vol. 18, no. 1, pp. 1–12, Jan. 2004.

[120] A. P. Wohl, H. Troilo, R. F. Collins, C. Baldock, and G. Sengle, "Extracellular Regulation of Bone Morphogenetic Protein Activity by the Microfibril Component Fibrillin-1," *J. Biol. Chem.*, vol. 291, no. 24, pp. 12732–12746, Jun. 2016.

[121] G. Murakami, T. Watabe, K. Takaoka, K. Miyazono, and T. Imamura, "Cooperative Inhibition of Bone Morphogenetic Protein Signaling by Smurf1 and Inhibitory Smads," *Mol. Biol. Cell*, vol. 14, no. 7, pp. 2809–2817, Jul. 2003.

[122] L. C. Fuentealba *et al.*, "Integrating patterning signals: Wnt/GSK3 regulates the duration of the BMP/Smad1 signal.," *Cell*, vol. 131, no. 5, pp. 980–93, Nov. 2007.

[123] B. Rath *et al.*, "Biomechanical forces exert anabolic effects on osteoblasts by activation of SMAD 1/5/8 through type 1 BMP receptor," *Biorheology*, vol. 48, pp. 37–48, 2011.

[124] J. Zhou *et al.*, "Force-specific activation of Smad1 / 5 regulates vascular endothelial cell cycle progression in response to disturbed flow," *Proc.*, vol. 109, pp. 1–6, 2012.

[125] J. Kopf, A. Petersen, G. N. Duda, and P. Knaus, "BMP2 and mechanical loading cooperatively regulate immediate early signalling events in the BMP pathway," *BMC Biol.*, vol. 10, no. 1, p. 37, 2012.

[126] Z. Zeng, X. Yin, X. Zhang, D. Jing, and X. Feng, "Cyclic stretch enhances bone morphogenetic protein-2-induced osteoblastic differentiation through the inhibition of Hey1.," *Int. J. Mol. Med.*, vol. 36, no. 5, pp. 1273–81, Nov. 2015.

[127] S. Kido *et al.*, "Mechanical Stress Activates Smad Pathway through PKCδ to Enhance Interleukin-11 Gene Transcription in Osteoblasts," *PLoS One*, vol. 5, no. 9, p. e13090, 2010.

[128] J. Zhou *et al.*, "BMP receptor-integrin interaction mediates responses of vascular endothelial Smad1/5 and proliferation to disturbed flow," *J. Thromb. Haemost.*, vol. 11, no. 4, pp. 741–755, 2013.

[129] L. Fourel *et al.*, "β3 integrin-mediated spreading induced by matrix-bound BMP-2 controls Smad signaling in a stiffness-independent manner.," *J. Cell Biol.*, vol. 212, no. 6, pp. 693–706, Mar. 2016.

[130] C.-F. Lai and S.-L. Cheng, "αvβ Integrins Play an Essential Role in BMP-2 Induction of Osteoblast Differentiation," *J. Bone Miner. Res.*, vol. 20, no. 2, pp. 330–340, 2004.

[131] A. Jikko, S. E. Harris, D. Chen, D. L. Mendrick, and C. H. Damsky, "Collagen Integrin Receptors Regulate Early Osteoblast Differentiation Induced by BMP-2," *J. Bone Miner. Res.*, vol. 14, no. 7, pp. 1075–1083, Jul. 1999.

[132] M. Brunner *et al.*, "β1 integrins mediate the BMP2 dependent transcriptional control of osteoblast differentiation and osteogenesis.," *PLoS One*, vol. 13, no. 4, p. e0196021, 2018.

[133] A. Kotzsch *et al.*, "Structure Analysis of Bone Morphogenetic Protein-2 Type I Receptor Complexes Reveals a Mechanism of Receptor Inactivation in Juvenile Polyposis Syndrome," *J. Biol. Chem.*, vol. 283, no. 9, pp. 5876–5887, Feb. 2008.

[134] Y. Zu, X. Liang, J. Du, S. Zhou, and C. Yang, "Binding of integrin α1 to bone morphogenetic protein receptor IA suggests a novel role of integrin α1β1 in bone morphogenetic protein 2 signalling," *J. Biomech.*, vol. 48, no. 14, pp. 3950–3954, Nov. 2015.

[135] H. A. North, L. Pan, T. L. McGuire, S. Brooker, and J. A. Kessler, "β1-Integrin Alters Ependymal Stem Cell BMP Receptor Localization and Attenuates Astrogliosis after Spinal Cord Injury," *J. Neurosci.*, vol. 35, no. 9, pp. 3725–3733, Mar. 2015.

[136] J. Du *et al.*, "Integrin activation and internalization on soft ECM as a mechanism of induction of stem cell differentiation by ECM elasticity.," *Proc. Natl. Acad. Sci. U. S. A.*, vol. 108, no. 23, pp. 9466–71, Jun. 2011.

[137] M. Delcommenne, C. Tan, V. Gray, L. Rue, J. Woodgett, and S. Dedhar, "Phosphoinositide-3-OH kinase-dependent regulation of glycogen synthase kinase 3 and protein kinase B/AKT by the integrin-linked kinase.," *Proc. Natl. Acad. Sci. U. S. A.*, vol. 95, no. 19, pp. 11211–6, Sep. 1998.

[138] C. Frantz, K. M. Stewart, and V. M. Weaver, "The extracellular matrix at a glance," *Journal of Cell Science*, vol. 123, no. 24. pp. 4195–4200, 15-Dec-2010.

[139] S. Ricard-Blum, "The Collagen Family," *Cold Spring Harb. Perspect. Biol.*, vol. 3, no. 1, pp. 1–19, Jan. 2011.

[140] J. Bella and D. J. S. Hulmes, "Fibrillar collagens," *Subcell. Biochem.*, vol. 82, pp. 457–490, Jan. 2017.

[141] H. NAGASE, R. VISSE, and G. MURPHY, "Structure and function of matrix metalloproteinases and TIMPs.," *Cardiovasc. Res.*, vol. 69, no. 3, pp. 562–573, 2006.

[142] D. Kessler *et al.*, "Fibroblasts in Mechanically Stressed Collagen Lattices Assume a 'Synthetic' Phenotype," *J. Biol. Chem.*, vol. 276, no. 39, pp. 36575–36585, Sep. 2001.

[143] V. Dumas *et al.*, "The effect of dual frequency cyclic compression on matrix deposition by osteoblast-like cells grown in 3D scaffolds and on modulation of VEGF variant expression," *Biomaterials*, vol. 30, no. 19, pp. 3279–3288, Jul. 2009.

[144] Y. He, E. J. Macarak, J. M. Korostoff, and P. S. Howard, "Compression and tension: Differential effects on matrix accumulation by periodontal ligaments fibroblasts in vitro," *Connect. Tissue Res.*, vol. 45, no. 1, pp. 28–39, 2004.

[145] J. D. Glaeser *et al.*, "Modulation of matrix metalloprotease-2 levels by mechanical loading of three-dimensional mesenchymal stem cell constructs: Impact on in vitro tube formation," *Tissue Eng. - Part A*, vol. 16, no. 10, pp. 3139–3148, Oct. 2010.

[146] A. Petersen, P. Joly, C. Bergmann, G. Korus, and G. N. Duda, "The Impact of Substrate Stiffness and Mechanical Loading on Fibroblast-Induced Scaffold Remodeling," *Tissue Eng. Part A*, vol. 18, no. 17–18, pp. 1804–1817, Sep. 2012.

[147] J. N. A. De Croos, S. S. Dhaliwal, M. D. Grynpas, R. M. Pilliar, and R. A. Kandel, "Cyclic compressive mechanical stimulation induces sequential catabolic and anabolic gene changes in chondrocytes resulting in increased extracellular matrix accumulation.," *Matrix Biol.*, vol. 25, no. 6, pp. 323–31, Aug. 2006.

[148] S. D. Waldman, D. C. Couto, M. D. Grynpas, R. M. Pilliar, and R. A. Kandel, "A single application of cyclic loading can accelerate matrix deposition and enhance the properties of tissue-engineered cartilage.," *Osteoarthr. Cartil.*, vol. 14, no. 4, pp. 323–30, Apr. 2006.

[149] E. N. Blaney Davidson, E. L. Vitters, P. L. E. M. van Lent, F. A. J. van de Loo, W. B. van den Berg, and P. M. van der Kraan, "Elevated extracellular matrix production and degradation upon bone morphogenetic protein-2 (BMP-2) stimulation point toward a role for BMP-2 in cartilage repair and remodeling.," *Arthritis Res. Ther.*, vol. 9, no. 5, p. R102, Jan. 2007.

[150] J. Li, K. S. Kim, J. S. Park, W. A. Elmer, W. C. Hutton, and S. T. Yoon, "BMP-2 and CDMP-2: Stimulation of chondrocyte production of proteoglycan," *J. Orthop. Sci.*, vol. 8, no. 6, pp. 829–835, 2003.

[151] D. Chen *et al.*, "Bone morphogenetic protein 2 (BMP-2) enhances BMP-3, BMP-4, and bone cell differentiation marker gene expression during the induction of mineralized bone matrix formation in cultures of fetal rat calvarial osteoblasts.," *Calcif. Tissue Int.*, vol. 60, no. 3, pp. 283–90, Mar. 1997.

[152] A. Marupanthorn, C. Tantrawatpan, P. Kheolamai, D. Tantikanlayaporn, and S. Manochantr, "Bone morphogenetic protein-2 enhances the osteogenic differentiation capacity of mesenchymal stromal cells derived from human bone marrow and umbilical cord," *Int. J. Mol. Med.*, vol. 39, no. 3, pp. 654–662, Mar. 2017.

[153] F. Lecanda, L. V Avioli, and S. L. Cheng, "Regulation of bone matrix protein expression and induction of differentiation of human osteoblasts and human bone marrow stromal cells by bone morphogenetic protein-2.," *J. Cell. Biochem.*, vol. 67, no. 3, pp. 386–96, Dec. 1997.

[154] P. Owens *et al.*, "Bone Morphogenetic Proteins Stimulate Mammary Fibroblasts to Promote Mammary Carcinoma Cell Invasion," *PLoS One*, vol. 8, no. 6, Jun. 2013.

[155] J. Li, S. T. Yoon, and W. C. Hutton, "Effect of bone morphogenetic protein-2 (BMP-2) on matrix production, other BMPs, and BMP receptors in rat intervertebral disc cells.," *J. Spinal Disord. Tech.*, vol. 17, no. 5, pp. 423–8, Oct. 2004.

[156] Y.-K. Wang *et al.*, "Bone morphogenetic protein-2-induced signaling and osteogenesis is regulated by cell shape, RhoA/ROCK, and cytoskeletal tension.," *Stem Cells Dev.*, vol. 21, no. 7, pp. 1176–86, May 2012.

[157] M. Werner, N. A. Kurniawan, G. Korus, C. V. C. Bouten, and A. Petersen, "Mesoscale substrate curvature overrules nanoscale contact guidance to direct bone marrow stromal cell migration.," *J. R. Soc. Interface*, vol. 15, no. 145, 2018.

[158] H. Schoof, J. Apel, I. Heschel, and G. Rau, "Control of pore structure and size in freeze-dried collagen sponges.," *J. Biomed. Mater. Res.*, vol. 58, no. 4, pp. 352–7, 2001.

[159] Petersen, Joly, Bergmann, Korus, and Duda, "The Impact of Substrate Stiffness and Mechanical Loading on Fibroblast-Induced Scaffold Remodeling," *Tissue Eng. Part A*, vol. 18, no. 17–18, pp. 1804–1817, 2012.

[160] J. Riedl *et al.*, "Lifeact: a versatile marker to visualize F-actin," *Nat. Methods*, vol. 5, no. 7, pp. 605–607, Jul. 2008.

[161] M. W. Pfaffl, "A new mathematical model for relative quantification in real-time RT-PCR.," *Nucleic Acids Res.*, vol. 29, no. 9, p. e45, 2001.

[162] C. Ramakers, J. M. Ruijter, R. H. L. Deprez, and A. F. M. Moorman, "Assumption-free analysis of quantitative real-time polymerase chain reaction (PCR) data.," *Neurosci. Lett.*, vol. 339, no. 1, pp. 62–6, Mar. 2003.

[163] B. Kappler *et al.*, "The cytoprotective capacity of processed human cardiac extracellular matrix.," *J. Mater. Sci. Mater. Med.*, vol. 27, no. 7, p. 120, Jul. 2016.

[164] X. Chen, O. Nadiarynkh, S. Plotnikov, and P. J. Campagnola, "Second harmonic generation microscopy for quantitative analysis of collagen fibrillar structure," *Nat. Protoc.*, vol. 7, no. 4, pp. 654–669, Apr. 2012.

[165] R. Rezakhaniha *et al.*, "Experimental investigation of collagen waviness and orientation in the arterial adventitia using confocal laser scanning microscopy," *Biomech. Model. Mechanobiol.*, vol. 11, no. 3–4, pp. 461–473, Mar. 2012.

[166] J.-Y. Tinevez *et al.*, "TrackMate: An open and extensible platform for single-particle tracking.," *Methods*, vol. 115, pp. 80–90, Feb. 2017.

[167] P. Baniukiewicz, S. Collier, and T. Bretschneider, "QuimP: analyzing transmembrane signalling in highly deformable cells.," *Bioinformatics*, vol. 34, no. 15, pp. 2695–2697, Aug. 2018.

[168] M. Becker *et al.*, "Towards a Novel Patch Material for Cardiac Applications: Tissue-Specific Extracellular Matrix Introduces Essential Key Features to Decellularized Amniotic Membrane.," *Int. J. Mol. Sci.*, vol. 19, no. 4, p. 1032, Mar. 2018.

[169] B. Ma *et al.*, "PEAKS: powerful software for peptide de novo sequencing by tandem mass spectrometry.," *Rapid Commun. Mass Spectrom.*, vol. 17, no. 20, pp. 2337–42, Oct. 2003.

[170] K. H. Vining and D. J. Mooney, "Mechanical forces direct stem cell behaviour in development and regeneration," *Nature Reviews Molecular Cell Biology*, vol. 18, no. 12. Nature Publishing Group, pp. 728–742, 01-Dec-2017.

[171] E. Brauer *et al.*, "Collagen Fibrils Mechanically Contribute to Tissue Contraction in an In Vitro Wound Healing Scenario," *Adv. Sci.*, vol. 6, no. 9, p. 1801780, May 2019.

[172] S. Schreivogel, V. Kuchibhotla, P. Knaus, G. N. Duda, and A. Petersen, "Load-induced osteogenic differentiation of mesenchymal stromal cells is caused by mechano-regulated autocrine signaling," *J. Tissue Eng. Regen. Med.*, Aug. 2019.

[173] F. Witt, G. N. Duda, C. Bergmann, and A. Petersen, "Cyclic Mechanical Loading Enables Solute Transport and Oxygen Supply in Bone Healing: An *In Vitro* Investigation," *Tissue Eng. Part A*, p. 140120073517006, Jan. 2014.

[174] T. Katagiri *et al.*, "Bone morphogenetic protein-2 converts the differentiation pathway of C2C12 myoblasts into the osteoblast lineage.," *J. Cell Biol.*, vol. 127, no. 6 Pt 1, pp. 1755–66, Dec. 1994.

[175] K. Yang *et al.*, "BMPR2-pSMAD1/5 signaling pathway regulates RUNX2 expression and impacts the progression of dedifferentiated chondrosarcoma.," *Am. J. Cancer Res.*, vol. 6, no. 6, pp. 1302–16, Jan. 2016.

[176] R. Nishimura, K. Hata, T. Matsubara, M. Wakabayashi, and T. Yoneda, "Regulation of bone and cartilage development by network between BMP signalling and transcription factors.," *J. Biochem.*, vol. 151, no. 3, pp. 247–54, Mar. 2012.

[177] C. Krause, A. Guzman, and P. Knaus, "Noggin," *Int. J. Biochem. Cell Biol.*, vol. 43, no. 4, pp. 478–481, Apr. 2011.

[178] I. S. Kim, Y. M. Song, T. H. Cho, J. Y. Kim, F. E. Weber, and S. J. Hwang, "Synergistic action of static stretching and BMP-2 stimulation in the osteoblast differentiation of C2C12 myoblasts.," *J. Biomech.*, vol. 42, no. 16, pp. 2721–7, 2009.

[179] L. Wang *et al.*, "Involvement of p38MAPK/NF-κB Signaling Pathways in Osteoblasts Differentiation in Response to Mechanical Stretch," *Ann. Biomed. Eng.*, vol. 40, no. 9, pp. 1884–1894, Sep. 2012.

[180] L. Wang *et al.*, "Involvement of BMPs/Smad signaling pathway in mechanical response in osteoblasts.," *Cell. Physiol. Biochem.*, vol. 26, no. 6, pp. 1093–102, Jan. 2010.

[181] M. A. Peake and A. J. El Haj, "Preliminary characterisation of mechanoresponsive regions of the c-fos promoter in bone cells," *FEBS Lett.*, vol. 537, no. 1–3, pp. 117–120, Feb. 2003.

[182] V. Kanoldt, L. Fischer, and C. Grashoff, "Unforgettable force – crosstalk and memory of mechanosensitive structures," *Biol. Chem.*, vol. 400, no. 6, pp. 687–698, Jun. 2019.

[183] J. S. Bennett, "Structure and function of the platelet integrin αIIbβ3," *J. Clin. Invest.*, vol. 115, no. 12, p. 3363, Dec. 2005.

[184] M. R. Bubb, I. Spector, B. B. Beyer, and K. M. Fosen, "Effects of jasplakinolide on the kinetics of actin polymerization. An explanation for certain in vivo observations.," *J. Biol. Chem.*, vol. 275, no. 7, pp. 5163–70, Feb. 2000.

[185] D. P. Berry, K. G. Harding, M. R. Stanton, B. Jasani, and H. P. Ehrlich, "Human wound contraction: Collagen organization, fibroblasts, and myofibroblasts," *Plast. Reconstr. Surg.*, vol. 102, no. 1, pp. 124–134, Jul. 1998.

[186] K. Runager, J. J. Enghild, and G. K. Klintworth, "Focus on molecules: Transforming growth factor beta induced protein (TGFBIp)," *Experimental Eye Research*, vol. 87, no. 4. pp. 298–299, Oct-2008.

[187] E. P. Sproul and W. S. Argraves, "A cytokine axis regulates elastin formation and degradation," *Matrix Biology*, vol. 32, no. 2. pp. 86–94, 11-Mar-2013.

[188] O. C. and D. J. Mooney, "Chaudhuri, Mooney - 2012 - Stem-cell differentiation Anchoring cell-fate cues.pdf," *Nat. Mater.*, vol. 11, pp. 568–569, 2012.

[189] M. Bottlang and F. Feist, "Biomechanics of Far Cortical Locking," *J. Orthop. Trauma*, vol. 25, pp. S21–S28, Feb. 2011.

[190] B. S. Klosterhoff *et al.*, "Wireless Implantable Sensor for Noninvasive, Longitudinal Quantification of Axial Strain Across Rodent Long Bone Defects," *J. Biomech. Eng.*, vol. 139, no. 11, p. 111004, Oct. 2017.

[191] C. Liu *et al.*, "Influence of perfusion and compression on the proliferation and differentiation of bone mesenchymal stromal cells seeded on polyurethane scaffolds," *Biomaterials*, vol. 33, no. 4, pp. 1052–1064, 2012.

[192] M. Morlock *et al.*, "Duration and frequency of every day activities in total hip patients.," *J. Biomech.*, vol. 34, no. 7, pp. 873–81, Jul. 2001.

[193] P. Ducy, R. Zhang, V. Geoffroy, A. L. Ridall, and G. Karsenty, "Osf2/Cbfa1: a transcriptional activator of osteoblast differentiation.," *Cell*, vol. 89, no. 5, pp. 747–54, May 1997.

[194] R. T. Franceschi and G. Xiao, "Regulation of the osteoblast-specific transcription factor, Runx2: Responsiveness to multiple signal transduction pathways," *J. Cell. Biochem.*, vol. 88, no. 3, pp. 446–454, 2003.

[195] Y. Shi *et al.*, "Continuous cyclic mechanical tension inhibited Runx2 expression in mesenchymal stem cells through RhoA-ERK1/2 pathway," *J. Cell. Physiol.*, vol. 226, no. 8, pp. 2159–2169, Aug. 2011.

[196] J. Klein-Nulend, J. Roelofsen, C. M. Semeins, A. L. Bronckers, and E. H. Burger, "Mechanical stimulation of osteopontin mRNA expression and synthesis in bone cell cultures.," *J. Cell. Physiol.*, vol. 170, no. 2, pp. 174–81, Feb. 1997.

[197] C. D. Toma, S. Ashkar, M. L. Gray, J. L. Schaffer, and L. C. Gerstenfeld, "Signal transduction

of mechanical stimuli is dependent on microfilament integrity: identification of osteopontin as a mechanically induced gene in osteoblasts.," *J. Bone Miner. Res.*, vol. 12, no. 10, pp. 1626–36, Oct. 1997.

[198] R. D. Sumanasinghe, S. H. Bernacki, and E. G. Loboa, "Osteogenic differentiation of human mesenchymal stem cells in collagen matrices: effect of uniaxial cyclic tensile strain on bone morphogenetic protein (BMP-2) mRNA expression.," *Tissue Eng.*, vol. 12, no. 12, pp. 3459–65, Dec. 2006.

[199] D. Wulsten *et al.*, "Time kinetics of bone defect healing in response to BMP-2 and GDF-5 characterised by in vivo biomechanics.," *Eur. Cell. Mater.*, vol. 21, pp. 177–92, Feb. 2011.

[200] M.-H. Lee *et al.*, "BMP-2-induced Runx2 expression is mediated by Dlx5, and TGF-beta 1 opposes the BMP-2-induced osteoblast differentiation by suppression of Dlx5 expression.," *J. Biol. Chem.*, vol. 278, no. 36, pp. 34387–94, Sep. 2003.

[201] R. P. Huang, C. T. Rubin, and K. J. McLeod, "Changes in postural muscle dynamics as a function of age.," *J. Gerontol. A. Biol. Sci. Med. Sci.*, vol. 54, no. 8, pp. B352-7, Aug. 1999.

[202] S. R. L. Young, R. Gerard-O'Riley, J. B. Kim, and F. M. Pavalko, "Focal adhesion kinase is important for fluid shear stress-induced mechanotransduction in osteoblasts," *J. Bone Miner. Res.*, vol. 24, no. 3, pp. 411–424, Mar. 2009.

[203] H.-J. Hsu, C.-F. Lee, and R. Kaunas, "A Dynamic Stochastic Model of Frequency-Dependent Stress Fiber Alignment Induced by Cyclic Stretch," *PLoS One*, vol. 4, no. 3, p. e4853, Mar. 2009.

[204] M. J. Qu, B. Liu, H. Q. Wang, Z. Q. Yan, B. R. Shen, and Z. L. Jiang, "Frequency-dependent phenotype modulation of vascular smooth muscle cells under cyclic mechanical strain," *J. Vasc. Res.*, vol. 44, no. 5, pp. 345–353, Aug. 2007.

[205] M. E. Goldschmidt, K. J. McLeod, and W. R. Taylor, "Integrin-mediated mechanotransduction in vascular smooth muscle cells: frequency and force response characteristics.," *Circ. Res.*, vol. 88, no. 7, pp. 674–80, Apr. 2001.

[206] C. H. Turner, M. R. Forwood, and M. W. Otter, "Mechanotransduction in bone: Do bone cells act as sensors of fluid flow?," *FASEB J.*, vol. 8, no. 11, pp. 875–878, 1994.

[207] Y. F. Hsieh and C. H. Turner, "Effects of loading frequency on mechanically induced bone formation," *J. Bone Miner. Res.*, vol. 16, no. 5, pp. 918–924, 2001.

[208] K. Marycz, D. Lewandowski, K. A. Tomaszewski, B. M. Henry, E. B. Golec, and M. Marędziak, "Low-frequency, low-magnitude vibrations (LFLM) enhances chondrogenic differentiation potential of human adipose derived mesenchymal stromal stem cells (hASCs)," *PeerJ*, vol. 2016, no. 2, 2016.

[209] R. Qin *et al.*, "Phosphorylation and turnover of paxillin in focal contacts is controlled by force and defines the dynamic state of the adhesion site.," *Cytoskeleton (Hoboken).*, vol. 72, no. 2, pp. 101–12, Feb. 2015.

[210] D. Choquet, D. P. Felsenfeld, and M. P. Sheetz, "Extracellular Matrix Rigidity Causes Strengthening of Integrin–Cytoskeleton Linkages," *Cell*, vol. 88, no. 1, pp. 39–48, Jan. 1997.

[211] D. Riveline *et al.*, "Focal Contacts as Mechanosensors," *J. Cell Biol.*, vol. 153, no. 6, pp. 1175–1186, Jun. 2001.

[212] C. Yang, M. W. Tibbitt, L. Basta, and K. S. Anseth, "Mechanical memory and dosing influence stem cell fate," *Nat. Mater.*, vol. 13, no. 6, pp. 645–652, Jun. 2014.

[213] Y. Zu, X. Liang, J. Du, S. Zhou, and C. Yang, "Binding of integrin α1 to bone morphogenetic protein receptor IA suggests a novel role of integrin α1β1 in bone morphogenetic protein 2 signalling," *J. Biomech.*, vol. 48, no. 14, pp. 3950–3954, Nov. 2015.

[214] H. L. Ashe, "Modulation of BMP signalling by integrins.," *Biochem. Soc. Trans.*, vol. 44,

no. 5, pp. 1465–1473, Oct. 2016.

[215] K. Haase, Z. Al-Rekabi, and A. E. Pelling, "Mechanical cues direct focal adhesion dynamics," in *Progress in Molecular Biology and Translational Science*, vol. 126, Elsevier B.V., 2014, pp. 103–134.

[216] E. A. Osborn, A. Rabodzey, C. F. Dewey, and J. H. Hartwig, "Endothelial actin cytoskeleton remodeling during mechanostimulation with fluid shear stress," *Am. J. Physiol. Physiol.*, vol. 290, no. 2, pp. C444–C452, Feb. 2006.

[217] L. P. Cramer, "Role of actin-filament disassembly in lamellipodium protrusion in motile cells revealed using the drug jasplakinolide," *Curr. Biol.*, vol. 9, no. 19, pp. 1095–1105, Oct. 1999.

[218] X. Zhang *et al.*, "Actin stabilization by jasplakinolide affects the function of bone marrow-derived late endothelial progenitor cells.," *PLoS One*, vol. 7, no. 11, p. e50899, Jan. 2012.

[219] W. C. Chen *et al.*, "BMP-2 induces angiogenesis by provoking integrin α6 expression in human endothelial progenitor cells," *Biochem. Pharmacol.*, vol. 150, pp. 256–266, Apr. 2018.

[220] D. Könnig, A. Herrera, G. N. Duda, and A. Petersen, "Mechanosensation across borders: fibroblasts inside a macroporous scaffold sense and respond to the mechanical environment beyond the scaffold walls," *J. Tissue Eng. Regen. Med.*, vol. 12, no. 1, pp. 265–275, Jan. 2018.

[221] R. Rudolph, "Contraction and the control of contraction.," *World J. Surg.*, vol. 4, no. 3, pp. 279–87, May 1980.

[222] G. Sedlmeier and J. P. Sleeman, "Extracellular regulation of BMP signaling: welcome to the matrix.," *Biochem. Soc. Trans.*, vol. 45, no. 1, pp. 173–181, Feb. 2017.

[223] N. Ghosh-Choudhury, S. L. Abboud, B. Chandrasekar, and G. Ghosh Choudhury, "BMP-2 regulates cardiomyocyte contractility in a phosphatidylinositol 3 kinase-dependent manner," *FEBS Lett.*, vol. 544, no. 1–3, pp. 181–184, Jun. 2003.

[224] T. Rothhammer, S. Braig, and A. K. Bosserhoff, "Bone morphogenetic proteins induce expression of metalloproteinases in melanoma cells and fibroblasts," *Eur. J. Cancer*, vol. 44, no. 16, pp. 2526–2534, Nov. 2008.

[225] R. Visse and H. Nagase, "Matrix metalloproteinases and tissue inhibitors of metalloproteinases: Structure, function, and biochemistry," *Circulation Research*, vol. 92, no. 8. pp. 827–839, 02-May-2003.

[226] C. Cangemi, M. L. Hansen, W. S. Argraves, and L. M. Rasmussen, "Fibulins and their role in cardiovascular biology and disease," in *Advances in Clinical Chemistry*, vol. 67, Academic Press Inc., 2014, pp. 245–265.

[227] M. A. Cooley *et al.*, "Fibulin-1 is required for bone formation and Bmp-2-mediated induction of Osterix," *Bone*, vol. 69, pp. 30–38, Sep. 2014.

[228] M. C. Sutcliffe and J. M. Davidson, "Effect of Static Stretching on Elastin Production by Porcine Aortic Smooth Muscle Cells," *Matrix*, vol. 10, no. 3, pp. 148–153, 1990.

[229] P. S. Howard, U. Kucich, R. Taliwal, and J. M. Korostoff, "Mechanical forces alter extracellular matrix synthesis by human periodontal ligament fibroblasts," *J. Periodontal Res.*, vol. 33, no. 8, pp. 500–508, Jun. 1998.

[230] B. Hinz, "Formation and function of the myofibroblast during tissue repair," *Journal of Investigative Dermatology*, vol. 127, no. 3. Nature Publishing Group, pp. 526–537, 2007.

[231] J. P. E. Junker, C. Kratz, A. Tollbäck, and G. Kratz, "Mechanical tension stimulates the transdifferentiation of fibroblasts into myofibroblasts in human burn scars," *Burns*, vol. 34, no. 7, pp. 942–946, Nov. 2008.

[232] I. Kii and H. Ito, “Periostin and its interacting proteins in the construction of extracellular architectures,” *Cellular and Molecular Life Sciences*, vol. 74, no. 23. Birkhauser Verlag AG, pp. 4269–4277, 01-Dec-2017.

[233] M. I. Uzel *et al.*, “Multiple Bone Morphogenetic Protein 1-related Mammalian Metalloproteinases Process Pro-lysyl Oxidase at the Correct Physiological Site and Control Lysyl Oxidase Activation in Mouse Embryo Fibroblast Cultures,” *J. Biol. Chem.*, vol. 276, no. 25, pp. 22537–22543, Jun. 2001.

[234] T. Maruhashi, I. Kii, M. Saito, and A. Kudo, “Interaction between periostin and BMP-1 promotes proteolytic activation of lysyl oxidase,” *J. Biol. Chem.*, vol. 285, no. 17, pp. 13294–13303, Apr. 2010.

[235] B. Merle and P. Garnero, “The multiple facets of periostin in bone metabolism,” *Osteoporosis International*, vol. 23, no. 4. Springer-Verlag, pp. 1199–1212, Apr-2012.

[236] I. Kii *et al.*, “Incorporation of tenascin-C into the extracellular matrix by periostin underlies an extracellular meshwork architecture,” *J. Biol. Chem.*, vol. 285, no. 3, pp. 2028–2039, Jan. 2010.

[237] K. Sato, O. Matsubara, E. Hase, T. Minamikawa, and T. Yasui, “Quantitative in situ time-series evaluation of osteoblastic collagen synthesis under cyclic strain using second-harmonic-generation microscopy,” *J. Biomed. Opt.*, vol. 24, no. 03, p. 1, Jan. 2019.

[238] C. Aparicio and M. P. Ginebra, *Biomineralization and Biomaterials: Fundamentals and Applications*. 2015.

[239] J. Chen *et al.*, “Therapeutic effects of whole-body vibration on fracture healing in ovariectomized rats: A systematic review and meta-analysis,” *Menopause*, vol. 26, no. 6. Lippincott Williams and Wilkins, pp. 677–686, 01-Jun-2019.

[240] R. Uchida *et al.*, “Vibration acceleration promotes bone formation in rodent models,” *PLoS One*, vol. 12, no. 3, p. e0172614, Mar. 2017.

Supplement

Supplement to section 1.3 of the introduction:

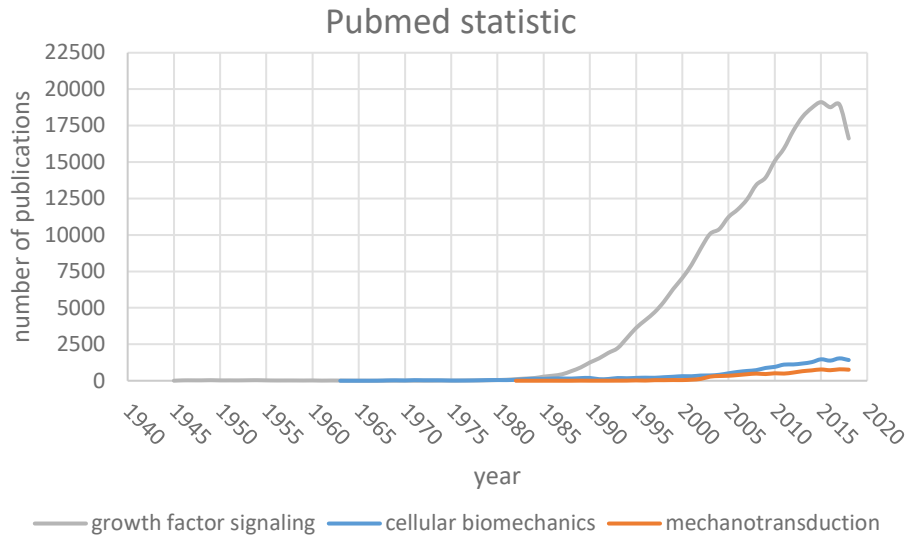

Figure 0-1 Pubmed search term statistics. Number of publications related to growth factor signaling (gray), cellular biomechanics (blue) or mechanotransduction (orange) listed per year. Since a long time, biochemical cues are recognized as important regulators of cellular behavior while the field of biomechanics only emerged around the year 2000. Biomechanics has gained increasing attention until now but is still underrepresented.

Supplement to section 4.1.4 of the results:

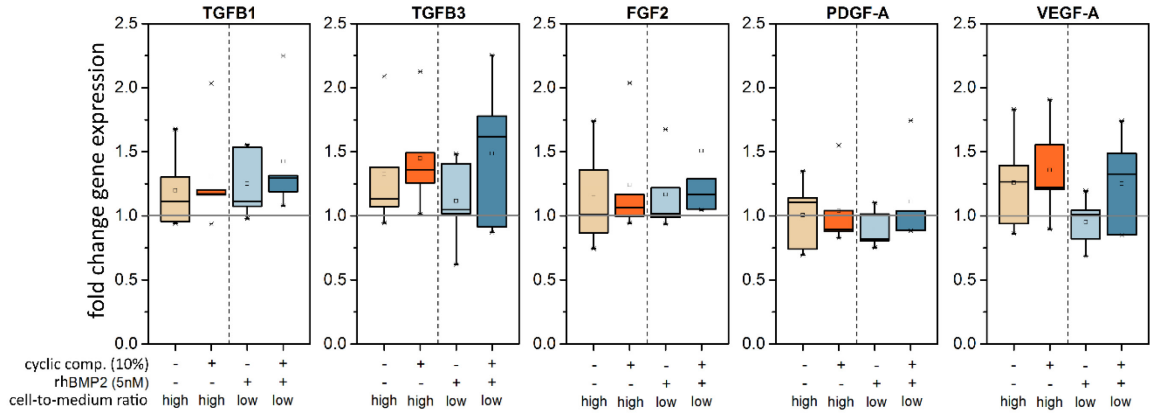

Figure 0-2: Gene expression changes of TGFβ1, TGFβ3, FGF2, PDGF-A and VEGF-A, growth factors that influence osteogenic differentiation. Under R_{high} conditions, only TGFβ3 expression is slightly increased in response to cyclic compression. Human BMSCs were seeded in collagen scaffolds (12.4 kPa) and stimulated with and without cyclic compression (f=1Hz, ε=10%) under increased cell-to-medium ratio or under concurrent rhBMP2 (5nM) stimulation. Fold change gene expression was analyzed by qPCR in comparison to the untreated control (low cell-to-medium ratio, without cyclic compression). HPRT1 was used as the reference gene. Box and whisker plots showing the following values from bottom to top: minimum value, low quartile, median, upper quartile, maximum value, □ mean; × outlier (n=5 hBMSC donors). Statistical significance was tested via Mann–Whitney test (two-sided) with Bonferroni correction.

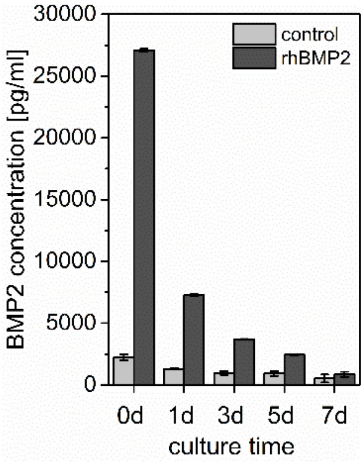

Figure 0-3: BMP2 stability during bioreactor culture. Bioreactor experiment without cultivation of cells. rhBMP2 (135ng/ml) was added at day 0 and medium samples were taken after 30min (0d), on day 1, 3, 5 and 7 to measure the BMP2 concentration by ELISA. Expansion medium without additional supplements served as a control (n=2).

Supplement to section 4.2.2 of the results:

Table 0-1: Fold change (F.I.) gene expression in response to 24h BMP-2 stimulation and/or mechanical loading of 1 Hz or 10 Hz. The heat map in Figure 4-8 is based on the log2(F.I.), n=4.

F.I.	c	B	L 1Hz	B/L 1Hz	L 10Hz	B/L 10Hz	**log2(F.I.)**	c	B	L 1Hz	B/L 1Hz	L 10Hz	B/L 10Hz
ID1	1	1.36	0.91	1.76	1.19	3.92	ID1	0	0.44	-0.13	0.81	0.25	1.97
ID2	1	1.16	0.98	1.43	1.19	2.06	ID2	0	0.21	-0.02	0.51	0.25	1.05
DLX2	1	1.29	1.19	1.24	1.47	1.86	DLX2	0	0.37	0.25	0.31	0.55	0.89
SMAD7	1	1.21	1.16	1.50	1.72	1.97	SMAD7	0	0.27	0.21	0.58	0.78	0.98
Noggin	1	1.18	1.13	1.42	1.31	2.87	Noggin	0	0.24	0.18	0.51	0.39	1.52
Smurf1	1	1.03	1.13	1.10	1.36	1.22	Smurf1	0	0.04	0.18	0.13	0.45	0.28
Smurf2	1	1.14	1.31	1.30	1.36	1.33	Smurf2	0	0.19	0.39	0.38	0.44	0.41
BR1A	1	1.08	1.14	1.15	1.21	1.06	BR1A	0	0.11	0.19	0.20	0.27	0.09
BR1B	1	0.96	1.20	1.41	1.74	1.62	BR1B	0	-0.06	0.27	0.50	0.80	0.70
BR2	1	1.05	1.23	1.22	1.22	1.10	BR2	0	0.07	0.30	0.28	0.29	0.13
c-fos	1	0.87	1.28	1.28	1.85	1.90	c-fos	0	-0.20	0.36	0.35	0.89	0.93
RUNX2	1	1.03	1.13	1.05	1.02	0.93	RUNX2	0	0.04	0.17	0.08	0.03	-0.11
SPP1	1	0.81	0.87	0.87	1.99	1.77	SPP1	0	-0.30	-0.20	-0.20	0.99	0.83
COL1A2	1	1.34	1.02	1.06	0.95	1.15	COL1A2	0	0.42	0.03	0.09	-0.08	0.20
RhoA	1	0.99	1.05	1.07	1.30	1.17	RhoA	0	-0.01	0.08	0.09	0.37	0.23
ROCK2	1	1.06	1.13	1.26	1.30	1.22	ROCK2	0	0.08	0.17	0.34	0.38	0.29
ITG a1	1	1.13	1.11	1.10	1.28	1.17	ITG a1	0	0.17	0.16	0.13	0.36	0.22
ITG a5	1	1.00	1.09	0.98	1.16	1.11	ITG a5	0	-0.01	0.13	-0.03	0.22	0.15
ITG av	1	0.98	1.06	1.14	1.46	1.31	ITG av	0	-0.03	0.09	0.19	0.55	0.39
ITG b1	1	1.16	1.32	1.31	1.42	1.32	ITG b1	0	0.21	0.40	0.39	0.50	0.40
ITG b3	1	1.03	1.26	1.85	1.57	1.92	ITG b3	0	0.04	0.34	0.89	0.65	0.94
ITG b5	1	1.08	1.10	1.10	1.03	1.07	ITG b5	0	0.12	0.14	0.14	0.04	0.10

Supplement to section 4.2.6 of the results:

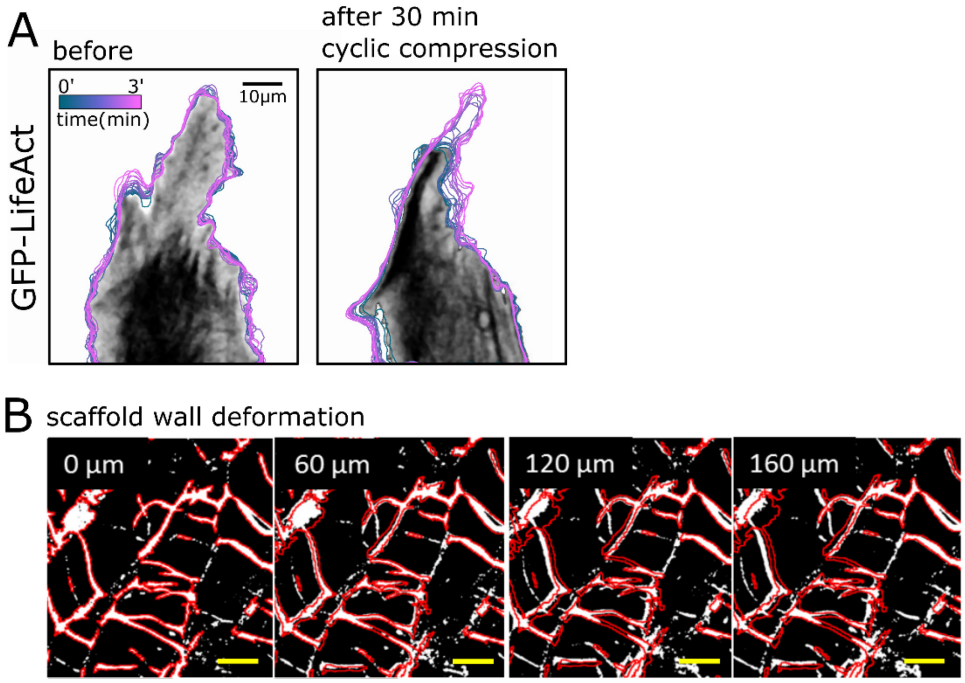

Figure 0-4: Dynamic actin remodeling induced by cyclic compression and scaffold wall deformation under compression visualized using the Bioreactor-Microscope-Setup. (A) GFP-LifeAct expressing hFOBs seeded in collagen scaffolds were stimulated with cyclic compression (1Hz, 10%) for 30 min. Fast actin remolding processes were recorded during 3 min before and after cyclic compression. Representative images show the cell outline change over 3 min. The cell outlines are colored according to frame number from blue to pink. (B) Scaffold wall crimping due to 10% compression (=160µm). Red lines indicate position of collagen scaffold walls before compression (scale bar = 100µm).

Supplement to section 4.3.2 of the results:

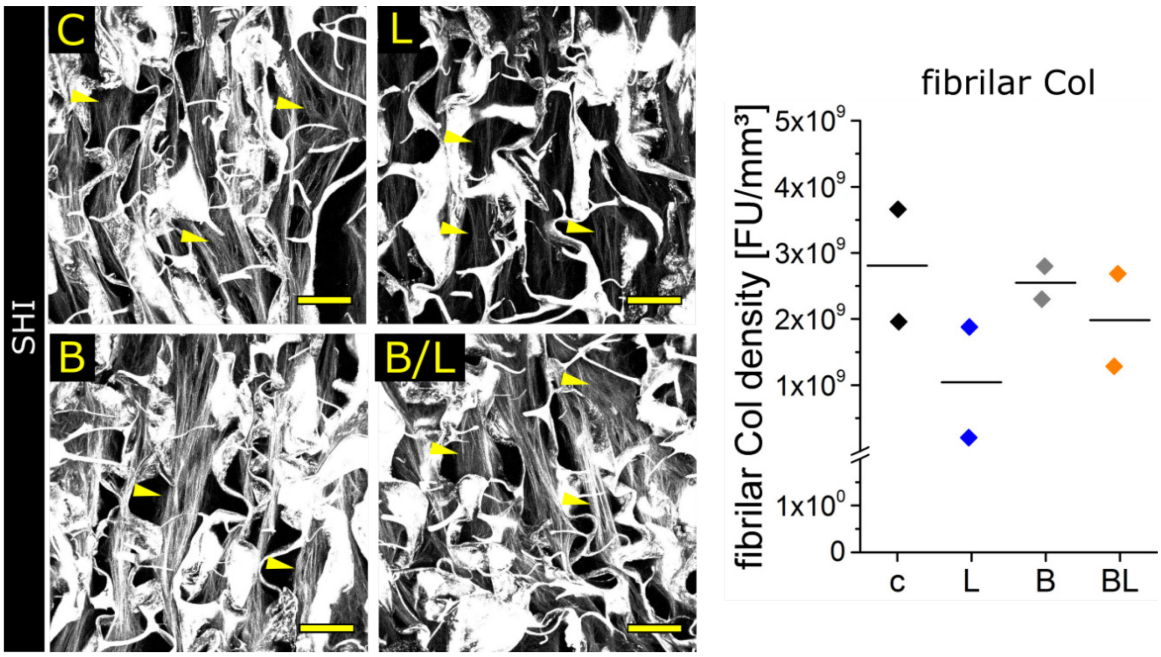

Figure 0-5: Fibrillar collagen density is reduced by cyclic compression after 2 weeks of cultivation. Human fibroblasts seeded in 1.5-wt% collagen scaffolds were cultured for 2 weeks in the bioreactor under intermitted cyclic compression (f=1Hz, ε=10%, 3h load, 5h break), rhBMP2 (5nM) or a combination of both. Representative confocal multiphoton images showing fibrillar collagen visualized by SHG (white). Yellow arrows indicate newly deposited collagen fibers

within the collagen walls of the scaffold. Scale bar = 100µm. Quantification of fibrillary collagen density inside scaffold pores (n=2).

Supplement to section 4.3.3 of the results:

Table 0-2: Gene expression analysis of selected ECM proteins and ECM modulators. Fold change (F.I.) gene expression analyzed after seven days in the bioreactor under intermitted cyclic compression (f=1Hz, ε=10%, 3h load, 5h break), rhBMP2 (5nM) or a combination of both. The heat map in Figure 4-23 is based on the log2(F.I.), n=3.

F.I.	c	L	B	B/L	**log2(F.I.)**	c	L	B	B/L
COL1A2	1	1.11	0.82	0.80	COL1A2	0	0.15	-0.29	-0.32
COL6A1	1	1.09	1.14	0.96	COL6A1	0	0.13	0.19	-0.06
FN	1	1.16	1.00	0.92	FN	0	0.21	-0.01	-0.13
FBLN1	1	1.84	1.42	1.26	FBLN1	0	0.88	0.50	0.33
ELN	1	1.91	0.64	1.22	ELN	0	0.94	-0.65	0.29
TNC	1	1.36	0.97	1.11	TNC	0	0.44	-0.04	0.15
THBS1	1	1.22	1.02	0.97	THBS1	0	0.29	0.03	-0.04
TGFBI	1	2.25	0.92	1.52	TGFBI	0	1.17	-0.12	0.60
POSTN	1	1.38	0.81	1.21	POSTN	0	0.47	-0.30	0.28
BMP1	1	1.48	1.00	1.18	LOX	0	0.39	-0.14	0.36
LOX	1	1.31	0.91	1.28	LOXL1	0	0.33	0.15	0.00
LOXL1	1	1.26	1.11	1.00	BMP1	0	0.57	0.00	0.24
MMP1	1	1.30	2.33	1.60	MMP1	0	0.38	1.22	0.68
MMP13	1	1.47	1.16	1.13	MMP13	0	0.55	0.21	0.18

Supplement to section 5.6 of the discussion:

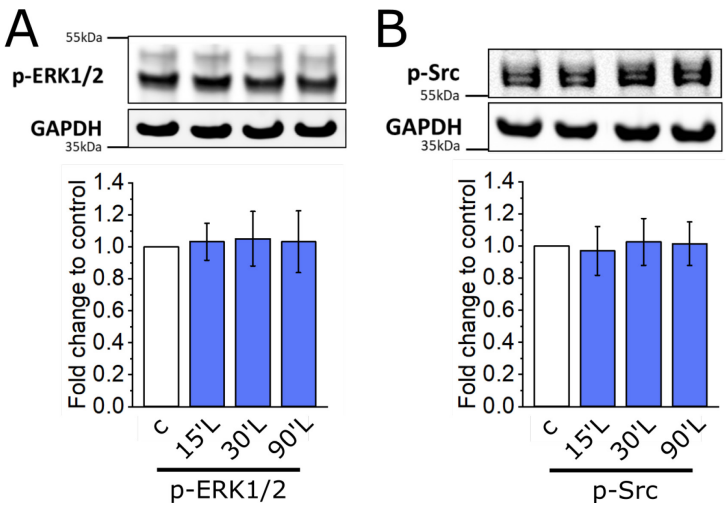

Figure 0-6: Cyclic compression did not induce ERK1/2 or Src phosphorylation. Human FOBs seeded in collagen scaffolds were subjected for 15, 30 or 90 min to cyclic compression (1Hz, 10%). The phosphorylation of ERK1/2 and Src were analyzed by western blotting. Phosphorylation intensities have been normalized to the uncompressed control (n=4).

Abbreviations

A

ALP	alkaline phosphatases

B

BISC	BMP-induced signaling complex
BMP	Bone Morphogenetic Protein
BMPR	BMP receptor
BSA	Bovine Serum Albumin

C

c	control
Col	collagen

D

DMEM	Dulbecco's modified Eagle medium
DMSO	Dimethyl sulfoxide

E

e.g.	exempli gratia
ECM	Extracellular matrix

F

FA	focal adhesion
FACS	fluorescence-activated cell sorting
FAK	focal adhesion kinase
FBS	fetal bovine serum
FC	focal complex
FDA	Food and Drug Administration
FGF-2	Fibroblast Growth Factor -2

G

GAG	glycosaminoglycan
GAPDH	glyceraldehyde 3-phosphate dehydrogenase
GPCRs	G-protein-coupled receptors
GSK3	glycogen synthase kinase 3

H

hdF	human dermal fibroblasts
hFOBs	human fetal osteoblasts
hMSCs	human mesenchymal stromal cells

I

I-Smads	inhibitory Smad
ID	inhibitor of DNA binding
IF	immunofluorescence
IFM	interfragmentary movement
IL	interleukin
ITG	integrin

J

Jas	Jasplakinolide

K

L

L	loading
LA	LifeAct
LOX	lysyl oxidases

M

MAPK	mitogen activated protein kinases myosin
MLC	light chain
MMPs	matrix metalloproteinases
MNE	mean normalized expression
mRNA	messenger RNA
MSC	mesenchymal stromal cell

N

NA	nascent adhesion
NEA	non-essential amino acids

O

OCN	osteocalcin
OSX	osterix
OPN	osteopontin
OSS	oscillatory shear stress

P

P/S	Penicillin/Streptomycin
PAA	polyacrylamide
PBS	Phosphate buffered saline
PCR	polymerase chain reaction
PDGF	Platelet-Derived Growth Factor
PDMS	polydimethylsiloxane
PEEK	polyether ether ketone
PFA	paraformaldehyde
PFCs	preformed complexes
PGs	proteoglycans
PI3K	phosphatidylinositol 3-kinase
POM	polyoxymethylene
PTHrP	parathyroid hormone-related peptide

Q

qPCR	quantitative polymerase chain reaction

R

R-Smad	receptor-regulated Smad
rh	recombinant human
RNA	ribonucleic acid
ROI	Region of interest
RT	Reverse transcription
RUNX2	Runt-related transcription factor 2

S

SHG	second harmonic generation
SHI	second harmonic imaging
siRNAs	small interfering RNA
Sox 9	SRY (sex determining region Y)-box
Src	proto-oncogene tyrosine-protein kinase 9

T

TGF-β	Transforming Growth Factor-β
TIMP	tissue inhibitors of metalloproteinases

U

V

W

WB	western blot
wt-%	weight percent

X

Y

YAP	yes-associated protein 1

Z